SWECO 7703
EMTR-801
SEPTEMBER 1977

MISSILE - BARRIER INTERACTION

A TOPICAL REPORT

PREPARED BY
STONE & WEBSTER ENGINEERING CORPORATION
BOSTON, MASSACHUSETTS

Z.D. JANKOV
CONSULTANT
ENGINEERING MECHANICS
DIVISION

J.A. SHANAHAN
SENIOR STRUCTURAL
ENGINEER
ENGINEERING MECHANICS
DIVISION

M.P. WHITE
CONSULTANT TO
STONE & WEBSTER

R.P. WESSEL
CHIEF ENGINEER
ENGINEERING MECHANICS
DIVISION

S.B. JACOBS
CHIEF LICENSING
ENGINEER

STONE & WEBSTER ENGINEERING CORPORATION

245 SUMMER STREET, BOSTON, MASSACHUSETTS

ADDRESS ALL CORRESPONDENCE TO P.O. BOX 2325, BOSTON, MASS. 02107

BOSTON
NEW YORK
CHERRY HILL, N.J.
DENVER
CHICAGO
HOUSTON
PORTLAND, OREGON
SAN DIEGO
WASHINGTON, D.C.

DESIGN
CONSTRUCTION
REPORTS
EXAMINATIONS
CONSULTING
ENGINEERING

September 23, 1977

Mr. John F. Stolz, Chief
Light Water Reactors Branch No. 1
Division of Project Management
U.S. Nuclear Regulatory Commission
Washington, DC 20555

Dear Sir:

STONE & WEBSTER ENGINEERING CORPORATION
TOPICAL REPORT - SWECO 7703
MISSILE-BARRIER INTERACTION

We are submitting, under separate cover, 50 copies of Stone & Webster Engineering Corporation (S&W) Topical Report, SWECO 7703. A copy of this transmittal letter is attached to each report copy.

In accordance with procedures outlined in your Elements of the Regulatory Staff Topical Report Review Program, S&W submits S&W Topical Report, SWECO 7703, "Missile-Barrier Interaction" for review and approval.

If you or members of your staff have questions or require clarification, please contact Mr. W. F. Bradley, Jr., of our Boston Office at 617-973-8092.

Very truly yours,

S. B. Jacobs

S. B. Jacobs
Chief Licensing Engineer

Enclosures

WFB:jmm

ABSTRACT

SWECO 7703, "Missile-Barrier Interaction," presents data of the missile barrier test program carried out at the Illinois Institute of Technology Research Institute under the direction of Stone & Webster Engineering Corporation. Methods are presented for design of both local and overall structural effects of missile impact on reinforced concrete barriers. The method of design for local effects is intended to prevent the phenomenon of scabbing, which is caused by movement of a shear plug. The method for overall structural response uses a single mass, single degree of freedom model to conservatively predict the response of the barrier.

DISCLAIMER OF RESPONSIBILITY

Neither Stone & Webster Engineering Corporation nor any of the contributors to this document makes any warranty or representation (expressed or implied) with respect to the accuracy, completeness, or usefulness of the information contained in this document. Stone & Webster Engineering Corporation assumes no responsibility for liability or damage which may result from the use of any of the information contained in this document.

TABLE OF CONTENTS

NOTE

This report has been previously printed by Stone & Webster Engineering Corporation and referenced in technical literature as EMTR-801, "Missile-Barrier Interaction," an Engineering Mechanics Division Technical Report.

ACKNOWLEDGEMENT

The authors wish to acknowledge the assistance given in the preparation of this report by Milton Nusbaum of the Illinois Institute of Technology Research Institute.

MISSILE-BARRIER INTERACTION

1.0 PURPOSE

The purpose of this report is to present missile barrier test data and to develop methods of analysis for local barrier damage and overall structural response. Specifically, the report has been developed to provide, in separately usable Appendices, unified simple procedures for designing barriers to withstand impact from those industrial missiles of concern to the nuclear power industry.

2.0 SUMMARY

The need to design nuclear plants for impact by various kinds of missiles has long been recognized. Until recently, however, the only available information for designing protection or for evaluating the threat has been the terminal ballistic data from tests of military projectiles against reinforced concrete protective structures. Unfortunately, the applicability of military test data to industrial missiles is very limited. Such tests consist of firing compact, nondeforming, pointed projectiles at relatively high velocities (generally 2,000 - 3,000 fps) against thick reinforced concrete (six to 12 times the thickness of the missile diameter). Industrial missiles, on the other hand, are normally of complex shape, frequently not compact, and not solid, so that they may deform during impact. Their velocities are usually in the range of 50-300 fps and seldom over 600 fps. Recognition of the importance of the problem created by this difference is the reason for undertaking this study. The barriers needed to protect nuclear plants from most industrial missiles range from less than 0.5 times the missile diameter for a tornado-borne automobile to 5 times the missile diameter for high energy turbine fragments.

Appendix A presents a detailed report on the extensive quarter-scale testing program carried out at the Illinois Institute of Technology Research Institute (IITRI) under the direction of Stone & Webster Engineering Corporation (S&W). Also in Appendix A is a report of a static penetration testing program which supplemented the S&W-IITRI tests. These tests were performed at the University of Massachusetts.

Two considerations involved in barrier design are treated in this report, namely, scabbing and overall structural deflection. Scabbing is discussed in Appendix B primarily on the basis of the S&W-ITTRI quarter-scale test program, but with supporting verification drawn from full-scale tests. The result is a method of determining sufficient barrier thickness to prevent scabbing caused by impact from various missiles. Alternatively, missile barriers can be designed with a thickness less than that required for no scabbing. The concrete coming off the back of the barrier can be contained by a scab plate. Appendix B also presents a method for designing steel scab plates.

The structural deflection of barriers due to missile impact is treated in Appendix C. The influence of other simultaneous loads such as static or dynamic pressure differentials is included. Two methods, a time history integration process and an analytical solution of the equations of motion, are presented.

The limit of barrier deflection is equal to or less than ten times the yield deflection of the barrier when either of the following conditions exist:

1. There is only one barrier between the missile and a missile protected zone, and
2. The barrier is required to carry other loads.

If a second barrier exists, able to stop possible secondary missiles, and if the barrier is not required to carry other loads, the first barrier impacted by the missile can be designed for structural response using a tension resisting mechanism. In this case the maximum barrier deflection is determined by the allowable tension strain in the rebar. The allowable tension strain in rebar for reinforced concrete barriers acting in tension is half the ultimate uniform strain of the rebar. This limit is the same as that for pipe whip restraints acting in tension, NUREG-75/087, Section 3.6.2.[4]

3.0 ANALYSIS AND EVALUATION OF TEST DATA

The initial objective of the S&W-IITRI testing program was to collect enough data to allow the design or evaluation of reinforced concrete missile barriers that would withstand impact by tornado-borne industrial missiles, especially steel pipes and wood poles. The final test program, however, included not only approximately scaled representations of the 13.5 in. diameter utility pole, the 12 in. diameter Schedule 40 and the 6 in. diameter Schedule 40 steel pipes required by the Nuclear Regulatory Commission (NRC)[3] as design basis tornado missiles but also certain additional missiles. These additional missile types, in all cases more damaging than the design basis tornado missiles, were chosen to try to document the capacity of barriers to resist a broad range of missiles.

In this program, described in detail in Appendix A, 48 missiles were fired against 22 reinforced concrete barriers of three different designs. There were nine missile types, three of which represented the three most damaging of the NRC steel pipe and wood pole missiles. Since the principal area of interest was the scabbing threshold, most of the missile shots were chosen so as to determine scabbing threshold velocities for different missile-barrier combinations. The tests showed that pipes are more damaging than wood missiles of equal weight and cross section and that, with respect to scabbing, the most damaging of the family of pipe and wood missiles specified as potential tornado threats by the NRC[3] is the 12 in. diameter 743 lb Schedule 40 pipe.

A general method of design and analysis is preferable to an ad hoc approach. In order to develop a general method, answers to certain specific questions needed to be obtained, the more important of which are the following:

1. Is back-face barrier scabbing by industrial missiles related to the formation of shock waves and their reflections within the barrier, or to the formation and displacement of a shear plug extending through the barrier?

   These tests indicate the latter to be the mechanism involved.

2. Does back-face scabbing, especially near the scabbing threshold, correlate with missile momentum, kinetic energy, or some other parameter?

   For these tests, which correspond to actual design conditions, the kinetic energy is shown to be the controlling parameter. Consequently, the estimate of a barrier's ability to withstand missile impact without scabbing is based on the barrier's kinetic energy absorption capacity, rather than on the depth of penetration as defined by the Modified Petry formula.

3. What role is played by the wall thickness of a pipe missile striking end-on?

   These tests show that wall thickness plays a very important role; a thick-walled pipe is far more damaging than a thin-walled pipe of equal total weight, velocity, and diameter. This shows that tests with pipe missiles can be misinterpreted unless this effect is considered.

4. How important is the material strength of the missile?

   These tests show that if the material strength is such that deformation or disintegration of the missile occurs during impact, the threat of scabbing is greatly reduced.

5. What is the role of concrete strength?

   This question is not resolved by this program since no consistent variation of concrete strength was investigated in the dynamic tests. However, the static penetration tests reported in Appendix A indicate that the effect of concrete strength on missile-barrier behavior is secondary.

6. What is the importance of the barrier reinforcing steel ratio on barrier performance?

   The results of these tests indicate that the scabbing threshold appears to be independent of the reinforcing ratio in the range of 0.3 to 1.0 percent, each way in each face. However, it is possible that the scabbing performance will be affected by changes in the size, spacing, and depth of concrete cover of the back-face rebars. It is found that levels of damage above the scabbing threshold are affected by the reinforcement ratio. Moreover, the analyses in Appendix C for structural response show that the amount of steel reinforcing and its strength play a direct role in determining structural response.

7. How reliable are reduced scale tests of missile-barrier interactions?

   These and other testing programs show that if all significant scaling relationships are satisfied, including the coarse aggregate of the concrete, model predictions are reliable. Evidence for this conclusion is the very close agreement between predictions based on these tests and the results of full-scale tests by others (especially the Bechtel-Calspan data which is discussed in Section B.3.1 of Appendix B).

4.0 RECOMMENDED DESIGN PROCEDURES

4.1 Design for Local Barrier Damage

Appendix B deals with the prevention and control of local damage, i.e., back-face scabbing of reinforced concrete barriers under impact by various industrial type missiles. The missiles specifically considered are:

1. Tornado-borne pipes
2. Tornado-borne automobile
3. Whipping pipes
4. Aircraft engine
5. Turbine rotor segment

Wooden missiles, such as the NRC utility pole, are not included since they are shown by the tests described in Appendix A to be less capable of causing scabbing than pipe missiles; specifically, the NRC-specified 743 lb 12 in. Schedule 40 pipe is more able to cause local damage than the 1500 lb utility pole.

All scabbing design computations are based on a single design diagram (Fig. B.3-1). This figure presents relationships among the following quantities:

1. Missile kinetic energy
2. Missile diameter
3. Average impact pressure (for whipping pipes and other missiles, except end-on pipe missiles) and pipe wall thickness (for end-on pipe missiles)
4. Barrier thickness

The design level corresponds to the scabbing threshold with some added conservatism on account of expected scattering of field or experimental data. In other words, on the average, Fig. B.3-1 somewhat overpredicts damage and underpredicts missile energy (or velocity) to cause scabbing of a given thickness barrier.

Illustrative examples for all missiles listed above except whipping pipes are given and include:

1. Comparison of observed and predicted full-scale test results.
2. Tabulations of required barrier thickness for both the NRC-specified 743 lb 12 in. Schedule 40 pipe and the 4,000 lb automobile for a range of striking velocities.

Appendix B also considers the corrections which may be necessary to compensate for barrier concrete weaker than that of the testing program; however, there is as yet no experimental evidence as to the necessity for such corrections.

The characteristics of secondary missiles (scab fragments) for impact above the scabbing threshold are treated, as is the design of scab plates, to control these secondary missiles.

4.2 Design for Barrier Overall Structural Response

Appendix C develops a method for calculating overall structural response to missile impact using a single equivalent mass and a nonlinear spring to model the dynamic response characteristics of the barrier. Numerical and analytical solutions for the barrier equation of motion are presented. These methods of calculating structural response use a square wave of force versus time to transfer the momentum of the missile to the barrier when the missile takes the same order of time or longer to stop in comparison with the time it takes the barrier to reach maximum deflection due to missile impact. The same method could be used for missiles which take a short time by comparison. However, in this case, considerable calculational effort is saved if the momentum is transferred to the barrier instantaneously, i.e., in zero time, thus giving the barrier an initial velocity. The barrier is brought to rest by its own structural stiffness.

At the present time, an analysis developed by Williamson and Alvy[1] is used by the NRC[2] for calculating structural response. This report shows that the Williamson and Alvy method is too conservative in the case of non-penetrating missiles such as the frame and body of the tornado-borne auto and whipping ruptured pipes. For short span barriers (10-15 ft) under impact by a tornado-borne automobile, the structural response predicted by the method in Appendix C is less by a factor of 10 or more than that predicted by Williamson and Alvy. The Williamson and Alvy method for non-penetrating missiles is, in fact, identical to the instantaneous momentum transfer method used here for missiles with short stopping time compared to the time it takes the barrier to reach maximum deflection.

A particular objective of this report was to investigate the adequacy of a 2 ft thick reinforced concrete barrier with No. 11 rebar, Grade 40, spaced each way and on each face of the barrier at 10 in. on center for protection against the horizontal motion of tornado-borne missiles. The governing Zone 1 tornado missile for structural response is the 4,000 lb automobile travelling at 59 meters per second as specified in NUREG-75/087 Section 3.5.1.4[3]. It is considered to have a 650 lb engine which transfers its momentum instantaneously and a 3,350 lb body and frame considered to transfer its momentum through a 300 kip square wave. The ductility ratio of the 2 ft thick barrier with a 10 ft span is 4.56; with a 15 ft span, 1.47; and with a 30 ft span, 0.50. The ductility ratio of the same barrier and missile using Williamson and Alvy is; for a 10 ft span, 68.42; for a 15 ft span, 19.14; and for a 30 ft span, 2.02. The 2 ft thick barrier is adequate in structural response for a 10 ft span. For 15 ft and 30 ft span barriers, less steel may be used and still remain below a ductility of 10.

The excessive conservatism of Williamson and Alvy in predicting structural response of certain non-penetrating missiles is evident in the case of the 4,000 lb auto given above. Both methods used in this report for calculating structural response, namely a square wave of force versus time and an instantaneous transfer of momentum give the same results as Williamsom and Alvy when the missile stopping time is short compared to the time it takes the barrier to reach maximum deflection due to the missile impact.

All other missiles or moving objects striking reinforced concrete barriers at nuclear power plants may also be analyzed for structural response by using a square wave of force versus time to transfer the missile momentum to the barrier. In the case where a missile or component of a missile transfers its momentum in a short time compared with the time the barrier takes to reach maximum deflection, the calculational effort is simplified by giving the mass of the barrier plus the mass of the missile or component a velocity so that its momentum is equal to the initial momentum of the missile. This instantaneous transfer of momentum is done in place of applying a square wave of force versus time to the barrier. This method of analyzing structural response to missile impact is used for whipping pipes, dropped equipment, flying pieces of equipment, aircraft, and tornado missiles.

5.0 CONCLUSIONS

The principal conclusions of this report are:

1. Tornado-generated missiles as specified by the NRC[3] do not cause scabbing or structural response greater than a ductility ratio of 10 for the standard Stone & Webster exterior missile barrier wall. This is reinforced concrete 2 feet thick with No. 11 size rebar 10 in. on center each way on each face. The specified material strengths are 3 ksi at 28 days for concrete and 40 ksi yield strength for rebar.

2. The principal type of local damage of concern to the designer is scabbing. A conservative method of designing to protect against scabbing for moving objects striking reinforced concrete at nuclear plants is provided in Appendix B. Scabbing is controlled by using either a barrier thick enough so that it does not scab or a thinner barrier with a steel scab plate on the far face of the barrier.

3. A conservative method of predicting the structural deflection caused by moving objects striking reinforced concrete at nuclear plants is provided in Appendix C. The barrier deflection is limited to a ductility of 10 or less when; a) there is only one barrier between missile and missile protected zone, or b) the barrier is required to carry other loads.

   If there is more than one barrier separating missile from missile protected zone, the primary barrier can be designed using its tension-resisting mechanism, if it is not required to carry other loads. The strain of the rebar in the barrier in a tension-resisting mechanism is permitted to go to half the ultimate uniform strain of the rebar.

4. Penetration into concrete by industrial missiles of concern to nuclear power plants is more varied for the range of missile types and less predictable than is the penetration of military type missiles. Penetration, therefore, is not used as a measure of predicting scabbing, as is done in the military formulas. Also, it is not used to determine structural response, as is done in Williamson and Alvy[1][2].

5. The method, given in[1],[2] to determine structural response for missiles which do not penetrate is too conservative when the missile stopping time is a large fraction of the time

to maximum barrier displacement. Therefore, the method given in Appendix C is used to evaluate the structural deflection to missile impact.

6.0 REFERENCES

(1) Williamson, R.A. and Alvy, R.R., "Impact Effect of Fragments Striking Structural Elements," Holmes and Narver, Inc., Revised November, 1973.

(2) NUREG-75/087, Section 3.5.3, "Barrier Design Procedures," U.S. Nuclear Regulatory Commission.

(3) NUREG-75/087, Section 3.5.1.4, "Missiles Generated by Natural Phenomena," U.S. Nuclear Regulatory Commission.

(4) NUREG-75/087, Section 3.6.2, "Determination of Break Location and Dynamic Effects Associated with the Postulated Rupture of Piping," U.S. Nuclear Regulatory Commission.

7.0 DEFINITIONS

Ductility Ratio

The ratio of the maximum barrier displacement to the displacement at the effective yield point of the barrier.

Penetration

The passage of the nose of a missile past the front face of a barrier.

Perforation

The passage of the nose of a missile past the rear face of a barrier.

Scabbing

The separation of concrete from the back face of a barrier due to missile impact.

Scabbing Threshold

The stage when the shear plug is moved from its original position and forced against the back-face reinforcing bars causing the separation of the fragments of concrete from the back-face of the barrier with small initial velocities (up to 4-5 fps).

Scabbing Threshold Velocity

The velocity of a given missile which causes a given barrier to reach the scabbing threshold.

Shear Plug Formation

The stage of an impact event when the applied load from a missile causes the formation of a truncated conical plug of concrete in front of the missile.

APPENDIX A

TEST DATA AND INTERPRETATION

TABLE OF CONTENTS

LIST OF TABLES

LIST OF FIGURES

APPENDIX A

TEST DATA AND INTERPRETATION

A.1 PURPOSE

The purpose of this Appendix is to present, analyze, and evaluate data from a series of quarter-scale missile-barrier interaction tests in order to establish a basis for the design of reinforced concrete missile barriers for nuclear facilities.

Another objective of this Appendix is to demonstate the validity of linear scaling for missile-barrier tests.

A.2 SUMMARY

Data from three series of tests are presented in this Appendix: 1) interaction tests of wood pole, steel pipe, and solid steel slug missiles with reinforced concrete barriers, 2) static punching shear tests of barriers, and 3) tests of static penetration of concrete by steel punches. Tabular, photographic, and graphic presentations of these tests are included.

The first series consisted of 48 tests that involved the firing of quarter-scale missiles at similarly scaled reinforced concrete panels. Among the missiles were several chosen to represent the tornado-generated missiles considered in the design of nuclear facilities. The barriers were similarly scaled so as to represent the 18 in. and 24 in. reinforced concrete panels currently used as missile barriers at nuclear facilities.

In the second series, nine tests were made to evaluate the static punching load capacity of the reinforced concrete barriers. Two barriers, one representing the current Stone & Webster Engineering Corporation's (S&W) 24 in. design for Category I walls and the other representing an 18 in. wall, were used in these tests.

The third series of tests, performed at the University of Massachusetts, consisted of seventeen static penetrations of concrete by solid and hollow cylindrical steel punches. Punch diameters varied from one-quarter in. to 1 in. and concrete strength from about 3 ksi to 7.4 ksi.

Since the dynamic tests presented in this Appendix were performed with quarter-scale missiles and barriers, the validity of linear scaling for missile-barrier interaction testing is demonstrated. This is done by using comparisons of the full-scale and one-tenth scale tests performed by the United States Naval Weapons Laboratory (USNWL)[1], and the full-scale tests performed by the Sandia Corporation[2] and Calspan[3] with the quarter-scale tests performed by IITRI.

Finally, the effects of the most damaging tornado missiles specified for nuclear facilities by the Nuclear Regulatory Commission (NRC)[5] are evaluated in terms of the S&W-IITRI tests.

A.3 MISSILE-BARRIER TESTS

The Illinois Institute of Technology Research Institute (IITRI) performed a series of missile-barrier impact tests for S&W at ITTRI's Gary, Indiana testing facility in August of 1975.

The tests yielded data about the following:

1. Missile velocity to initiate back-face scabbing
2. Missile deformation
3. Barrier resistance to initial penetration
4. Missile perforation of barrier
5. Velocity of scabbing particles
6. Size of barrier rear-face crater
7. Size of barrier front-face crater
8. Barrier support reactions

Forty-eight missile-barrier tests were made using 22 barriers. The first shot at each barrier was generally a missile traveling either in the order of 200 fps or at a velocity near the estimated scabbing threshold. The second shot at a barrier was either an exploratory shot with a new kind of missile or a shot aimed at investigating the barrier's perforation limit.

Twenty-nine of the 48 tests are classified as primary hits because the results of

these tests were not significantly affected by previous hits on the same barrier. The primary hit test results are given in Table A.3.3-1.

The other nineteen tests are classified as multiple hits because previous hits had significantly damaged the barrier. The multiple hit test results are given in Table A.3.5-1.

It is important to note that the pipe missiles in the test program were not scaled exactly to the NRC pipe missiles, but had somewhat greater wall thicknesses. Consequently, the corresponding NRC missiles are less damaging than the scaled-up test missiles.

A.3.1 Missiles

The missiles listed in Table A.3.1-1 were selected because of their similarity to the three missiles (listed and described in Table A.3.1-2) specified by the NRC as among those which the structures within a nuclear facility must withstand. The similarities and differences between the nine test missiles and the three NRC-specified missiles are as follows:

1. Wood pole (3.375 in. diameter, 23.4 lb): This missile had approximately one-quarter the linear dimensions and one sixty-fourth the weight of the NRC utility pole listed in Table A.3.1-2. The test missile was machined from yellow pine to 3.75 in. in diameter and was about 11.25 ft long.

2. Steel pipe (1.69 in. OD, 4.6 lb): This missile had approximately one-quarter the outside diameter and one sixty-fourth the weight of the second NRC missile listed in Table A.3.1-2. The outside diameter and wall thickness of the NRC 6 in. pipe are 6.625 in. and 0.28 in., respectively. At full size, missile No. 2 would have a 6.75 in. OD and a wall thickness of 0.48 in. Thus, the wall thickness and cross-sectional area of test missile No. 2 are about 70 percent greater at full size than the NRC 6 in. pipe. Therefore, tests with missile No. 2 should produce more barrier damage than a missile that is scaled to exactly one quarter of the NRC 6 in. pipe.

3. Missile No. 3 was about double the weight of missile No. 2 with the same cross section. At full size, it would approximate a 30 ft long pipe missile.

4. Steel pipe (3.0 in. OD, 12.3 lb): This missile had approximately one quarter the diameter of the NRC 12 in. Schedule 40 pipe and had one sixty-fourth its weight. The outside diameter and wall thickness of the NRC 12 in. pipe are 12.75 in. and 0.375 in., respectively. The diameter and wall thickness of test missile No. 4 at full size would be 12 in. and 0.48 in., respectively. Thus, at full size, the wall thickness of test missile No. 4 is 28 percent greater than that of the NRC 12 in. pipe, and the difference in steel areas is 19 percent.

5. Missile No. 5 was approximately double the weight of test missile No. 4 with the same cross section. At full size, it would approximate a 30 ft long pipe missile 12 in. in diameter.

6. Steel Pipe (3.50 in. OD, 11.25 lb): This missile had approximately one quarter the outside diameter of the NRC 12 in. Schedule 40 pipe. The outside diameter and wall thickness of test missile No. 6 at full size would be 14.00 in. and 0.864 in., respectively. The wall thickness and cross-sectional area of test missile No. 6 are, respectively, 112 and 127 percent greater than those of the NRC 12 in. pipe.

7. Missile No. 7 was a solid steel slug with the same weight and diameter (3 in.) as test missile No. 4 and approximately the same weight as test missile No. 6.

8. Missile No. 8 was a solid steel slug twice the weight of test missile No. 7 with the same cross section.

9. Missile No. 9 was a special missile. Unlike all the other test missiles, it had an impact diameter greater than the barrier thickness. Its weight was four times that of the heaviest of the eight other missiles. At full size, its weight would be 6,976 lb with an impact diameter of 40 in. It was essentially a non-deforming missile and, therefore, provided basic information on the upper boundary of barrier damage for other missiles of the same weight, diameter, and velocity.

A.3.2 Barriers

Historically, the Category I S&W exterior wall barrier for tornado-borne missiles has been 24 in. thick with No. 11 A615 Gr 40 reinforcing bars placed 10 in. on center (OC) each way and in each face (EWEF) with 2 in. of concrete cover. This corresponds to 0.757 percent steel EWEF.

Three quarter-scale three foot square barriers designated Types I, II, and III were used in the tests. They were designed with the specifications shown in Table A.3.2-1. At full size, they would have the specifications listed in Table A.3.2-2.

The Type I barrier had No. 3 rebar 2.5 in. OC, EWEF with 1/2 in. of cover. The steel percentage was 0.859 EWEF.

Type II was 4.5 in. thick with No. 2 undeformed rebar, 3 in. OC, EWEF, giving a steel percentage of 0.444 EWEF. At full size, this corresponds to an 18 in. barrier with No. 8 rebar at 12 in. OC, EWEF, with 0.444 percent steel EWEF. The Type III barrier was 6 in. thick with the same rebar as in Type II giving a steel percentage of 0.317 EWEF. This corresponds to a 24 in. barrier with No. 8 rebar at 12 in. OC with 0.317 percent steel EWEF.

For all barriers, the specified concrete cylinder compression strength f_c' was 3.0 ksi. However, the actual concrete strength at testing was higher (see Section A.4.1). The 3/8 in. coarse aggregate used in the concrete was approximately one quarter the size used in full-scale construction.

A.3.3 Primary Hit Data and Photographs

Twenty-nine of the 48 missile barrier tests were primary hits (i.e., not affected by previous hits); the data from these tests is listed in Table A.3.3-1. This table is organized according to missile type, missile velocity, and barrier type. The barrier damage details are given in Table A.3.3-2.

Photographs of the front and rear face of the barrier, profile of rear rebar or concrete, profile of back crater after excavation, and missile damage for each primary hit test are shown in Figs. A.3.3-1 through A.3.3-29. The profiles of the rear rebar or concrete and the back crater show a white board with seven black lines on it for scale. The black lines are 0.5 in. wide and 0.5 in. apart. This shows the amount of outward movement of the rear concrete surface or the rear rebar and the depth of the back crater. In the back crater photographs, the nails shown were held in place by two eye hooks and then pushed in until the tips touched the surface of the back crater. The heads of the nails then give the profile of the back crater. The nails were spaced one in. apart.

The same white board with 0.5 in. black stripes was used as a scale in the missile photographs. The missile was positioned so that the original front end of the missile would be at the edge of the board. Thus, the amount of deformation is recorded in the photograph.

A.3.4 Primary Hit Load Cell Time Histories

The time histories of the load cells supporting the primary hit barriers are given in Figs. A.3.4-1 through A.3.4-29.

A.3.5 Multiple Hit Data and Photographs

Nineteen of the 48 missile barrier tests were multiple hit tests (i.e., the tests were influenced by previous hits on the same barrier). Data from these tests is listed in Table A.3.5-1. The table is organized according to missile type, missile velocity, and barrier type. The barrier damage details are listed in Table A.3.5-2.

Photographs of the front and rear face of the barrier, profile of rear rebar or concrete, profile of back crater, and missile damage for each multiple hit test are shown in Figs. A.3.5-1 through A.3.5-19.

A.3.6 Multiple Hit Load Cell Time Histories

The time histories of the load cells supporting the multiple hit barriers are given in Figs. A.3.6-1 through A.3.6-19.

A.4 MATERIAL TESTS AND SPECIFICATIONS FOR MISSILES AND BARRIERS

A.4.1 Barrier Concrete

The specified concrete compressive strength for all barriers at 28 days was 3.0 ksi. The tested strength for the Type I barriers averaged 4.3 ksi; for the Type II barriers, 3.2 ksi; and for the Type III barriers, 3.9 ksi. The split cylinder strength for Type I averaged 0.433 ksi; for Type II, 0.345 ksi; and for Type III, 0.360 ksi. These tested strengths of concrete are for the day of missile impact which ranged from 40 to 60 days after the concrete was poured.

A.4.2 Barrier Rebar

The specified yield strength for the No. 2 and No. 3 rebar was 40 ksi. The No. 2 rebar in Types II and III had a yield stress of 56 ksi and an ultimate stress of 80 ksi. The No. 3 rebar in Type I had a tested yield stress of 80 ksi and an ultimate stress of 115 ksi.

A.4.3 Wood Missiles

The wood missiles had an average ultimate static compression stress of 6.9 ksi. The strength of the wood missiles during impact is determined by equating the kinetic energy of the missile to the work done in permanent distortion of the wood. This can only be done when penetration, shear plug movement, and large barrier deformations do not occur. The strength of the wood missiles during missile impact was 3.0 ksi. This was determined by

equating the kinetic energy of the wood missile, 24.6 ft-kips, to the irreversible work done in deforming the missile 11 in. The missile has a cross-sectional area of 8.94 sq in.

A.4.4 Pipe Missiles

The 1.69 in. diameter pipe had a tensile yield stress of 24 ksi and an ultimate stress of 90 ksi. The 3 in. diameter pipe had a tensile yield stress of 52 ksi and an ultimate stress of 61 ksi. The 3.5 in. diameter pipe had a tensile yield stress of 36 ksi and an ultimate stress of 61 ksi.

The static strength of the pipe missiles was determined by cutting out a section of the missile, flattening it, and then testing it in tension. The 1.69 in. diameter pipe had the greatest curvature and, therefore, underwent more deformation in being flattened prior to tension tests. This contributed to the low yield strength, 24 ksi, of the 1.69 in. diameter pipe missiles.

A.5 BARRIER STATIC PUNCHING SHEAR TESTS

Two barriers were not used during the 48 dynamic tests so that static load capacity evaluations could be performed. These were one Type I barrier, 6 in. thick, and one Type II barrier, 4.5 in. thick. Both barriers were quartered to provide multiple samples. Fourteen in. and 3.5 in. (inside) diameter ring dies provided two support conditions.

Composite photographs illustrating the static punching tests are presented in Figs. A.5-1 through A.5-9.

The force-deflection curves for a 3 in. punch as it moved the shear plug into the Type II barriers are shown in Fig. A.5-10.

A.6 STATIC PENETRATION OF CONCRETE BY STEEL PUNCHES

Seventeen static penetration tests were made on massive concrete by 1/4 in. to 1 in. in diameter solid and tubular cylindrical steel penetrators (see Figs. A.6-1 to A.6-17). Concrete compressive strengths ranged from 3.0 ksi to 7.4 ksi.

A.7 DYNAMIC PENETRATION OF CONCRETE BY STEEL MISSILES

If the missile does not deform and a shear plug is not formed, all of the kinetic energy is dissipated by the work of penetration. This can be expressed by the following equation

$$KE = \sigma \times A \times d \qquad \text{(A.7-1)}$$

where

KE = kinetic energy of missile

σ = average penetration resistance stress of concrete

A = cross-sectional area of missile

d = depth of penetration

A certain amount of information on penetration resistance of concrete barriers to impacting pipe and slug missiles can be drawn from the S&W-IITRI test program. However, great caution is required in doing this, since most of those tests involved not only missile penetration but also shear plug displacement and missile deformation, so that application of Eq. A.7-1 to these cases would give spurious results.

The use of Eq. A.7-1 on tests which had shear plug movement would give apparent resistances well below the actual penetration resistance. Consequently, these tests have not been used to calculate the average penetration resistance stress. However, an approximate correction for missile deformation (by a corresponding increase in d) can be applied to Eq. A.7-1.

Rotz[3] gives penetration resistances of 55 ksi for 1 in. rods and 57 ksi for 8 in. slugs. An independent analysis of that data using Eq. A.7-1 gives values of 48 ksi for both cases. A value of 50 ksi is used in this report.

A.8 SCALED REPLICA MODEL TESTING

A.8.1 Scaling Relations

Scaled models have been used for many years for investigating the static and dynamic behavior of all kinds of mechanical systems subjected to a wide assortment of loadings. The reliability of predictions based on model studies is generally acknowledged. In a scaled model, all significant lengths bear a constant ratio to corresponding lengths in the prototype; this ratio is the length scale factor, usually called the scale factor, λ . A replica model uses materials with the same physical properties as in the prototype.

An obvious condition for validity of a model test is that model and prototype behave alike. This requirement can be satisfied by use of various approaches (e.g., the Buckingham Pi Theorem[1][4]). Another method is to specify that all the significant forces that control the response of the model bear a constant relationship to the corresponding forces in the prototype; this defines a force scale factor, λ_F . One can define other scale factors: velocity ratio, λ_V , time scale factor, λ_T , etc.

In the case of missile-barrier interaction, the significant forces are the internal forces due to deformations of all kinds and the inertia forces due to

accelerations within the system. The internal forces are equal to internal stresses as functions of unit strain, $\sigma(\epsilon)$, multiplied by area. This gives $L_F = \sigma\lambda^2$. The inertia forces equal material density, ρ, multiplied by volume, L^3, and by acceleration, L/T^2. This gives $\lambda_F = \rho\lambda^4/\lambda_T^2$. Combining relations gives $\sigma/\rho = \lambda^2/\lambda_T^2$. Since model and prototype are composed of the same materials, it follows that the time scale equals the length scale ($\lambda_T = \lambda$). Other scale factor relationships can be developed as required. For the quarter-scale tests reported here, the scale factor relations are given below:

Length	$\lambda = 1/4$
Time	$\lambda_T = \lambda = 1/4$
Force	$\lambda_F = \lambda^2 = 1/16$
Velocity	$\lambda_V = \lambda^0 = 1$
Acceleration	$\lambda_A = \lambda^{-1} = 4$

In other words, model lengths and model times are one quarter prototype lengths and times; model forces are one sixteenth those in the prototype; model and prototype velocities are equal; and model accelerations are four times those of the prototype.

Obviously, sufficient care must be taken to be sure that all significant forces in model and prototype have been considered in making up the scaling factors. For example, if the force of gravity had also been of importance, problems would arise since the gravity forces have the form $\rho g L^3$ which is not compatible with the relations derived here.

It is also essential that all significant characteristics of the prototype be correctly scaled in the model. This condition is illustrated by World War II experience with terminal ballistic studies of concrete penetration and perforation by projectiles. It was discovered that large projectiles did not behave as was predicted by simple scaling, since they penetrated further than expected. The reason for this apparent violation of the scaling laws is simply that the coarse aggregate used in the small caliber and large caliber tests was not scaled in proportion to the projectile caliber. This has been shown by USNWL[1] in a program of full-scale and one-tenth scale projectile penetration firings against concrete barriers of the same strength but with scaled coarse aggregate. In these tests, the small and large scale data coincided when striking velocity was plotted against dimensionless penetration into massive concrete.

A.8.2 Reasons for Scaled Model Testing of Missile Barriers

Model testing is generally less expensive and less time-consuming than full-scale testing. The ability to obtain large amounts of data (due to decreased costs) was especially attractive since it was possible to explore the effect of changing parameters such as velocity, missile dimensions, barrier reinforcement and dimensions, etc. Another factor in the decision was that the other barrier programs in process or planned were at full scale and would provide full-scale data which could furnish comparison and verification of model test data.

A.8.3 Comparison of Quarter-Scale and Full-Scale Tests

Figures A.8.2-1 through A.8.2-6 allow comparison between full-scale missile-barrier tests made by the Sandia Corporation for EPRI[2] and nearly comparable one-quarter scale tests conducted by IITRI (see Section A.3). These photographs indicate a good degree of correlation between the two groups of test results. The characteristics of missiles and barriers for this comparison are given in Table A.8.2-1. See also Section B.3-1.

A.8.4 Full-Scale Extrapolation of the IITRI Test Data

Full-scale extrapolations for the primary hit tests in Table A.3.3-1 are given in Table A.8.4-1.

Full-scale extrapolations for the multiple hit tests in Table A.3.5-1 are given in Table A.8.4-2.

A.9 INTERPRETATION OF TEST DATA

A.9.1 General Remarks

Although the tests utilized a considerable range of velocities for most of the missiles, and produced levels of damage from slight to extreme, the major concern was to determine the scabbing threshold velocity for a given missile and a given barrier, and the dependence of that velocity on the various parameters of missile and barrier.

It is emphasized that any conclusions drawn from these tests are valid only within the limits of the dimensionless parameters of the tests.

A.9.2 Mechanism of Scabbing

If scabbing were the result of shock-wave reflection at the back face of a barrier, there would generally be undamaged concrete in the middle between the front crater and the scabbed area. This is not the case: excavation of the back faces of barriers after impact showed that above some velocity level (but considerably lower than the scabbing threshold) a shear plug is formed in the form of a frustum of a cone. The small end of the shear plug near the barrier front face is the size of the impacting missile, and the total angle at the apex of the cone is approximately

120 deg. As the velocity is increased, the shear plug is displaced. Cracks on the back face of the barrier define the larger end of the shear plug. Eventually, at the scabbing threshold velocity, scabbing occurs.

Estimates were made of scabbing threshold velocities for those missile-barrier combinations for which enough data was obtained and these velocities are listed in Table A.9.2-1.

A.9.3 Scabbing Threshold Correlation with Impact Parameters

Examination of the scabbing threshold velocities for light and heavy slugs (Nos. 7 and 8) and for light and heavy 3 in. pipe (Nos. 4 and 5) in Table A.9.2-1 shows that, under the conditions of these tests, for a given type and size of missile, scabbing occurs at a given level of kinetic energy, not momentum.

A.9.4 Scabbing Threshold Dependence on Pipe Wall Thickness

Comparison of scabbing threshold velocities for steel missiles of about the same weight and diameter but with different cross sections (slugs, thin- and thick-walled pipes - Nos. 4, 6, and 8 in Table A.3.1-1) shows that pipe wall thickness plays a very strong role in missile performance. For example, the 3.5 in. pipe (No. 6) requires about 50-60 percent higher velocity than the 3 in. slug (or well over twice the kinetic energy) to reach the scabbing threshold. The thinner-walled 3 in. pipe (No. 4) requires about 80 percent higher velocity than the 3 in. slug for the same effect on the barrier. (A small difference in the value of T/D has little effect on the damage level.)

The 3.5 in. pipe is not significantly deformed during impact, except at points of contact with rebars. The difference between its performance and that of a solid slug is that the latter only slightly penetrates the barrier and is, therefore, brought to rest more quickly and in a shorter distance than the pipe. Consequently, the slug exerts a greater peak force on the barrier than the pipe and produces equal damage at a lower velocity.

With the thin-walled 3 in. pipe, the effect on scabbing threshold velocity would be greater than with the thicker walled pipe, but the situation is complicated further by the simultaneous crumpling of the nose of the missile. The combined effect is to increase even further the duration of the impact process and to decrease the peak force on the barrier, hence requiring still greater velocity and more kinetic energy to reach the scabbing threshold.

It is important to note that the pipe missiles in the test program were not scaled exactly to the NRC pipe missiles, but had somewhat greater wall thicknesses. Consequently, the NRC pipe missiles would be less damaging than the scaled-up test missiles.

A.9.5 Effect of Concrete Strength

The question of the effect of concrete strength is not answered by the test data, since no systematic variation of f_c was included in the program. There was a considerable difference between the strengths of the 4.5 in. barrier (f_c = 3.2 ksi) and the two 6 in. barriers (f_c = 3.9 and 4.3 ksi) but no conclusions can be drawn from the data. The static penetration tests indicate relatively little difference between the resistance of 3.0 ksi and 7.4 ksi concrete (Figs. A.6-1 through A.6-17).

A.9.6 Effect of Missile Strength

It is clear that missile strength (i.e., material strength combined with end geometry) is an important factor in missile performance. The wood missile with about 3.3 times the kinetic energy of the short 3 in. pipe accomplished far less barrier damage as shown by comparison of Tests 1, 2, 3, and 4. How much of the difference in performance between missiles 4 (3 in. pipe) and 6 (3.5 in. pipe) is due to their different diameters and wall thickness, and how much to the crumpling of the former, is uncertain. However, it is to be expected that local missile distortion will reduce back face damage.

A.9.7 Role of Reinforcement Ratio of Barrier

These tests revealed no apparent difference of scabbing threshold velocities for barrier Types I and III (both 6 in. thick, but with steel percentages of 0.859 and 0.317, respectively). This is not unexpected since scabbing occurs with very little displacement of the shear plug. In other words, at the scabbing threshold the difference between the two levels of reinforcing has little effect. However, a barrier with no reinforcing steel at all might well break up under moderate impact. On the other hand, under severe impact resulting in a high degree of damage, including extensive shear plug displacement or disintegration, the quantity of steel plays an important role.

It is possible that a considerable effect on the scabbing threshold might result from changing the number of rear face reinforcing bars without changing the percentage of steel.

Tack welds were used at several points to connect rebar of different layers to facilitate construction of the targets. For levels of damage above the scabbing threshold but below the perforation limit (i.e., significant movement of the shear plug), the rear face rebar was ruptured at

the weld points. This effect would tend to decrease the strength of the barrier for overall structural response. Therefore, as recommended in ACI 318[6] and ACI 349[7], tack welds of rebar shall not be used in the missile-barrier construction.

A.10 CONCLUSIONS

For a particular missile type and barrier type, the scabbing threshold corresponds to a given kinetic energy of missile, not its momentum. This means that the scabbing threshold velocity varies inversely with the square root of the mass of the missile.

For pipe missiles that neither buckle nor crush, the scabbing threshold velocity decreases as the ratio of missile wall thickness/radius (2t/D) increases. The scabbing threshold velocity increases when 1) the missile nose crushes or buckles, and 2) the entire missile buckles. If the material of the missile yields or disintegrates during impact, the scabbing threshold velocity increases.

The scabbing threshold velocity appears to be unaffected by changes in the reinforcement ratio within the range of 0.3 to 1.0 percent each way in each face. However, this conclusion does not apply to higher levels of damage.

The concrete strength referred to in this Appendix is the average strength of test cylinders on the day of missile test. The variation of missile-barrier strengths in the S&W-IITRI tests and the variation of strength of the static penetration tests, mentioned in Section A.6, indicate that the scabbing threshold velocity is not sensitive to changes in concrete strength from 3 ksi to 5 ksi.

Scabbing of concrete on the rear face of the barrier is caused by formation and movement of a shear plug. For an illustration of this, see the photo labeled, "Profile of Back Crater," and photo labeled, "Barrier Rear Face," in Fig. A.3.3-16. The data in Fig. A.3.3-16 and the photo labeled, "Barrier Rear Face" show that the pipe missile impacted the barrier at the scabbing threshold velocity. The photo labeled, "Profile of Back Crater" shows a black and white profile gage recording the crater left by removing the shear plug. In the lower left quarter of the photo is the solid shear plug which was easily removed after cutting the rear face rebar.

If stress waves had caused scabbing particles to come off the rear face of the barrier, this concrete plug would not be solid.

A.11 REFERENCES

(1) U.S. Naval Weapons Laboratory Technical Report 2057 "Development of a Scaling Law and Techniques to Investigate Penetration in Concrete", J.A. Caulfied and I.G. Clator, 1966.

(2) Stephenson, A.E., "Full-Scale Tornado-Missile Impact Tests", Electric Power Research Institute, EPRI NP-148 Interim Report, April, 1976.

(3) Rotz, J.V., "Results of Missile Impact Tests on Reinforced Concrete Panels", Second ASCE Specialty Conference on Structural Design of Nuclear Power Plant Facilities, December, 1975.

(4) Langhaar, Henry L., "Dimensional Analysis and Theory of Models", John Wiley and Sons, Inc., New York, 1954.

(5) U.S. Nuclear Regulatory Commission Standard Review Plan, NUREG-75/087, Section 3.5.1.4 "Missiles Generated by Natural Phenomena." Rev. 1.

(6) ACI Standard 318-71, "Building Code Requirements for Reinforced Concrete."

(7) ACI Standard 349-76 and Commentary, "Code Requirements for Nuclear Safety Related Concrete Structures."

TABLE A.3.1-1

IITRI QUARTER-SCALE MISSILE DATA

Missile No./Type	Outside Diameter (in.)	Weight (lb)	Wall Thickness (in.)	Wall Thickness/ Radius (2t/D)
1. Wood Pole	3.375	23.42	Solid	1.000
2. Steel Pipe	1.69	4.60	0.12	0.142
3. Steel Pipe	1.69	10.40	0.12	0.142
4. Steel Pipe	3.00	12.30	0.12	0.080
5. Steel Pipe	3.00	26.50	0.12	0.080
6. Steel Pipe	3.50	11.25	0.216	0.123
7. Steel Slug	3.00	12.60	Solid	1.000
8. Steel Slug	3.00	23.50	Solid	1.000
9. Composite Missile*	-	-	-	-
Pipe	3.50	76.00	0.216	1.000
Plate	10.00	33.00	Solid	1.000
		109.00**		

*Welded assembly
**Total weight of pipe and plate

TABLE A.3.1-2

NRC FULL-SCALE MISSILE DATA

	Missile	Outside Diameter (in.)	Weight (lb)	Wall Thickness (in.)	Wall Thickness/ Radius (2t/D)
1.	13.5 In. Utility Pole	13.5	1,490	Solid	1.000
2.	6 In. Sch. 40 Steel Pipe	6.625	285	0.28	0.085
3.	12 In. Sch. 40 Steel Pipe	12.75	743	0.375	0.059

TABLE A.3.2-1

IITRI QUARTER-SCALE BARRIER DATA

Barrier Type	28 day Specified Concrete Strength (psi)	Day of Test Concrete Strength (psi)	Barrier Dimensions	$p = \frac{100\ A_s}{bd}$	Rebar Size No.	Rebar Spacing (in.)
I	3,000	4,300	6.0"x3'-0"x3'-0"	0.859	3	2.5
II	3,000	3,200	4.5"x3'-0"x3'-0"	0.444	2	3
III	3,000	3,900	6.0"x3'-0"x3'-0"	0.317	2	3

* d = barrier thickness minus cover** minus one rebar diameter.
** cover = 0.5 inches.

TABLE A.3.2-2

FULL-SCALE PROTOTYPE BARRIFR DATA

Barrier Type	28 day Specified Concrete Strength (psi)	Barrier Dimensions	$p = \frac{A_s}{bd} \times 100$	Rebar Size No.	Rebar Spacing (in.)
I	3,000	24" x 12' x 12'	0.757	11	10"
II	3,000	18" x 12' x 12'	0.44	8	12"
III	3,000	24" x 12' x 12'	0.31	8	12"

TABL

PRIMARY HIT MISS

Line No.	Missile Description	Velocity, (fps)	Location	Ba Thickness, (in.)
WOOD POLE				
1	3.375" OD Wood Pole, 23.42 lb, Solid	258	Rebound	4.5
2	3.375" OD Wood Pole, 23.42 lb, Solid	265	Rebound	6.0
SINGLE LENGTH PIPE				
3	1.69" OD Steel Pipe, 4.6 lb, 0.12" Wall	313	Rebound	6.0
4	1.69" OD Steel Pipe, 4.6 lb, 0.12" Wall	394	Rebound	6.0
5	1.69" OD Steel Pipe, 4.6 lb, 0.12" Wall	470	Rebound	6.0
6	3.0" OD Steel Pipe, 12.3 lb, 0.12" Wall	159	Rebound	4.5
7	3.0" OD Steel Pipe, 12.3 lb, 0.12" Wall	195	Rebound	4.5
8	3.0" OD Steel Pipe, 12.3 lb, 0.12" Wall	211	Rebound	4.5
9	3.0" OD Steel Pipe, 12.3 lb, 0.12" Wall	317	Perforated	4.5
10	3.0" OD Steel Pipe, 12.3 lb, 0.12" Wall	403	In Target	4.5
11	3.0" OD Steel Pipe, 12.3 lb, 0.12" Wall	207	Rebound	6.0
12	3.0" OD Steel Pipe, 12.3 lb, 0.12" Wall	245	Rebound	6.0
13	3.0" OD Steel Pipe, 12.3 lb, 0.12" Wall	211	Rebound	6.0
14	3.0" OD Steel Pipe, 12.3 lb, 0.12" Wall	244	Rebound	6.0
15	3.5" OD Steel Pipe, 11.25 lb, 0.216" Wall	131	Rebound	4.5
16	3.5" OD Steel Pipe, 11.25 lb, 0.216" Wall	206	Rebound	6.0
17	3.5" OD Steel Pipe, 11.25 lb, 0.216" Wall	203	Rebound	6.0

E A.3.3-1

ILE BARRIER TEST DATA

Barrier Characteristics				Rear Face Scabbing Particle Velocity, (fps)	Rear Face Scabbing Particle Distance from Barrier, (ft)	Rear Face Scabbing Particle Cube Dimension, (in.)	Test Nos. of Previous Impact On Same Target	Test No.
f'c ksi)	p = A_s/ bd x 100	Rebar fy, (ksi)	Rebar Spacing, (in.)					
3.2	0.444	56	3.0	None	None	NA	None	3
3.9	0.317	56	3.0	None	None	NA	None	1
4.3	0.859	80	2.5	None	None	NA	None	35
4.3	0,859	80	2.5	None	None	NA	35	36
4.3	0.859	80	2.5	1	1	0.6	39	40
3.2	0.444	56	3.0	1	1	0.6	None	41
3.2	0.444	56	3.0	50	60	0.9	None	28
3.2	0.444	56	3.0	None	None	NA	None	7
3.2	0.444	56	3.0	110	250	1.2	None	12
3.2	0.444	56	3.0	105	220	1.3	None	10
3.9	0.317	56	3.0	None	None	NA	1	2
3.9	0.317	56	3.0	1	1	0.8	None	30
4.3	0.859	80	2.5	None	None	NA	None	5
4.3	0.859	80	2.5	1	1	0.7	None	22
3.2	0.444	56	3.0	1	1	0.8	None	43
3.9	0.317	56	3.0	1	1	0.9	None	21
4.3	0.859	80	2.5	None	None	NA	None	39

TABL

PRIMARY HIT MISSILE

Line No.	Missile Description	Velocity, (fps)	Location	Ba Thickness, (in.)
DOUBLE LENGTH PIPE				
18	1.69" OD Steel Pipe, 10.4 lb, 0.12" Wall	383	In Target	6.0
19	3.0" OD Steel Pipe, 26.5 lb, 0.12" Wall	160	In Target	6.0
20	3.0" OD Steel Pipe, 26.5 lb, 0.12" Wall	193	In Target	6.0
21	3.0" OD Steel Pipe, 26.5 lb, 0.12" Wall	162	Rebound	6.0
22	3.0" OD Steel Pipe, 26.5 lb, 0.12" Wall	200	In Target	6.0
SINGLE LENGTH STEEL SLUG				
23	3.0" OD Steel Slug, 12.6 lb, Solid	89	Rebound	4.5
24	3.0" OD Steel Slug, 12.6 lb, Solid	101	Rebound	6.0
25	3.0" OD Steel Slug, 12.6 lb, Solid	135	Rebound	6.0
26	3.0" OD Steel Slug, 12.6 lb, Solid	205	Rebound	6.0
27	3.0" OD Steel Slug, 12.6 lb, Solid	183	Rebound	6.0
DOUBLE LENGTH STEEL SLUG				
28	3.0" OD Steel Slug, 23.5 lb, Solid	95	Rebound	6.0
29	3.0" OD Steel Slug, 23.5 lb, Solid	128	Rebound	6.0

E A.3.3-1

BARRIER TEST DATA (CONT'D)

Barrier Characteristics				Rear Face Scabbing Particle Velocity, (fps)	Rear Face Scabbing Particle Distance from Barrier, (ft)	Rear Face Scabbing Particle Cube Dimension, (in.)	Test Nos. of Previous Impact On Same Target	Test No.
f'c ksi)	p = A_s/ bd x 100	Rebar fy, (ksi)	Rebar Spacing, (in.)					
4.3	0.859	80	2.5	30	30	1.2	35, 36, 37	38
3.9	0.317	56	3.0	25	20	1.3	None	47
3.9	0.317	56	3.0	65	95	1.3	None	32
4.3	0.859	80	2.5	None	None	NA	None	26
4.3	0.859	80	2.5	25	20	2.4	None	45
3.2	0.444	56	3.0	1	1	0.6	41	42
3.9	0.317	56	3.0	None	None	NA	14	15
3.9	0.317	56	3.0	None	None	NA	None	19
3.9	0.317	56	3.0	25	20	1.3	None	14
4.3	0.859	80	2.5	1	1	1.2	None	24
3.9	0.317	56	3.0	1	1	1.2	None	17
3.9	0.317	56	3.0	15	10	1.3	17	18

Line No.	Sketch Dimensions: Barrier Thickness (In.) Barrier Rebar (Size, No. and Spacing (In.))	Front Face a: Diam Of Loose Concrete At Surface (In.)	b: Neck Diam (In.)	c: Neck Depth (In.)	d: Depth To Solid Plug (In.)
Wood Pole					
1	4.5 2 at 3	0.0	0	0.0	0
2	6.0 2 at 3	0.0	0.0	0.0	0
Single Length Pipe					
3	6.0 3 at 2.5	8.0	2.0	1.2	1.50
4	6.0 3 at 2.5	6.0	1.8	1.5	1.75
5	6.0 3 at 2.5	9.0	3.0	1.5	1.89
6	4.5 2 at 3	4.5	3.2	0.7	2.00
7	4.5 2 at 3	5.0	4.0	0.5	2.45
8	4.5 2 at 3	6.2	4.0	0.6	1.25
9	4.5 2 at 3	6.2	4.2	1.0	Plug gone
10	4.5 2 at 3	7.0	4.0	1.0	Plug gone
11	6.0 2 at 3	6.7	3.0	1.4	1.50
12	6.0 2 at 3	5.5	3.5	1.0	1.87
13	6.0 3 at 2.5	5.5	3.5	1.2	1.87
14	6.0 3 at 2.5	6.0	3.5	1.5	1.50
15	4.5 2 at 3	6.0	4.0	0.9	0.75

TABLE A.3.3-2

PRIMARY HIT MISSILE BARRIER DAMAGE DIMENSIONS

Rear Face										
		e	f	g	h			θ		
Rebar Broken	Rebar Hit	Diam Of Loose Concrete At Surface (In.)	Diam Of Plug (In.)	Rear Surface Moved (In.)	Rear Rebar Moved (In.)	Rebar Broken	Rebar Hit	Angle Of Plug (Deg)	Total Volume Of Rear Crater To Neck (c) (cu Ft)	Test No.
0	0	20.6	None	0.0	0.0	0	0	60	0.16	3
0	0	0	None	0.0	0.0	0	0	None	None	1
1	2	None	None	0.0	0.0	0	0	No data taken	No data taken	35
0	1	None	None	0.0	0.0	0	0	No data taken	No data taken	36
0	4	18.0	None	0.0	0.0	0	0	None	None	40
0	3	24.9	12	0.8	0.8	0	0	50	0.32	41
1	2	29.7	14	0.8	0.8	0	0	50	0.21	28
0	1	22.0	13	0.0	0.0	0	0	60	0.43	7
2	2	23.5	Gone	Gone	2.5	1	2	55	0.32	12
2	2	29.9	Gone	Gone	3.3	1	3	60	0.33	10
0	1	16.7	None	0.0	0.0	0	0	None	None	2
0	2	29.3	14	0.5	0.5	0	0	55	0.47	30
0	3	24.7	None	0.0	0.0	0	0	55	0.51	5
0	2	None	None	0.0	0.0	0	0	None	None	22
0	3	23.0	17	0.2	0.2	0	0	50	0.20	43

Line No.	Sketch Dimensions: Barrier Thickness (In.) Barrier Rebar (Size, No. and Spacing (In.))	Front Face a: Diam Of Loose Concrete At Surface (In.)	b: Neck Diam (In.)	c: Neck Depth (In.)	d: Depth To Solid Plug (In.)
16	6.0 2 at 3	6.0	3.5	1.5	1.12
17	6.0 3 at 2.5	6.5	4.0	1.0	1.25
Double Length Pipe					
18	6.0 3 at 2.5	7.0	2.0	2.0	Not availa
19	6.0 2 at 3	5.0	3.5	1.5	2.50
20	6.0 2 at 3	7.0	3.5	1.1	3.0
21	6.0 3 at 2.5	5.0	3.0	2.0	2.00
22	6.0 3 at 2.5	5.1	3.3	1.0	2.25
Single Length Steel Slug					
23	4.5 2 at 3	4.0	1.2	1.0	0.19
24	6.0 2 at 3	6.5	2.5	1.2	0.15
25	6.0 2 at 3	-	3.5	0.7	0.13
26	6.0 2 at 3	7.0	3.5	0.9	0.43
27	6.0 3 at 2.5	3.0	3.0	0.2	0.37
Double Length Steel Slug					
28	6.0 2 at 3	3.0	3.0	0.2	0.19
29	6.0 2 at 3	6.7	3.0	0.4	0.37

TABLE A.3.3-2

RIMARY HIT MISSILE BARRIER DIMENSIONS (CONT'D)

		Rear Face								
		e	f	g	h			θ		
Rebar Broken	Rebar Hit	Diam Of Loose Concrete At Surface (In.)	Diam Of Plug (In.)	Rear Surface Moved (In.)	Rear Rebar Moved (In.)	Rebar Broken	Rebar Hit	Angle Of Plug (Deg)	Total Volume Of Rear Crater To Neck (c) (Cu Ft)	Test No.
0	3	28.5	17	0.2	0.2	0	0	60	0.58	21
0	3	22.5	17	0.0	0.0	0	0	None	None	39
0	2	24.0	12	0.5	0.5	0	0	50	0.33	38
2	2	28.0	12	0.6	0.6	0	0	50	0.44	47
2	3	28.9	17	2.2	2.2	0	0	55	0.50	32
0	2	30.2	17	0.0	0.0	0	0	60	0.53	26
0	3	22.5	15	0.7	0.7	0	0	45	No data taken	45
0	1	19.2	10	0.2	0.2	0	0	55	0.15	42
0	1	None	None	0.0	0.0	0	0	None	None	15
0	1	27.1	None	0.1	0.1	0	0	60	0.39	19
0	2	21.4	8	0.5	0.5	0	2	55	0.21	14
0	0	25.3	16	0.3	0.3	0	0	No data taken	No data taken	24
0	0	20.0	12	0.0	0.0	0	0	None	None	17
0	0	23.4	12	0.3	0.3	0	0	50	0.27	18

TA

MULTIPLE HIT M

Line No.	Missile Description	Velocity, (fps)	Location	Barr: Thickness, (in.)	f (k
WOOD POLE					
1	3.375" OD Wood Pole, 23.42 lb, Solid	426	In Target	4.5	3.
2	3.375" OD Wood Pole, 23.42 lb, Solid	378	In Target	6.0	3.
SINGLE LENGTH PIPE					
3	1.69" OD Steel Pipe, 4.6 lb, 0.12" Wall	215	Rebound	6.0	3.
4	1.69" OD Steel Pipe, 4.6 lb, 0.12" Wall	517	Rebound	6.0	4.
5	3" OD Steel Pipe, 12.3 lb, 0.12" Wall	216	Rebound	4.5	3.
6	3" OD Steel Pipe, 12.3 lb, 0.12" Wall	296	Perforated	4.5	3.
7	3" OD Steel Pipe, 12.3 lb, 0.12" Wall	329	Perforated	4.5	3.
8	3" OD Steel Pipe, 12.3 lb, 0.12" Wall	399	In Target	4.5	3.
9	3" OD Steel Pipe, 12.3 lb, 0.12" Wall	403	Rebound	4.5	3.
10	3" OD Steel Pipe, 12.3 lb, 0.12" Wall	403	In Target	4.5	3.
11	3" OD Steel Pipe, 12.3 lb, 0.12" Wall	343	Rebound	6.0	4.
12	3" OD Steel Pipe, 12.3 lb, 0.12" Wall	369	Rebound	6.0	4.
13	3.5" OD Steel Pipe, 11.25 lb, 0.216" Wall	208	Rebound	6.0	3.
14	3.5" OD Steel Pipe, 11.25 lb, 0.216" Wall	413	Rebound	6.0	4.
DOUBLE LENGTH PIPE					
15	1.69" OD Steel Pipe, 10.4 lb, 0.12" Wall	373	In Target	6.0	3.
16	3" OD Steel Pipe, 26.5 lb, 0.12" Wall	329	Perforated	6.0	3.
17	3" OD Steel Pipe, 26.5 lb, 0.12" Wall	340	Perforated	6.0	4
SINGLE LENGTH STEEL SLUG					
18	3" OD Steel Slug, 12.6 lb, Solid	207	In Target	6.0	3
COMPOSITE STEEL PLATE AND PIPE					
19	10" OD Steel Plate with Pipe - See Table A.3.4-1, 109 lb, Solid	200	In Target	6.0	4.

BLE A.3.5-1

ISSILE BARRIER TEST DATA

ier Characteristics				Rear Face Scabbing Particle Velocity, (fps)	Rear Face Scabbing Particle Distance from Barrier, (ft)	Rear Face Scabbing Particle Cube Dimension, (in.)	Test Nos. of Previous Impact On Same Target	Test No.
c si)	p = A_s/ bd x 100	Rebar fy, (ksi)	Rebar Spacing, (in.)					
2	.444	56	3.0	55	70	1.7	43	44
9	.317	56	3.0	30	30	2.6	32	33
9	.317	56	3.0	None	None	NA	33, 32	34
3	.859	80	2.5		Missile Tumbled on Impact		35, 36	37
2	.444	56	3.0	30	30	2.1	3	4
2	.444	56	3.0	100	200	2.3	28	29
2	.444	56	3.0	100	200	1.7	12	13
2	.444	56	3.0	105	220	1.3	10	11
2	.444	56	3.0	None	Hit Edge of Target	NA	7	8
2	.444	56	3.0	105	220	1.0	8, 7	9
3	.859	80	2.5	50	60	2.1	5	6
3	.859	80	2.5	65	100	0.8	22	23
9	.317	56	3.0	25	20	1.3	19	20
3	.859	80	2.5	80	145	1.6	24	25
9	.317	56	3.0	70	110	2.0	47	48
9	.317	56	3.0	110	240	2.4	30	31
3	.859	80	2.5	105	230	1.9	26	27
9	.317	56	3.0		Hit Edge of Target		15, 14	16
3	.859	80	2.5	115	260	1.5	45	46

Secondary Particles Stopped by 3/4" Plywood Behind Barrier

Line No.	Sketch Dimensions: Barrier Thickness (In.) Barrier Rebar (Size, No. and Spacing (In.))	Front Face: a Diam Of Loose Concrete At Surface (In.)	b Neck Diam (In.)	c Neck Depth (In.)	d Depth To Solid Plug (In.)
Wood Pole					
1	4.5 2 at 3	4.0	4.0	0.0	N/A
2	6.0 2 at 3	3.4	3.4	0.6	N/A
Single Length Pipe					
3	6.0 2 at 3	3.7	1.8	1.2	1.25
4	6.0 3 at 2.5	6.0	2.0	0.8	1.62
5	4.5 2 at 3	7.5	3.7	1.0	2.75
6	4.5 2 at 3	6.0	4.0	0.7	Plug gone
7	4.5 2 at 3	7.2	4.0	1.0	Plug gone
8	4.5 2 at 3	12.0	5.0	1.0	Plug gone
9	4.5 2 at 3	7.0	4.7	1.1	Hit edge of target
10	4.5 2 at 3	7.0	4.1	0.9	Plug gone
11	6.0 3 at 2.5	5.6	4.0	0.7	2.00
12	6.0 3 at 2.5	11.5	4.5	1.5	Not available
13	6.0 2 at 3	6.2	0.2	0.7	1.00
14	6.0 3 at 2.5	8.5	4.0	1.5	2.75

TABLE A.3.5-2

TIPLE HIT MISSILE BARRIER DAMAGE DIMENSIONS

Rear Face										
		e	f	g	h			θ		
Rebar Broken	Rebar Hit	Diam Of Loose Concrete At Surface (In.)	Diam Of Plug (In.)	Rear Surface Moved (In.)	Rear Rebar Moved (In.)	Rebar Broken	Rebar Hit	Angle Of Plug (Deg)	Total Volume Of Rear Crater To Neck (c) (Cu Ft)	Test No.
0	4	28.3	N/A	N/A	N/A	0	0	55	0.19	44
0	2	28.8	N/A	N/A	N/A	0	0	No data taken	No data taken	33
2	2	None	None	0.0	0.0	0	0	No data taken	No data taken	34
0	0	None	None	0.0	0.0	0	0	No data taken	No data taken	37
2	2	20.8	10	1.5	1.5	0	0	55	0.26	4
2	3	28.0	Gone	Gone	3.5	2	3	55	0.28	29
2	2	24.5	Gone	Gone	3.0	1	2	55	0.29	13
2	2	29.5	Gone	Gone	2.8	1	3	55	0.28	11
2	2	Hit edge of target	N/A	N/A	N/A	2	3	None	None	8
0	1	24.0	Gone	Gone	2.5	0	0	65	0.45	9
0	3	24.7	13	0.5	0.5	0	0	55	0.66	6
2	4	25.7	13	Gone	1.4	1	0	50	0.50	23
0	2	24.9	12	0.1	0.1	0	0	45	0.47	20
3	3	22.7	17	Gone	1.7	1	0	55	0.53	25

Line No.	Sketch Dimensions: Barrier Thickness (In.) Barrier Rebar (Size, No. and Spacing (In.))	Front Face: a Diam Of Loose Concrete At Surface (In.)	b Neck Diam (In.)	c Neck Depth (In.)	d Depth To Solid Plug (In.)
Double Length Pipe					
15	6.0 2 at 3	5.0	2.2	1.4	1.25
16	6.0 2 at 3	7.0	4.5	1.5	Plug gone
17	6.0 3 at 2.5	6.0	4.0	1.3	Plug gone
Single Length Steel Slug					
18	6.0 2 at 3	3.0	3.0	0.6	0.62
Composite Steel Plate and Pipe					
19	6.0 3 at 2.5	10.5	10.5	0.5	Plug gone

TABLE A.3.5-2

E HIT MISSILE BARRIER DAMAGE DIMENSIONS (CONT'D)

Rear Face										
		e	f	g	h			θ		
Rebar Broken	Rebar Hit	Diam Of Loose Concrete At Surface (In.)	Diam Of Plug (In.)	Rear Surface Moved (In.)	Rear Rebar Moved (In.)	Rebar Broken	Rebar Hit	Angle Of Plug (Deg)	Total Volume Of Rear Crater To Neck (c) (Cu Ft)	Test No.
0	0	21.4	N/A	N/A	N/A	2	2	50	0.30	48
2	2	26.6	Gone	Gone	3.0	2	2	60	0.45	31
2	2	30.5	Gone	Gone	0.8	3	3	45	0.32	27
0	0	14.4	N/A	N/A	N/A	0	0	None	None	16
8	7	29.7	Gone	Gone	6.0	5	7	No data taken	No data taken	46

TABLE A.8.2-1

COMPARISON DATA FOR IITRI QUARTER-SCALE
AND SANDIA FULL-SCALE 12 INCH PIPE MISSILE-BARRIER TESTS

	Missile Data				Barrier Data					Barrier rear face scabbing particles travel distance (ft)	Test Results	
12 in. Steel Pipe 18 in. Barrier Test No.	Diameter (in.)	2t/D	Weight (lbs)	Velocity (fps)	Thickness (in.)	Rebar percentage	Rebar (ksi)	Concrete fc (ksi)	Edge Beam Type		Diameter of barrier back face crater (in.)	Peak force at barrier edge beam (kips)
IITRI-7	3.0	.080	12.3	211	4.5	.444	56[1]	3.2[1]	6I12.5[4]	0[3]	30.5	25.5
IITRI-28	3.0	.080	12.3	195	4.5	.444	56[1]	3.2[1]	6I12.5[4]	60	30.6	23.8
Sandia-4	12.75	.059	743.0	202	18.0	.438	60[2]	3.6[1]	1"x3"RC[5]	49.5	99.0	400
12 in. Steel Pipe 24 in. Barrier Test No.												
IITRI-2	3.0	.080	12.3	207	6.0	.317	56[1]	3.9[1]	6I12.5[4]	0	None	27.9
IITRI-30	3.0	.080	12.3	245	6.0	.317	56[1]	3.9[1]	6I12.5[4]	0	None	25.1
Sandia-8	12.75	.059	743.0	202	24.0	.313	60[2]	3.6[1]	1"x3"RC[5]	0	None	Not Available

NOTES:

1. measured material strength, concrete strength on day of test
2. specified material strength
3. IITRI Test 7 had identical rear face damage pattern to IITRI Test 28 and Sandia Test 4. The loose concrete at the perimeter of the shear plug in IITRI Test 7 is ready to come off and, if it did, would travel as fast as the particles in IITRI Test 28 and Sandia Test 8.
4. I = structural steel shape
5. RC = reinforced concrete

TABLE

PRIMARY HIT

Line No.	Missile Description	Test No.	Missile Characteristics: Weight, (lb)	Length, (ft)	Velocity, (fps)	Pipe Wall Thickness, (in.)	Thickn (in.
WOOD POLE							
1	13.5" OD Wood Pole	3	1,499	35	258	Solid	18
2	13.5" OD Wood Pole	1	1,499	35	265	Solid	24
SINGLE LENGTH PIPE							
3	6.75" OD Steel Pipe	35	294	15	313	0.48	24
4	6.75" OD Steel Pipe	36	294	15	394	0.48	24
5	6.75" OD Steel Pipe	40	294	15	470	0.48	24
6	12.00" OD Steel Pipe	41	787	15	159	0.48	18
7	12.00" OD Steel Pipe	28	787	15	195	0.48	18
8	12.00" OD Steel Pipe	7	787	15	211	0.48	18
9	12.00" OD Steel Pipe	12	787	15	317	0.48	18
10	12.00" OD Steel Pipe	10	787	15	403	0.48	18
11	12.00" OD Steel Pipe	2	787	15	207	0.48	24
12	12.00" OD Steel Pipe	30	787	15	245	0.48	24
13	12.00" OD Steel Pipe	5	787	15	211	0.48	24
14	12.00" OD Steel Pipe	22	787	15	244	0.48	24
15	14.00" OD Steel Pipe	43	752	15	131	0.86	18
16	14.00" OD Steel Pipe	21	720	15	206	0.86	24
17	14.00" OD Steel Pipe	39	720	15	203	0.86	24

*Obtained from one-quarter scale t
material properties constant, per
**Test number of previous missile i

FULL SIZE DATA*

Barrier Characteristics								
ess,)	f'c (ksi)	p = A_s/ bd x 100	Rebar fy, (ksi)	Rebar Spacing, (in.)	Missile Location	Rear Face Scabbing Particle Velocity, (fps)	Rear Face Scabbing Particle Cube Dimension, (in.)	Previous** Missile Impacts
	3.2	0.444	56	12	Rebound	None	NA	None
	3.9	0.317	56	12	Rebound	None	NA	None
	4.3	0.859	80	10	Rebound	None	NA	None
	4.3	0.859	80	10	Rebound	None	NA	35
	4.3	0.859	80	10	Rebound	1	2.4	39
	3.2	0.444	56	12	Rebound	1	2.4	None
	3.2	0.444	56	12	Rebound	50	3.6	None
	3.2	0.444	56	12	Rebound	None	NA	None
	3.2	0.444	56	12	Perforated Target	110	4.8	None
	3.2	0.444	56	12	In Target	105	5.2	None
	3.9	0.317	56	12	Rebound	None	NA	1
	3.9	0.317	56	12	Rebound	1	3.2	None
	4.3	0.859	80	10	Rebound	None	NA	None
	4.3	0.859	80	10	Rebound	1	2.8	None
	3.2	0.444	56	12	Rebound	1	3.2	None
	3.9	0.317	56	12	Rebound	1	3.6	None
	4.3	0.859	80	10	Rebound	None	NA	None

est data by multiplying dimensions by four, keeping
centage of rebar constant, and velocity constant.
mpact

PRIMARY HIT

Line No.	Missile Description	Test No.	Missile Characteristics				Thickne (in.)
			Weight, (lb)	Length, (ft)	Velocity, (fps)	Pipe Wall Thickness, (in.)	
DOUBLE LENGTH PIPE							
18	6.75" OD Steel Pipe	38	668	30	383	0.48	24
19	12.00" OD Steel Pipe	47	1,696	30	160	0.48	24
20	12.00" OD Steel Pipe	32	1,696	30	193	0.48	24
21	12.00" OD Steel Pipe	26	1,696	30	162	0.48	24
22	12.00" OD Steel Pipe	45	1,696	30	200	0.48	24
SINGLE LENGTH STEEL SLUG							
23	12.00" OD Steel Slug	42	806	2.1	89	Solid	18
24	12.00" OD Steel Slug	15	806	2.1	101	Solid	24
25	12.00" OD Steel Slug	19	806	2.1	135	Solid	24
26	12.00" OD Steel Slug	14	806	2.1	205	Solid	24
27	12.00" OD Steel Slug	24	806	2.1	183	Solid	24
DOUBLE LENGTH STEEL SLUG							
28	12.00" OD Steel Slug	17	1,504	3.9	95	Solid	24
29	12.00" OD Steel Slug	18	1,504	3.9	128	Solid	24

TABLE A.8.4-1

FULL SIZE DATA* (CONT'D)

Barrier Characteristics								
ss,	f'c (ksi)	p = A_s/ bd x 100	Rebar fy, (ksi)	Rebar Spacing, (in.)	Missile Location	Rear Face Scabbing Particle Velocity, (fps)	Rear Face Scabbing Particle Cube Dimension, (in.)	Previous** Missile Impacts
	4.3	0.859	80	10	In Target	30	4.8	35, 36, 37
	3.9	0.317	56	12	In Target	25	5.2	None
	3.9	0.317	56	12	In Target	65	5.2	None
	4.3	0.859	80	10	Rebound	None	NA	None
	4.3	0.859	80	10	In Target	25	9.6	None
	3.2	0.444	56	12	Rebound	1	2.4	41
	3.9	0.317	56	12	Rebound	None	NA	14
	3.9	0.317	56	12	Rebound	None	NA	None
	3.9	0.317	56	12	Rebound	25	5.2	None
	4.3	0.859	80	10	Rebound	1	4.8	None
	3.9	0.317	56	12	Rebound	1	4.8	None
	3.9	0.317	56	12	Rebound	15	5.2	17

TAB

MULTIPLE H

Line No.	Missile Description	Velocity, (fps)	Location	Thickness, (in.)
WOOD POLE				
1	13.5" OD Wood Pole, 1,499 lb, Solid	426	In Target	18
2	13.5" OD Wood Pole, 1,499 lb, Solid	378	In Target	24
SINGLE LENGTH PIPE				
3	6.75" OD Steel Pipe, 294 lb, 0.48" Wall	215	Rebound	24
4	6.75" OD Steel Pipe, 294 lb, 0.48" Wall	517	Rebound	24
5	12.00" OD Steel Pipe, 787 lb, 0.48" Wall	216	Rebound	18
6	12.00" OD Steel Pipe, 787 lb, 0.48" Wall	296	Perforated	18
7	12.00" OD Steel Pipe, 787 lb, 0.48" Wall	329	Perforated	18
8	12.00" OD Steel Pipe, 787 lb, 0.48" Wall	399	In Target	18
9	12.00" OD Steel Pipe, 787 lb, 0.48" Wall	403	Rebound	18
10	12.00" OD Steel Pipe, 787 lb, 0.48" Wall	403	In Target	18
11	12.00" OD Steel Pipe, 787 lb, 0.48" Wall	343	Rebound	24
12	12.00" OD Steel Pipe, 787 lb, 0.48" Wall	369	Rebound	24
13	14.00" Steel Pipe, 720 lb, 0.86" Wall	208	Rebound	24
14	14.00" Steel Pipe, 720 lb, 0.86" Wall	413	Rebound	24
DOUBLE LENGTH PIPE				
15	6.75" OD Steel Pipe, 668 lb, 0.48" Wall	373	In Target	24
16	12.00" OD Steel Pipe, 1,696 lb, 0.48" Wall	329	Perforated	24
17	12.00" OD Steel Pipe, 1,696 lb, 0.48" Wall	340	Perforated	24
SINGLE LENGTH STEEL SLUG				
18	12.00" OD Steel Slug, 806 lb, Solid	207	Rebound	24
COMPOSITE STEEL PLATE AND PIPE				
19	40" OD Steel Plate with Pipe - See Table A.3.1-1, 6,976 lb, Solid Nose	200	In Target	24

LE A.8.4-2

IT FULL SIZE DATA

Barrier Characteristics				Rear Face Scabbing Particle Velocity, (fps)	Rear Face Scabbing Particle Cube Dimension, (in.)	Test Nos. of Previous Impact On Same Target	Test No.
f'c (ksi)	p = A_s/ bd x 100	Rebar fy, (ksi)	Rebar Spacing, (in.)				
3.2	.444	56	12.0	55	6.8	43	44
3.9	.317	56	12.0	30	10.4	32	33
3.9	.317	56	12.0	None	None	33, 32	34
4.3	.859	80	10.0	Missile Tumbled		35, 36	37
3.2	.444	56	12.0	30	8.4	3	4
3.2	.444	56	12.0	100	9.2	28	29
3.2	.444	56	12.0	100	6.8	12	13
3.2	.444	56	12.0	105	5.2	10	11
3.2	.444	56	12.0	None	Hit Edge of Target	7	8
3.2	.444	56	12.0	105	4.0	8, 7	9
4.3	.859	80	10.0	50	8.4	5	6
4.3	.859	80	10.0	65	3.2	22	23
3.9	.317	56	12.0	25	5.2	19	20
4.3	.859	80	10.0	80	6.4	24	25
3.9	.317	56	12.0	70	8.0	47	48
3.9	.317	56	12.0	110	9.2	30	31
4.3	.859	80	10.0	105	7.6	26	27
3.9	.317	56	12.0	Hit Edge of Target		15, 14	16
4.3	.859	80	10.0	115	6.0	45	46

Secondary Particles - Stopped by Plywood 3/4" Thick Behind Barrier

Also Available On Aperture Card

TABLE A.9.2-1

SCABBING THRESHOLD VELOCITIES DEDUCED FROM TEST DATA

Missile No. Figure No.	Missile Type	Barriers I and III, T = 6 in. Velocity (fps)	Momentum (kip-sec)	Kinetic Energy (kip-in.)	Barrier II, T = 4.5 in. Velocity (fps)	Momentum (kip-sec)	Kinetic Energy (kip-in.)
2 A.3.3-5	1.69 in. Pipe 4.6 lb	>470	0.07	189.3	-	-	-
3 A.3.3-18	1.69 in. Pipe 10.4 lb	<380	0.12	279.8	-	-	-
4 A.3.3-14	3.0 in. Pipe 12.3 lb	240	0.09	132.0	150	0.06	51.6
5 A.3.3-21	3.0 in. Pipe 26.5 lb	165	0.14	134.4	-	-	-
6 A.3.3-16,17	3.5 in. Pipe 11.25 lb	205	0.07	88.1	130	0.05	35.4
7 A.3.3-25	3.0 in. Slug 12.6 lb	135	0.05	42.8	80	0.03	15.0
8 A.3.3-28	3.0 in. Slug 23.5 lb	95	0.07	39.5	-	-	-

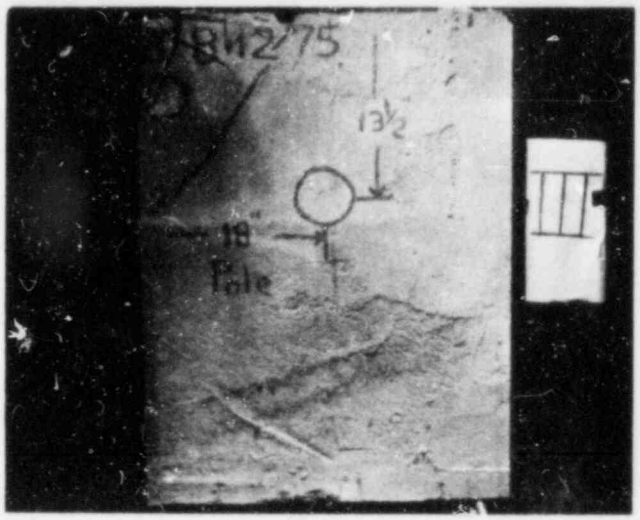

Barrier Front Face

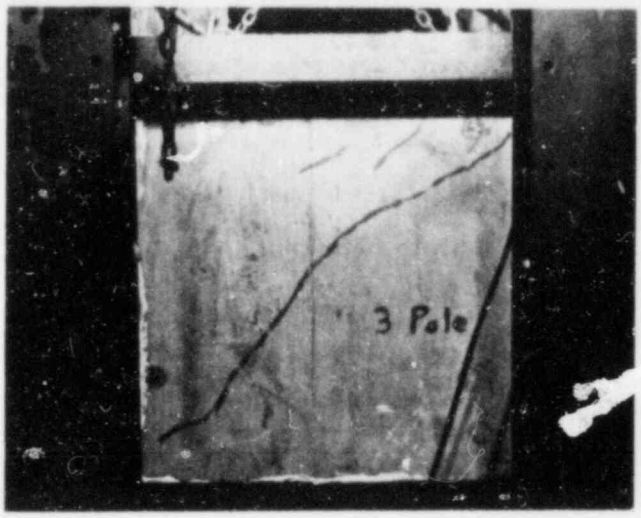

Barrier Rear Face

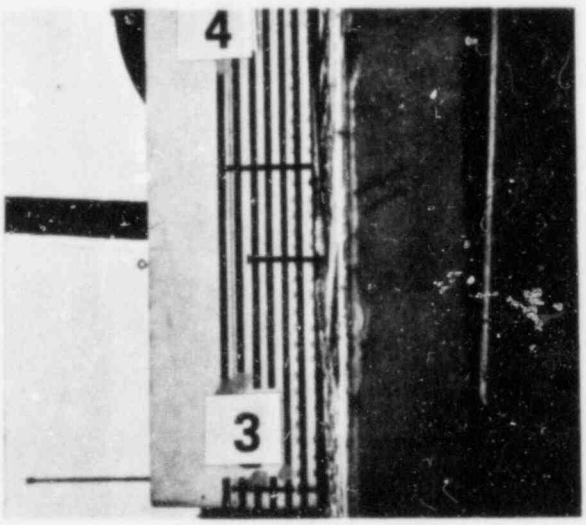

Profile of Rear Rebar or Concrete

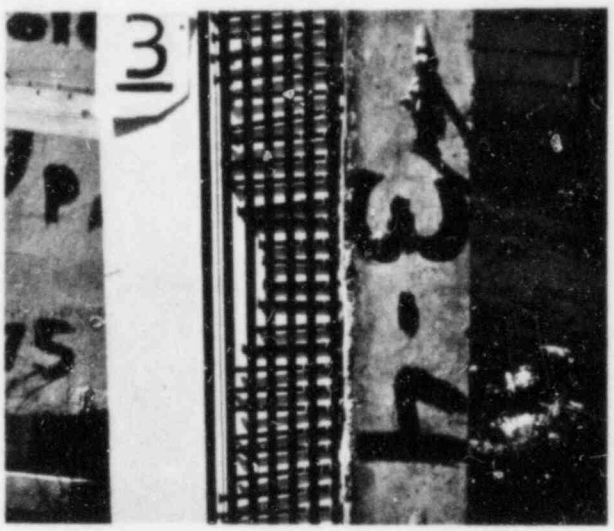

Profile of Back Crater

No Photo Taken

V = 258 fps

3.375" OD Wood Pole
23.42 lb Solid

Missile

Final Missile Location Rebound

Secondary Concrete Missiles

Particle size NA in.
Particle traveled NA ft
Particle velocity NA fps

Barrier

Thickness 4.5 in.
Rebar # 2 at 3.0 in.

Figure A.3.3-1 Primary Hit Test No. 3 Table A.3.3-1 Line 1

Barrier Front Face

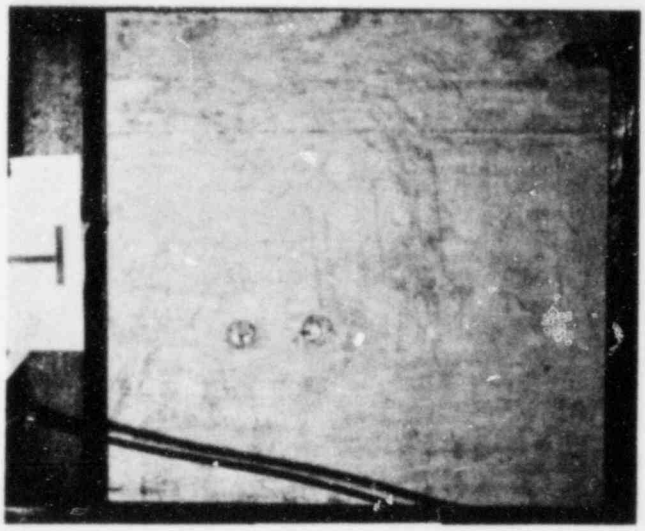

Barrier Rear Face

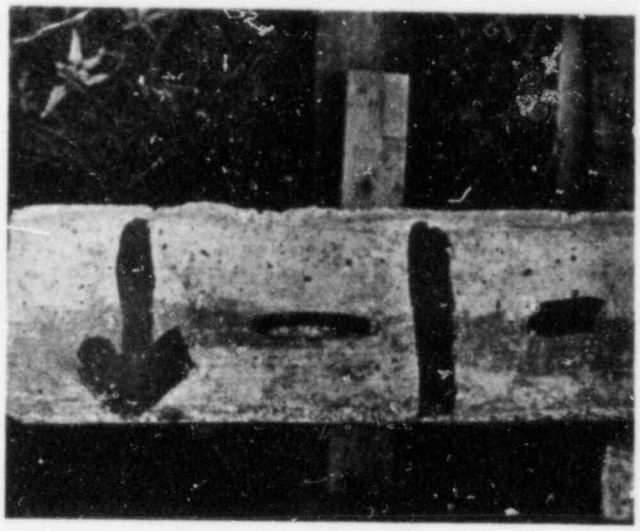

Profile of Rear Rebar or Concrete

No crater formed

Profile of Back Crater

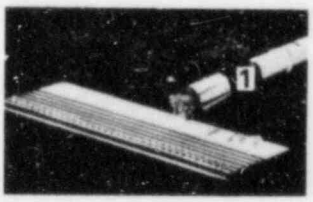

V = 265 fps

3.375" OD Wood Pole
23.42 lb Solid

Missile

Final Missile Location Rebound

Secondary Concrete Missiles

Particle size	NA	in.
Particle traveled	NA	ft
Particle velocity	NA	fps

Barrier

Thickness	6.0	in.
Rebar	# 2 at 3.0	in.

Figure A.3.3-2 Primary Hit Test No. 1 Table A.3.3-1 Line 2

Barrier Front Face

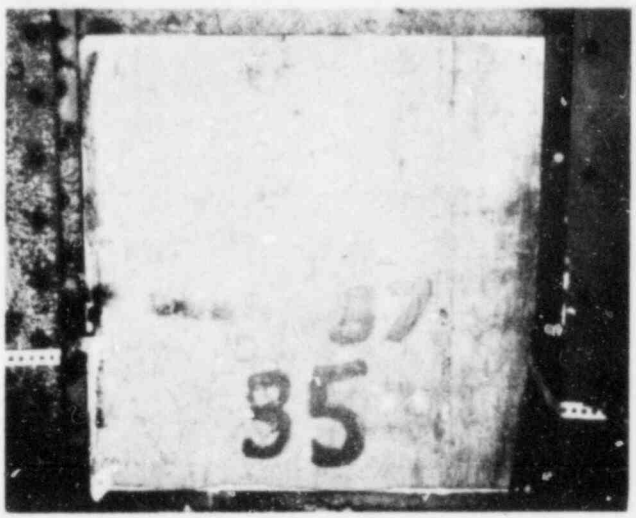

Barrier Rear Face

No crater formed

Profile of Rear Rebar or Concrete

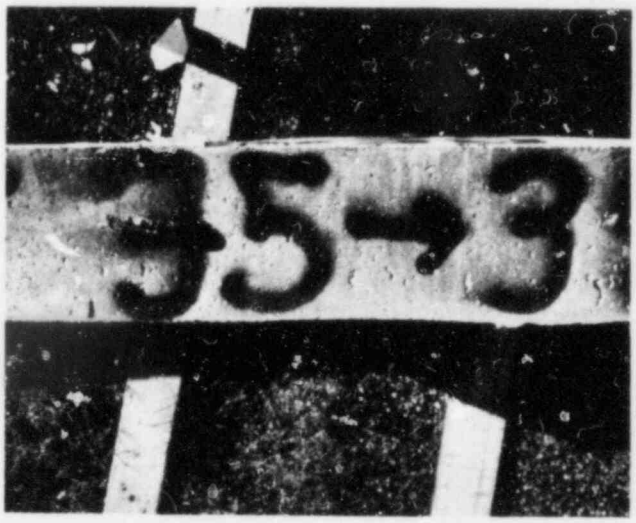

Profile of Back Crater

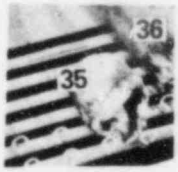

V = 313 fps

1.69" OD Steel Pipe
4.6 lb 0.12" Thick

Missile

Final Missile Location Rebound

Secondary Concrete Missiles

Particle size	NA	in.
Particle traveled	NA	ft
Particle velocity	NA	fps

Barrier

Thickness	6.0	in.
Rebar	# 3 at 2.5	in.

Figure A.3.3-3 Primary Hit Test No. 35 Table A.3.3-1 Line 3

Barrier Front Face

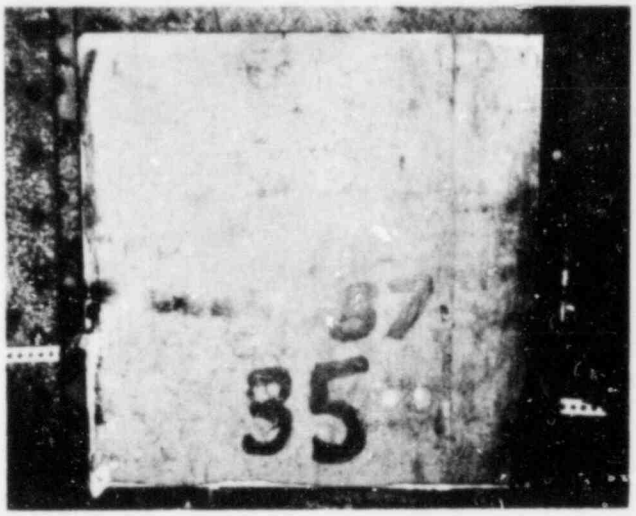

Barrier Rear Face

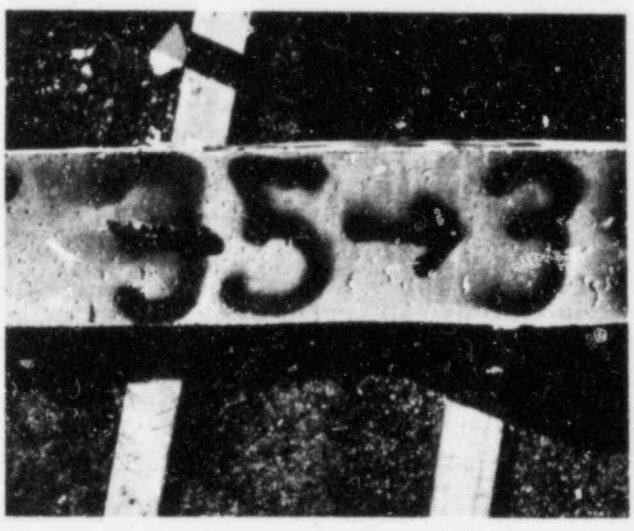

Profile of Rear Rebar or Concrete

No crater formed

Profile of Back Crater

V = 394 fps

1.69" OD Steel Pipe
4.6 lb 0.12" Thick

Missile

Final Missile Location Rebound

Secondary Concrete Missiles

Particle size	NA	in.
Particle traveled	NA	ft
Particle velocity	NA	fps

Barrier

Thickness	6.0	in.
Rebar	# 3 at 2.5	in.

Figure A.3.3-4 Primary Hit Test No. 36 Table A.3.3-1 Line 4

Barrier Front Face

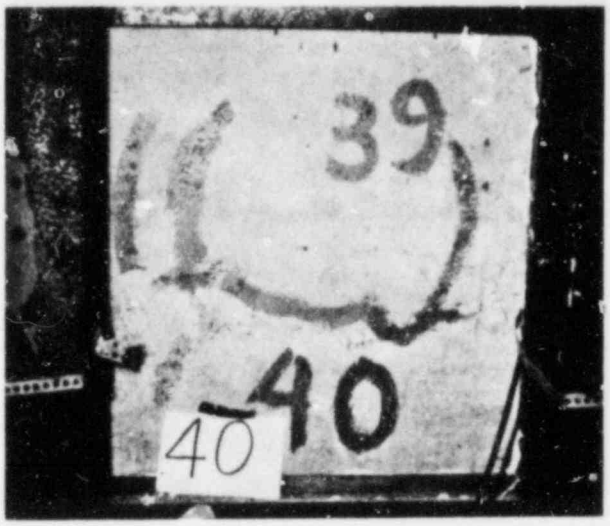

Barrier Rear Face

Profile of Rear Rebar or Concrete

No crater formed

Profile of Back Crater

V = 470 fps

1.69 OD Steel Pipe
4.6 lb 0.12" Thick

Missile

Final Missile Location Rebound

Secondary Concrete Missiles

Particle size	0.6	in.
Particle traveled	1	ft
Particle velocity	1	fps

Barrier

Thickness	6.0	in.
Rebar	# 3 at 2.5	in.

Figure A.3.3-5 Primary Hit Test No. 40 Table A.3.3-1 Line 5

Barrier Front Face

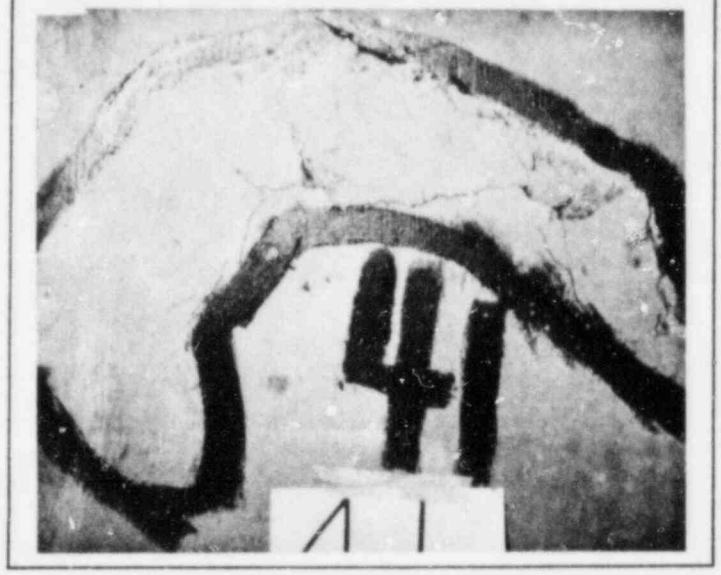

Barrier Rear Face

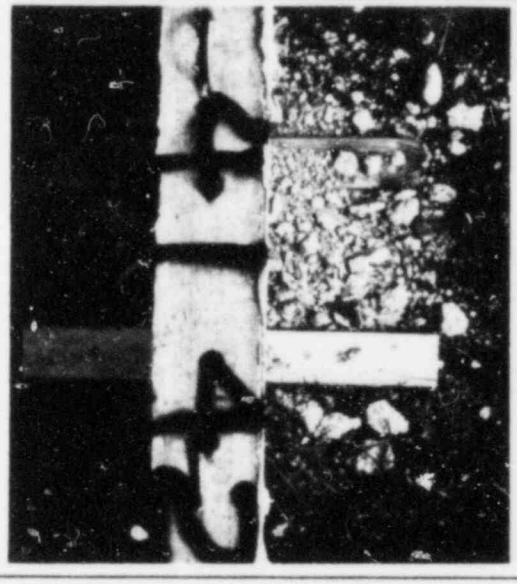

Profile of Rear Rebar or Concrete

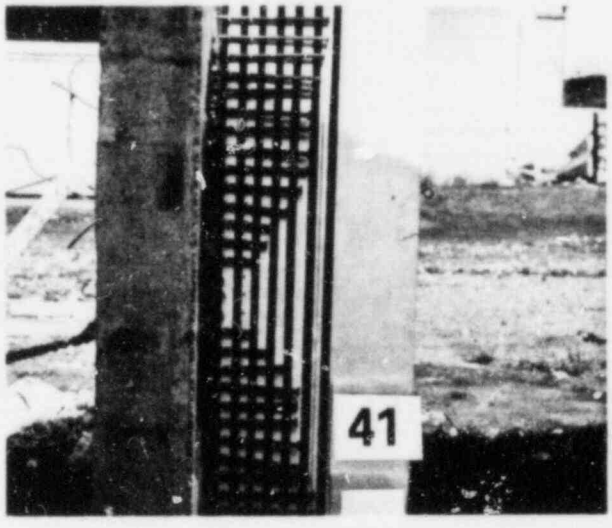

Profile of Back Crater

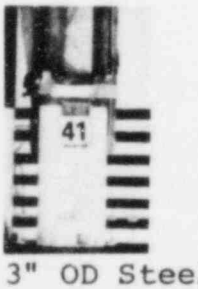

V = 159 fps

3" OD Steel Pipe
12.3 lb 0.12" Thick

Missile

Final Missile Location Rebound

Secondary Concrete Missiles

Particle size	0.6	in.
Particle traveled	1	ft
Particle velocity	1	fps

Barrier

Thickness	4.5	in.
Rebar	# 2 at 3.0	in.

Figure A.3.3-6 Primary Hit Test No. 41 Table A.3.3-1 Line 6

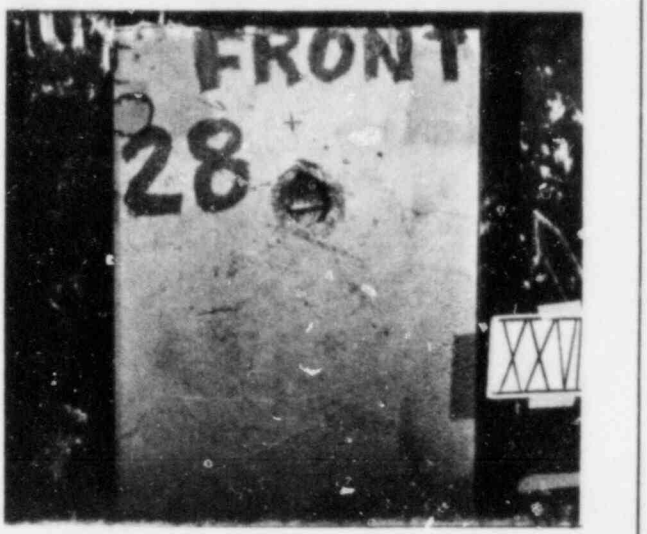

Barrier Front Face

Barrier Rear Face

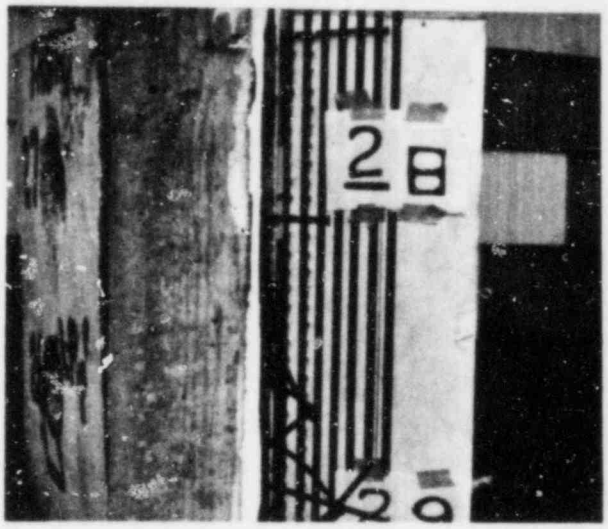

Profile of Rear Rebar or Concrete

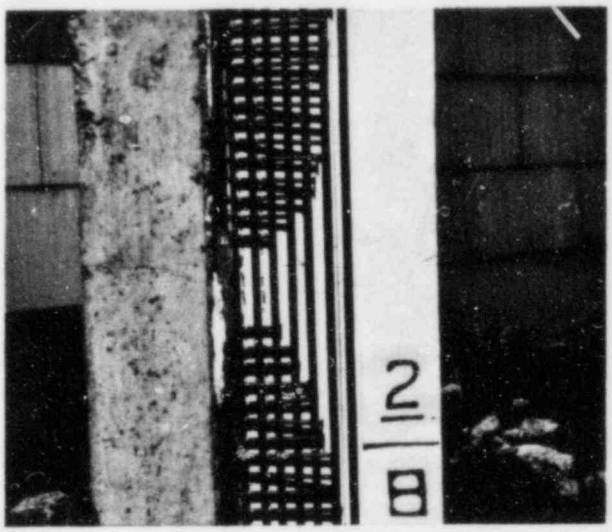

Profile of Back Crater

V = 195 fps

3" OD Steel Pipe
12.3 lb 0.12" Thick

Missile

Final Missile Location Rebound

Secondary Concrete Missiles

Particle size	0.9	in.
Particle traveled	60	ft
Particle velocity	50	fps

Barrier

Thickness	4.5	in.
Rebar	# 2 at 3.0	in.

Figure A.3.3-7 Primary Hit Test No. 28 Table A.3.3-1 Line 7

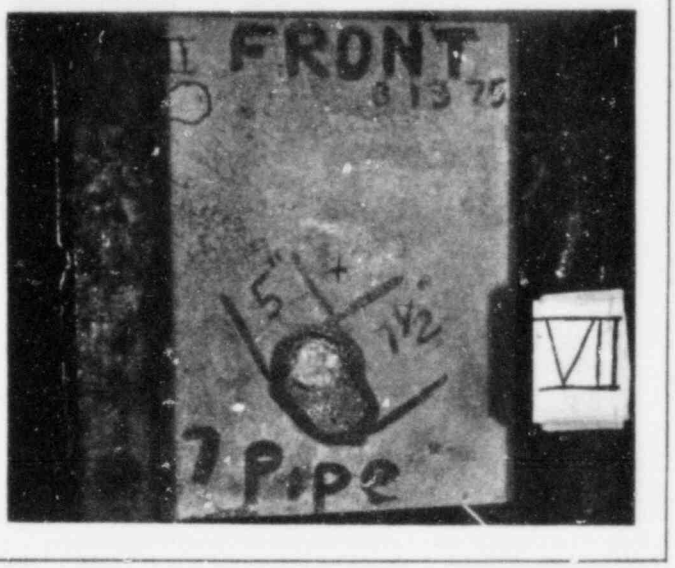

Barrier Front Face

Barrier Rear Face

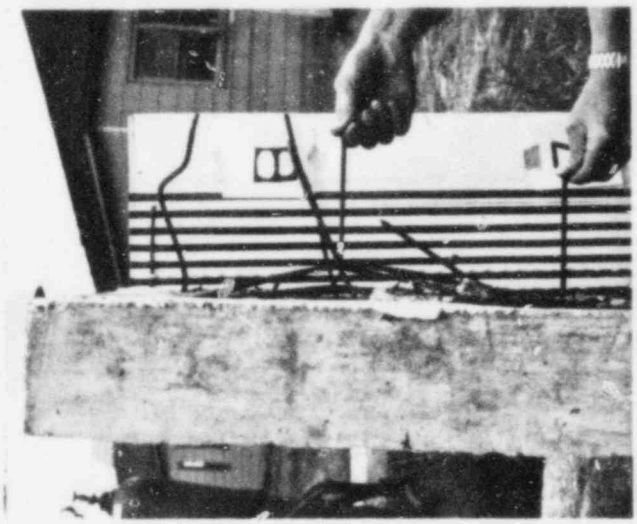

Profile of Rear Rebar or Concrete

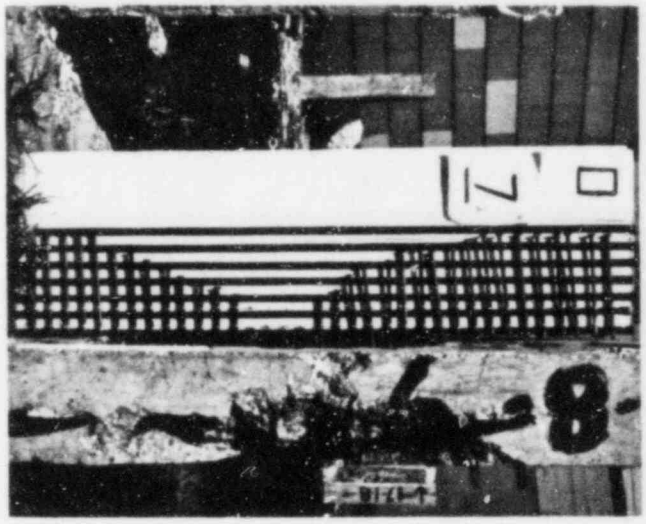

Profile of Back Crater

V = 211 fps

3" OD Steel Pipe
12.3 lb 0.12" Thick

Missile

Final Missile Location Rebound

Secondary Concrete Missiles

Particle size	NA	in.
Particle traveled	NA	ft
Particle velocity	NA	fps

Barrier

Thickness	4.5	in.
Rebar	# 2 at 3.0	in.

Figure A.3.3-8 Primary Hit Test No. 7 Table A.3.3-1 Line 8

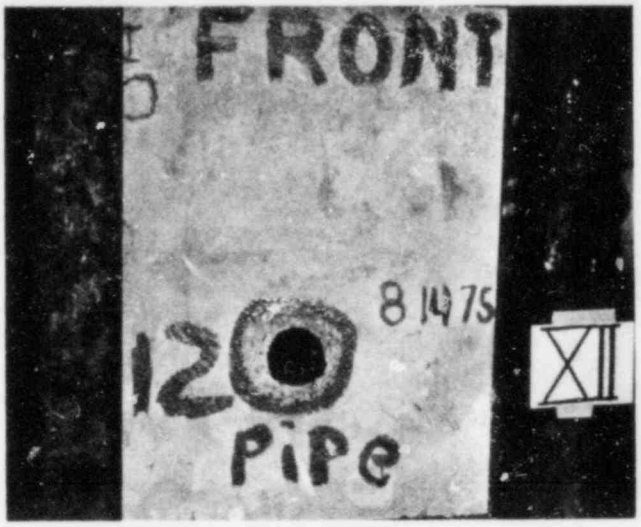

Barrier Front Face

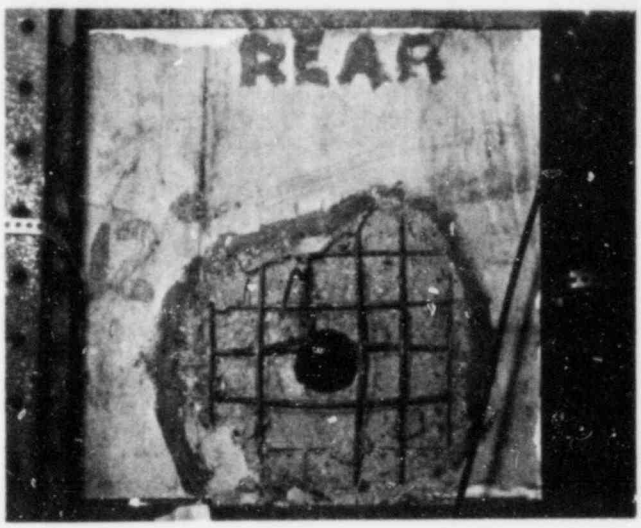

Barrier Rear Face

Profile of Rear Rebar or Concrete

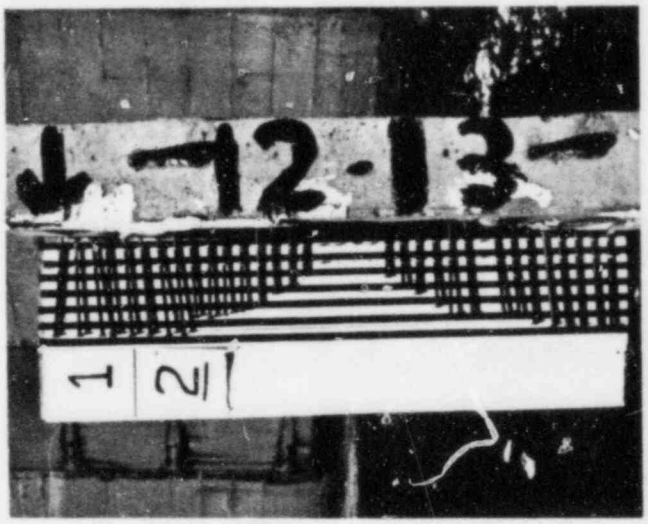

Profile of Back Crater

V = 317 fps

3" OD Steel Pipe
12.3 lb 0.12" Thick

Missile

Final Missile Location Perforated

Secondary Concrete Missiles

Particle size	1.2	in.
Particle traveled	250	ft
Particle velocity	110	fps

Barrier

Thickness	4.5		in.
Rebar	# 2	at 3.0	in.

Figure A.3.3-9 Primary Hit Test No. 12 Table A.3.3-1 Line 9

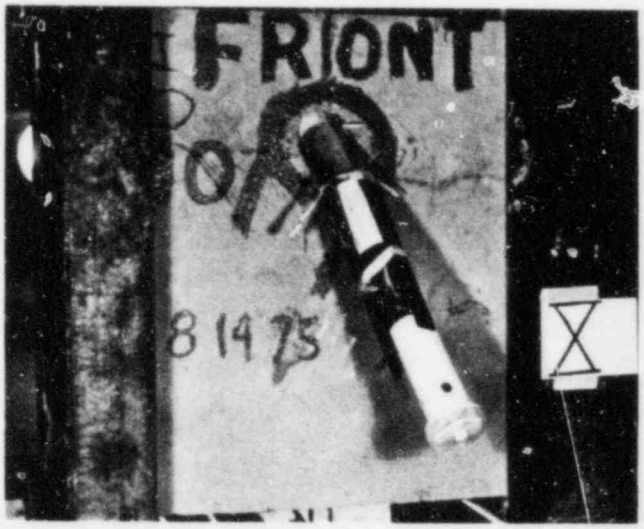

Barrier Front Face

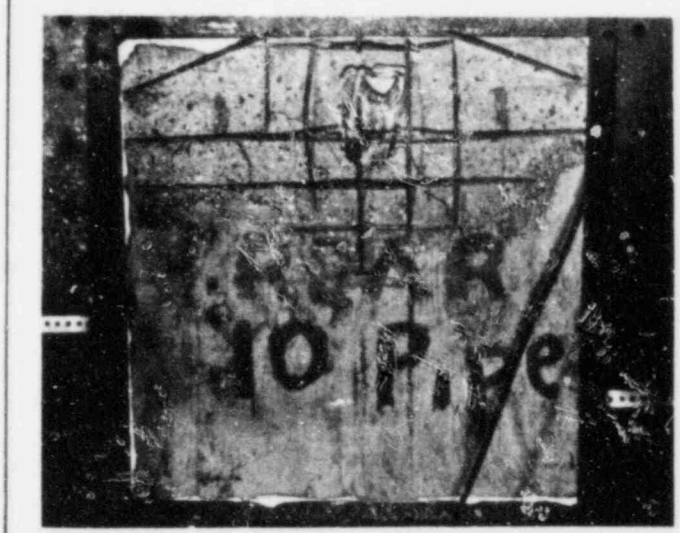

Barrier Rear Face

Profile of Rear Rebar or Concrete

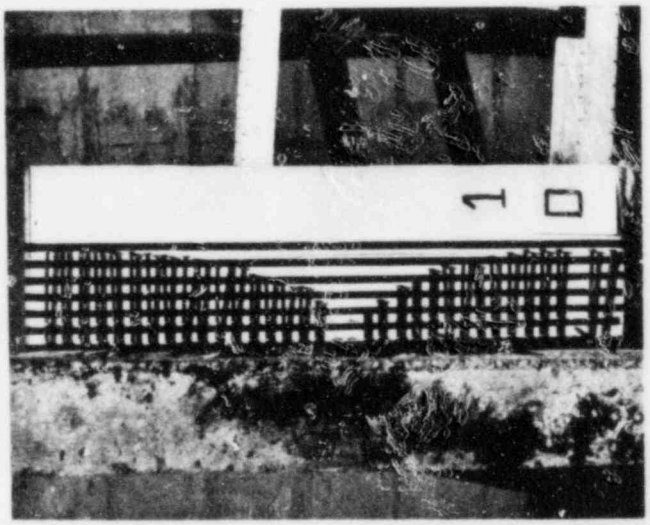

Profile of Back Crater

V = 403 fps

3" OD Steel Pipe
12.3 lb 0.12" Thick

Missile

Final Missile Location In Target

Secondary Concrete Missiles

Particle size	1.3	in.
Particle traveled	220	ft
Particle velocity	105	fps

Barrier

Thickness	4.5	in.
Rebar	# 2 at 3.0	in.

Figure A.3.3-10 Primary Hit Test No. 10 Table A.3.3-1 Line 10

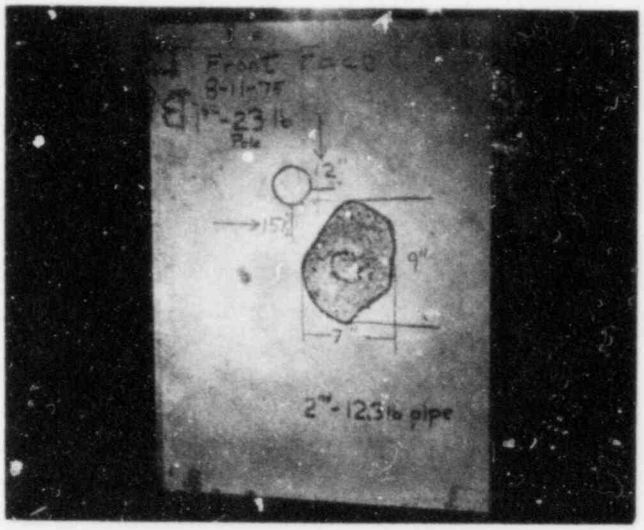

Barrier Front Face

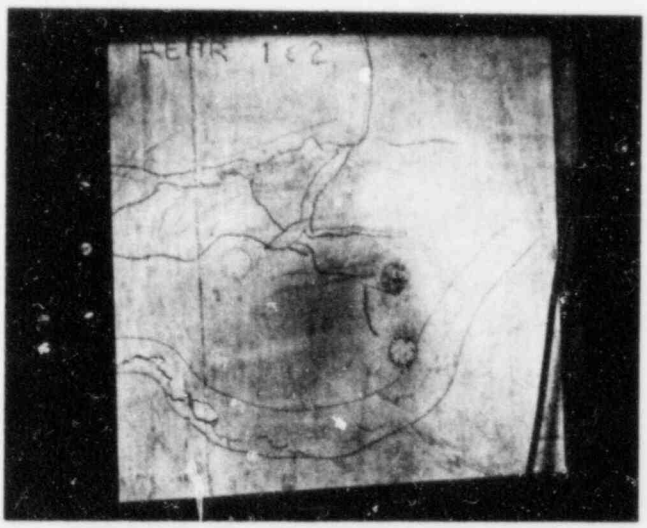

Barrier Rear Face

Profile of Rear Rebar or Concrete

No crater formed

Profile of Back Crater

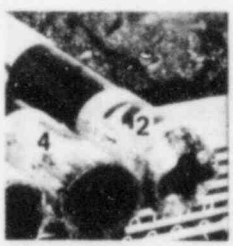

V = 207 fps

3" OD Steel Pipe
12.3 lb 0.12" Thick

Missile

Final Missile Location Rebound

Secondary Concrete Missiles

Particle size	NA	in.
Particle traveled	NA	ft
Particle velocity	NA	fps

Barrier

Thickness	6.0	in.
Rebar	# 2 at 3.0	in.

Figure A.3.3-11 Primary Hit Test No. 2 Table A.3.3-1 Line 11

Barrier Front Face

Barrier Rear Face

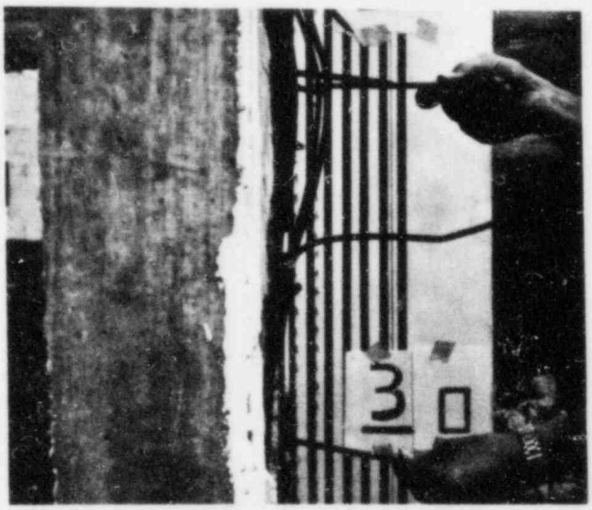

Profile of Rear Rebar
or Concrete

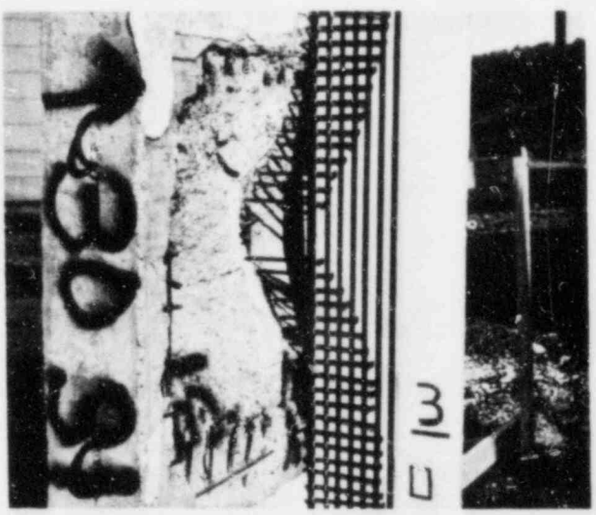

Profile of Back Crater

V = 245 fps

3" OD Steel Pipe
12.3 lb 0.12" Thick

Missile

Final Missile Location Rebound

Secondary Concrete Missiles

Particle size	0.8	in.
Particle traveled	1	ft
Particle velocity	1	fps

Barrier

Thickness	6.0	in.
Rebar	# 2 at 3.0	in.

Figure A.3.3-12 Primary Hit Test No. 30 Table A.3.3-1 Line 12

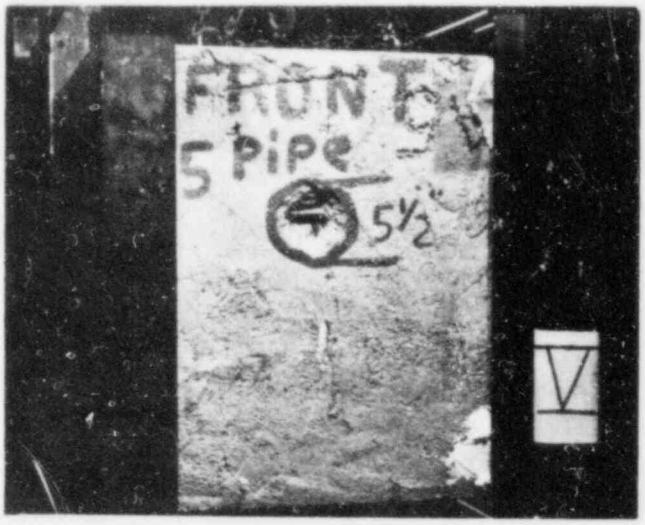

Barrier Front Face

Barrier Rear Face

Profile of Rear Rebar or Concrete

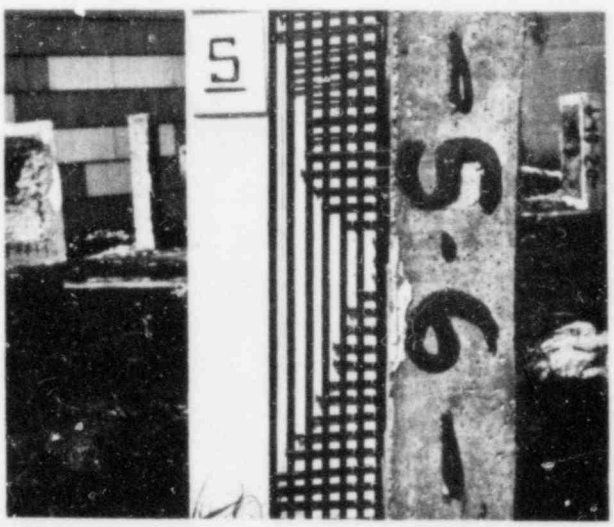

Profile of Back Crater

V = 211 fps

3" OD Steel Pipe
12.3 lb 0.12" Thick

Missile

Final Missile Location Rebound

Secondary Concrete Missiles

Particle size	NA	in.
Particle traveled	NA	ft
Particle velocity	NA	fps

Barrier

Thickness	6.0	in.
Rebar	# 3 at 2.5	in.

Figure A.3.3-13 Primary Hit Test No. 5 Table A.3.3-1 Line 13

Barrier Front Face

Barrier Rear Face

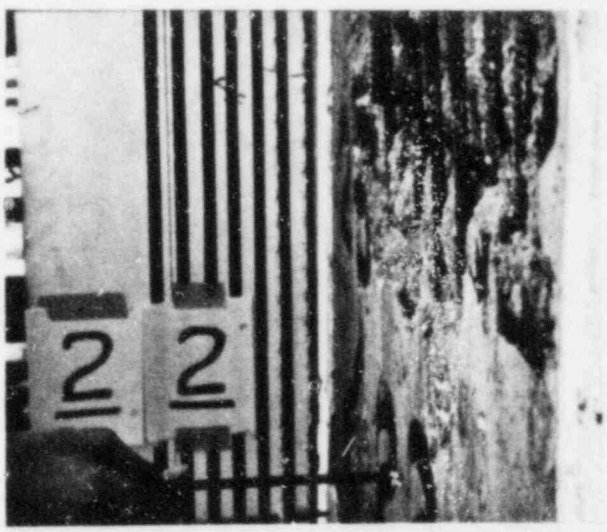

Profile of Rear Rebar or Concrete

No crater formed

Profile of Back Crater

V = 244 fps

3" OD Steel Pipe
12.3 lb 0.12" Thick

Missile

Final Missile Location Rebound

Secondary Concrete Missiles

Particle size	0.7	in.
Particle traveled	1	ft
Particle velocity	1	fps

Barrier

Thickness	6.0	in.
Rebar	# 3 at 2.5	in.

Figure A.3.3-14 Primary Hit Test No. 22 Table A.3.3-1 Line 14

Barrier Front Face

Barrier Rear Face

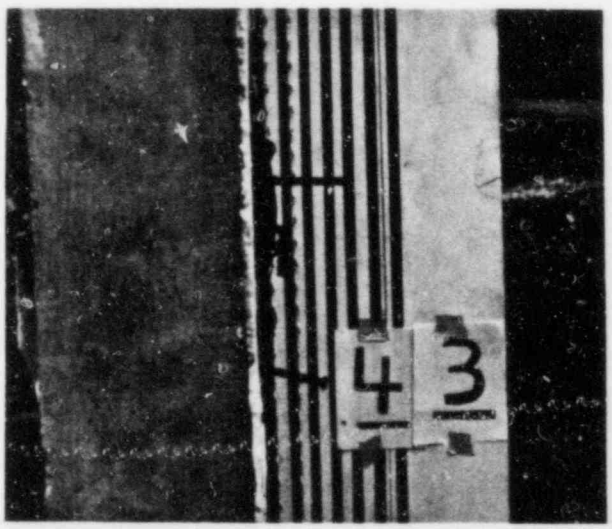

Profile of Rear Rebar or Concrete

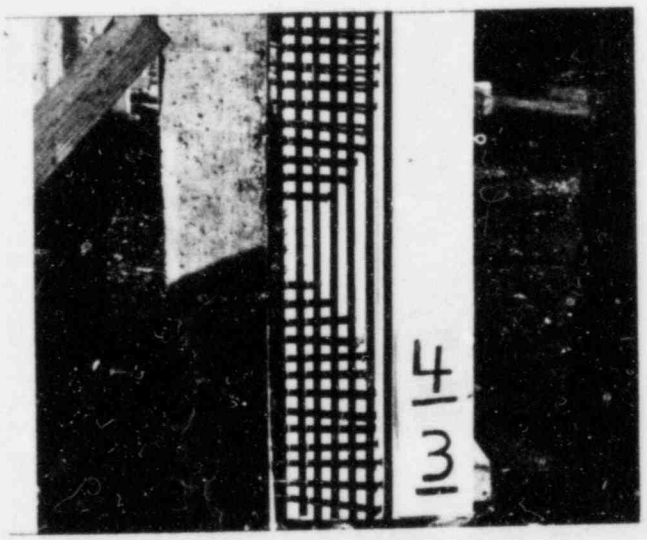

Profile of Back Crater

V = 131 fps

3.5" OD Steel Pipe
11.25 lb 0.216 " Thick

Missile

Final Missile Location Rebound

Secondary Concrete Missiles

Particle size	0.8	in.
Particle traveled	1	ft
Particle velocity	1	fps

Barrier

Thickness	4.5	in.
Rebar	# 2 at 3.0	in.

Figure A.3.3-15 Primary Hit Test No. 43 Table A.3.3-1 Line 15

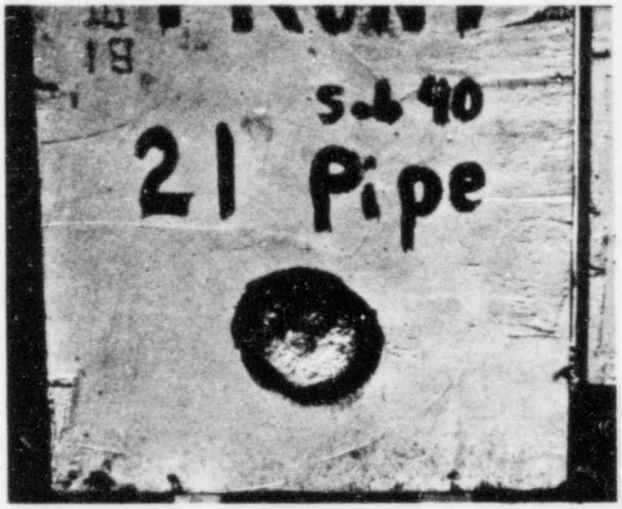

Barrier Front Face

Barrier Rear Face

Profile of Rear Rebar or Concrete

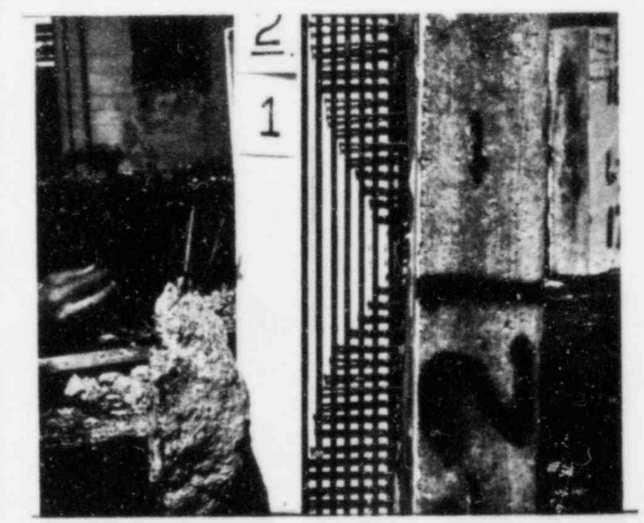

Profile of Back Crater

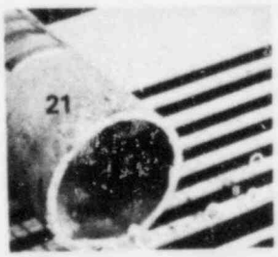

V = 206 fps

3.5" OD Steel Pipe
11.25 lb 0.216" Thick

Missile

Final Missile Location Rebound

Secondary Concrete Missiles

Particle size	0.9	in.
Particle traveled	1	ft
Particle velocity	1	fps

Barrier

Thickness	6.0	in.
Rebar	# 2 at 3.0	in.

Figure A.3.3-16 Primary Hit Test No. 21 Table A.3.3-1 Line 16

Barrier Front Face

Barrier Rear Face

Profile of Rear Rebar or Concrete

No crater formed

Profile of Back Crater

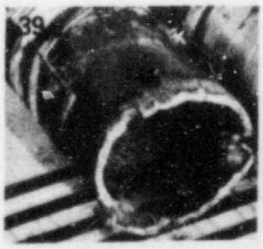

V = 203 fps

3.5" OD Steel Pipe
11.25 lb 0.216" Thick

Missile

Final Missile Location Rebound

Secondary Concrete Missiles

Particle size	NA	in.
Particle traveled	NA	ft
Particle velocity	NA	fps

Barrier

Thickness	6.0	in.
Rebar	# 3 at 2.5	in.

Figure A.3.3-17 Primary Hit Test No. 39 Table A.3.3-1 Line 17

Barrier Front Face

Barrier Rear Face

Profile of Rear Rebar or Concrete

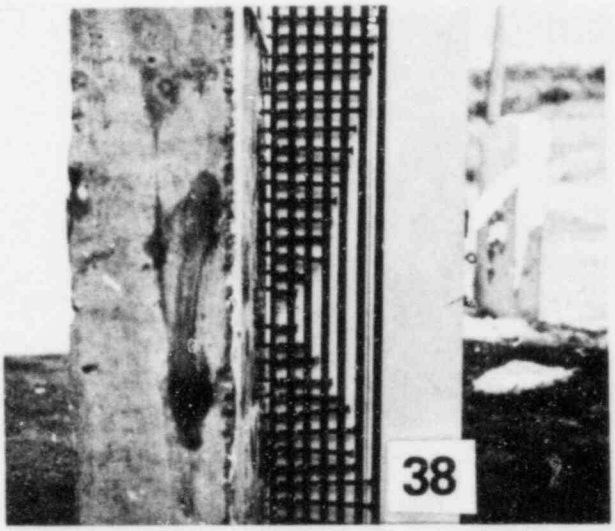

Profile of Back Crater

V = 383 fps

1.69" OD Steel Pipe
10.4 lb 0.12" Thick

Missile

Final Missile Location In Target

Secondary Concrete Missiles

Particle size	1.2	in.
Particle traveled	30	ft
Particle velocity	30	fps

Barrier

Thickness	6.0	in.
Rebar	# 3 at 2.5	in.

Figure A.3.3-18 Primary Hit Test No. 38 Table A.3.3-1 Line 18

Barrier Front Face

Barrier Rear Face

Profile of Rear Rebar or Concrete

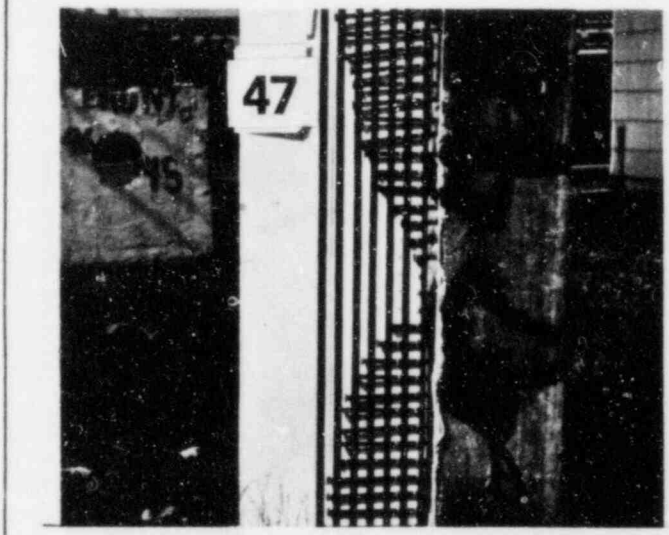

Profile of Back Crater

V = 160 fps

3" OD Steel Pipe
26.5 lb 0.12" Thick

Missile

Final Missile Location In Target

Secondary Concrete Missiles

Particle size	1.3	in.
Particle traveled	20	ft
Particle velocity	25	fps

Barrier

Thickness	6.0	in.
Rebar	# 2 at 3.0	in.

Figure A.3.3-19 Primary Hit Test No. 47 Table A.3.3-1 Line 19

Barrier Front Face

Barrier Rear Face

Profile of Rear Rebar or Concrete

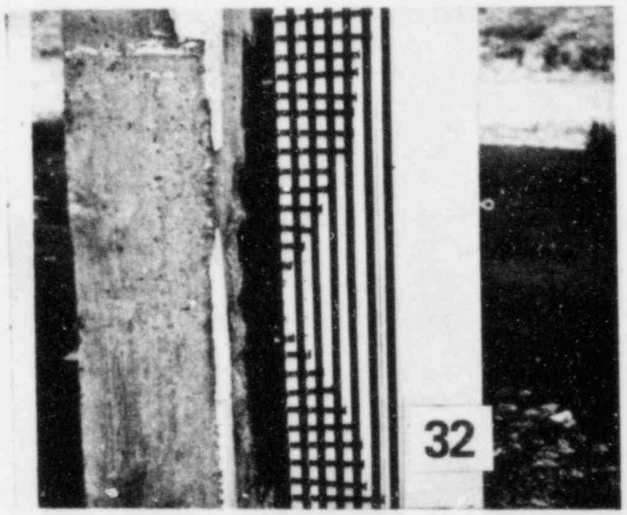

Profile of Back Crater

V = 193 fps

3" OD Steel Pipe
26.5 lb 0.12" Thick

Missile

Final Missile Location In Target

Secondary Concrete Missiles

Particle size	1.3	in.
Particle traveled	95	ft
Particle velocity	65	fps

Barrier

Thickness	6.0	in.
Rebar	# 2 at 3.0	in.

Figure A.3.3-20 Primary Hit Test No. 32 Table A.3.3-1 Line 20

Barrier Front Face

Barrier Rear Face

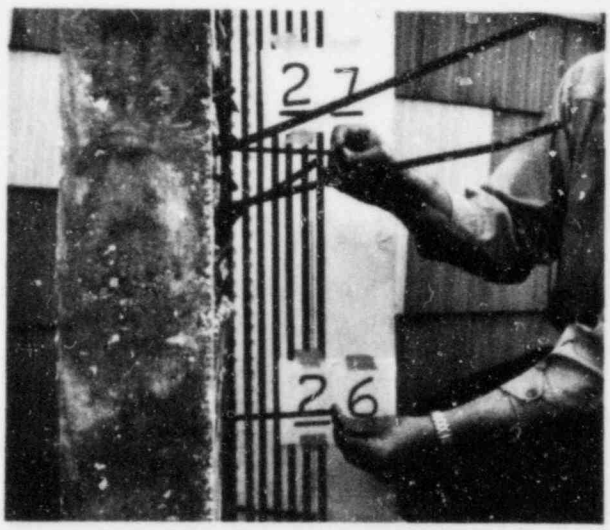

Profile of Rear Rebar or Concrete

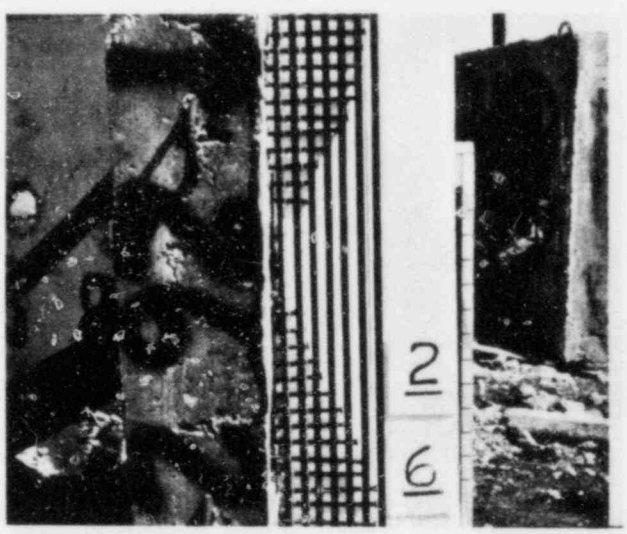

Profile of Back Crater

V = 162 fps

3" OD Steel Pipe
26.5 lb 0.12" Thick

Missile

Final Missile Location Rebound

Secondary Concrete Missiles

Particle size	NA	in.
Particle traveled	NA	ft
Particle velocity	NA	fps

Barrier

Thickness	6.0	in.
Rebar	# 3 at 2.5	in.

Figure A.3.3-21 Primary Hit Test No. 26 Table A.3.3-1 Line 21

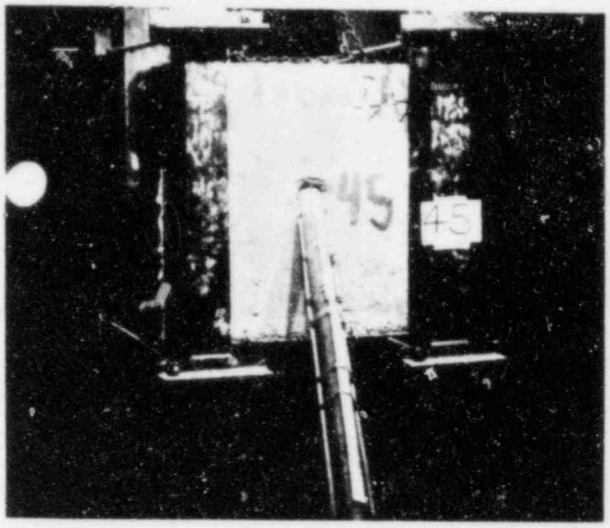

Barrier Front Face

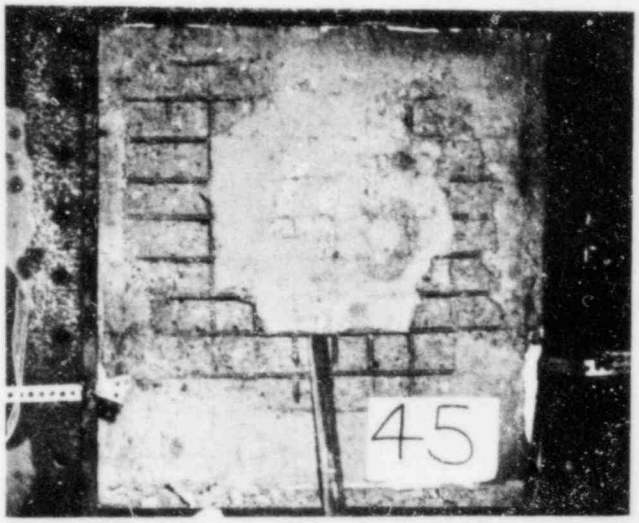

Barrier Rear Face

Test 45 data

destroyed by Test 46

Profile of Rear Rebar or Concrete

Test 45 data

destroyed by Test 46

Profile of Back Crater

V = 200 fps

3" OD Steel Pipe
26.5 lb 0.12" Thick

Missile

Final Missile Location In Target

Secondary Concrete Missiles

Particle size	2.4	in.
Particle traveled	20	ft
Particle velocity	25	fps

Barrier

Thickness	6.0	in.
Rebar	# 3 at 2.5	in.

Figure A.3.3-22 Primary Hit Test No. 45 Table A.3.3-1 Line 22

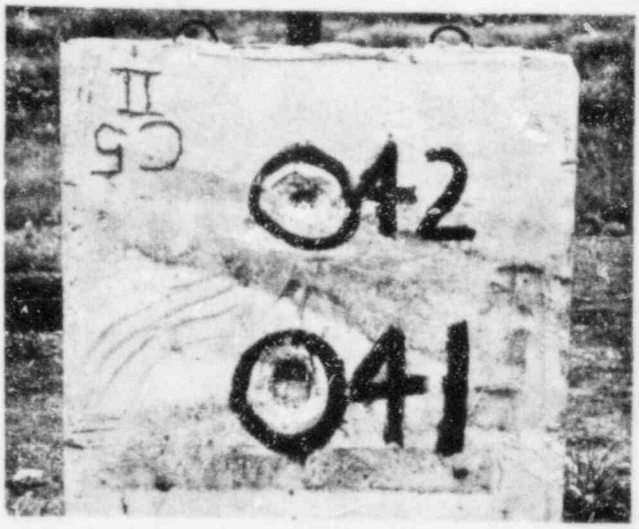

Barrier Front Face

Barrier Rear Face

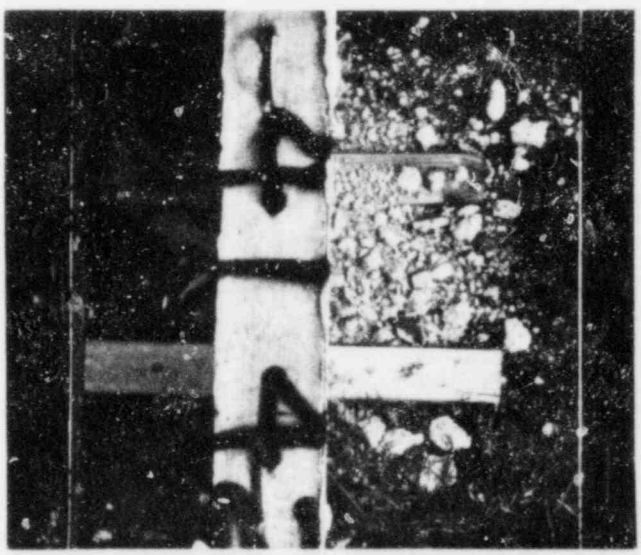

Profile of Rear Rebar or Concrete

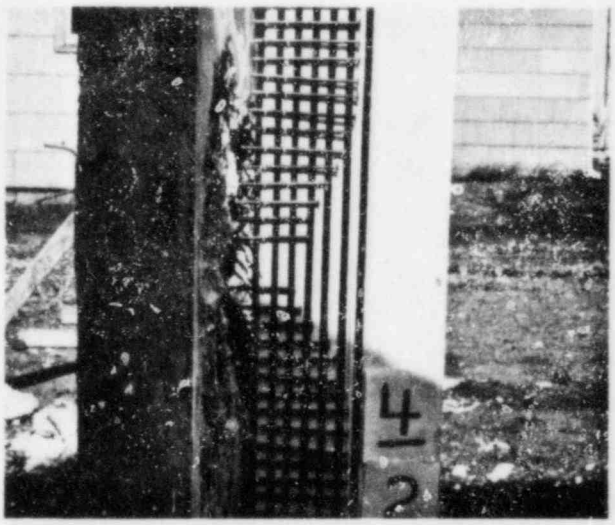

Profile of Back Crater

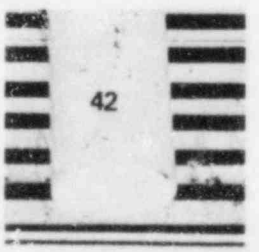

V = 89 fps

3" OD Steel Slug
12.6 lb Solid

Missile

Final Missile Location Rebound

Secondary Concrete Missiles

Particle size	0.6	in.
Particle traveled	1	ft
Particle velocity	1	fps

Barrier

Thickness	4.5	in.
Rebar	# 2 at 3.0	in.

Figure A.3.3-23 Primary Hit Test No. 42 Table A.3.3-1 Line 23

Barrier Front Face

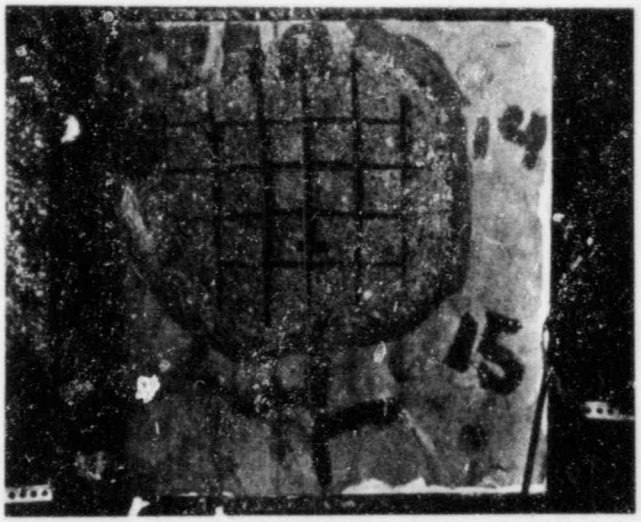

Barrier Rear Face

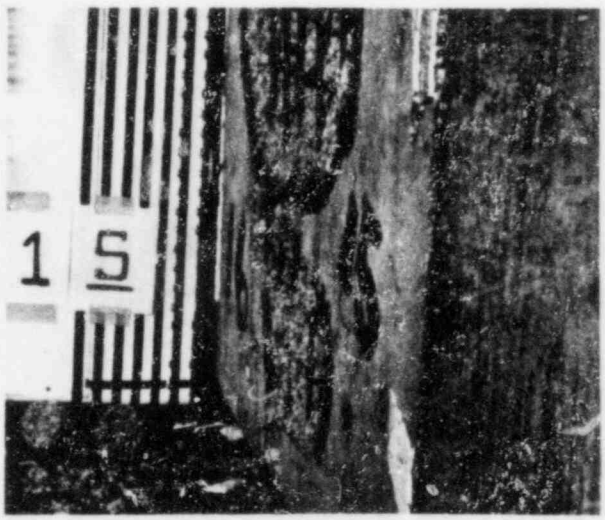

Profile of Rear Rebar or Concrete

No profile taken

Profile of Back Crater

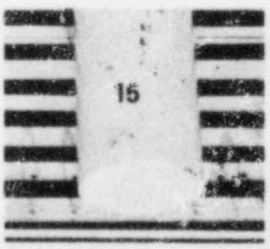

V = 101 fps

3" OD Steel Slug
12.6 lb Solid

Missile

Final Missile Location Rebound

Secondary Concrete Missiles

Particle size	NA	in.
Particle traveled	NA	ft
Particle velocity	NA	fps

Barrier

Thickness	6.0	in.
Rebar	# 2 at 3.0	in.

Figure A.3.3-24 Primary Hit Test No. 15 Table A.3.3-1 Line 24

Barrier Front Face

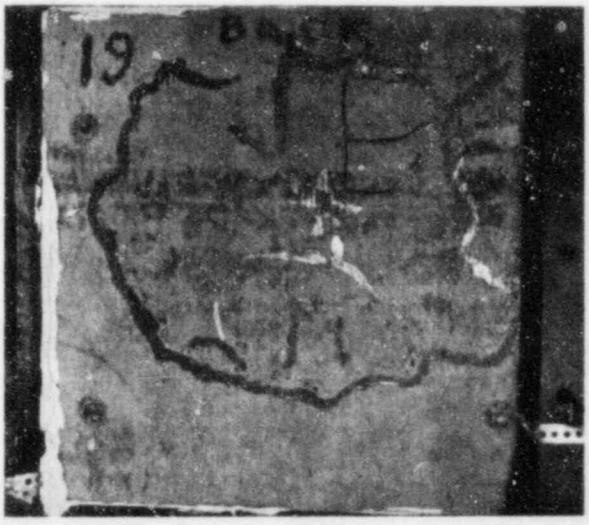

Barrier Rear Face

Profile of Rear Rebar or Concrete

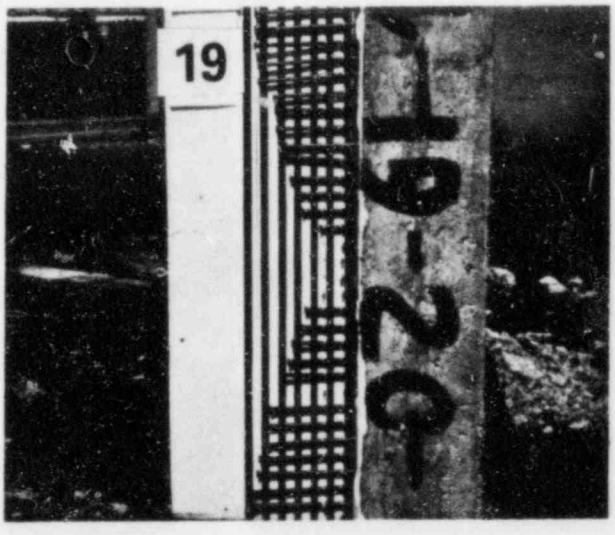

Profile of Back Crater

V = 135 fps

3" OD Steel Slug
12.6 lb Solid

Missile

Final Missile Location Rebound

Secondary Concrete Missiles

Particle size	NA	in.
Particle traveled	NA	ft
Particle velocity	NA	fps

Barrier

Thickness	6.0	in.
Rebar	# 2 at 3.0	in.

Figure A.3.3-25 Primary Hit Test No. 19 Table A.3.3-1 Line 25

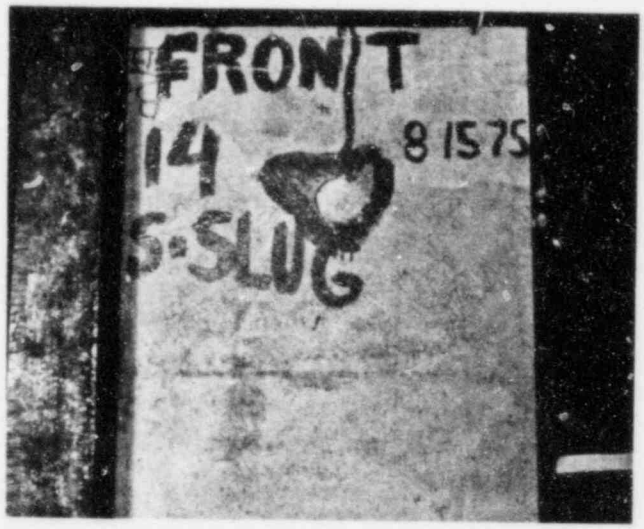

Barrier Front Face

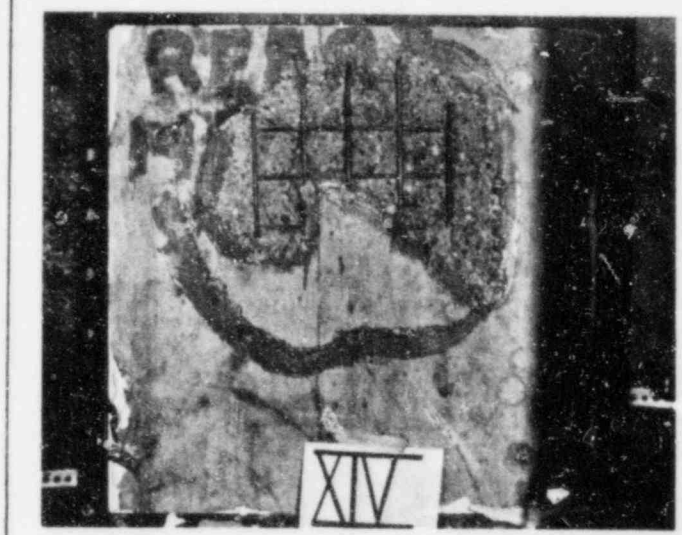

Barrier Rear Face

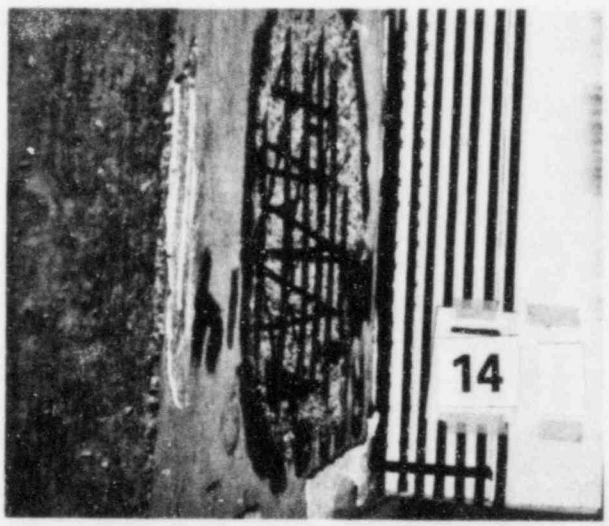

Profile of Rear Rebar or Concrete

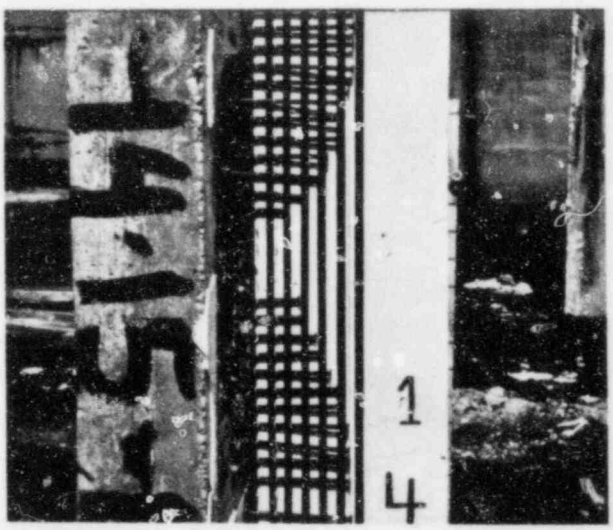

Profile of Back Crater

V = 205 fps

3" OD Steel Slug
12.6 lb Solid

Missile

Final Missile Location Rebound

Secondary Concrete Missiles

Particle size	1.3	in.
Particle traveled	20	ft
Particle velocity	25	fps

Barrier

Thickness	6.0	in.
Rebar	# 2 at 3.0	in.

Figure A.3.3-26 Primary Hit Test No. 14 Table A.3.3-1 Line 26

Barrier Front Face

Barrier Rear Face

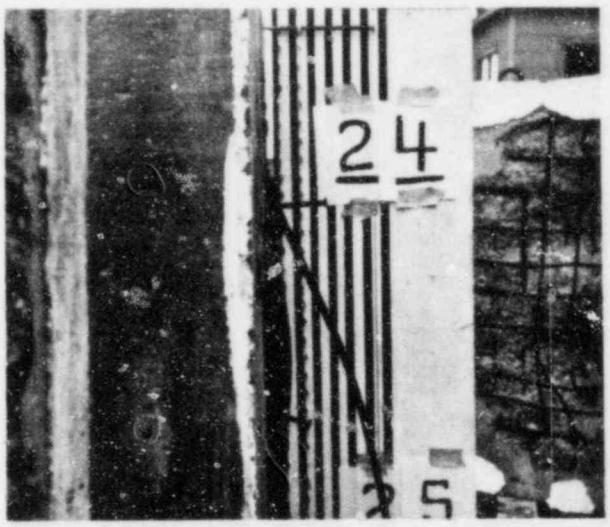

Profile of Rear Rebar or Concrete

No data taken

Profile of Back Crater

V = 183 fps

3" OD Steel Slug
12.6 lb Solid

Missile

Final Missile Location Rebound

Secondary Concrete Missiles

Particle size	1.2	in.
Particle traveled	1	ft
Particle velocity	1	fps

Barrier

Thickness	6.0	in.
Rebar	# 3 at 2.5	in.

Figure A.3.3-27 Primary Hit Test No. 24 Table A.3.3-1 Line 27

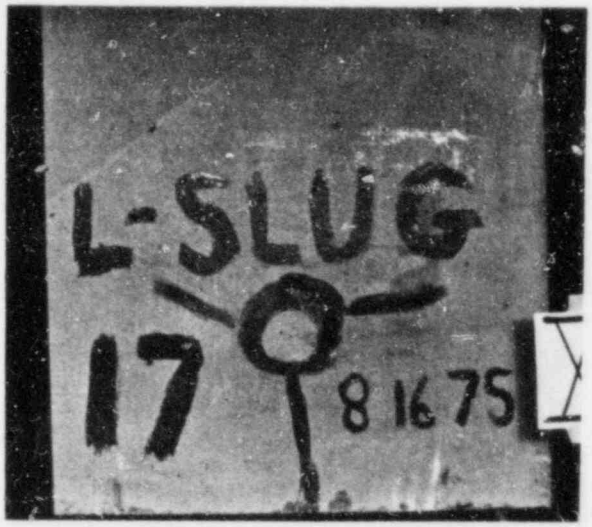

Barrier Front Face

Barrier Rear Face

Profile of Rear Rebar or Concrete

No crater formed

Profile of Back Crater

V = 95 fps

3" OD Steel slug
23.5 lb Solid

Missile

Final Missile Location Rebound

Secondary Concrete Missiles

Particle size	1.2	in.
Particle traveled	1	ft
Particle velocity	1	fps

Barrier

Thickness	6.0	in.
Rebar	# 2 at 3.0	in.

Figure A.3.3-28 Primary Hit Test No. 17 Table A.3.3-1 Line 28

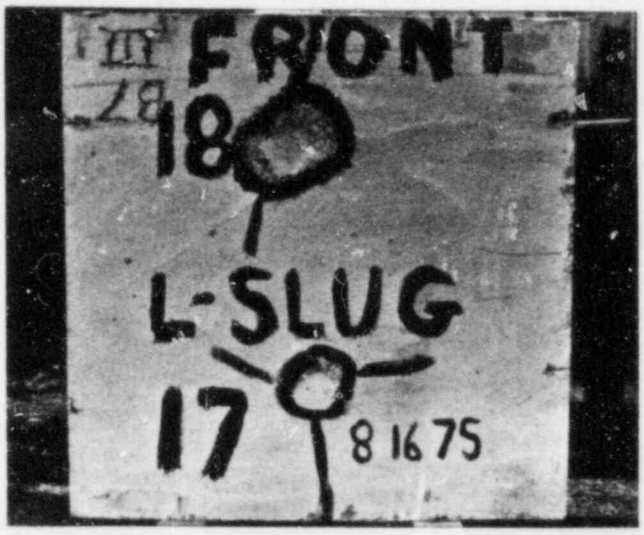

Barrier Front Face

Barrier Rear Face

Profile of Rear Rebar or Concrete

Profile of Back Crater

V = 128 fps

3" OD Steel Slug
23.5 lb Solid

Missile

Final Missile Location Rebound

Secondary Concrete Missiles

Particle size	1.3	in.
Particle traveled	10	ft
Particle velocity	15	fps

Barrier

Thickness	6.0	in.
Rebar	# 2 at 3.0	in.

Figure A.3.3-29 Primary Hit Test No. 18 Table A.3.3-1 Line 29

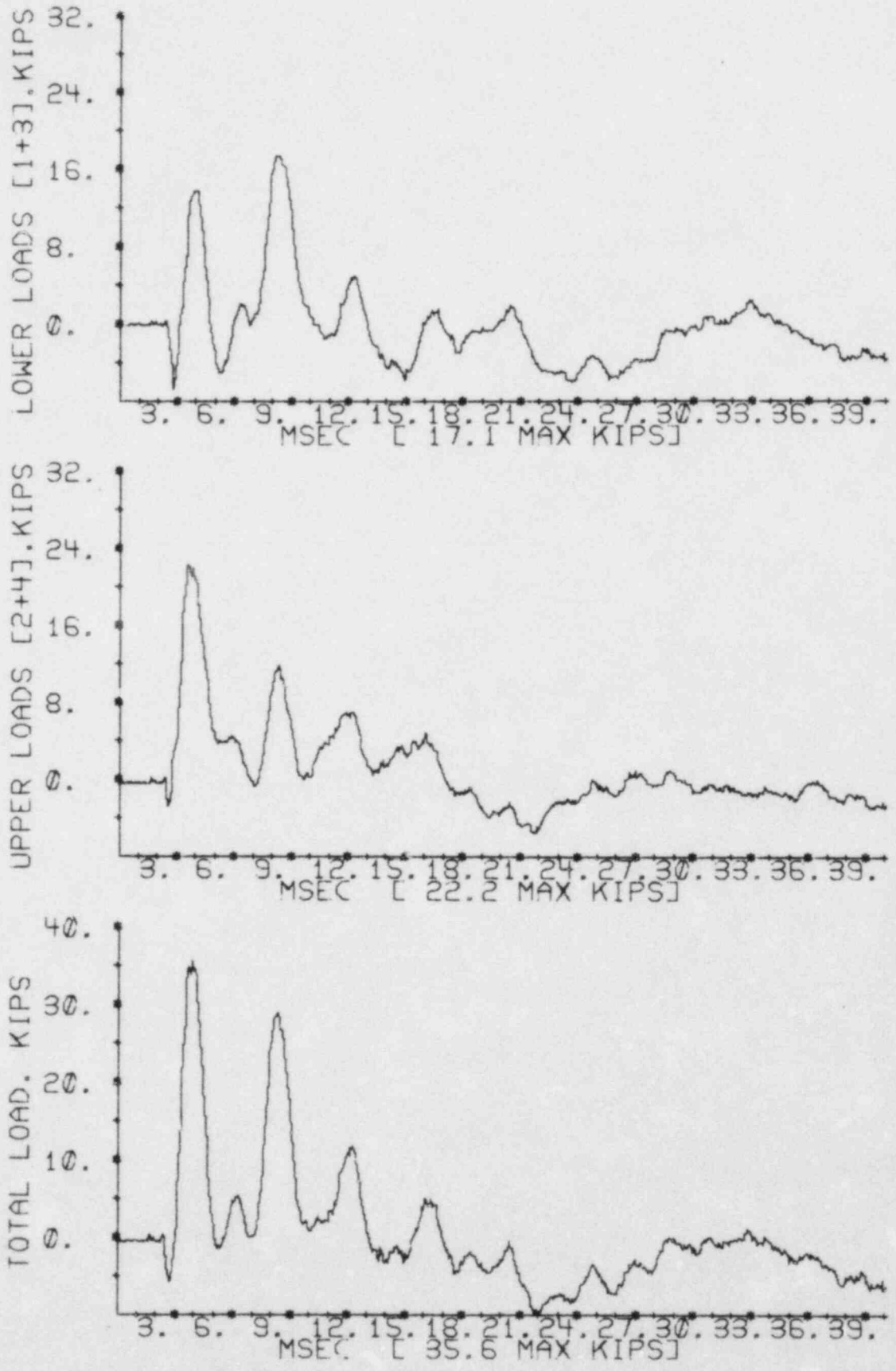

Figure A.3.4-1 Load Cell Data, Experiment Number 3

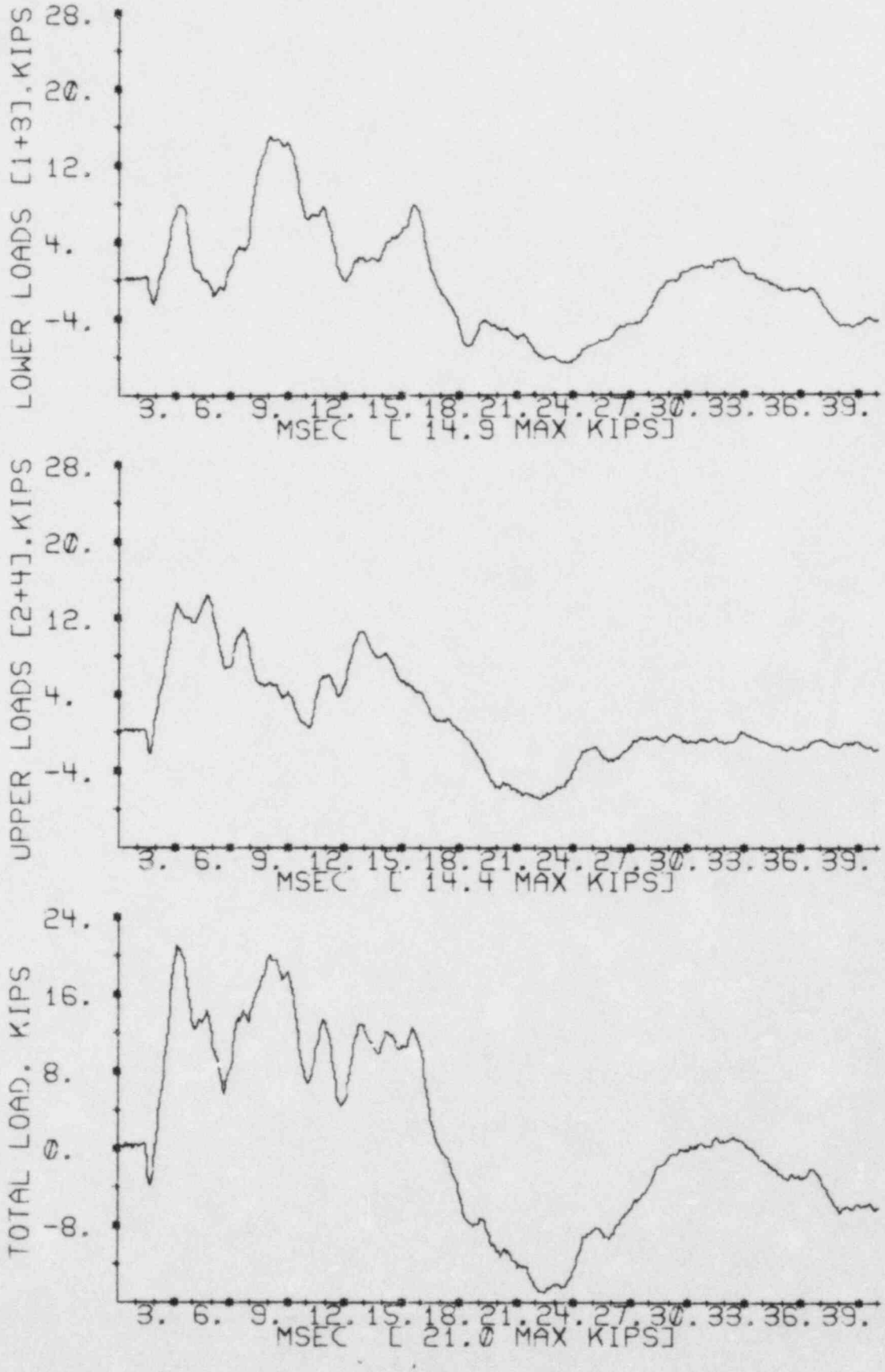

Figure A.3.4-2 Load Cell Data, Experiment Number 1

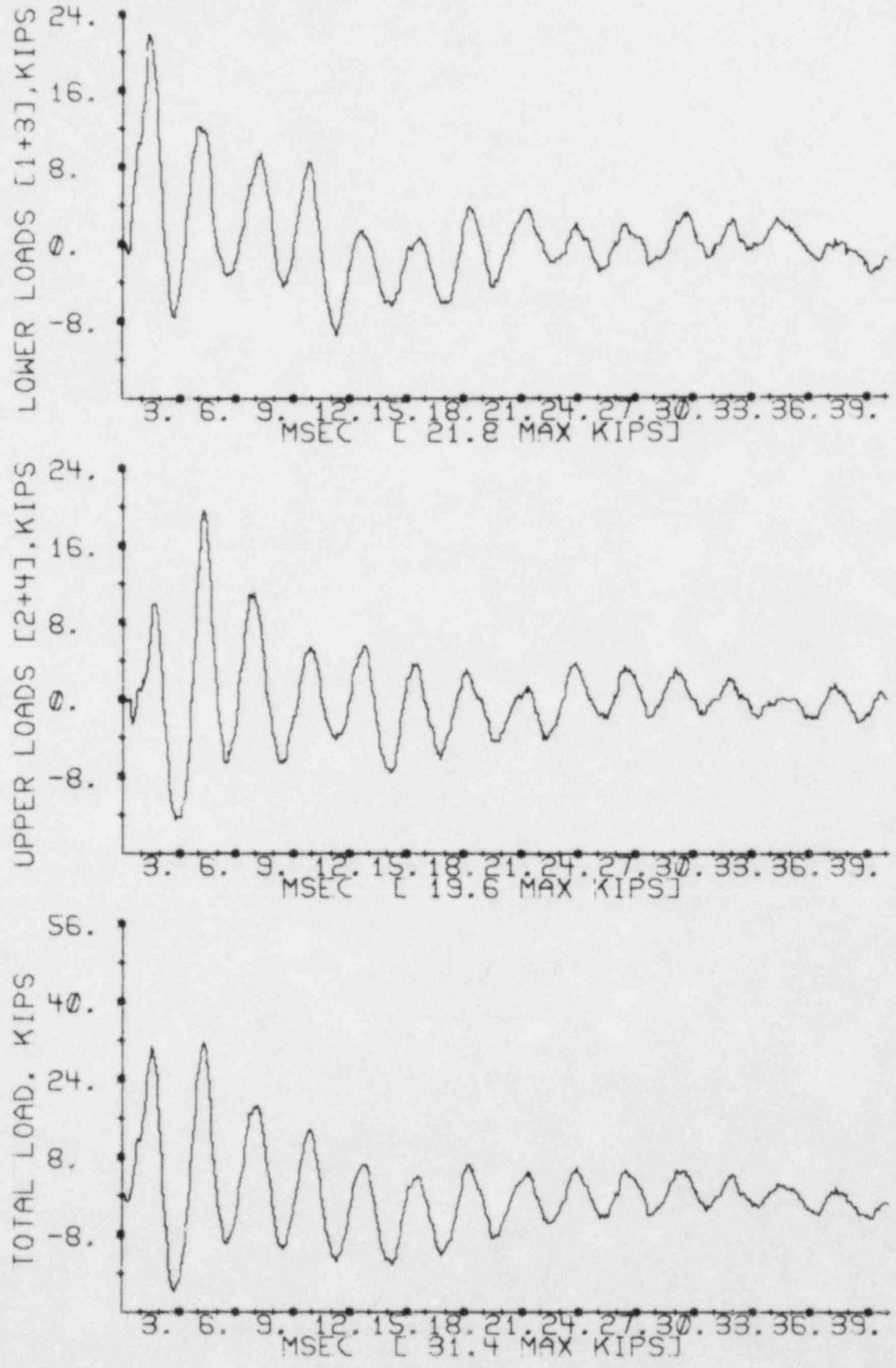

Figure A.3.4-3 Load Cell Data, Experiment Number 35

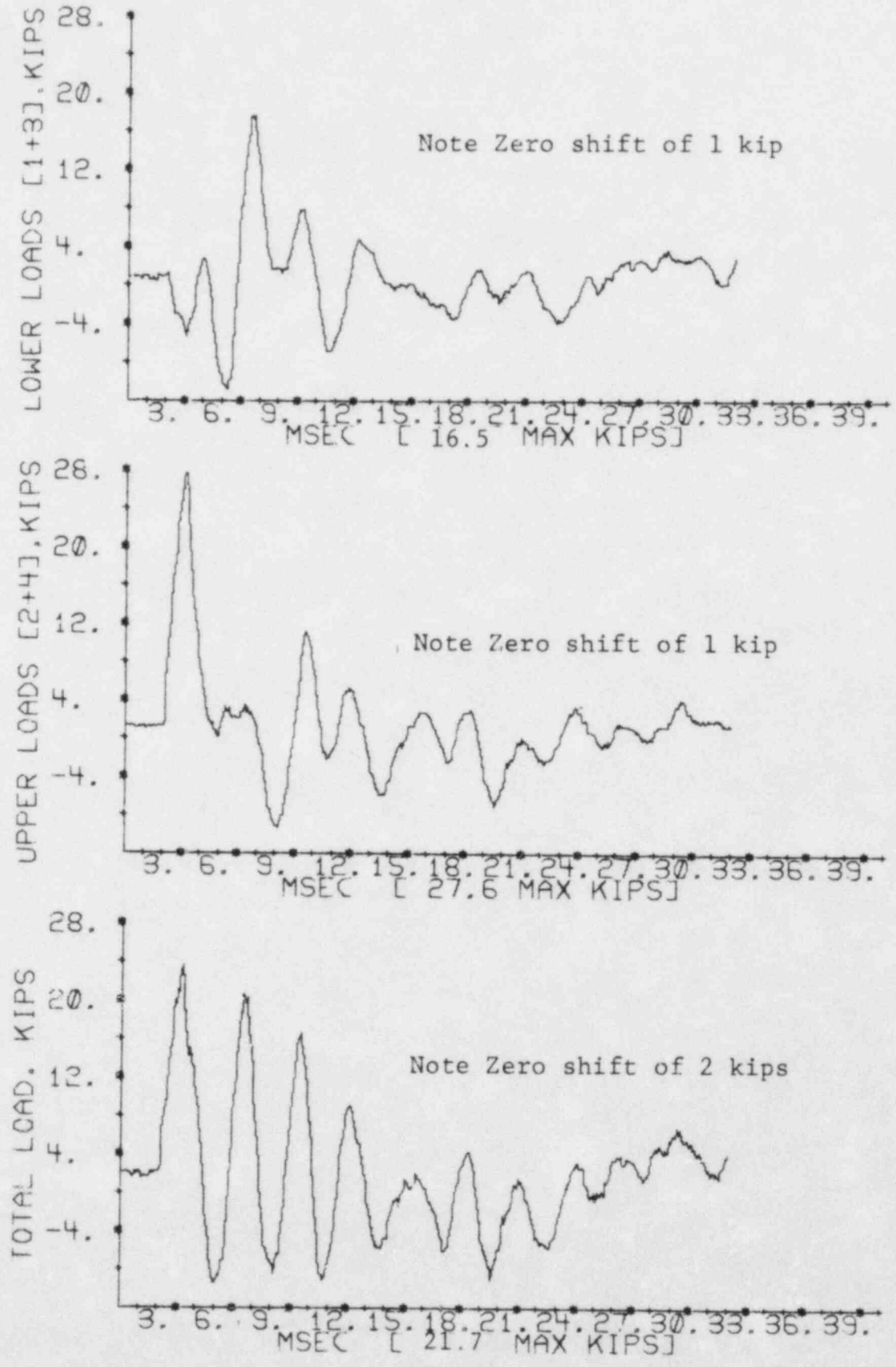

Figure A.3.4-4 Load Cell Data, Experiment Number 36

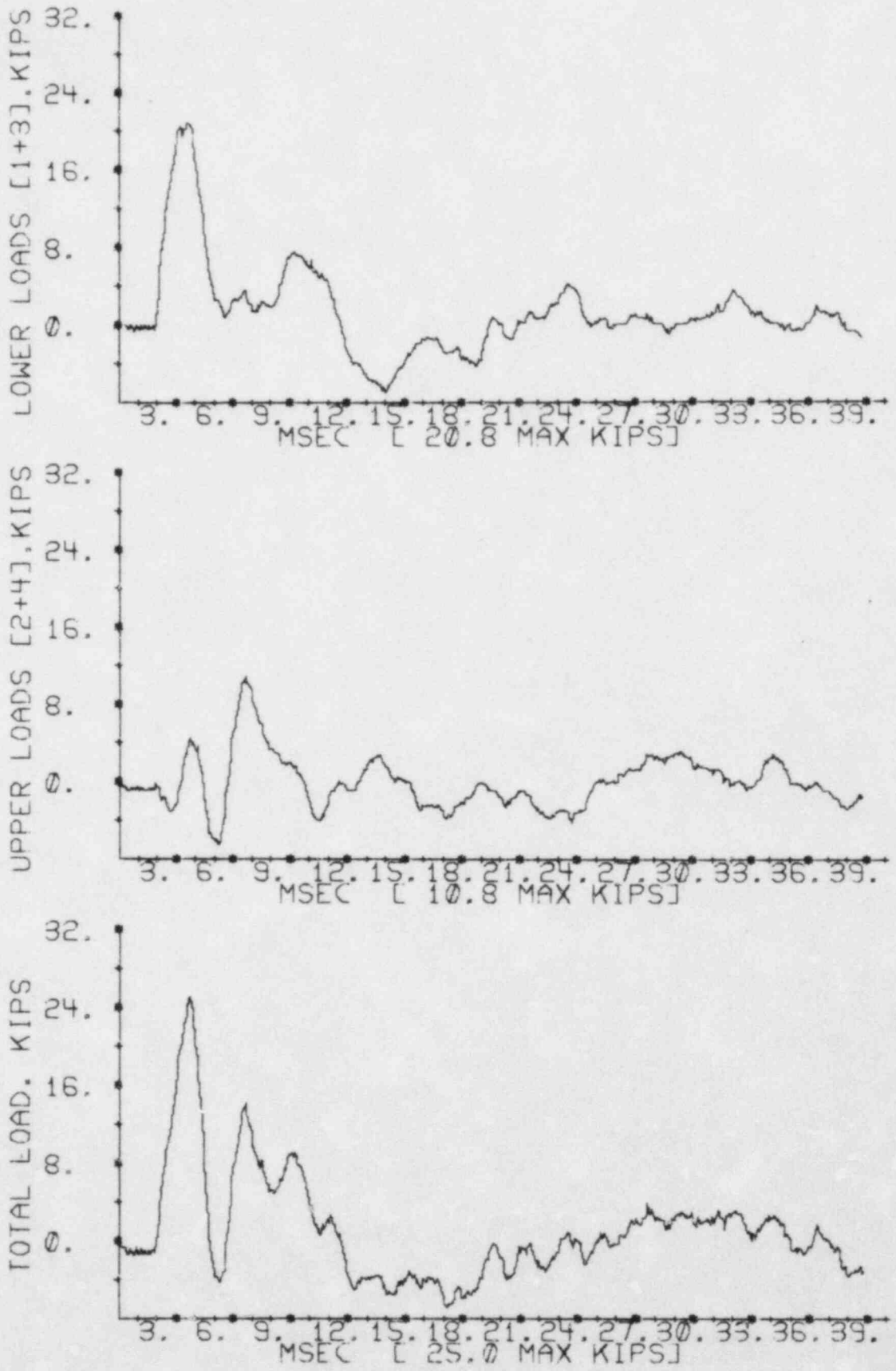

Figure A.3.4-5 Load Cell Data, Experiment Number 40

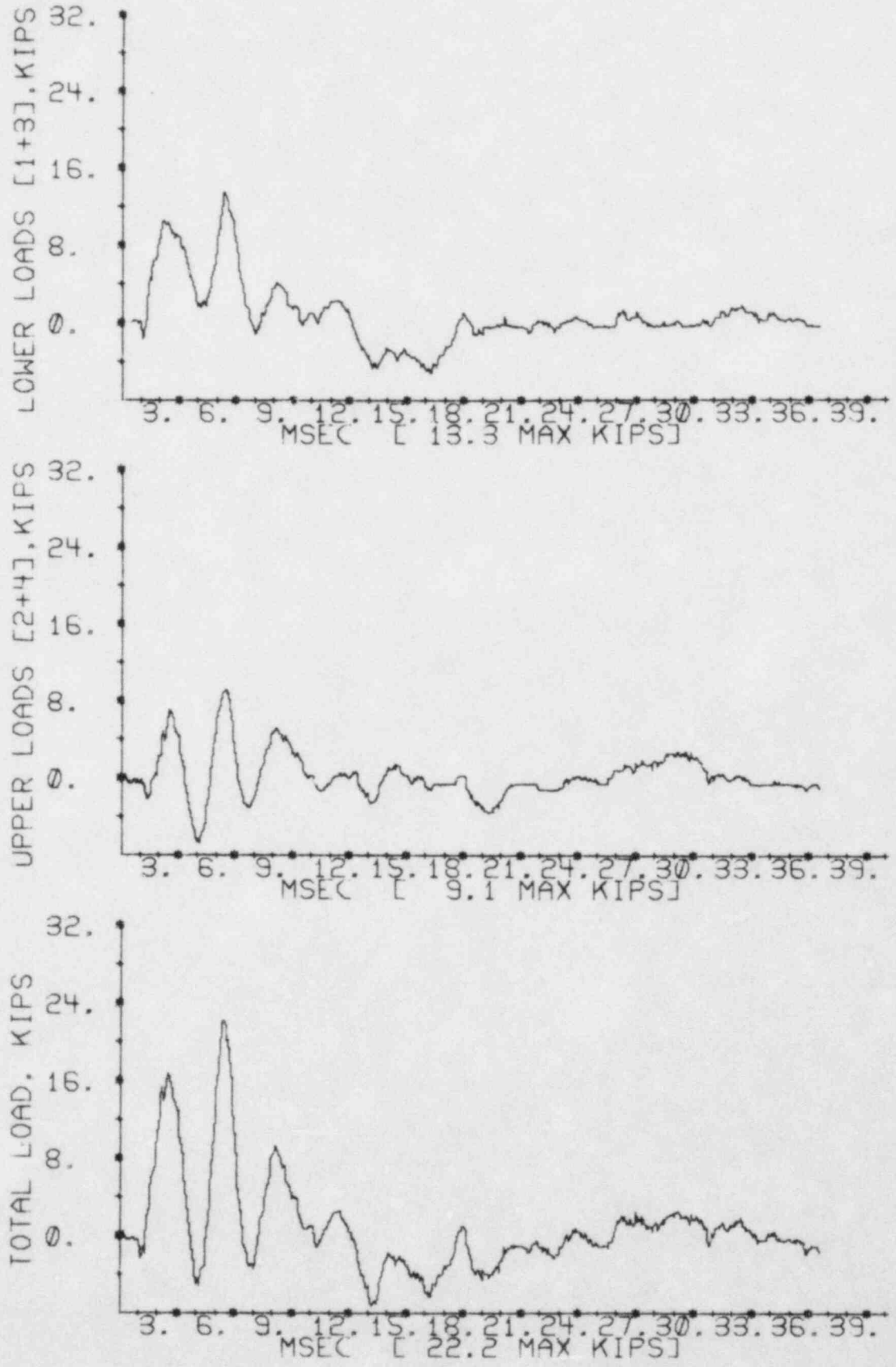

Figure A.3.4-6 Load Cell Data, Experiment Number 41

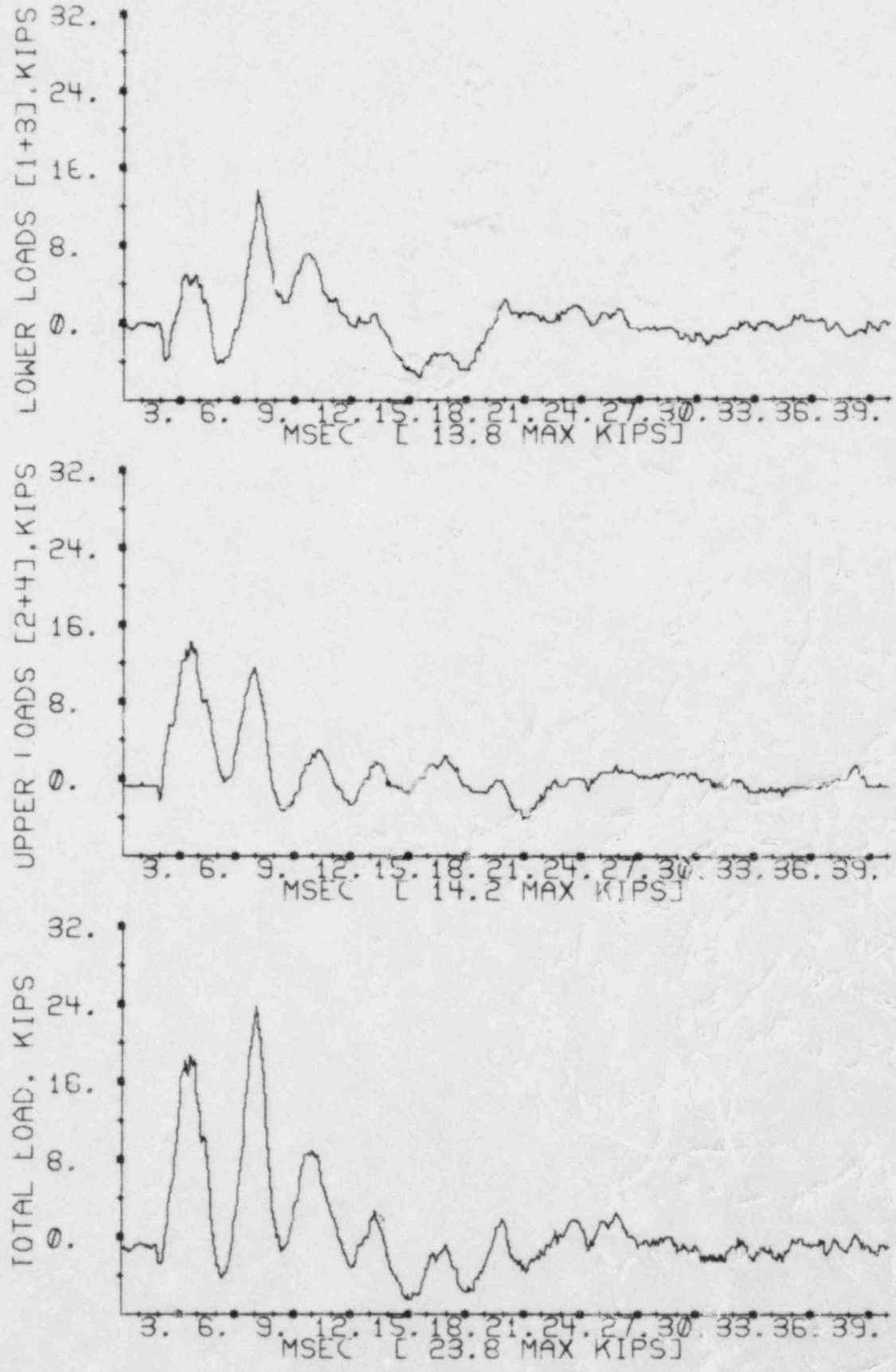

Figure A.3.4-7 Load Cell Data, Experiment Number 28

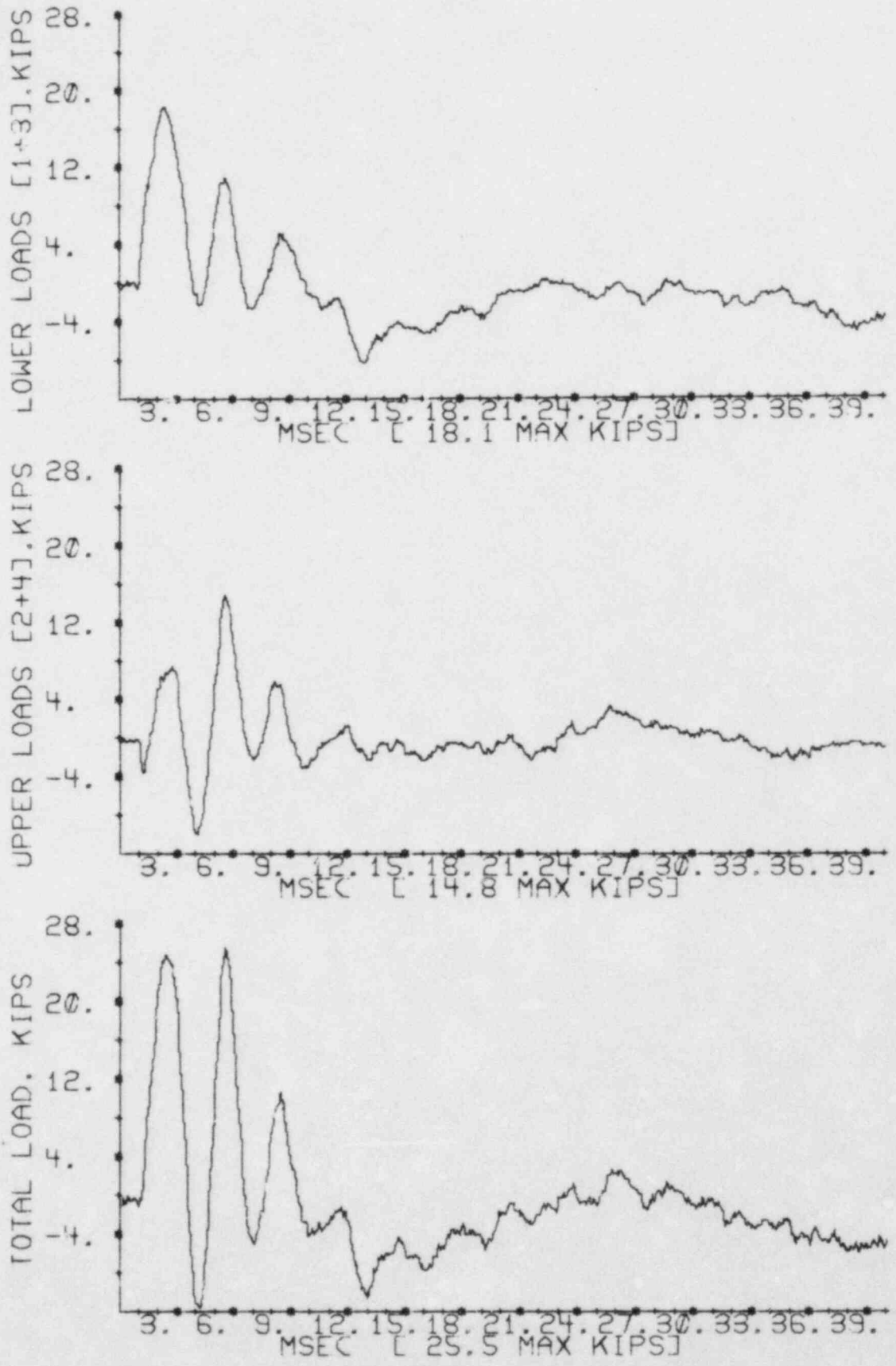

Figure A.3.4-8 Load Cell Data, Experiment Number 7

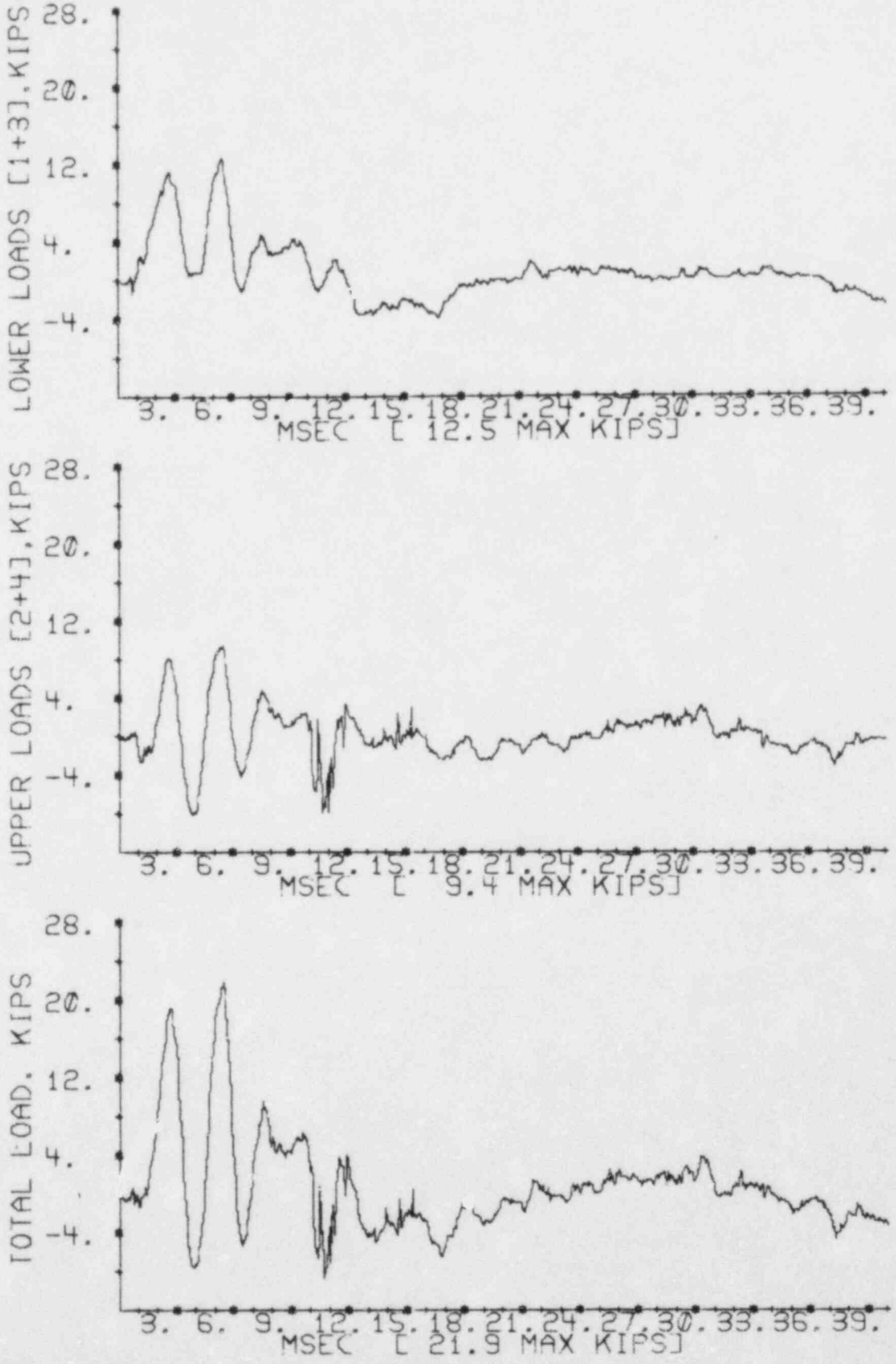

Figure A.3.4-9 Load Cell Data, Experiment Number 12

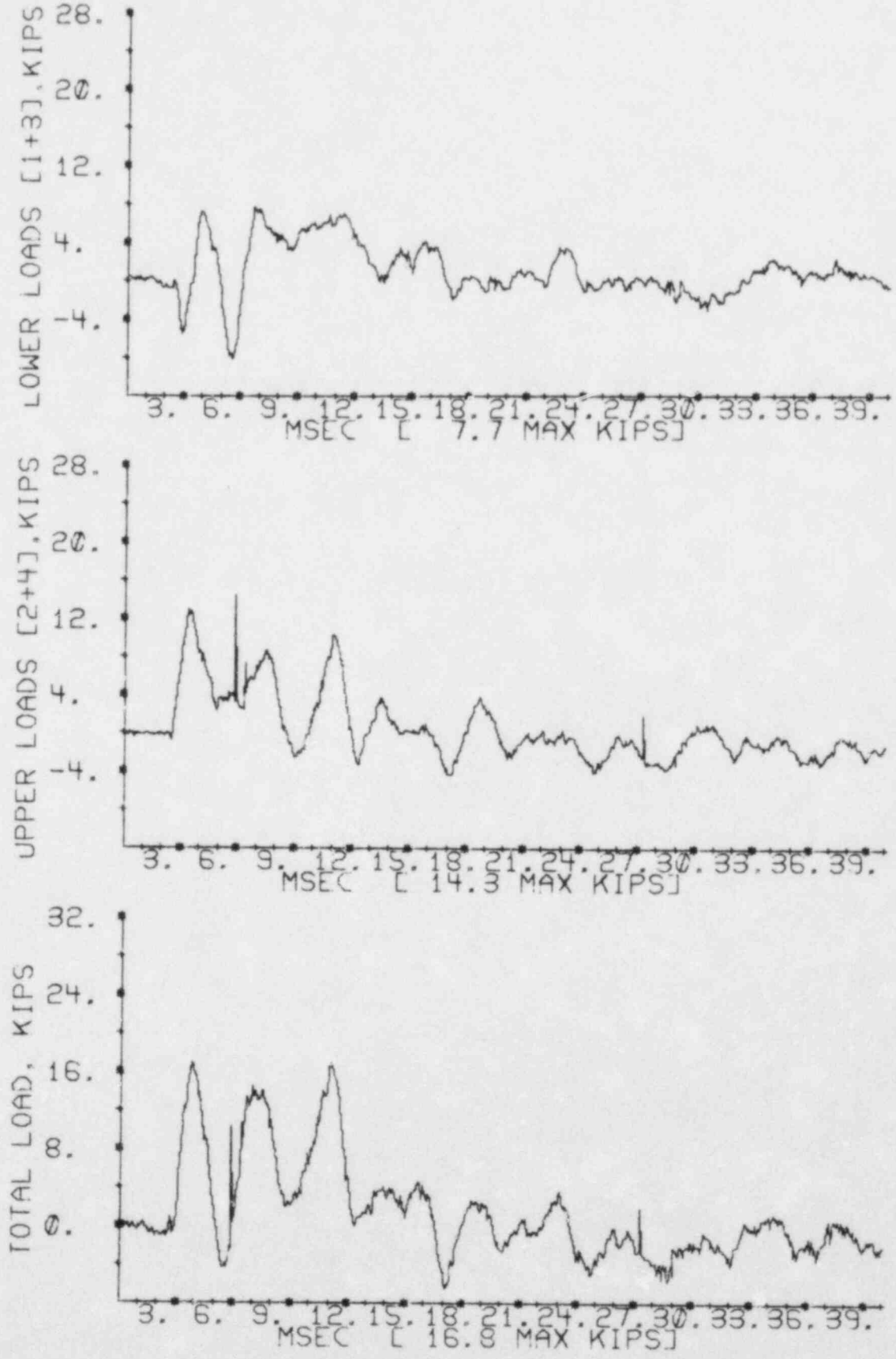

Figure A.3.4-10 Load Cell Data, Experiment Number 10

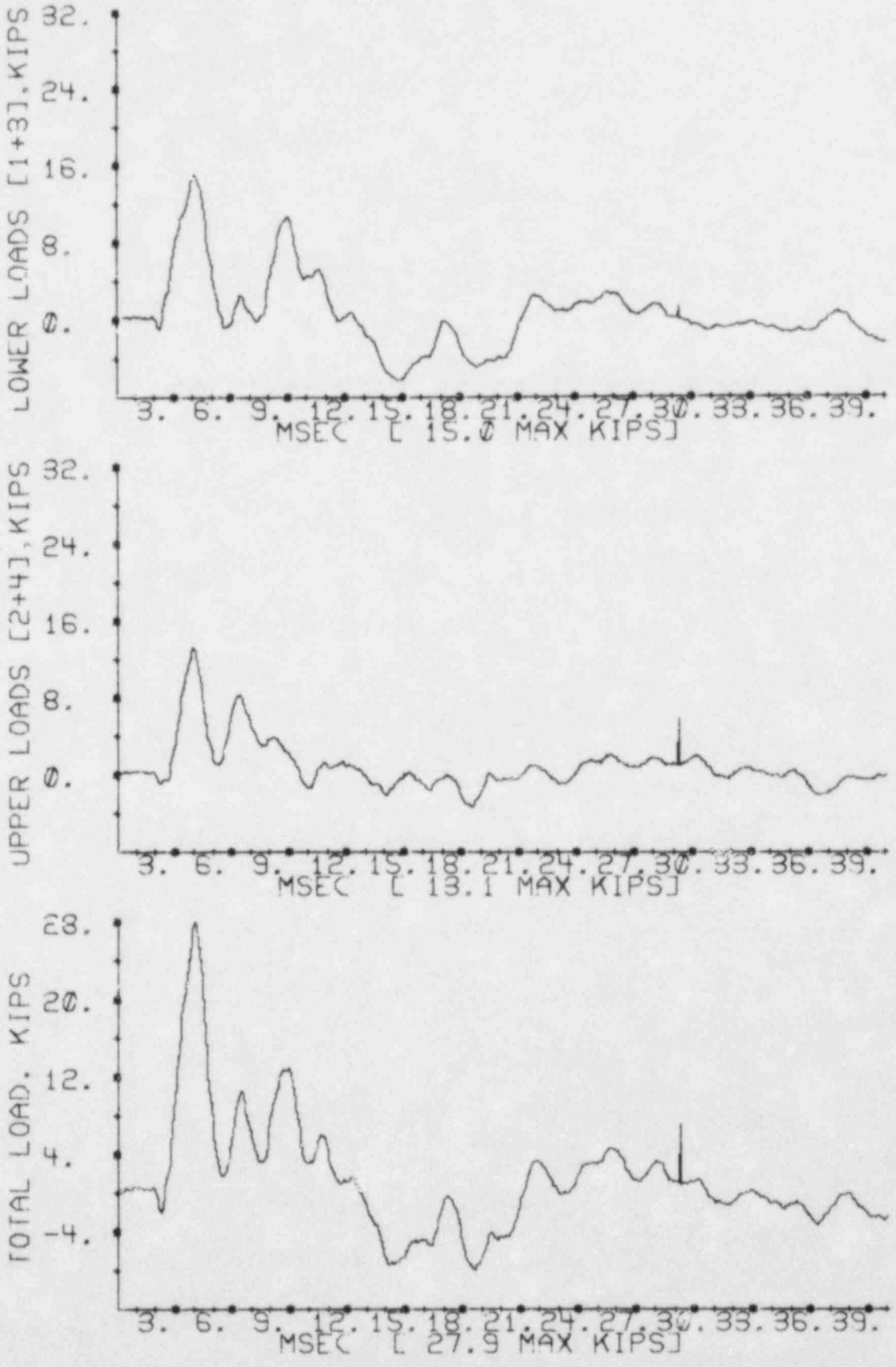

Figure A.3.4-11 Load Cell Data, Experiment Number 2

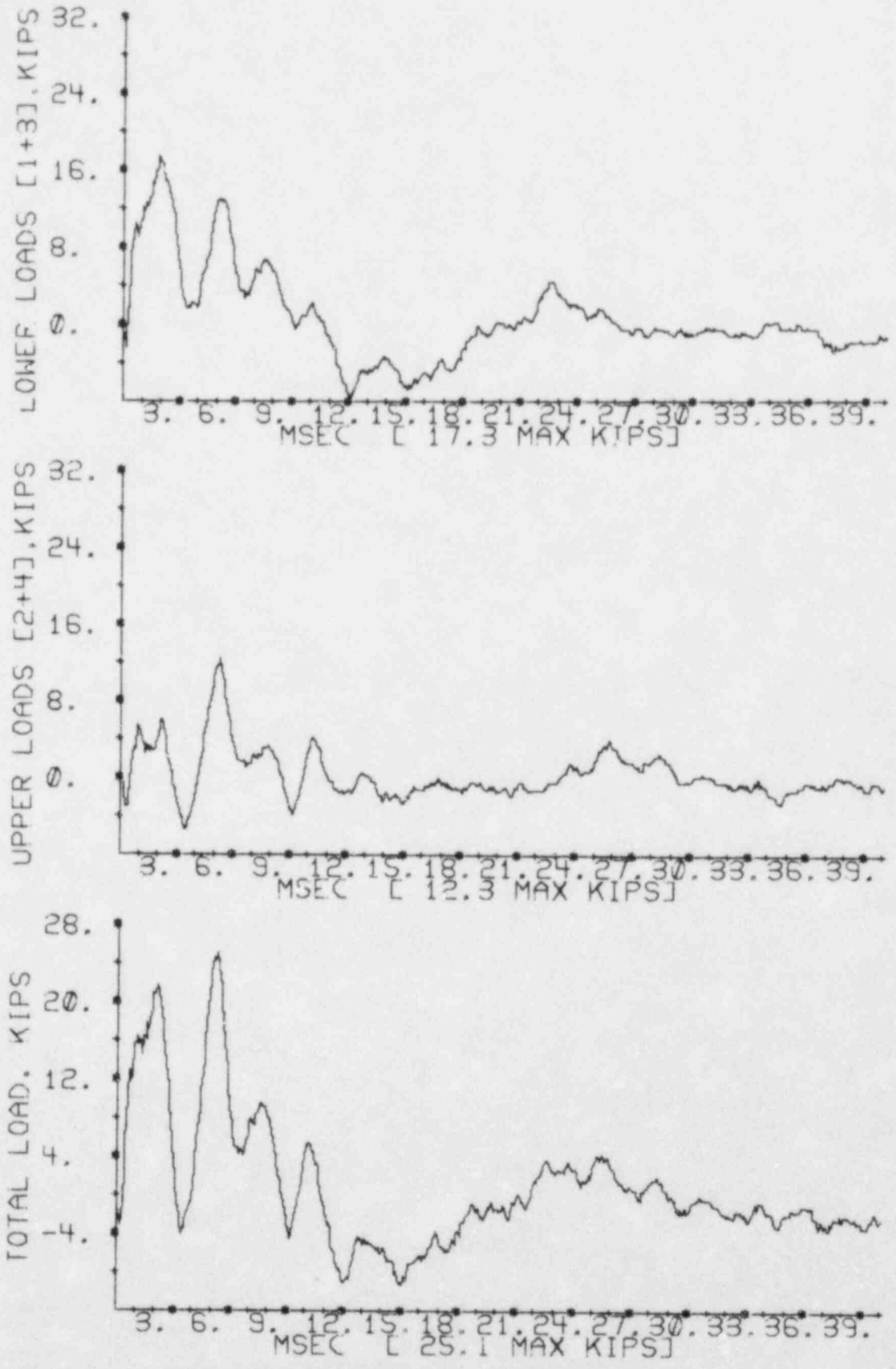

Figure A.3.4-12 Load Cell Data, Experiment Number 30

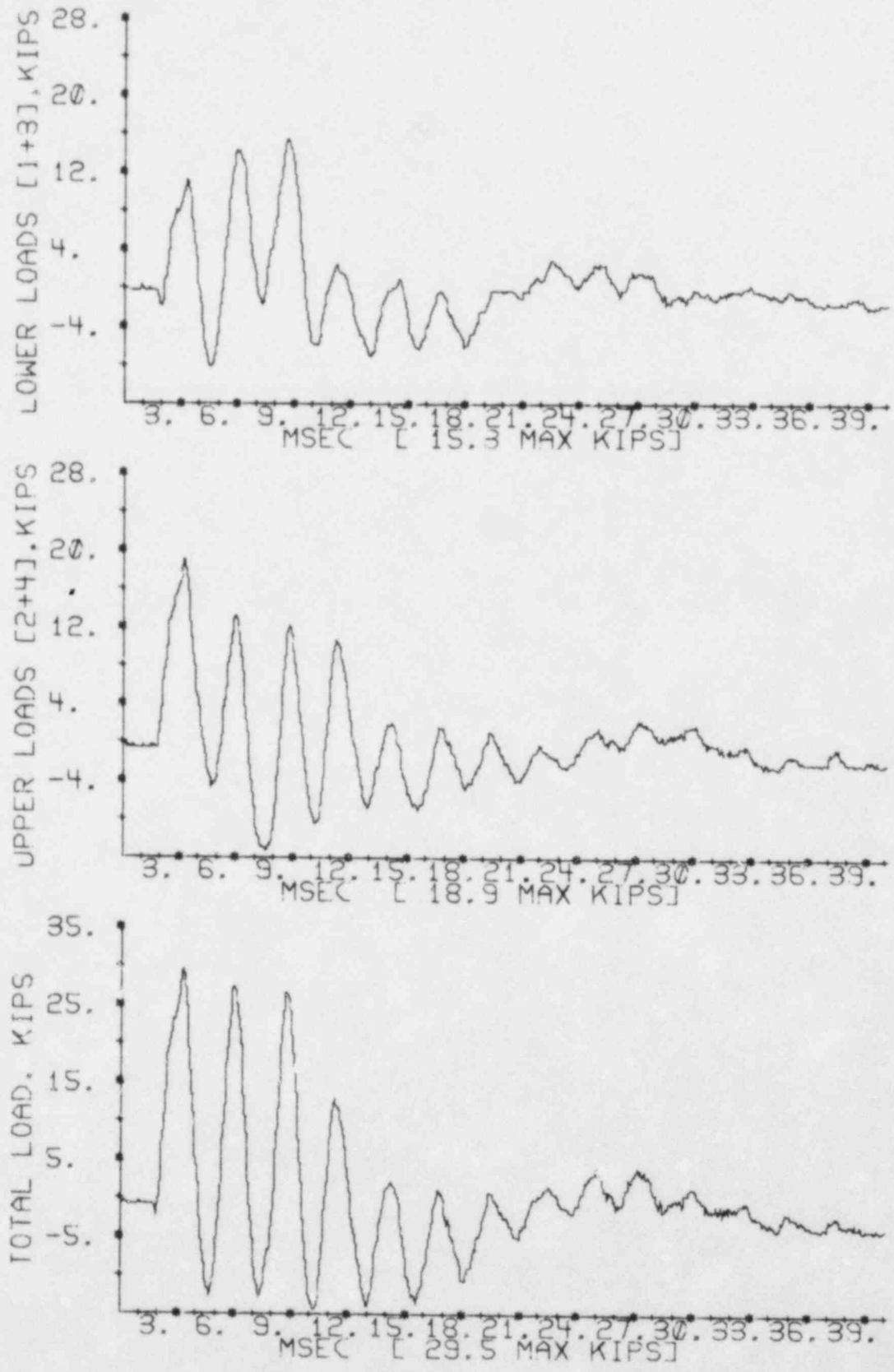

Figure A.3.4-13 Load Cell Data, Experiment Number 5

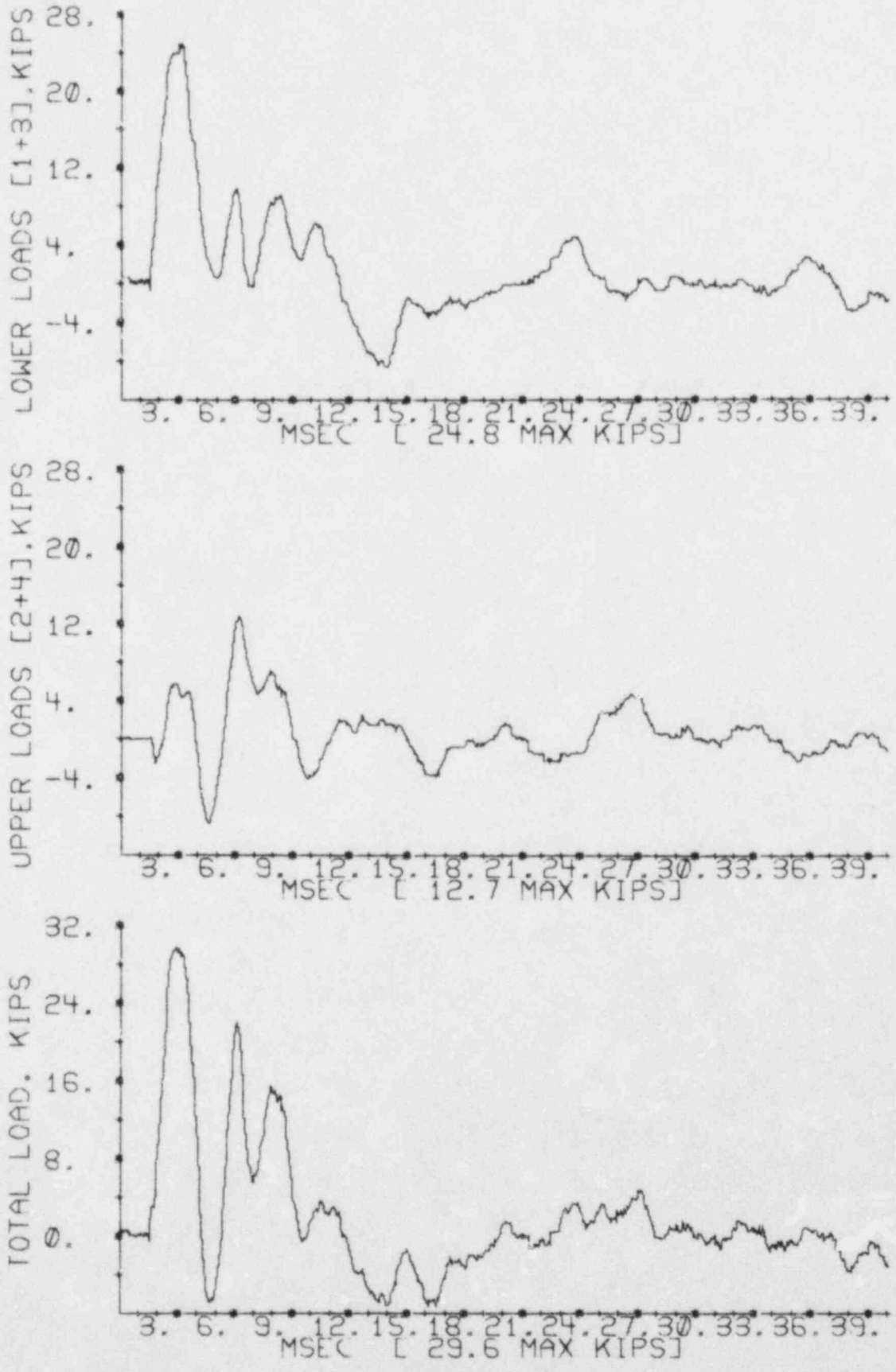

Figure A.3.4-14 Load Cell Data, Experiment Number 22

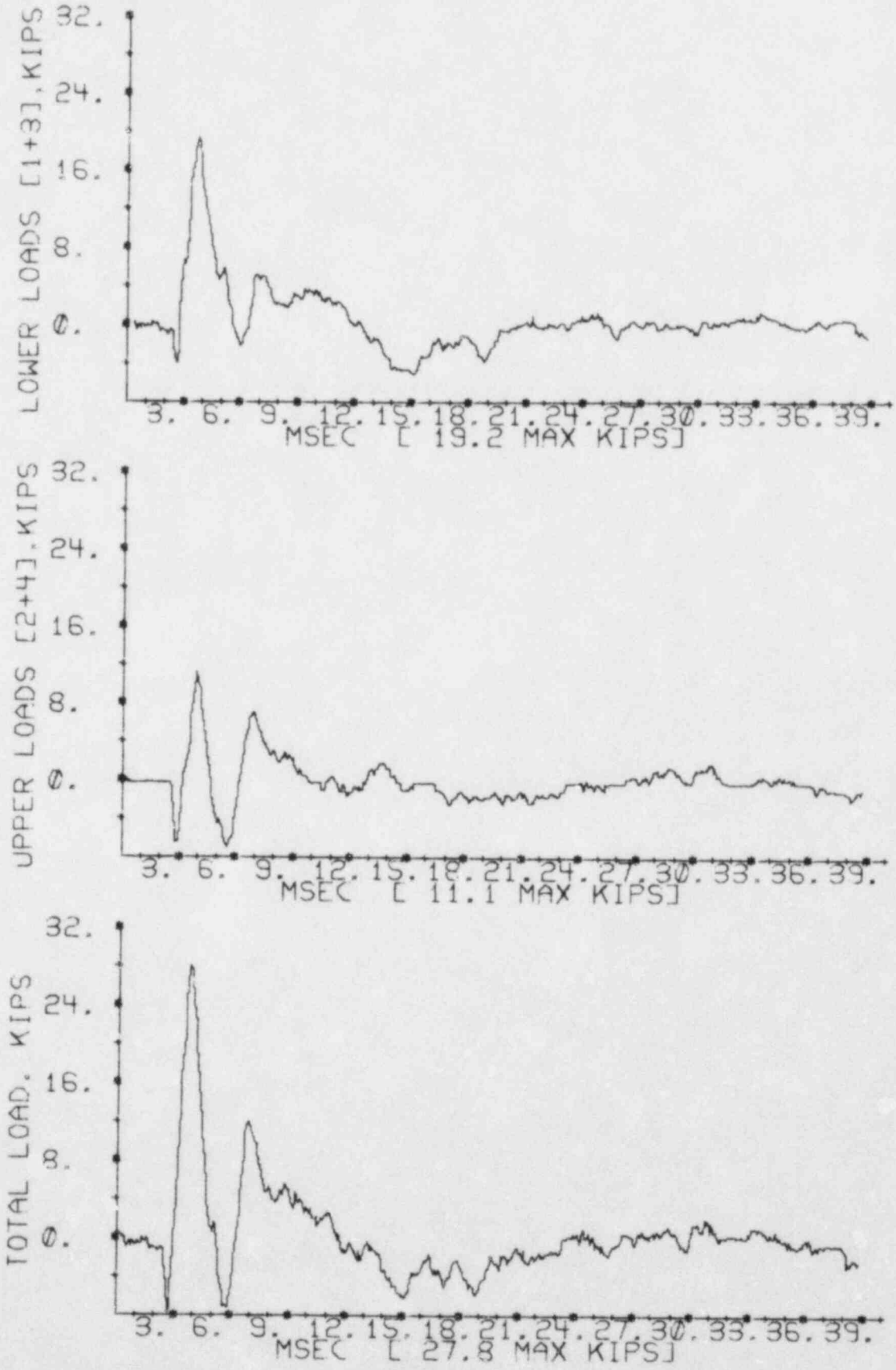

Figure A.3.4-15 Load Cell Data, Experiment Number 43

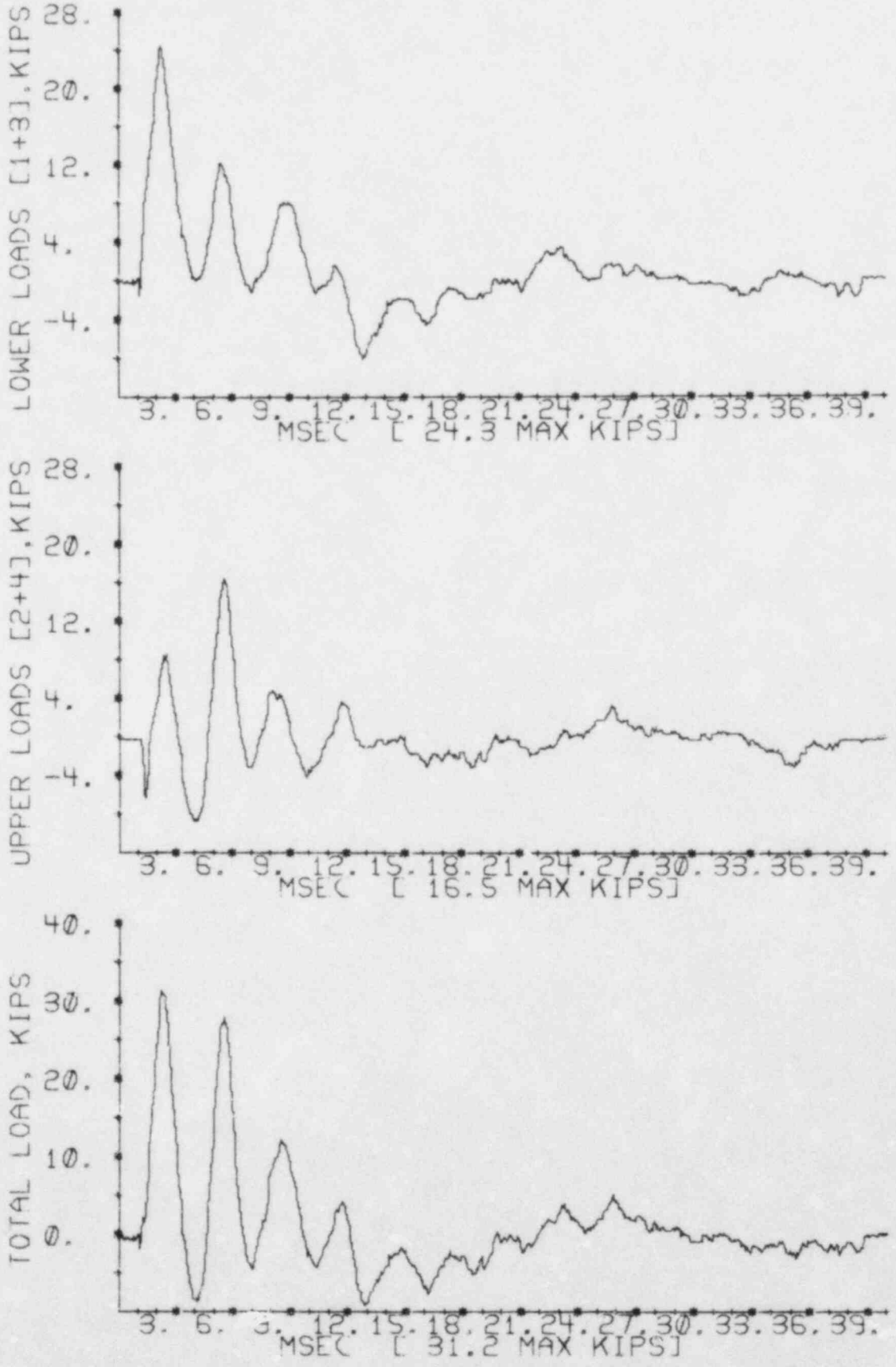

Figure A.3.4-16 Load Cell Data, Experiment Number 21

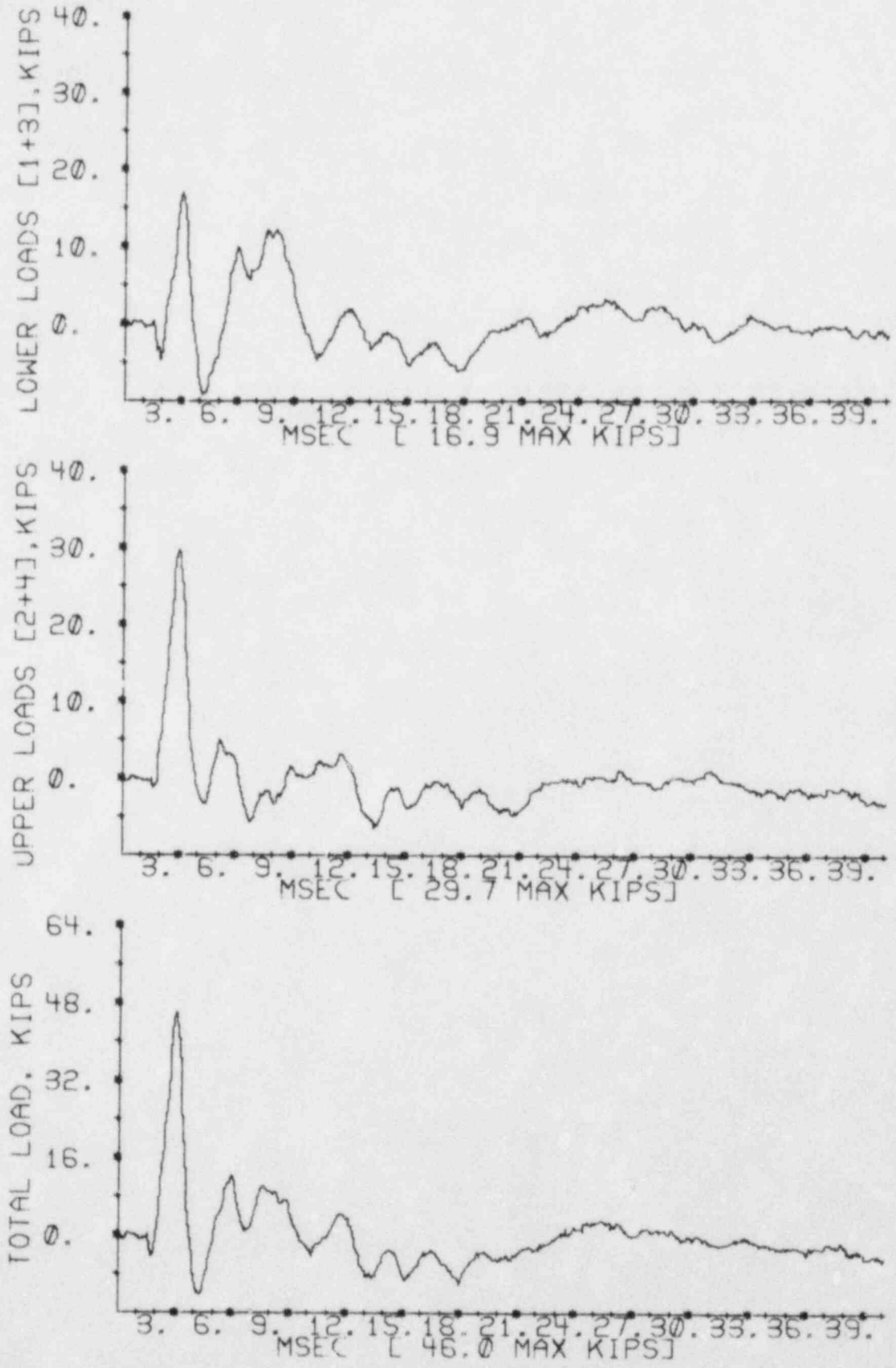

Figure A.3.4-17 Load Cell Data, Experiment Number 39

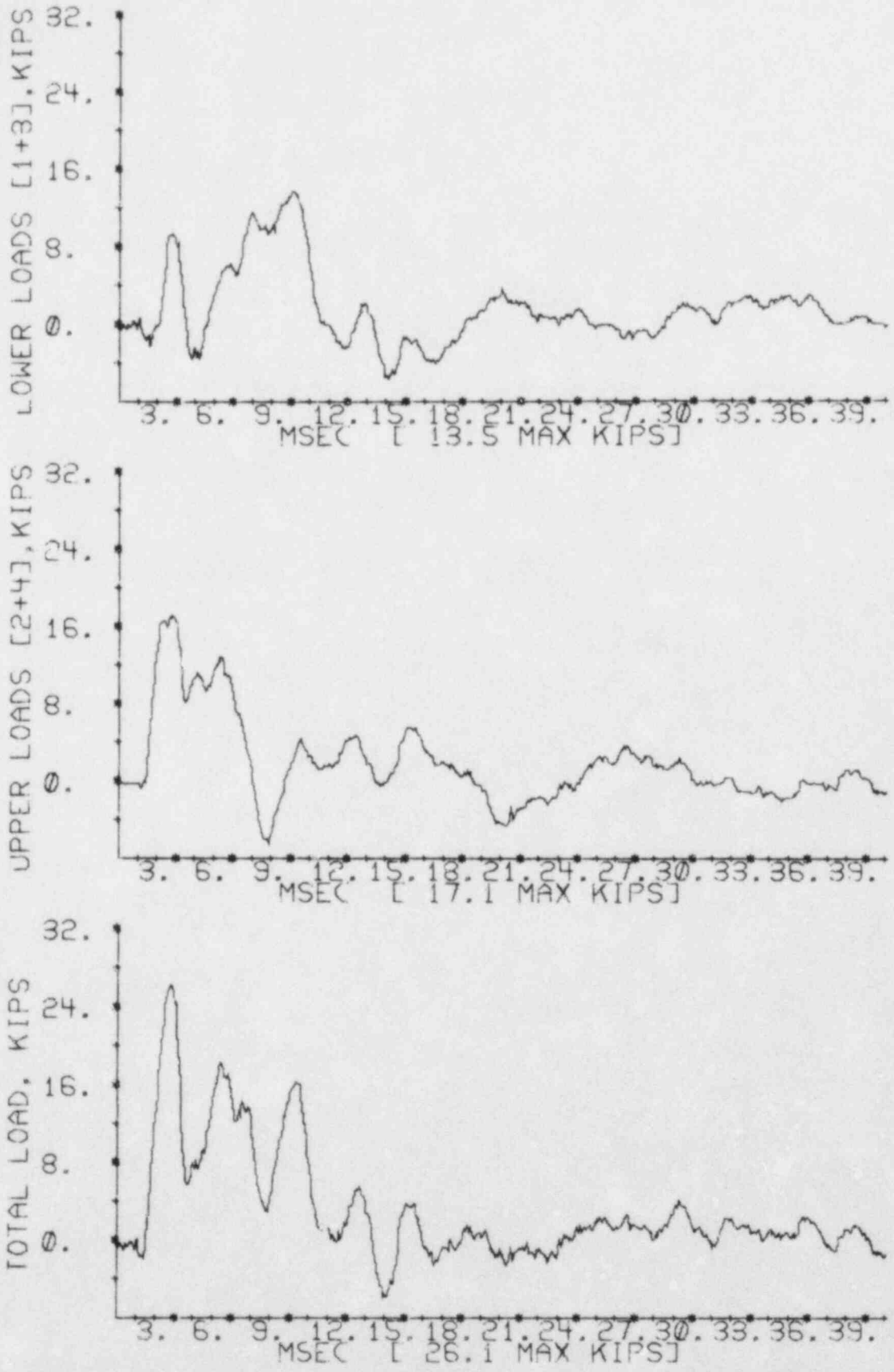

Figure A.3.4-18 Load Cell Data, Experiment Number 38

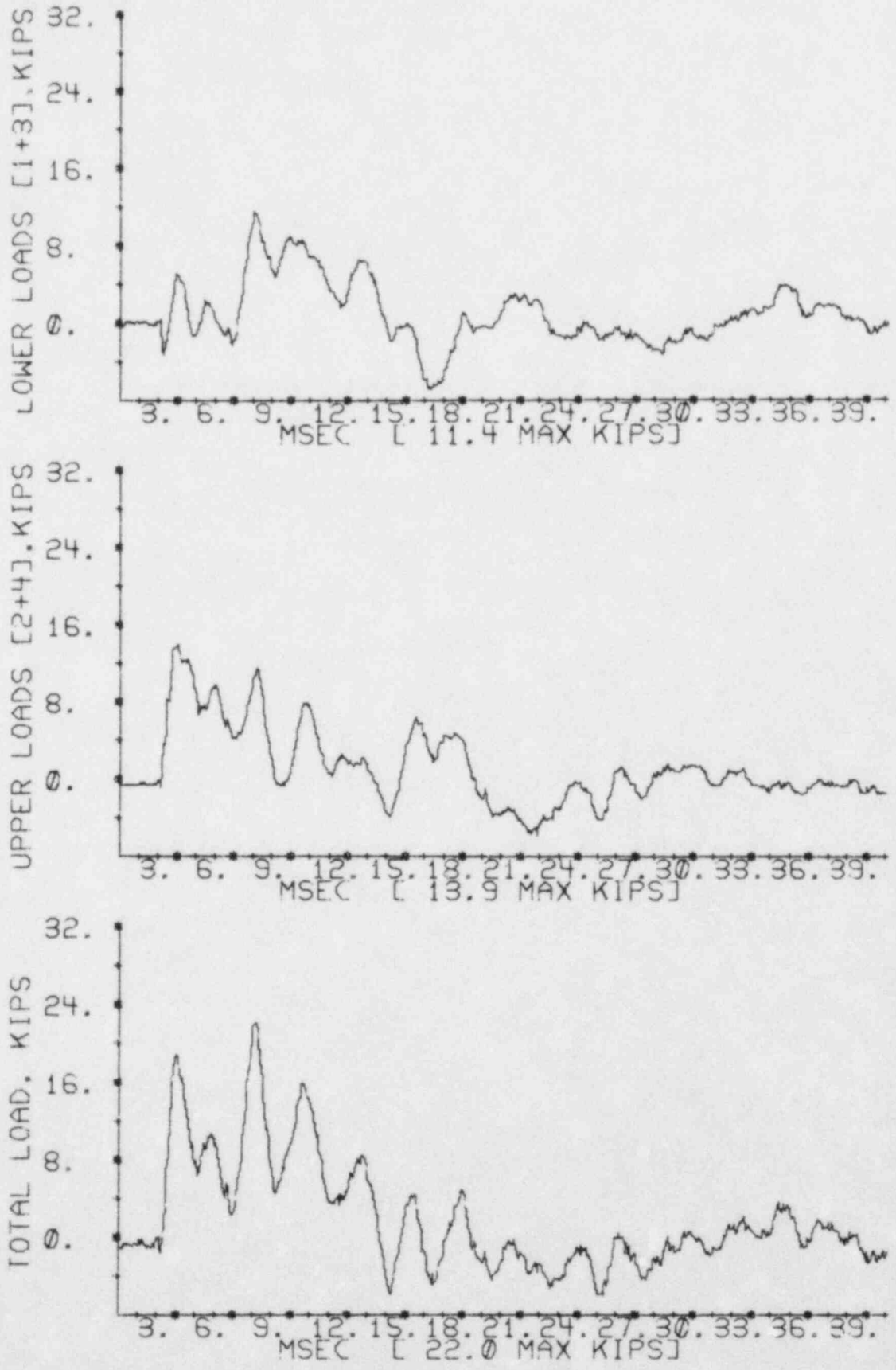

Figure A.3.4-19 Load Cell Data, Experiment Number 47

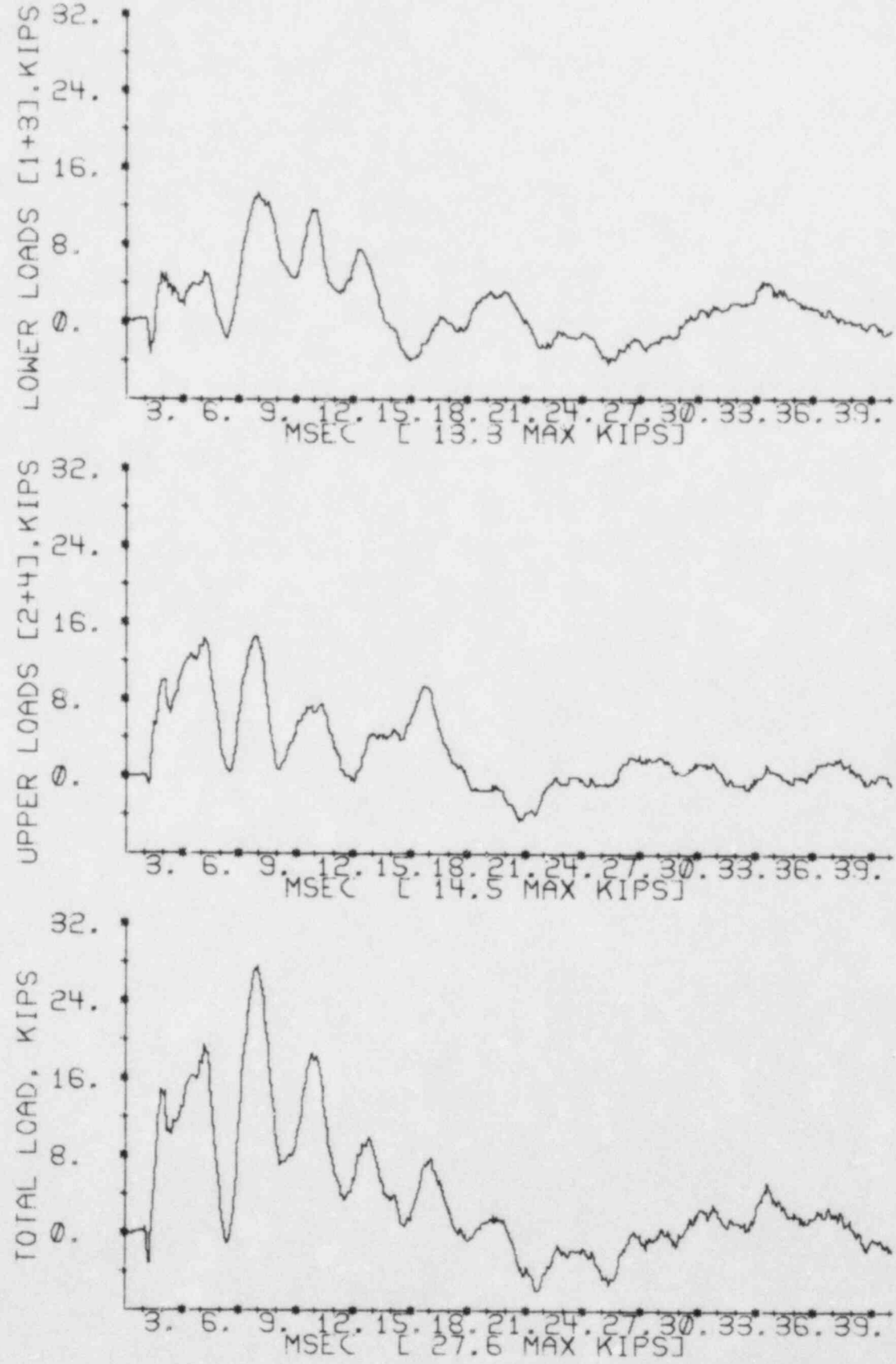

Figure A.3.4-20 Load Cell Data, Experiment Number 32

Data not Obtained

Figure A.3.4-21 Load Cell Data, Experiment Number 26

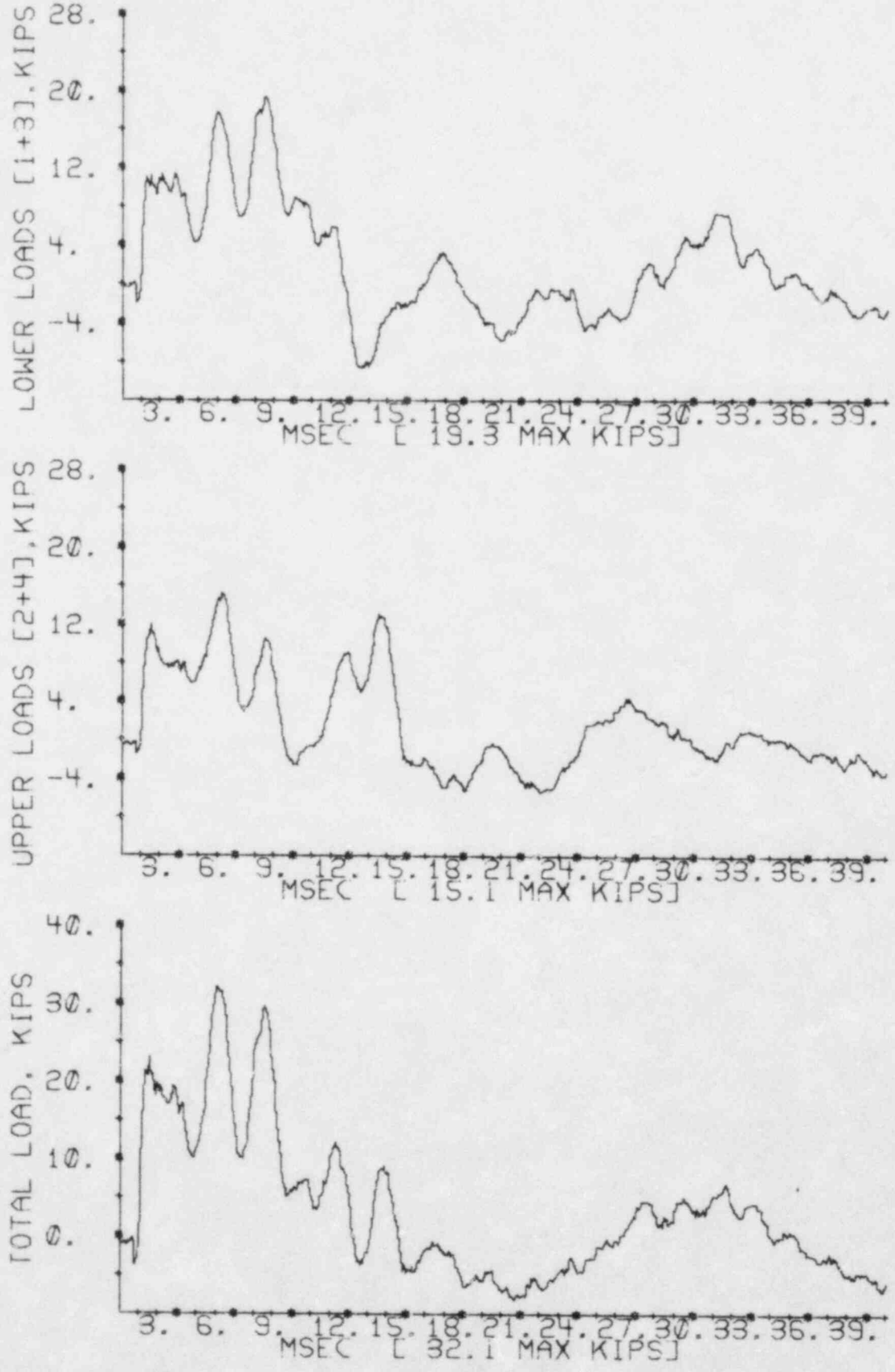

Figure A.3.4-22 Load Cell Data, Experiment Number 45

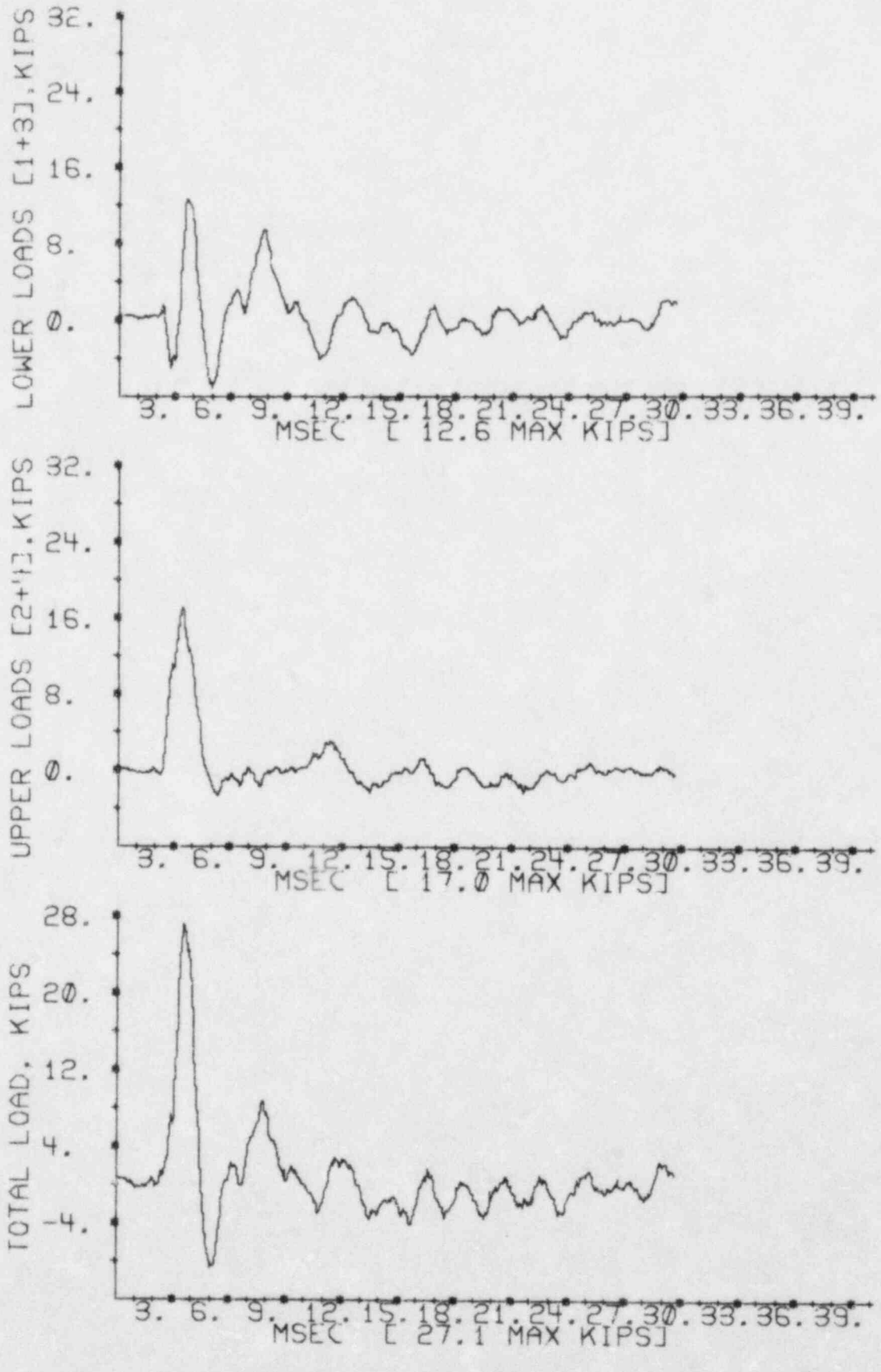

Figure A.3.4-23 Load Cell Data, Experiment Number 42

Data not Obtained

Figure A.3.4-24 Load Cell Data, Experiment Number 15

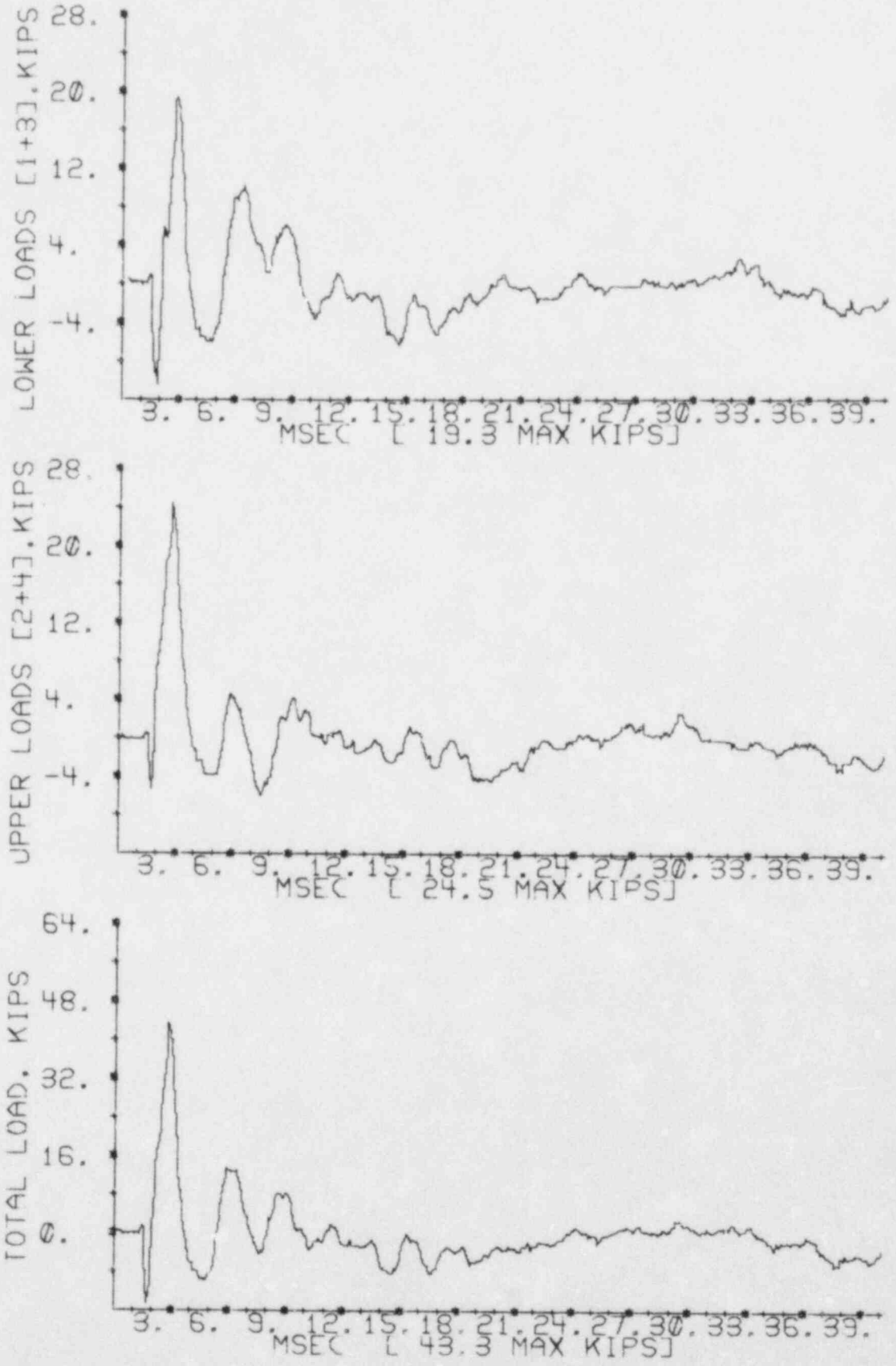

Figure A.3.4-25 Load Cell Data, Experiment Number 19

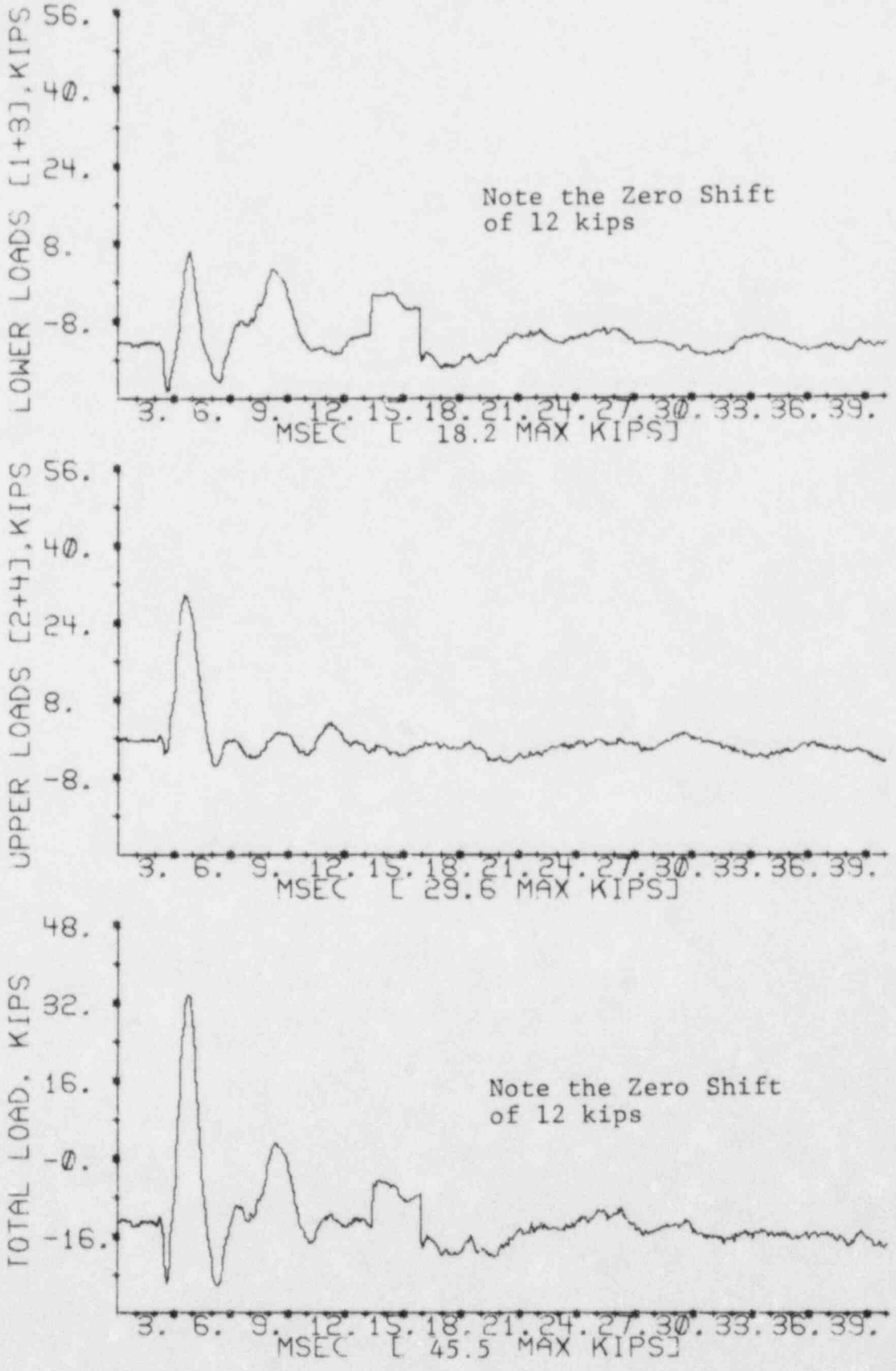

Figure A.3.4-26 Load Cell Data, Experiment Number 14

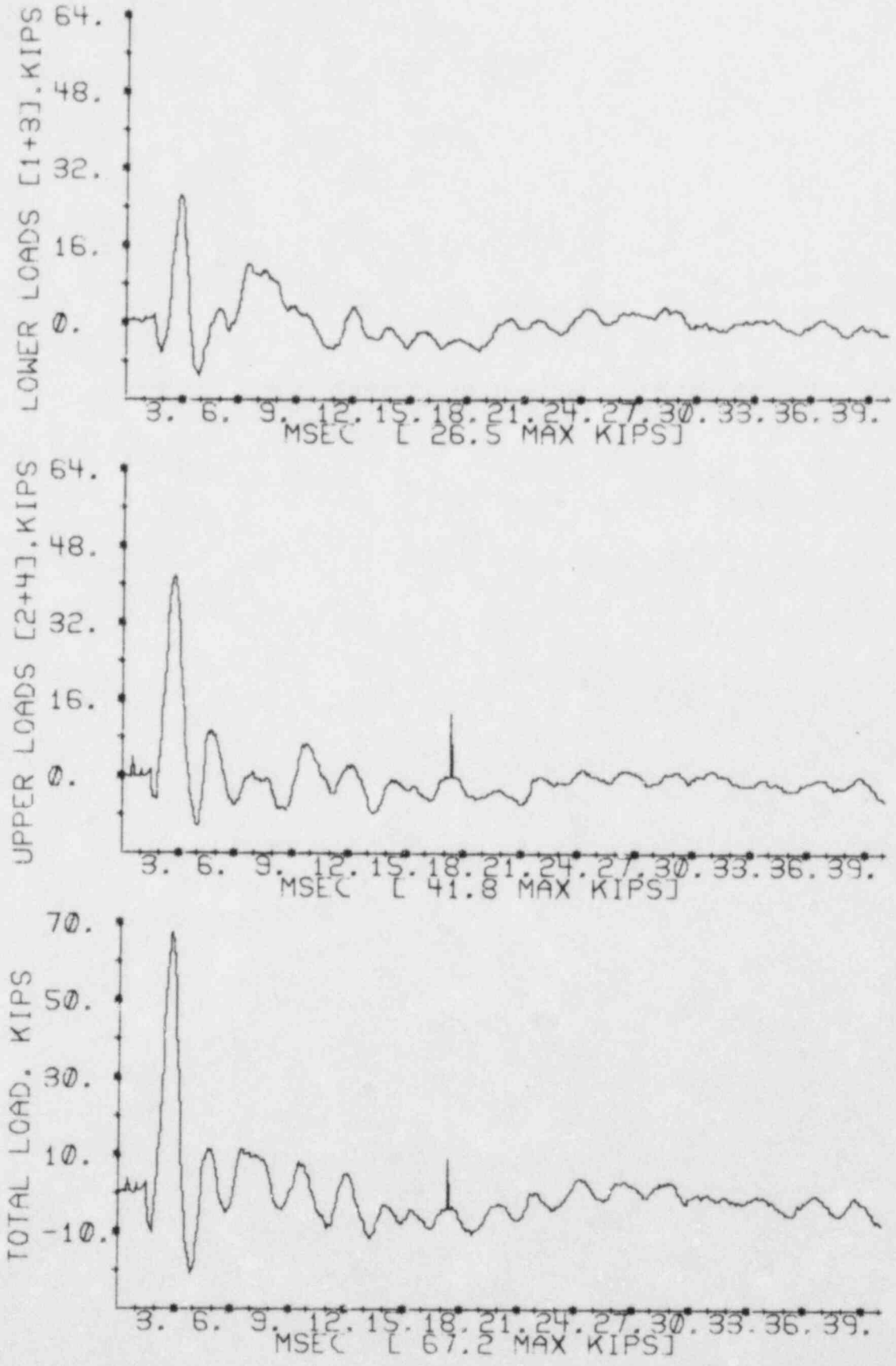

Figure A.3.4-27 Load Cell Data, Experiment Number 24

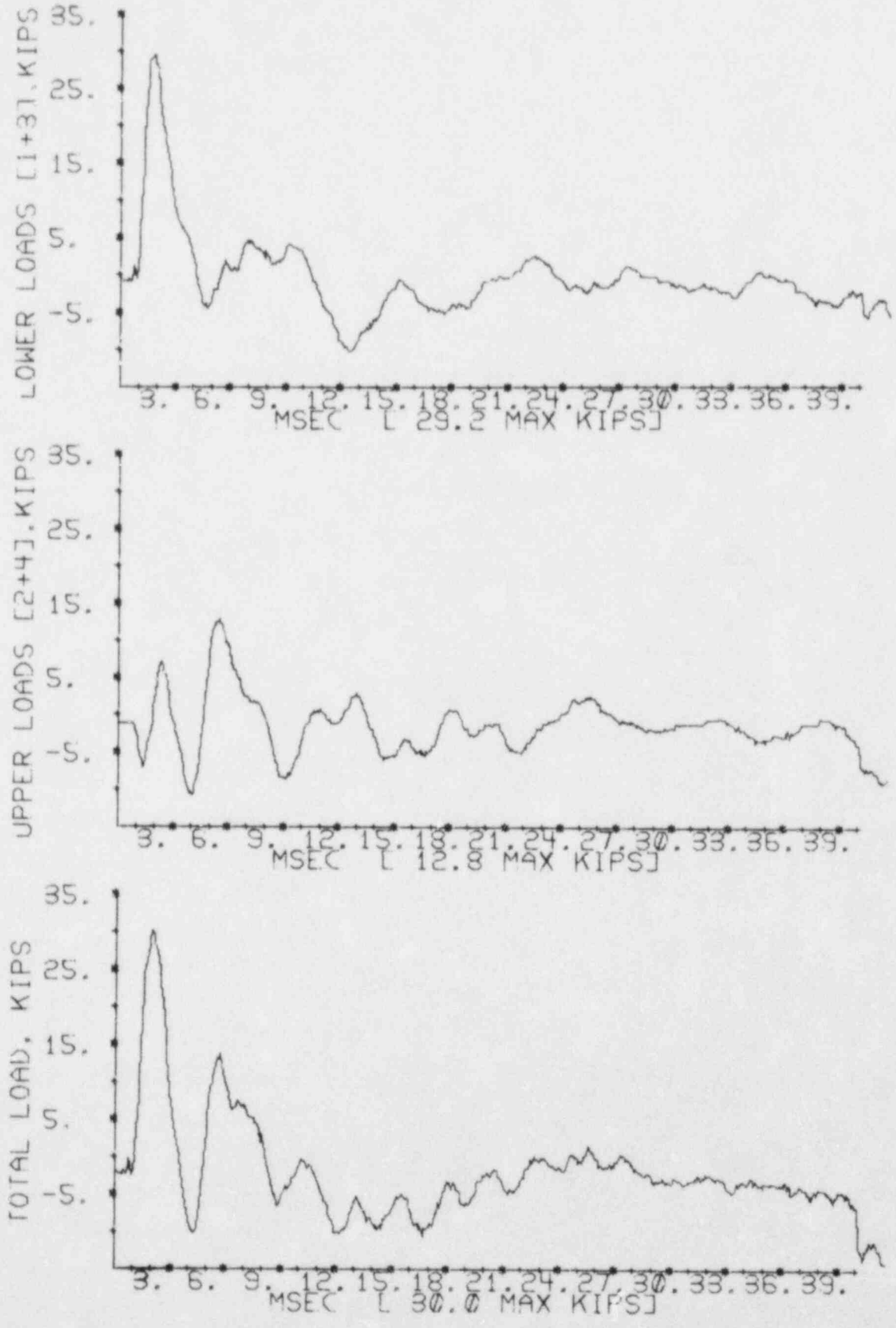

Figure A.3.4-28 Load Cell Data, Experiment Number 17

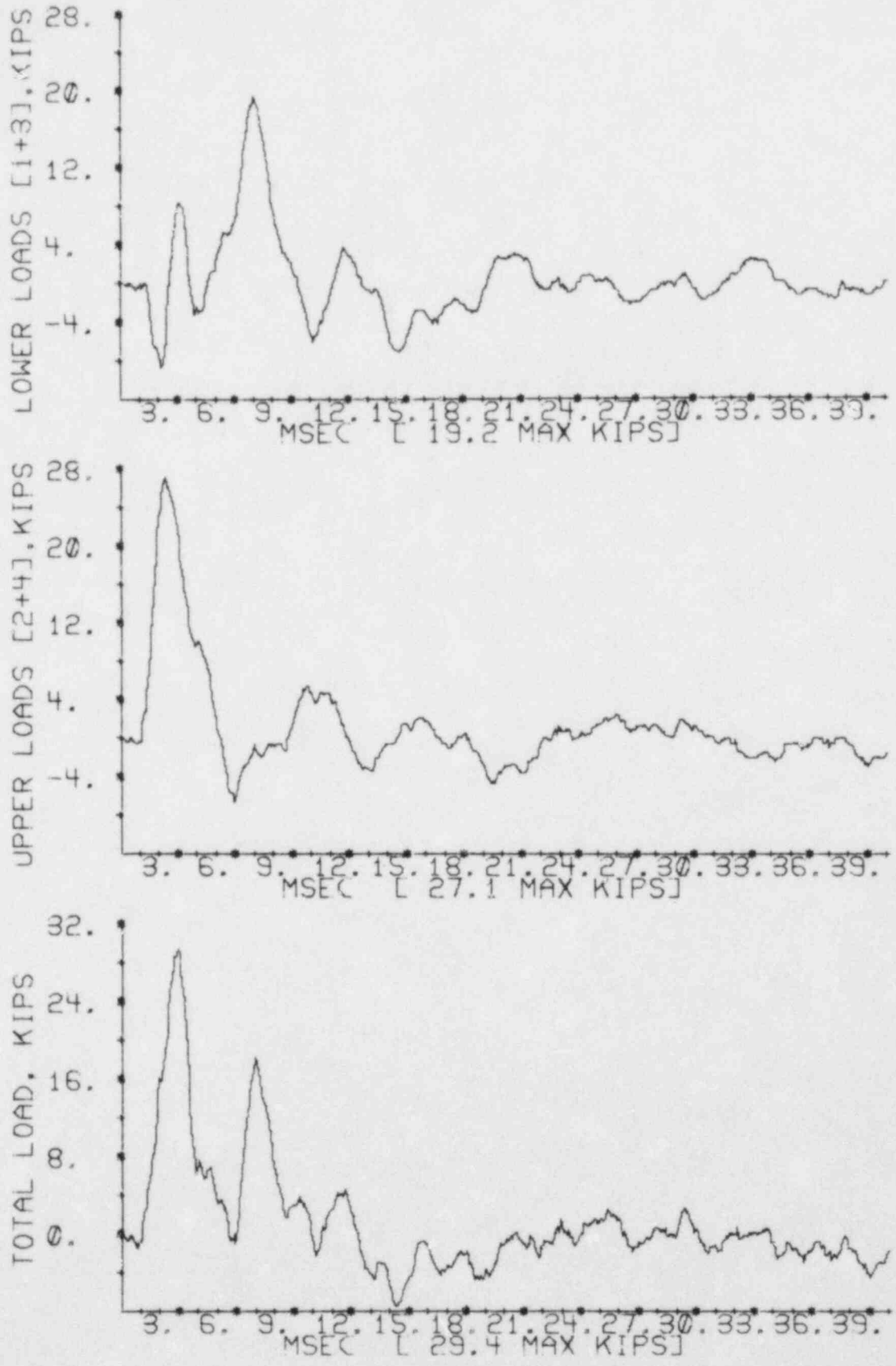

Figure A.3.4-29 Load Cell Data, Experiment Number 18

Barrier Front Face

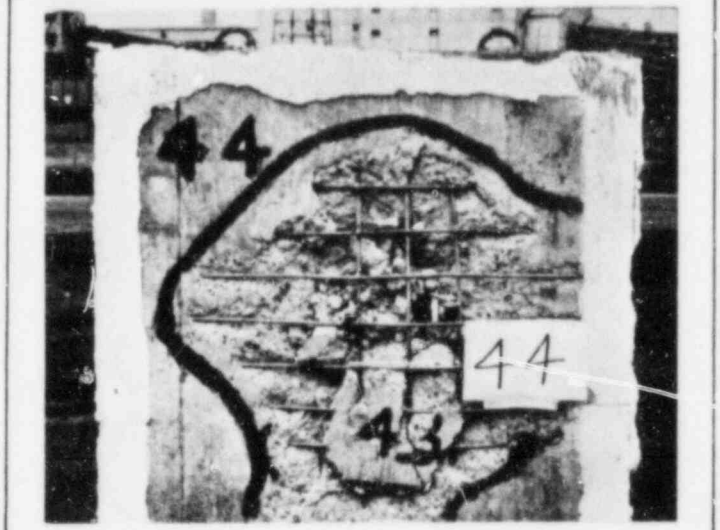

Barrier Rear Face

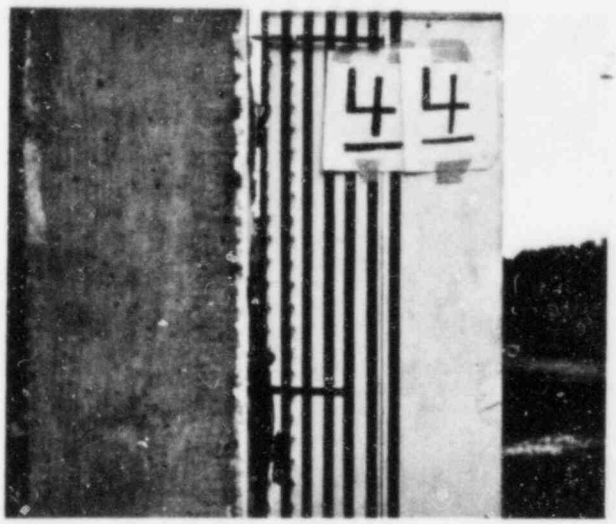

Profile of Rear Rebar or Concrete

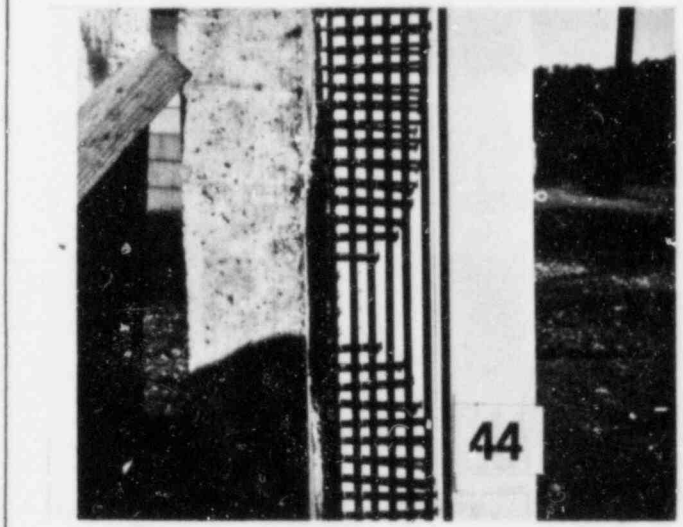

Profile of Back Crater

V = 426 fps

3.375" OD Wood Pole
23.42 lb Solid

Missile

Final Missile Location In Target

Secondary Concrete Missiles

Particle size	1.7	in.
Particle traveled	70	ft
Particle velocity	55	fps

Barrier

Thickness	4.5	in.		
Rebar	# 2	at	3.0	in.

Figure A.3.5-1 Multiple Hit Test No. 44 Table A.3.5-1 Line 1

Barrier Front Face

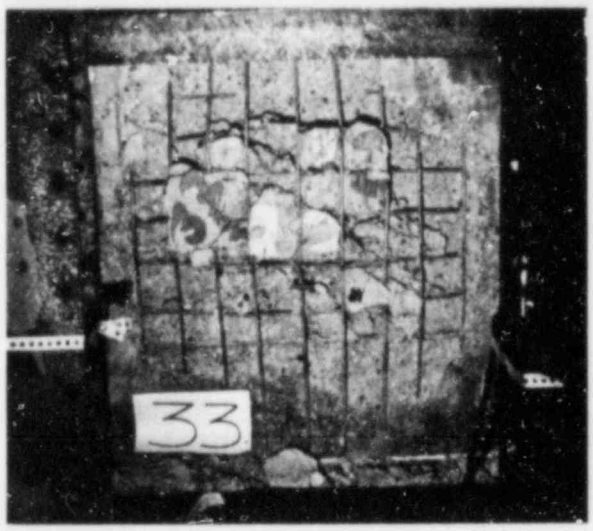

Barrier Rear Face

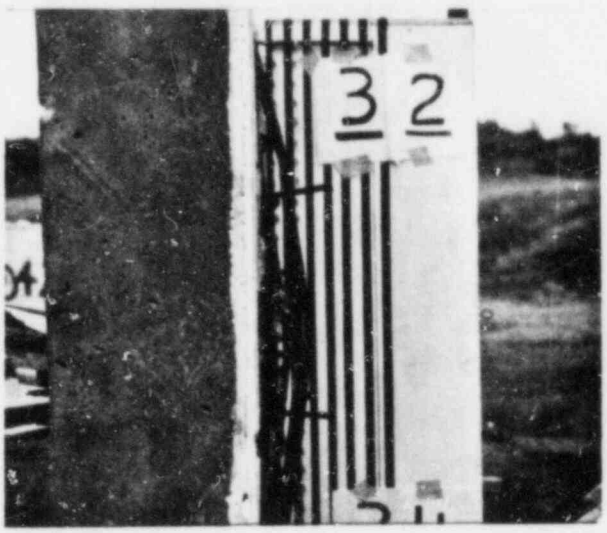

Profile of Rear Rebar or Concrete

No data taken

Profile of Back Crater

V = 378 fps

3.375"OD Wood Pole
23.42 lb Solid

Missile

Final Missile Location In Target

Secondary Concrete Missiles

Particle size	2.6	in.
Particle traveled	30	ft
Particle velocity	30	fps

Barrier

Thickness	6.0	in.
Rebar	# 2 at 3.0	in.

Figure A.3.5-2 Multiple Hit Test No. 33 Table A.3.5-1 Line 2

Barrier Front Face

Barrier Rear Face

Profile of Rear Rebar or Concrete

No data taken

Profile of Back Crater

V = 215 fps

1.69" OD Steel Pipe
4.6 lb 0.12" Thick

Missile

Final Missile Location Rebound

Secondary Concrete Missiles

Particle size	NA	in.
Particle traveled	NA	ft
Particle velocity	NA	fps

Barrier

Thickness	6.0	in.
Rebar	# 2 at 3.0	in.

Figure A.3.5-3 Multiple Hit Test No. 34 Table A.3.5-1 Line 3

Barrier Front Face

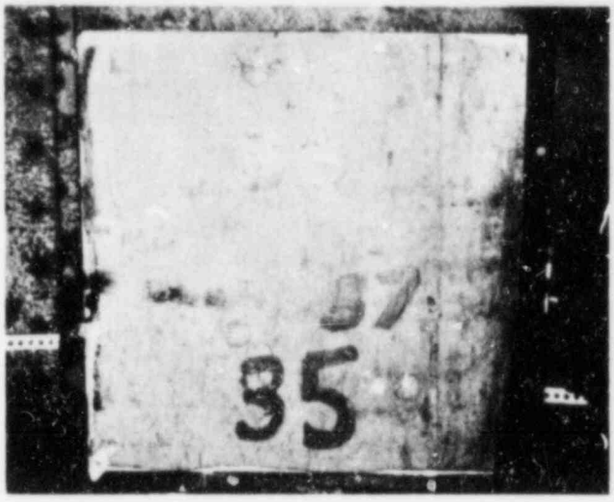

Barrier Rear Face

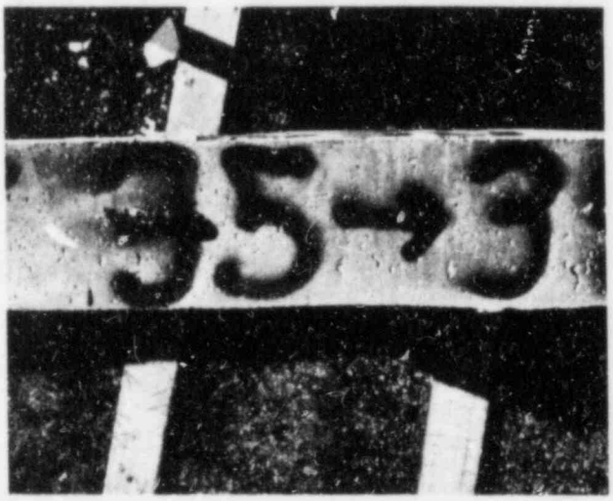

Profile of Rear Rebar or Concrete

Missile tumbled on impact

Profile of Back Crater

V = 517 fps

1.69" OD Steel Pipe
4.6 lb 0.12" Thick

Missile

Final Missile Location Rebound

Secondary Concrete Missiles

Particle size	Missile	in.
Particle traveled	Tumbled	ft
Particle velocity	on Impact	fps

Barrier

Thickness 6.0 in.
Rebar # 3 at 2.5 in.

Figure A.3.5-4 Multiple Hit Test No. 37 Table A.3.5-1 Line 4

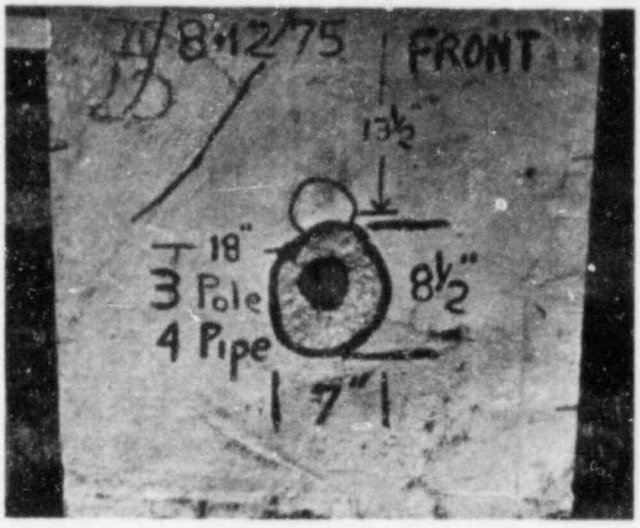

Barrier Front Face

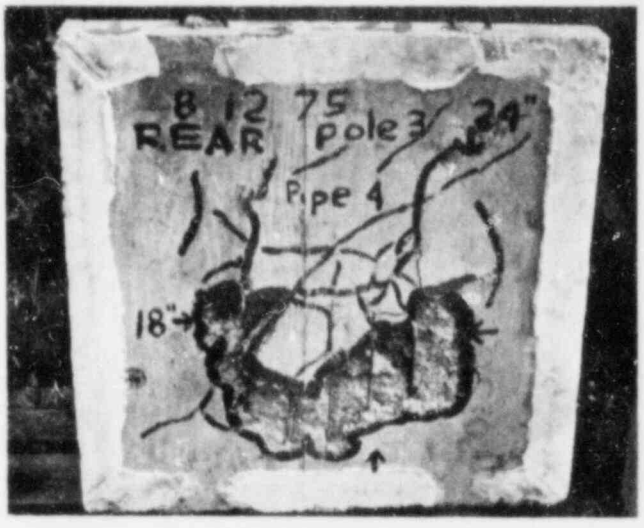

Barrier Rear Face

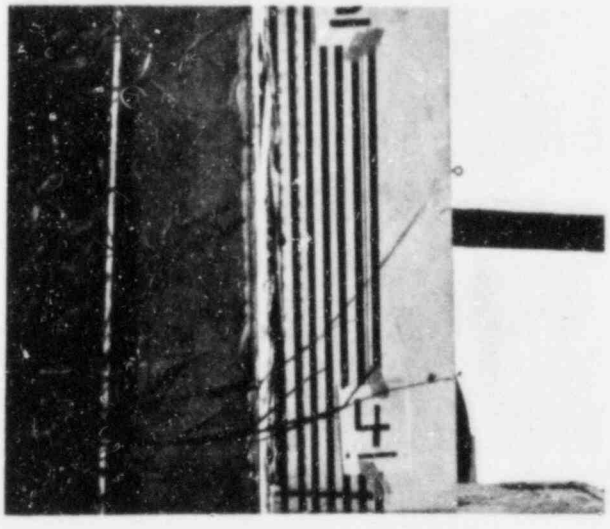

Profile of Rear Rebar or Concrete

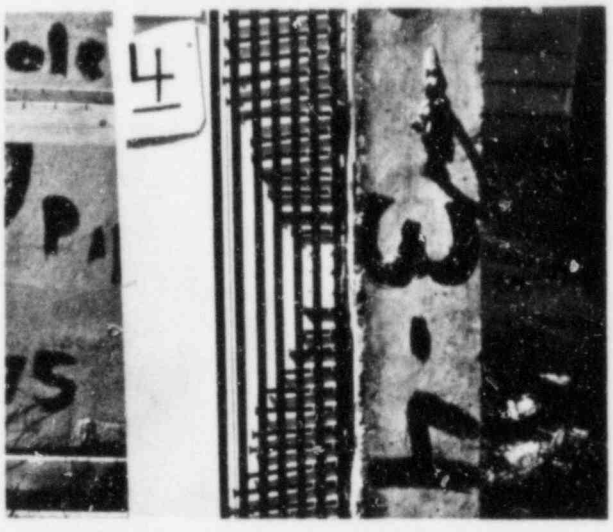

Profile of Back Crater

V = 216 fps

3" OD Steel Pipe
12.3 lb 0.12" Thick

Missile

Final Missile Location Rebound

Secondary Concrete Missiles

Particle size	2.1	in.
Particle traveled	30	ft
Particle velocity	30	fps

Barrier

Thickness	4.5	in.
Rebar	# 2 at 3.0	in.

Figure A.3.5-5 Multiple Hit Test No. 4 Table A.3.5-1 Line 5

Barrier Front Face

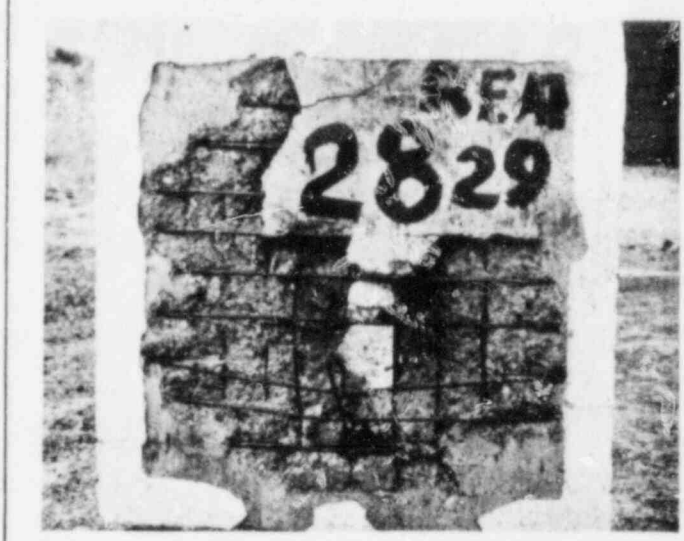

Barrier Rear Face

Profile of Rear Rebar or Concrete

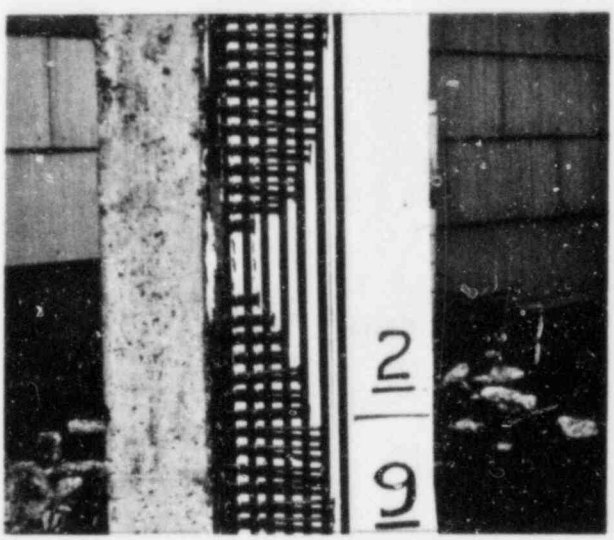

Profile of Back Crater

V = 296 fps

3" OD Steel Pipe
12.3 lb 0.12" Thick

Missile

Final Missile Location Perforated

Secondary Concrete Missiles

Particle size	2.3	in.
Particle traveled	200	ft
Particle velocity	100	fps

Barrier

Thickness	4.5	in.
Rebar	# 2 at 3.0	in.

Figure A.3.5-6 Multiple Hit Test No. 29 Table A.3.5-1 Line 6

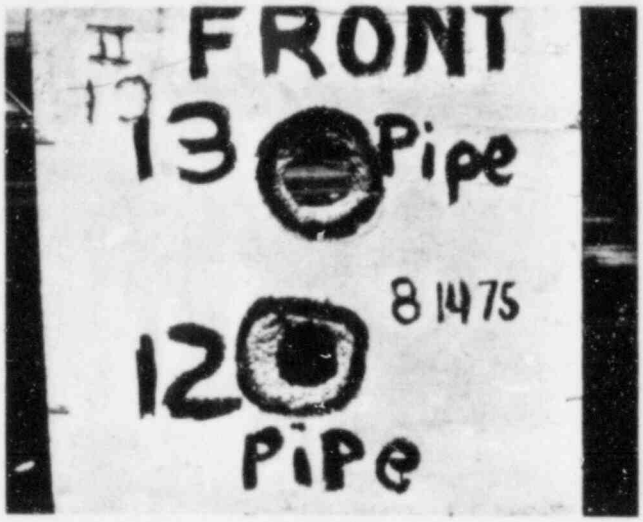

Barrier Front Face

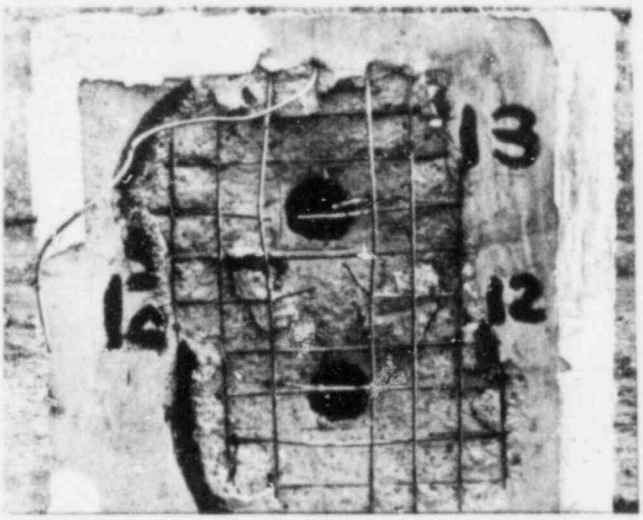

Barrier Rear Face

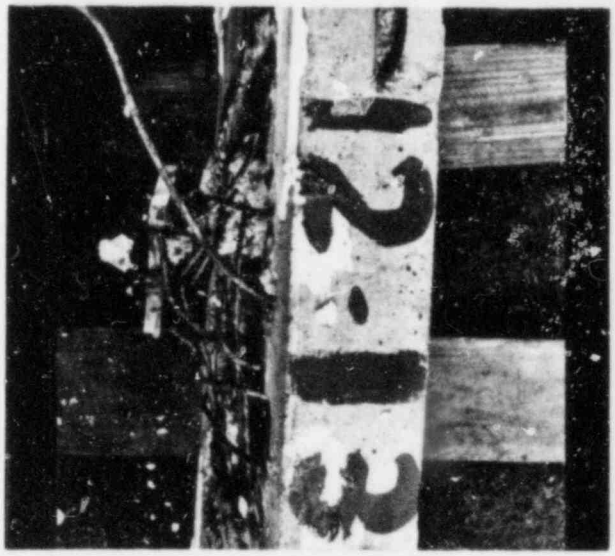

Profile of Rear Rebar or Concrete

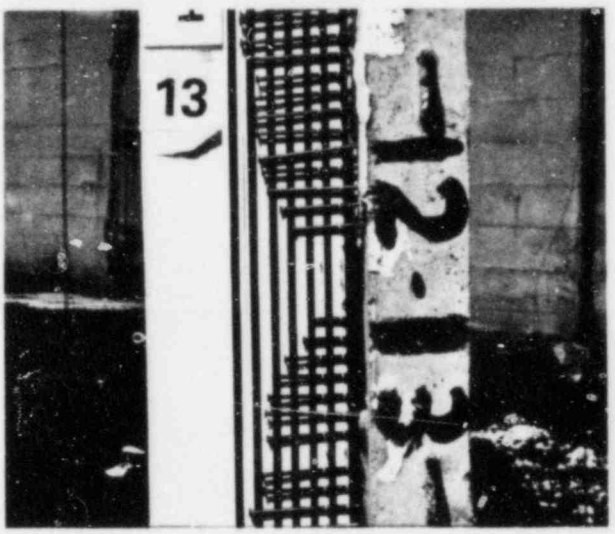

Profile of Back Crater

V = 329 fps

3" OD Steel Pipe
12.3 lb 0.12" Thick

Missile

Final Missile Location Perforated

Secondary Concrete Missiles

Particle size	1.7	in.
Particle traveled	200	ft
Particle velocity	100	fps

Barrier

Thickness	4.5	in.
Rebar	# 2 at 3.0	in.

Figure A.3.5-7 Multiple Hit Test No. 13 Table A.3.5-1 Line 7

Barrier Front Face

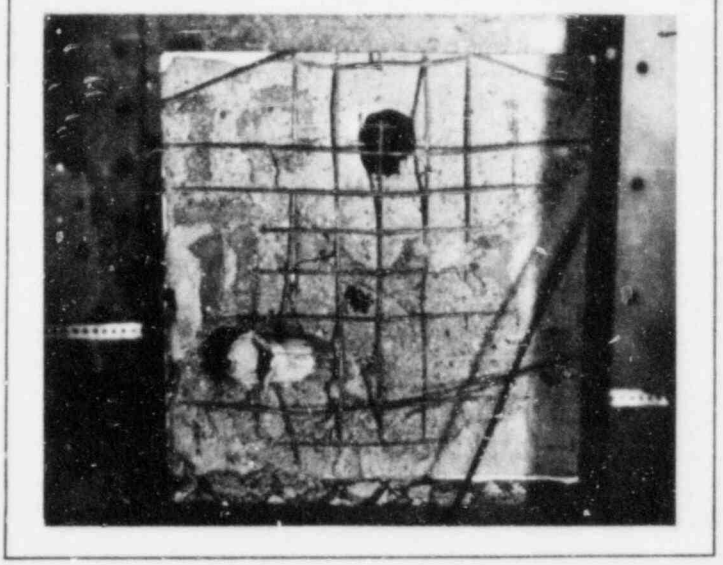

Barrier Rear Face

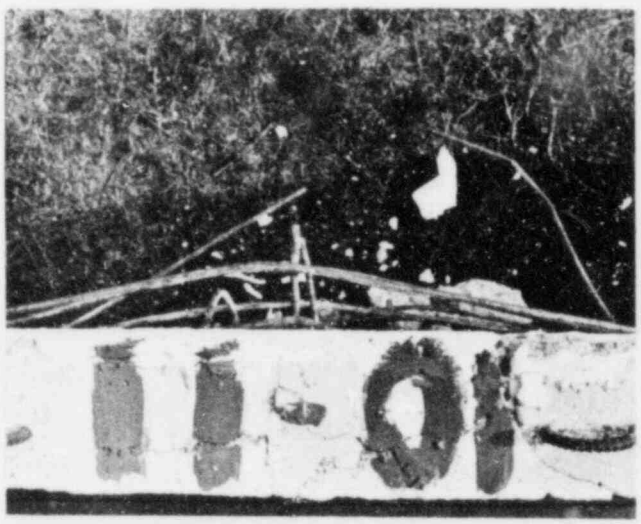

Profile of Rear Rebar or Concrete

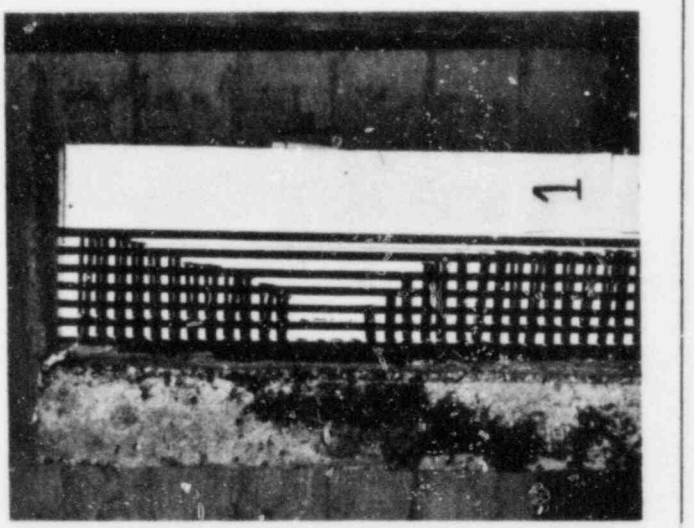

Profile of Back Crater

V = 399 fps

3" OD Steel Pipe
12.3 lb 0.12" Thick

Missile

Final Missile Location In Target

Secondary Concrete Missiles

Particle size	1.3	in.
Particle traveled	220	ft
Particle velocity	105	fps

Barrier

Thickness	4.5	in.
Rebar	# 2 at 3.0	in.

Figure A.3.5-8 Multiple Hit Test No. 11 Table A.3.5-1 Line 8

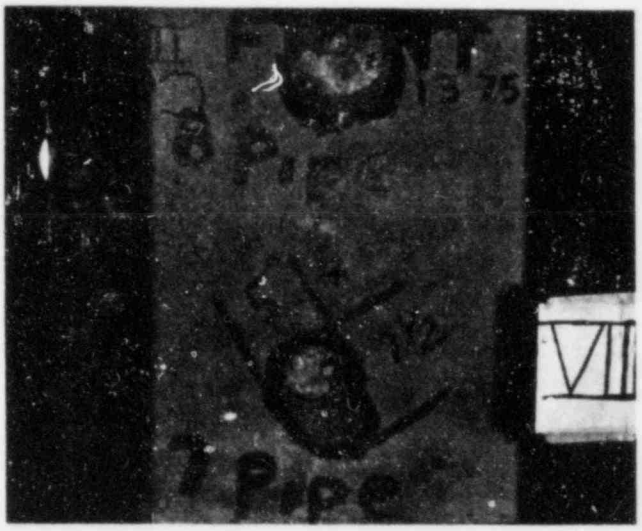

Barrier Front Face

Barrier Rear Face

No data

Missile hit at edge beam

Profile of Rear Rebar or Concrete

No data

Missile hit at edge beam

Profile of Back Crater

V = 403 fps

3" OD Steel Pipe
12.3 lb 0.12" Thick

Missile

Final Missile Location Rebound

Secondary Concrete Missiles

Particle size	Hit	in.
Particle traveled	Edge	ft
Particle velocity	of Target	fps

Barrier

Thickness 4.5 in.
Rebar # 2 at 3.0 in.

Figure A.3.5-9 Multiple Hit Test No. 8 Table A.3.5-1 Line 9

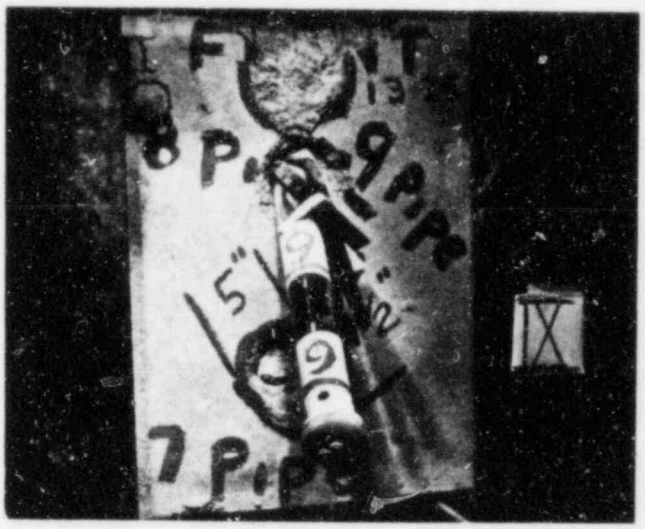

Barrier Front Face

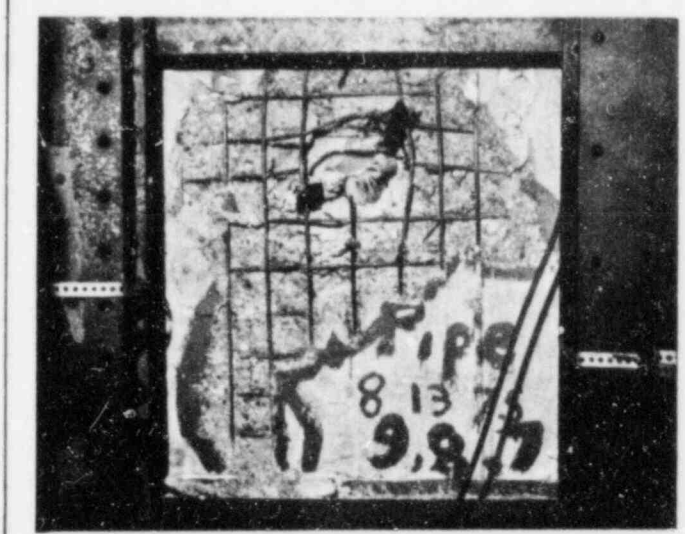

Barrier Rear Face

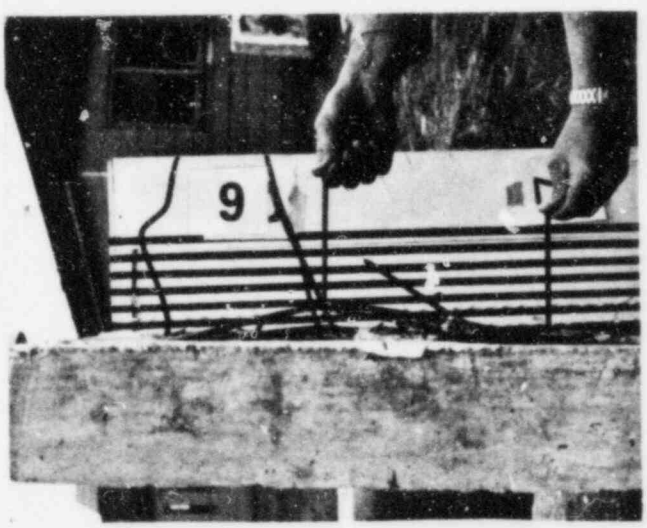

Profile of Rear Rebar or Concrete

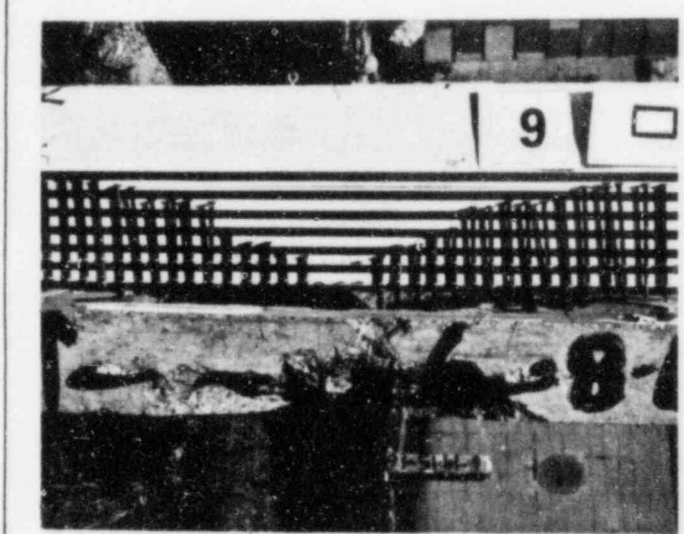

Profile of Back Crater

V = 403 fps

3" OD Steel Pipe
12.3 lb 0.12" Thick

Missile

Final Missile Location In Target

Secondary Concrete Missiles

Particle size	1.0	in.
Particle traveled	220	ft
Particle velocity	105	fps

Barrier

Thickness	4.5	in.
Rebar	# 2 at 3.0	in.

Figure A.3.5-10 Multiple Hit Test No. 9 Table A.3.5-1 Line 10

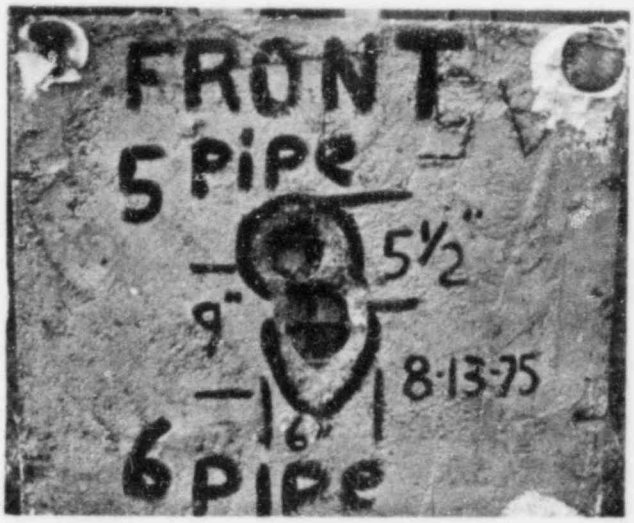

Barrier Front Face

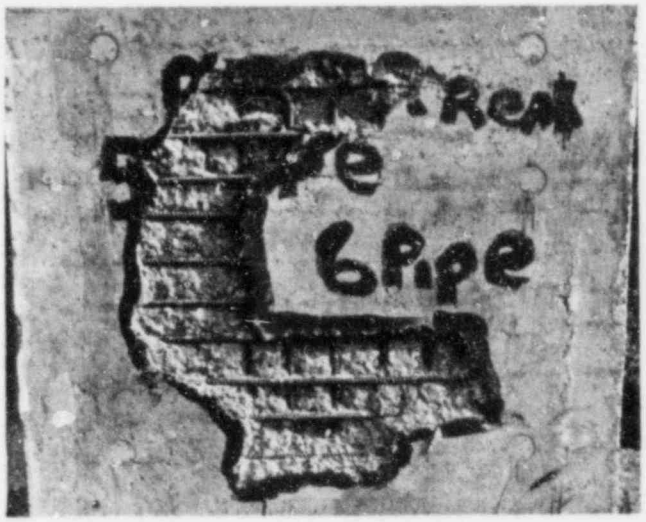

Barrier Rear Face

Profile of Rear Rebar or Concrete

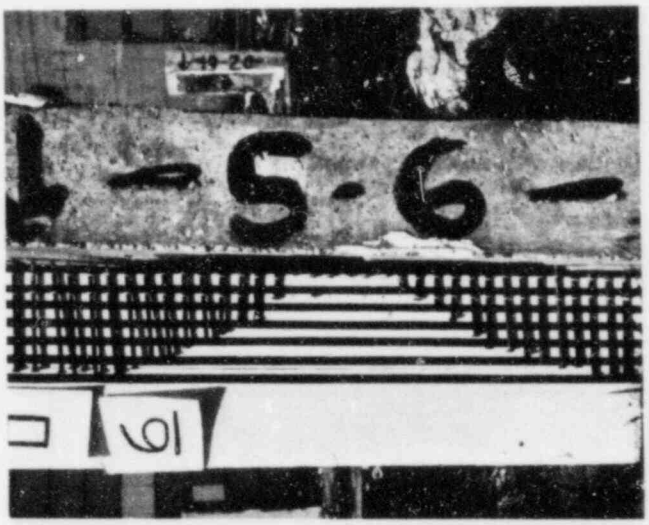

Profile of Back Crater

V = 343 fps

3" OD Steel Pipe
12.3 lb 0.12" Thick

Missile

Final Missile Location Rebound

Secondary Concrete Missiles

Particle size	2.1	in.
Particle traveled	60	ft
Particle velocity	50	fps

Barrier

Thickness	6.0	in.
Rebar	# 3 at 2.5	in.

Figure A.3.5-11 Multiple Hit Test No. 6 Table A.3.5-1 Line 11

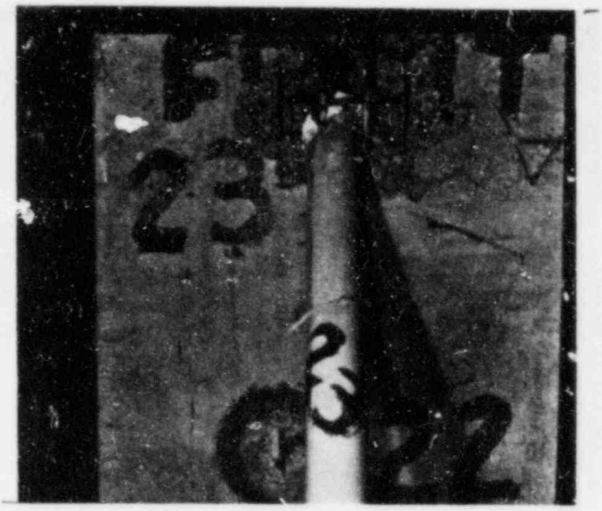

Barrier Front Face

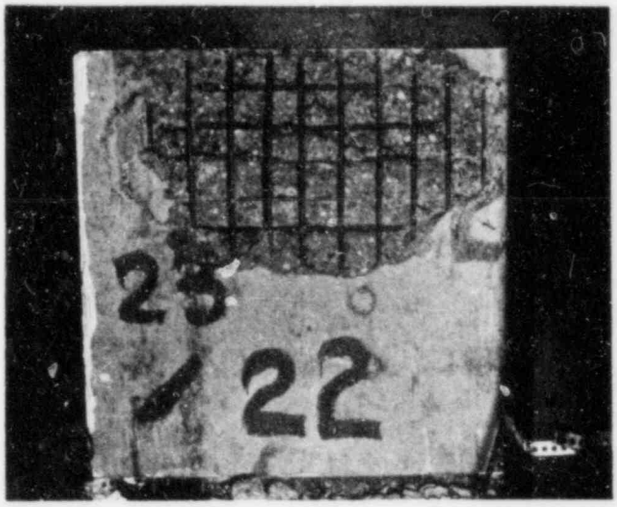

Barrier Rear Face

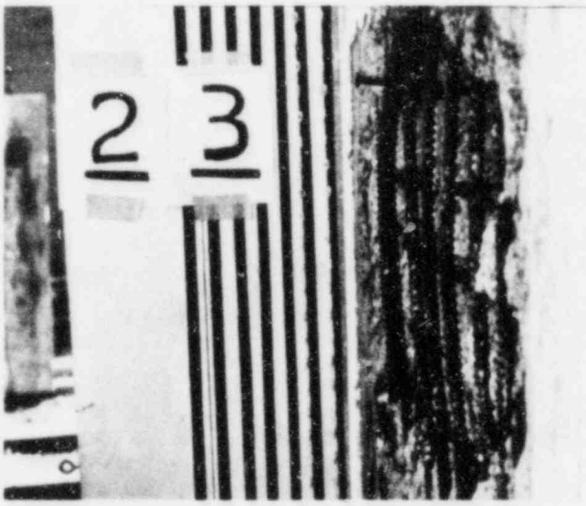

Profile of Rear Rebar or Concrete

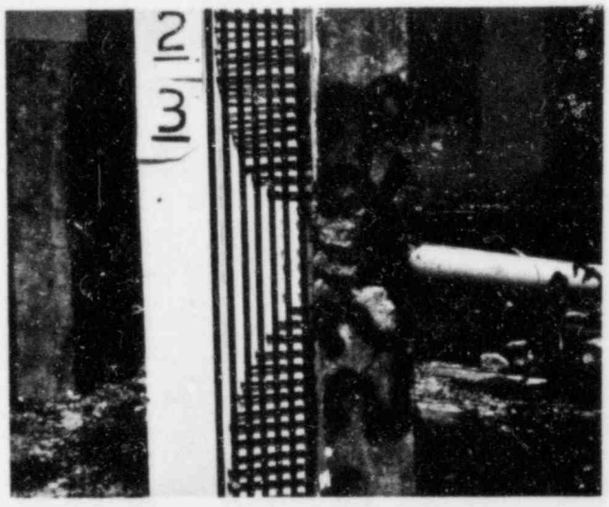

Profile of Back Crater

No Photo Taken

V = 369 fps

3" OD Steel Pipe
12.3 lb 0.12" Thick

Missile

Final Missile Location Rebound

Secondary Concrete Missiles

Particle size	0.8	in.
Particle traveled	100	ft
Particle velocity	65	fps

Barrier

Thickness	6.0	in.
Rebar	# 3 at 2.5	in.

Figure A.3.5-12 Multiple Hit Test No. 23 Table A.3.5-1 Line 12

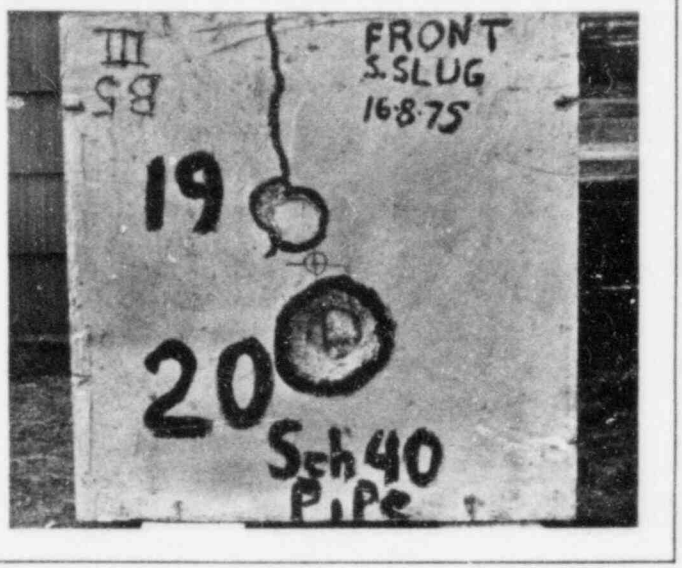

Barrier Front Face

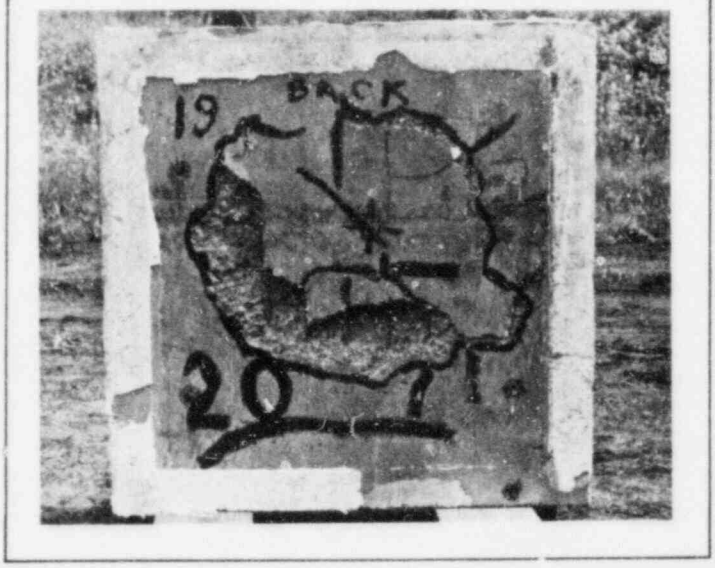

Barrier Rear Face

Profile of Rear Rebar or Concrete

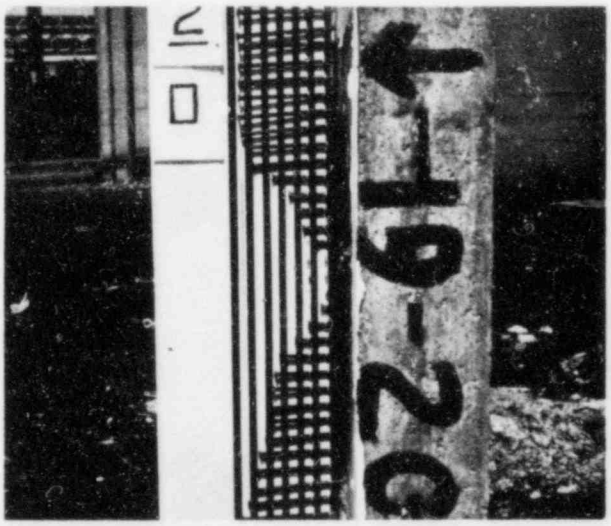

Profile of Back Crater

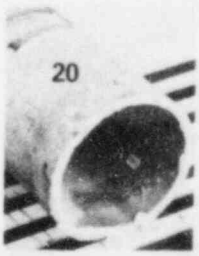

V = 208 fps

3.5" OD Steel Pipe
11.25 lb 0.216" Thick

Missile

Final Missile Location Rebound

Secondary Concrete Missiles

Particle size	1.3	in.
Particle traveled	20	ft
Particle velocity	25	fps

Barrier

Thickness	6.0	in.
Rebar	# 2 at 3.0	in.

Figure A.3.5-13 Multiple Hit Test No. 20 Table A.3.5-1 Line 13

Barrier Front Face

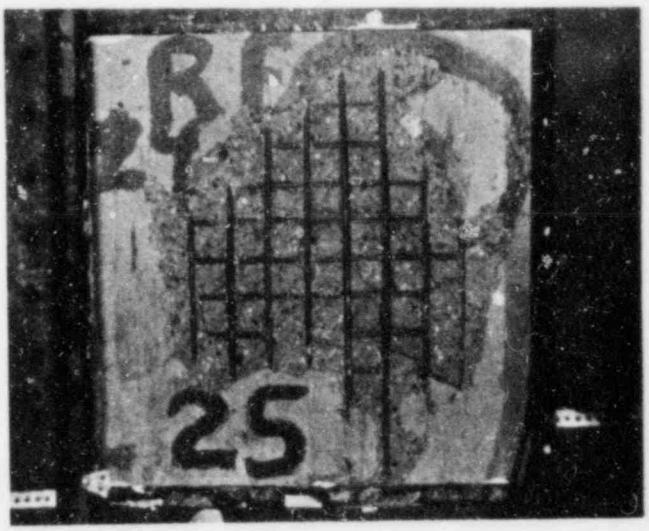

Barrier Rear Face

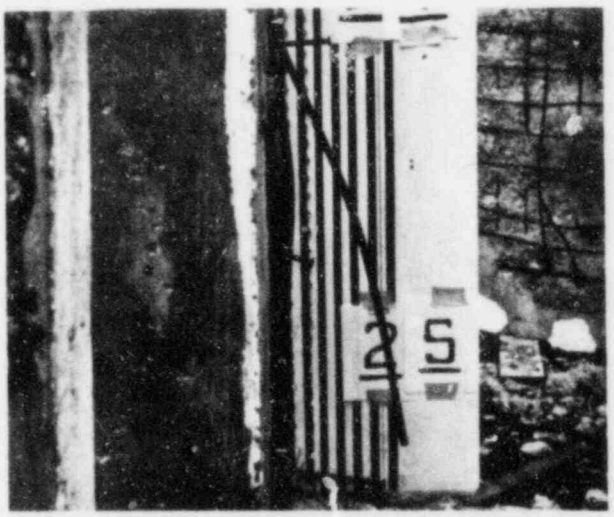

Profile of Rear Rebar or Concrete

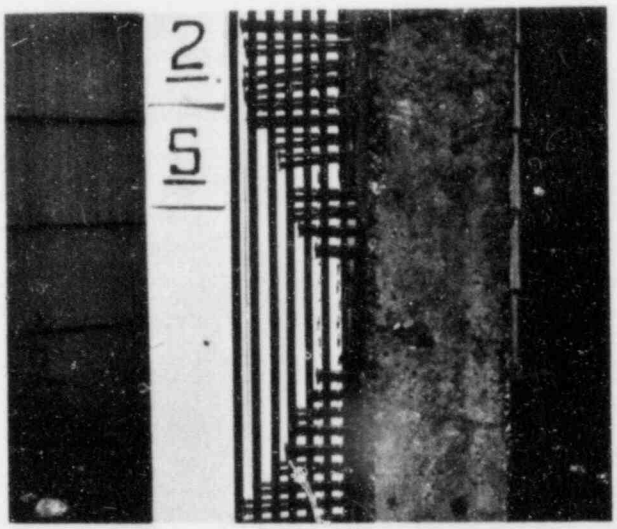

Profile of Back Crater

V = 413 fps

3.5" Steel Pipe
11.25 lb 0.216" Thick

Missile

Final Missile Location Rebound

Secondary Concrete Missiles

Particle size	1.6	in.
Particle traveled	145	ft
Particle velocity	80	fps

Barrier

Thickness	6.0	in.
Rebar	# 3 at 2.5	in.

Figure A.3.5-14 Multiple Hit Test No. 25 Table A.3.5-1 Line 14

Barrier Front Face

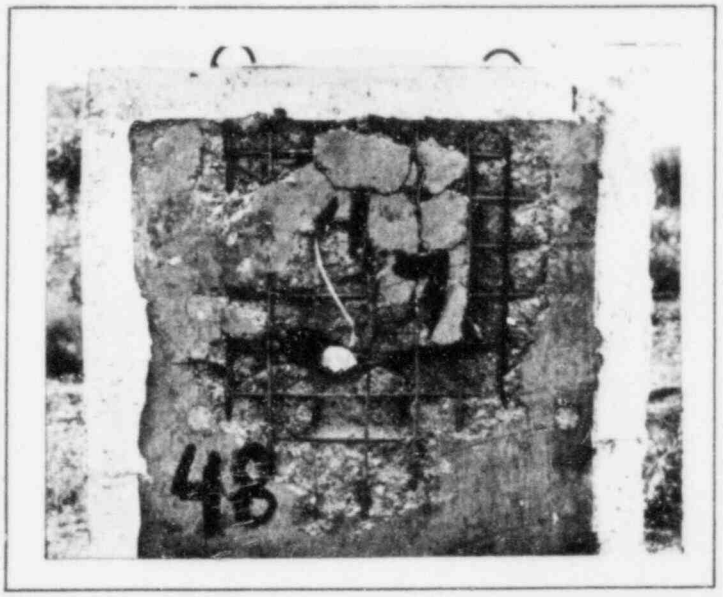

Barrier Rear Face

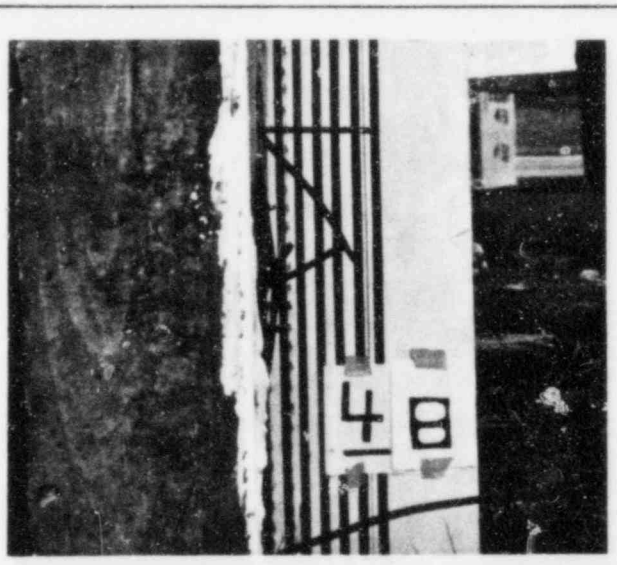

Profile of Rear Rebar or Concrete

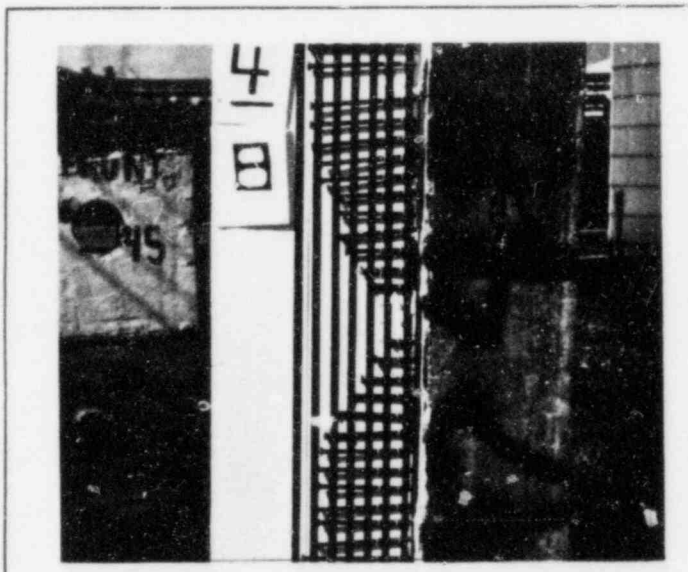

Profile of Back Crater

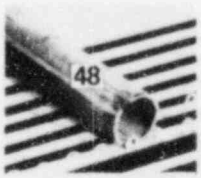

V = 373 fps

1.69" OD Steel Pipe
10.4 lb 0.12" Thick

Missile

Final Missile Location In Target

Secondary Concrete Missiles

Particle size	2.0	in.
Particle traveled	110	ft
Particle velocity	70	fps

Barrier

Thickness	6.0	in.
Rebar	# 2 at 3.0	in.

Figure A.3.5-15 Multiple Hit Test No. 48 Table A.3.5-1 Line 15

Barrier Front Face

Barrier Rear Face

Profile of Rear Rebar or Concrete

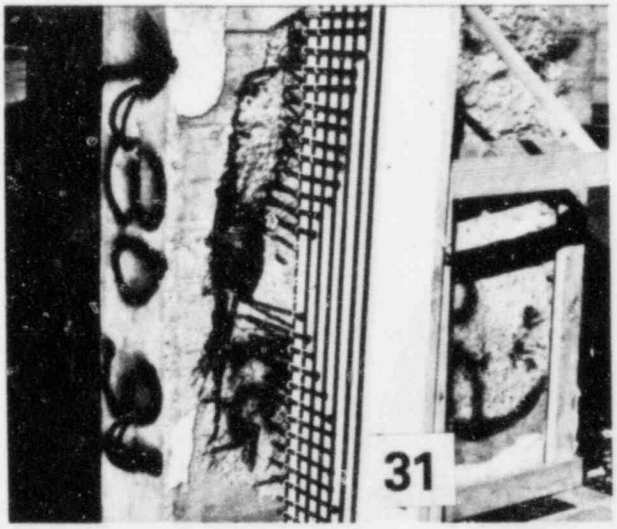

Profile of Back Crater

V = 329 fps

3" OD Steel Pipe
26.5 lb 0.12" Thick

Missile

Final Missile Location Perforated

Secondary Concrete Missiles

Particle size	2.4	in.
Particle traveled	240	ft
Particle velocity	110	fps

Barrier

Thickness	6.0	in.
Rebar	# 2 at 3.0	in.

Figure A.3.5-16 Multiple Hit Test No. 31 Table A.3.5-1 Line 16

Barrier Front Face

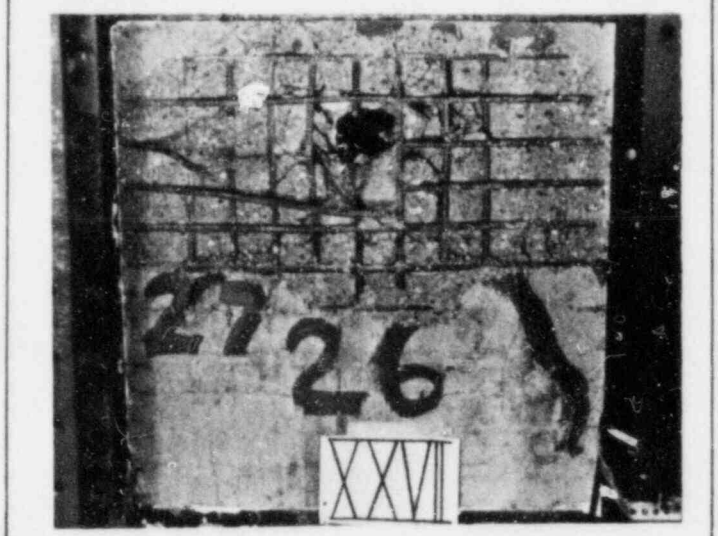

Barrier Rear Face

Profile of Rear Rebar or Concrete

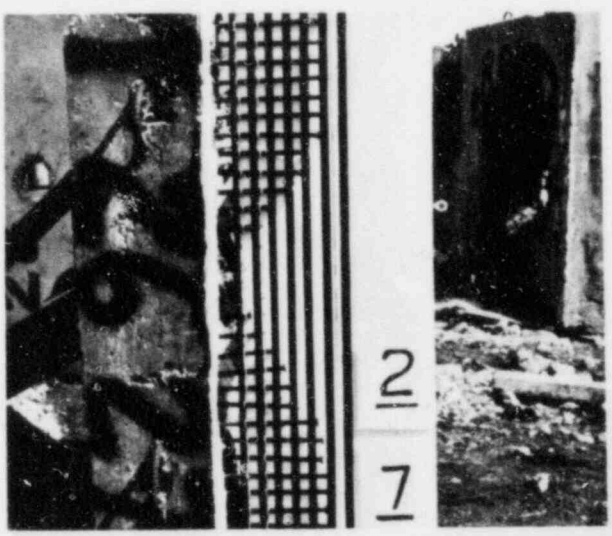

Profile of Back Crater

V = 340 fps

3" OD Steel Pipe
26.5 lb 0.12" Thick

Missile

Final Missile Location Perforated

Secondary Concrete Missiles

Particle size	1.9	in.
Particle traveled	230	ft
Particle velocity	105	fps

Barrier

Thickness	6.0	in.
Rebar	# 3 at 2.5	in.

Figure A.3.5-17 Multiple Hit Test No. 27 Table A.3.5-1 Line 17

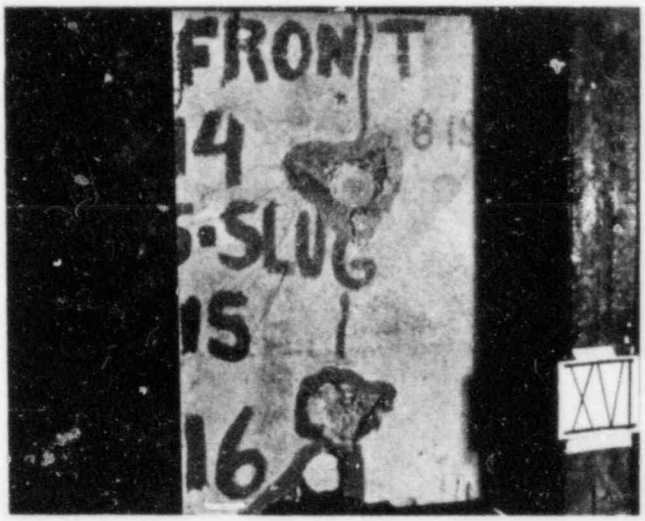

Barrier Front Face

Barrier Rear Face

Profile of Rear Rebar or Concrete

No profile taken

Profile of Back Crater

V = 207 fps

3" OD Steel Slug
12.6 lb Solid

Missile

Final Missile Location In Target

Secondary Concrete Missiles

Particle size	Hit	in.
Particle traveled	Edge	ft
Particle velocity	of Target	fps

Barrier

Thickness	6.0	in.
Rebar	# 2 at 3.0	in.

Figure A.3.5-18 Multiple Hit Test No. 16 Table A.3.5-1 Line 18

Barrier Front Face

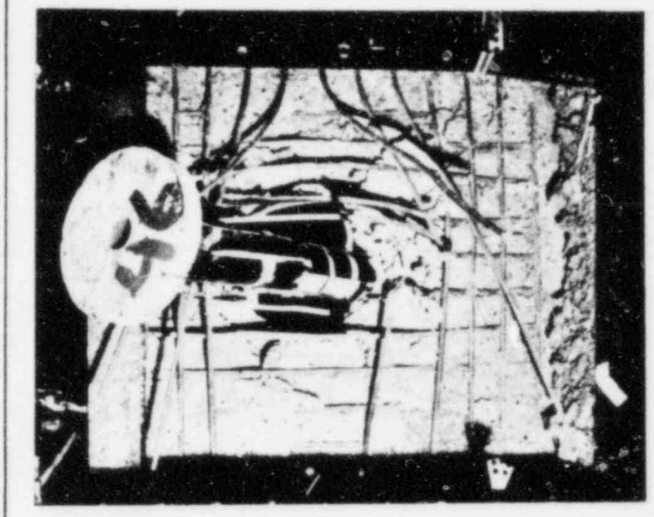

Barrier Rear Face

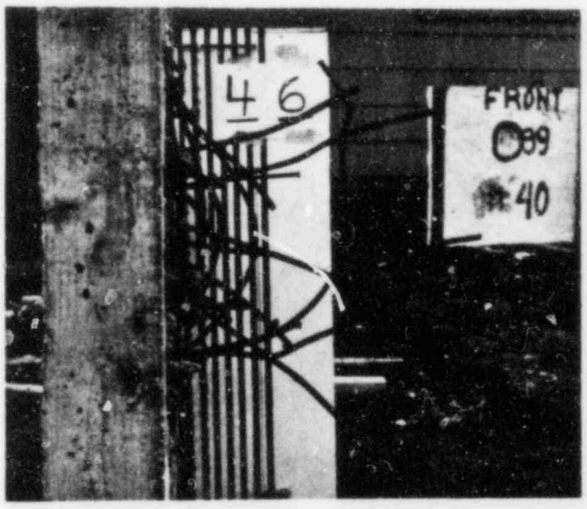

Profile of Rear Rebar or Concrete

No profile taken

Profile of Back Crater

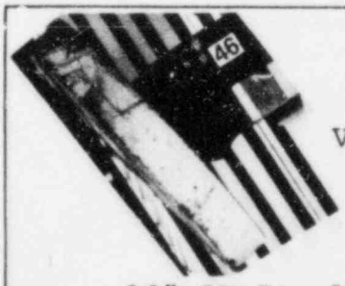

V = 200 fps

10" OD Steel Plate with Pipe

Missile

Final Missile Location In Target

Secondary Concrete Missiles

Particle size	1.5	in.
Particle traveled	260	ft
Particle velocity	115	fps

Barrier

Thickness	6.0	in.
Rebar	# 3 at 2.5	in.

Figure A.3.5-19 Multiple Hit Test No. 46 Table A.3.5-1 Line 19

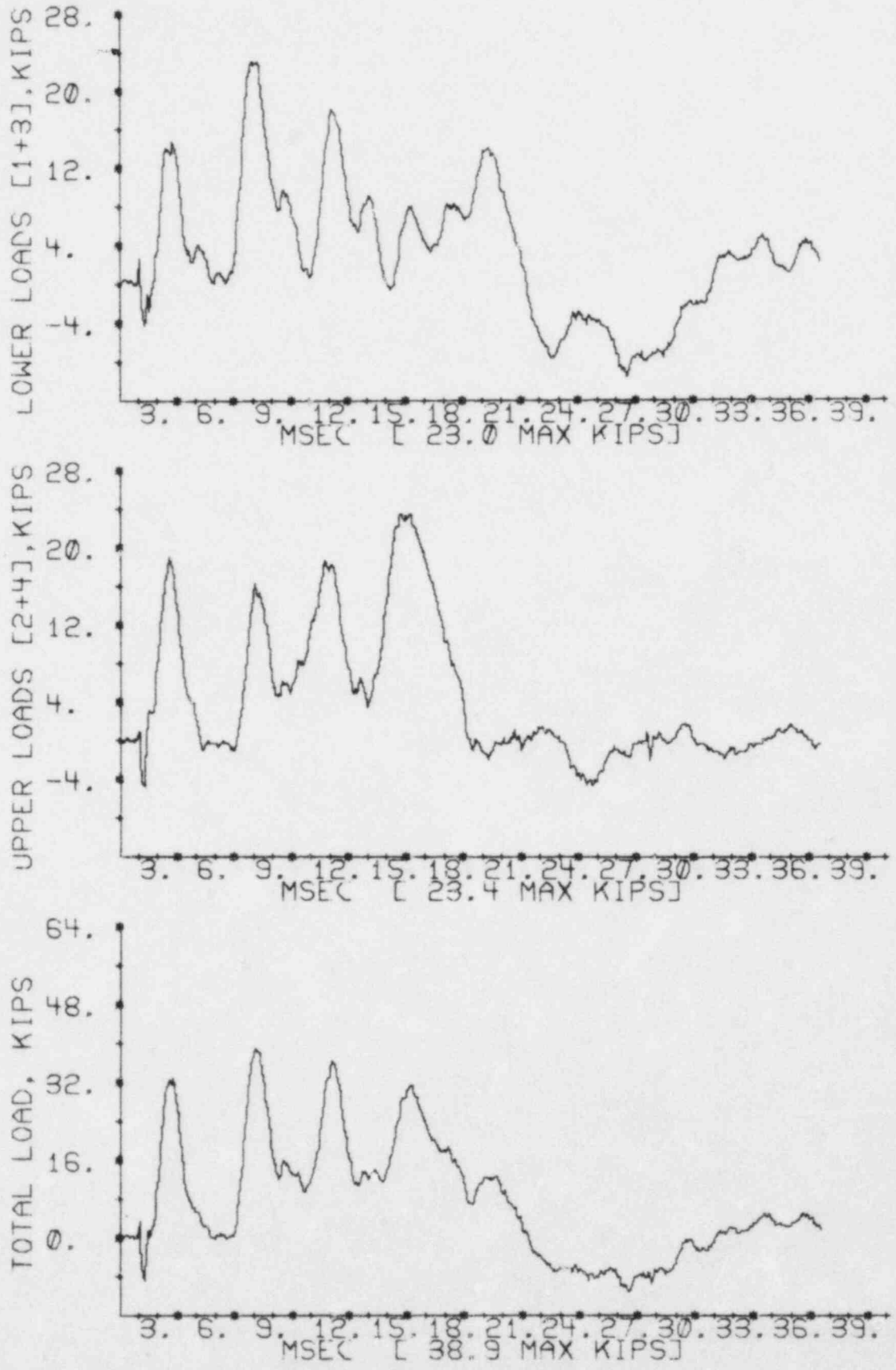

Figure A.3.6-1 Load Cell Data, Experiment Number 44

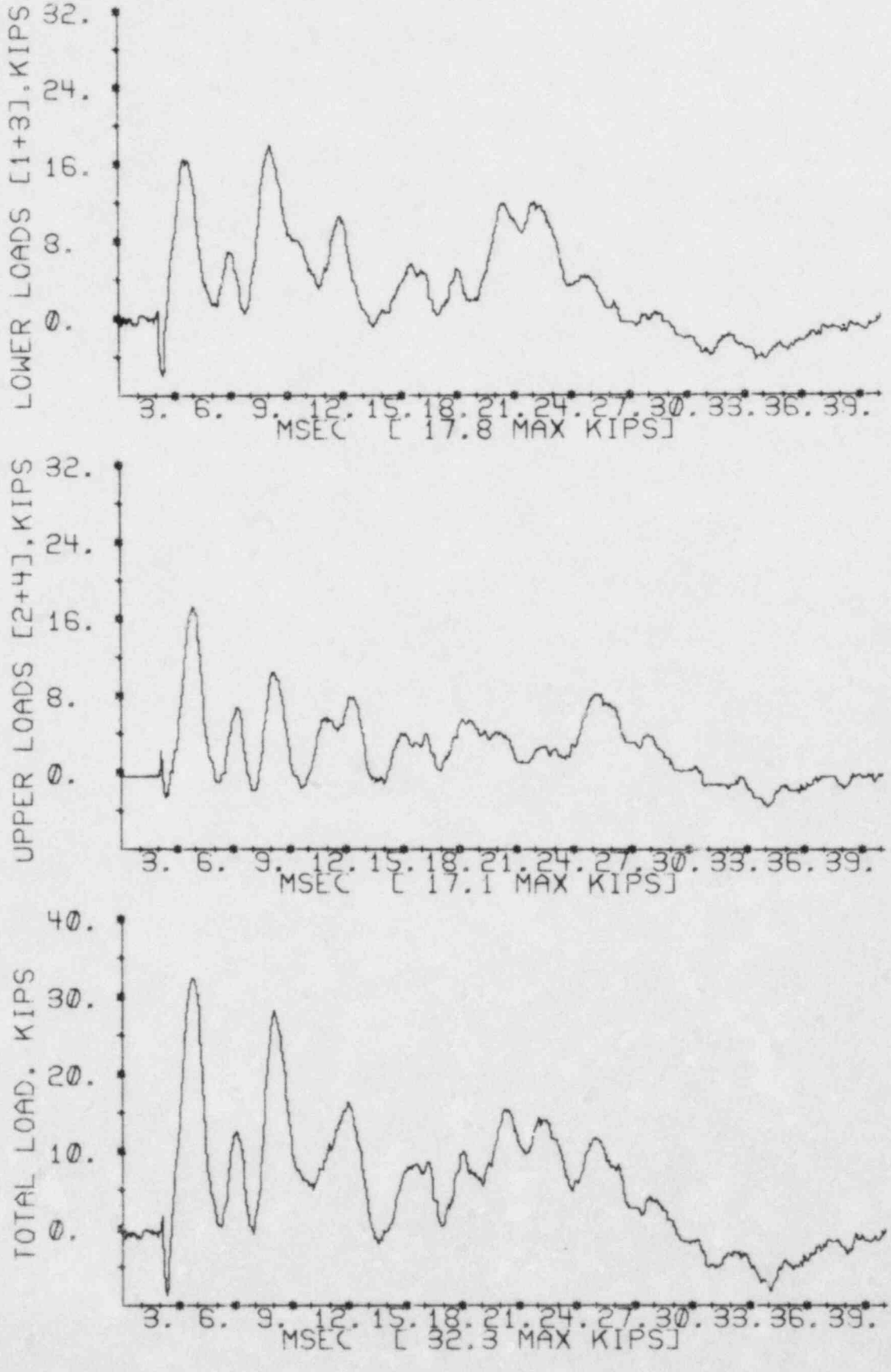

Figure A.3.6-2 Load Cell Data, Experiment Number 33

Data Not Obtained

Figure A.3.6-3 Load Cell Data, Experiment Number 34

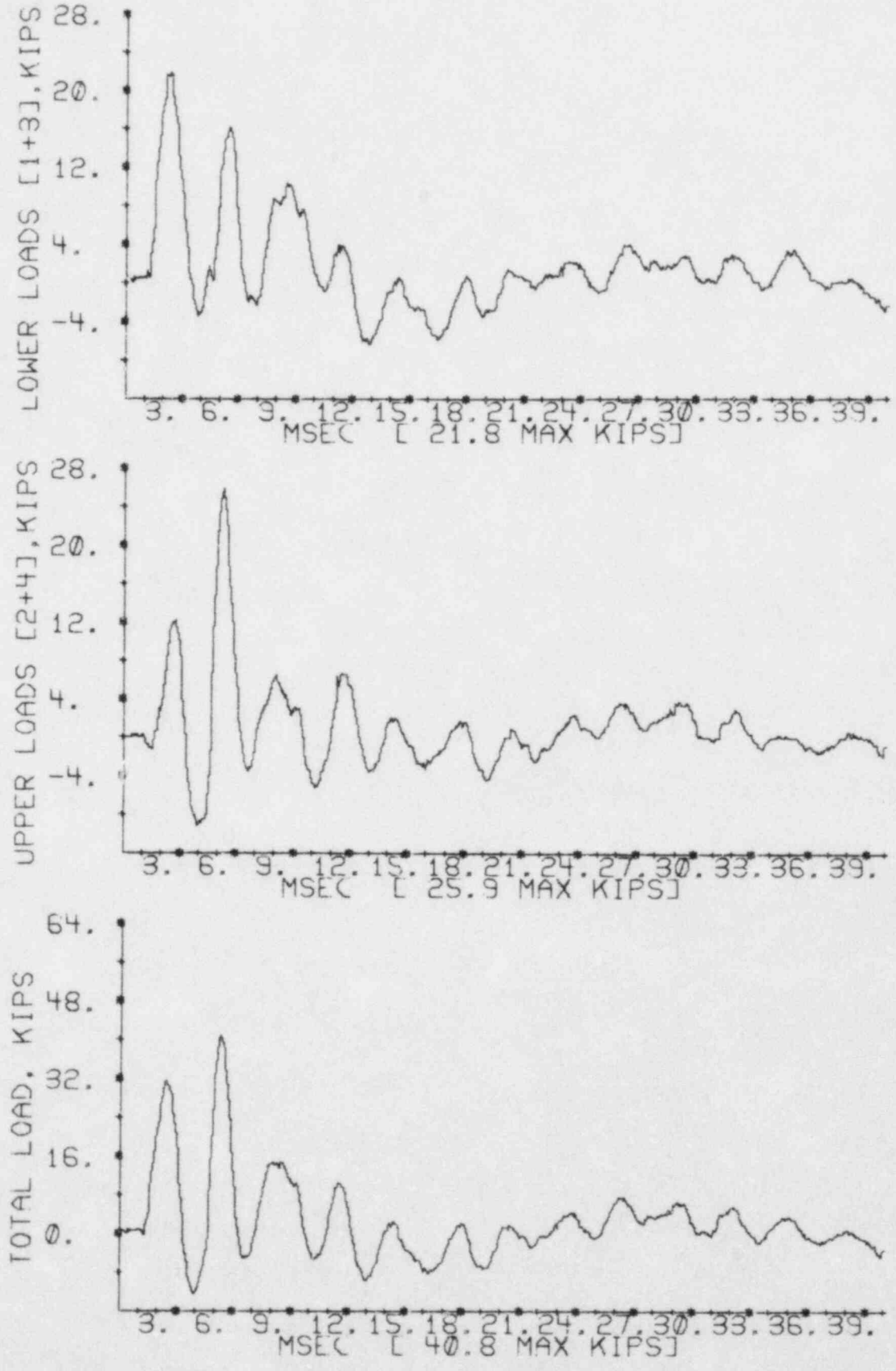

Figure A.3.6-4 Load Cell Data, Experiment Number 3

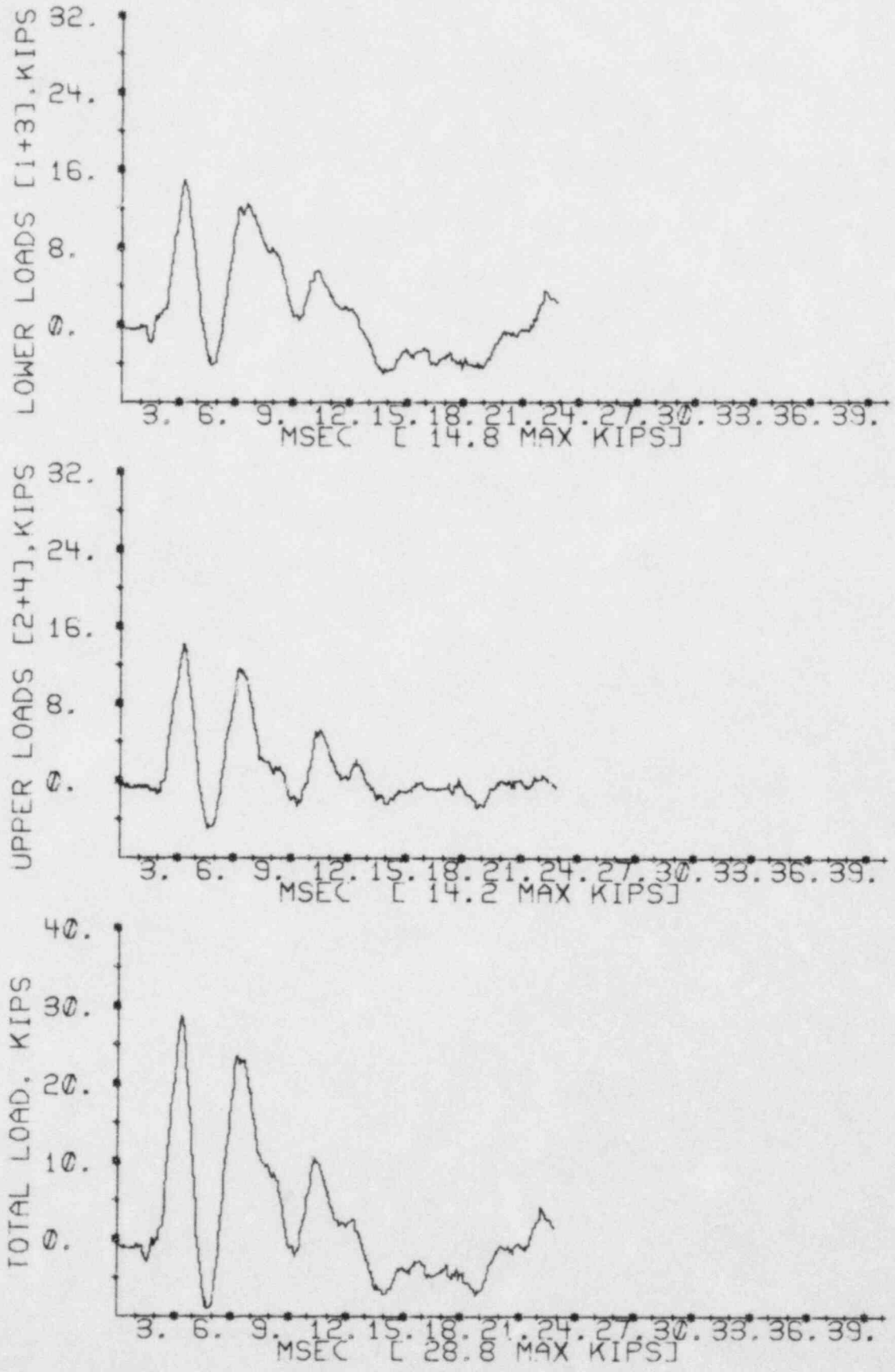

Figure A.3.6-5 Load Cell Data, Experiment Number 4

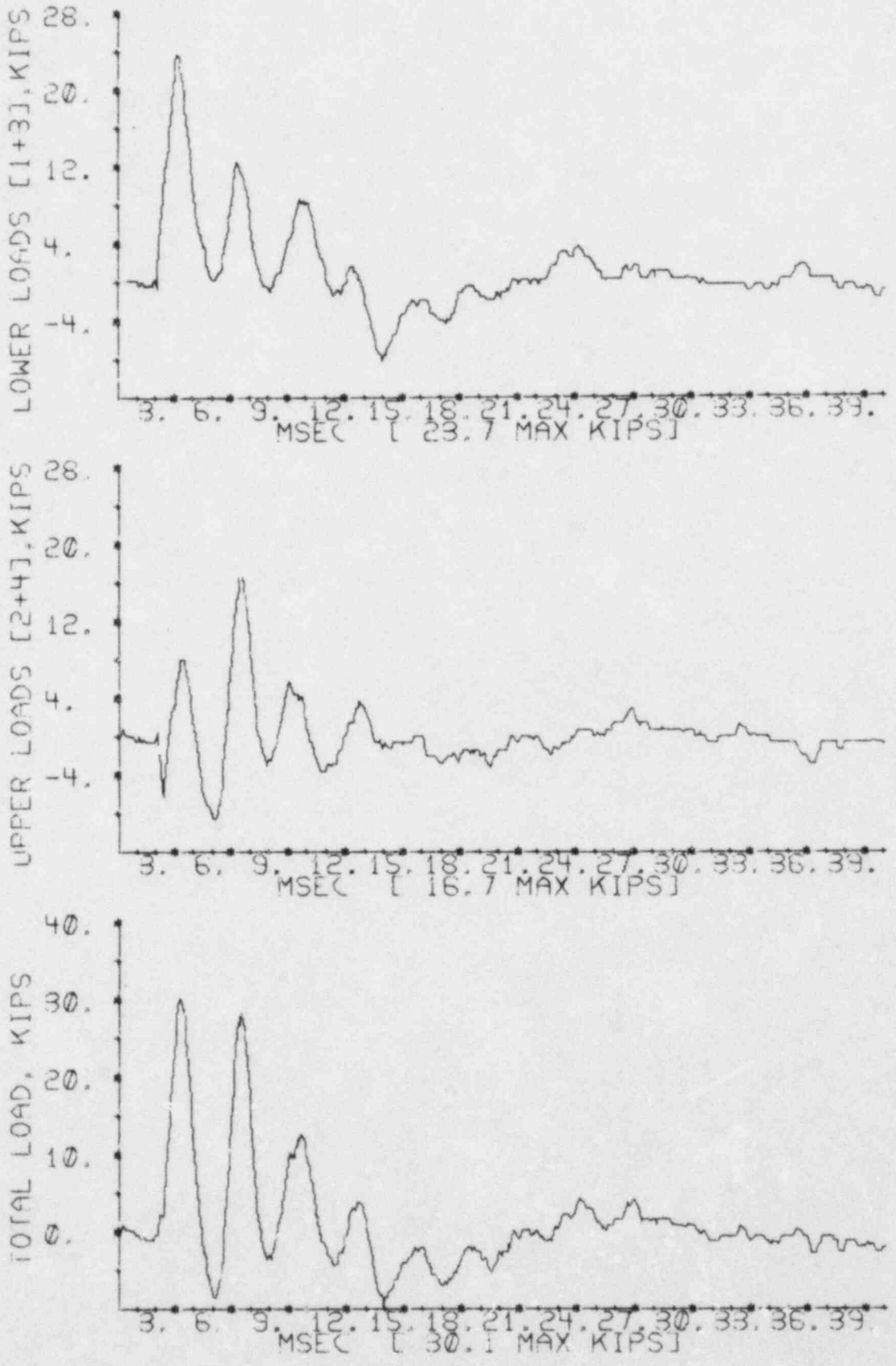

Figure A.3.6-6 Load Cell Data, Experiment Number 29

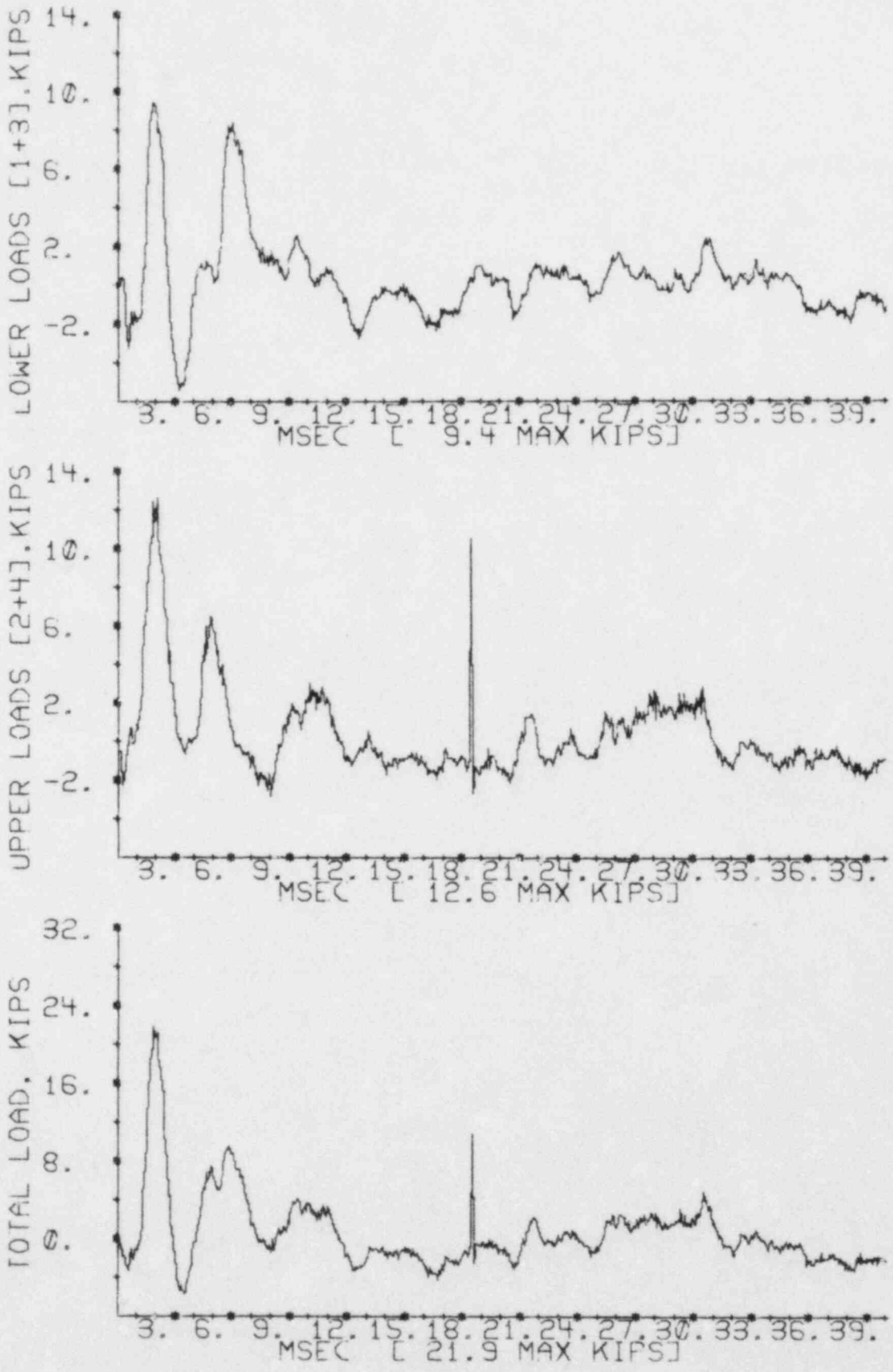

Figure A.3.6-7 Load Cell Data, Experiment Number 13

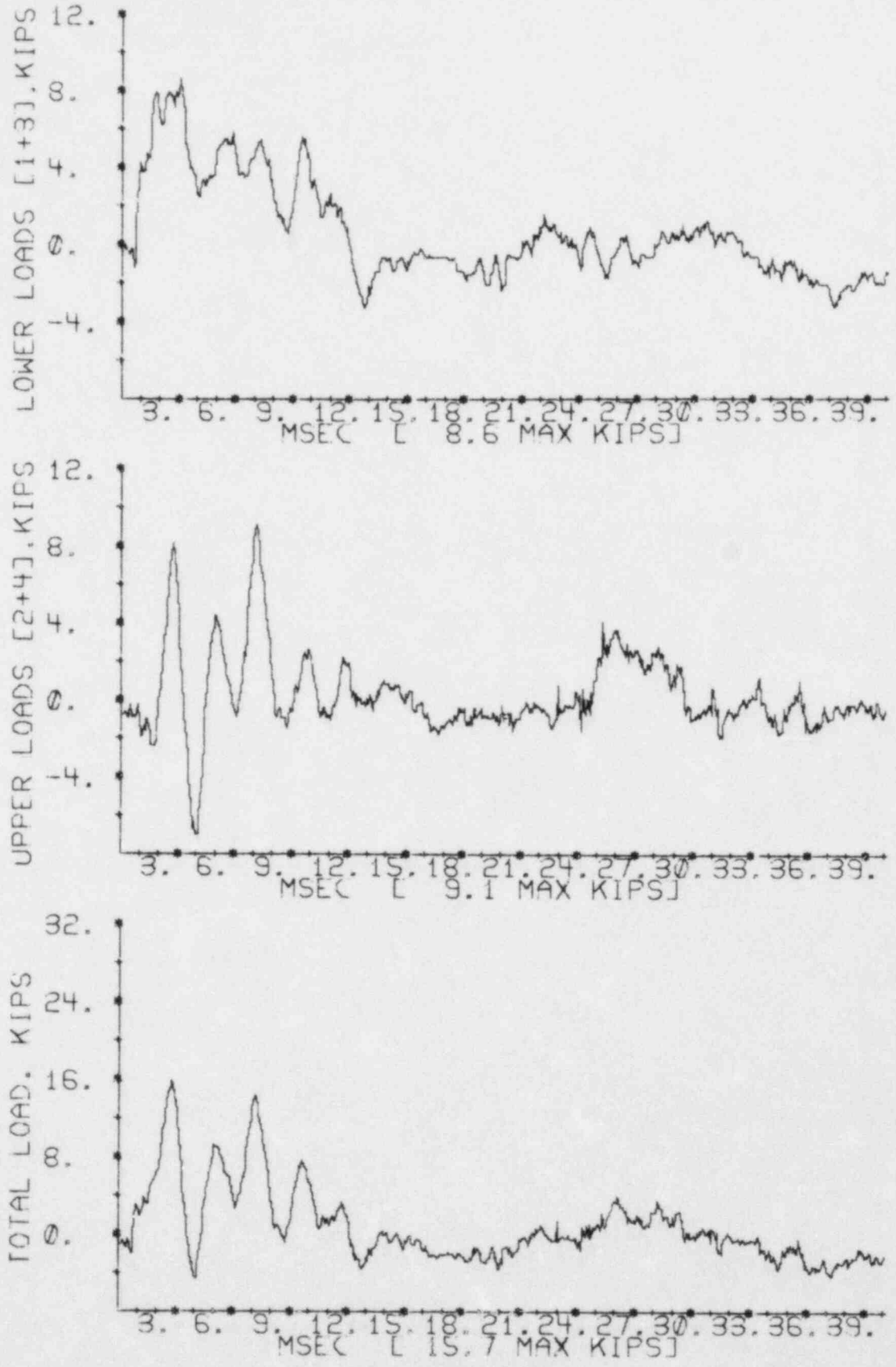

Figure A.3.6-8 Load Cell Data, Experiment Number 11

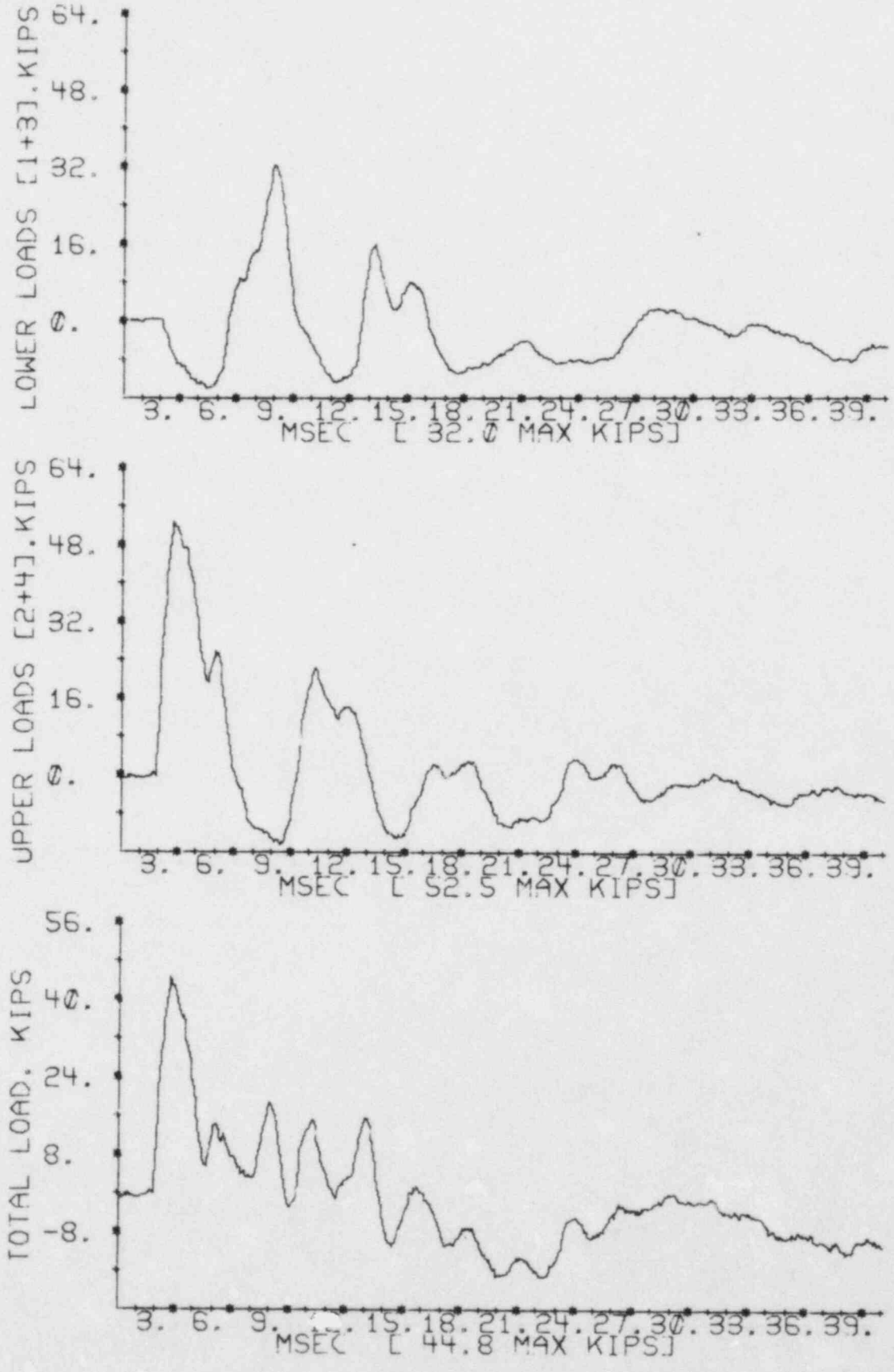

Figure A.3.6-9 Load Cell Data, Experiment Number 8

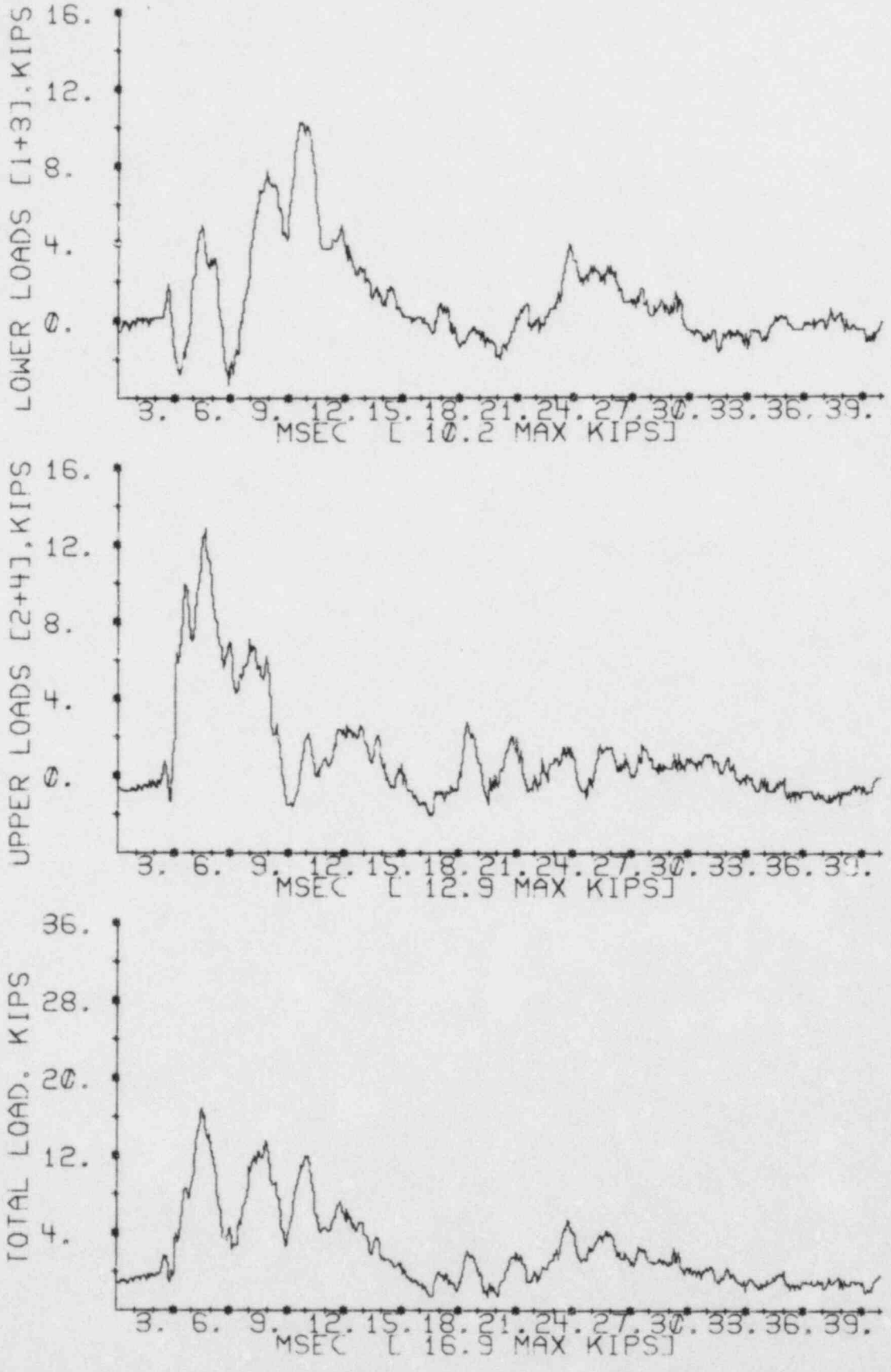

Figure A.3.6-10 Load Cell Data, Experiment Number 9

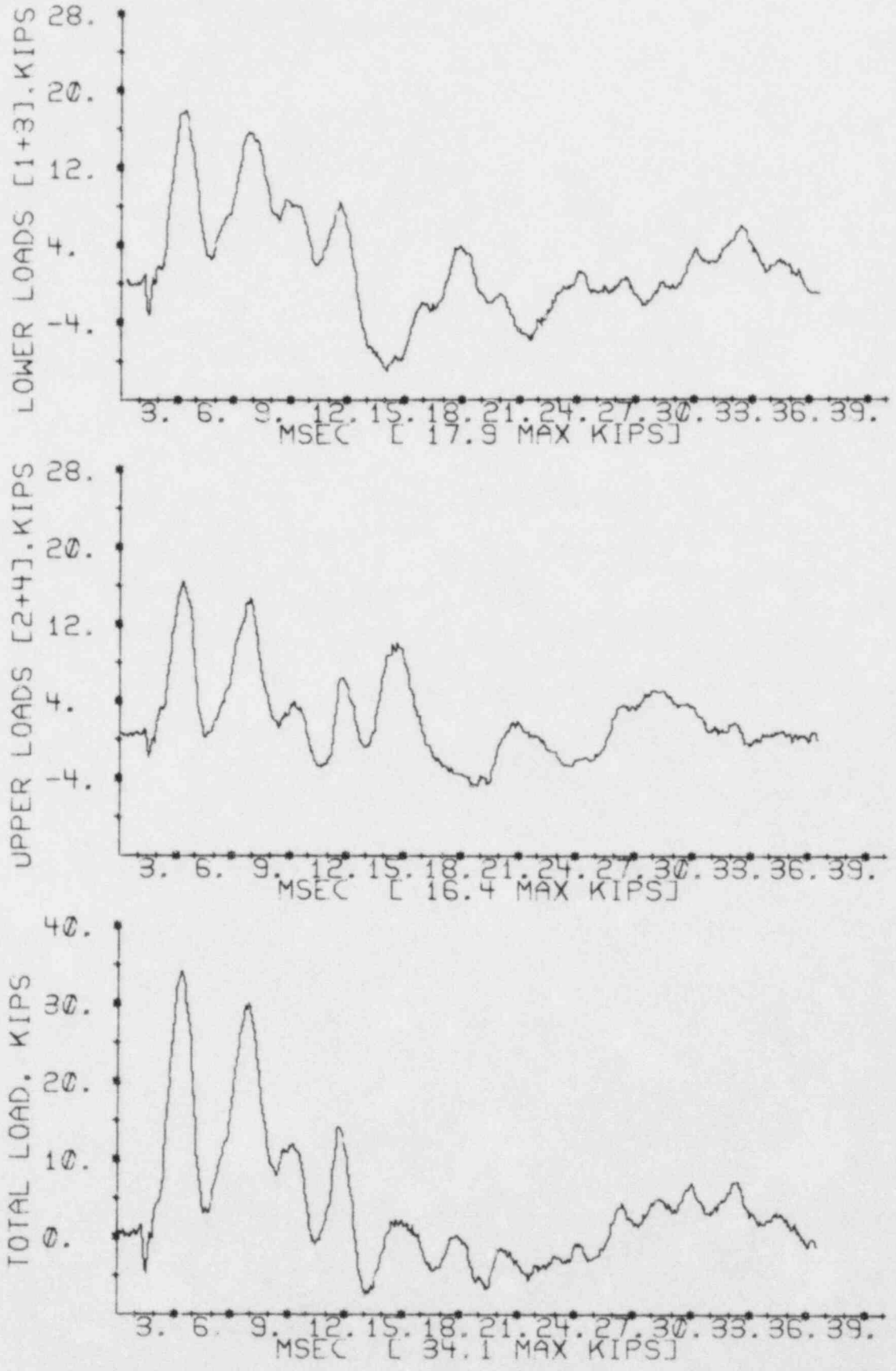

Figure A.3.6-11 Load Cell Data, Experiment Number 6

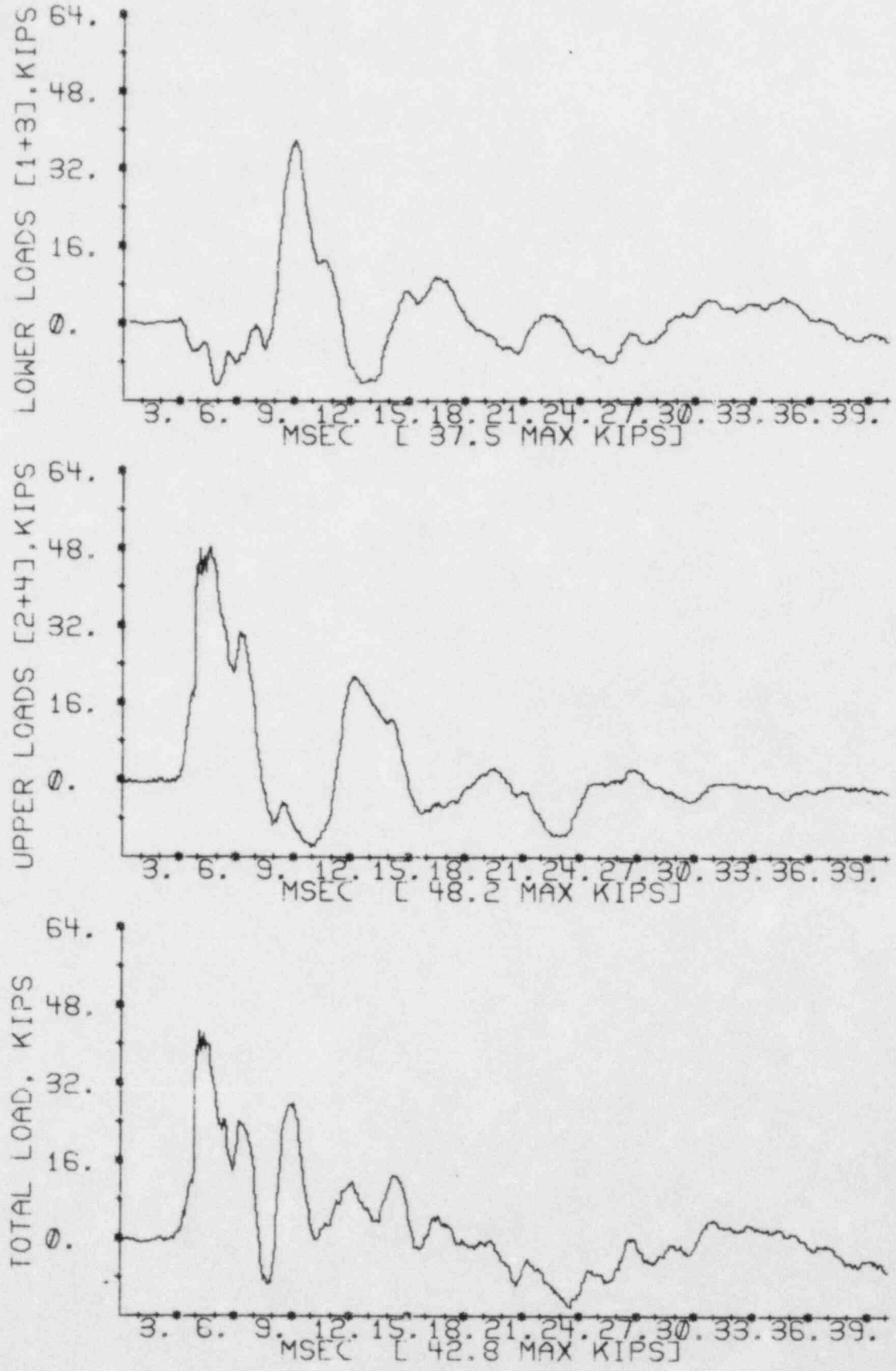

Figure A.3.6-12 Load Cell Data, Experiment Number 23

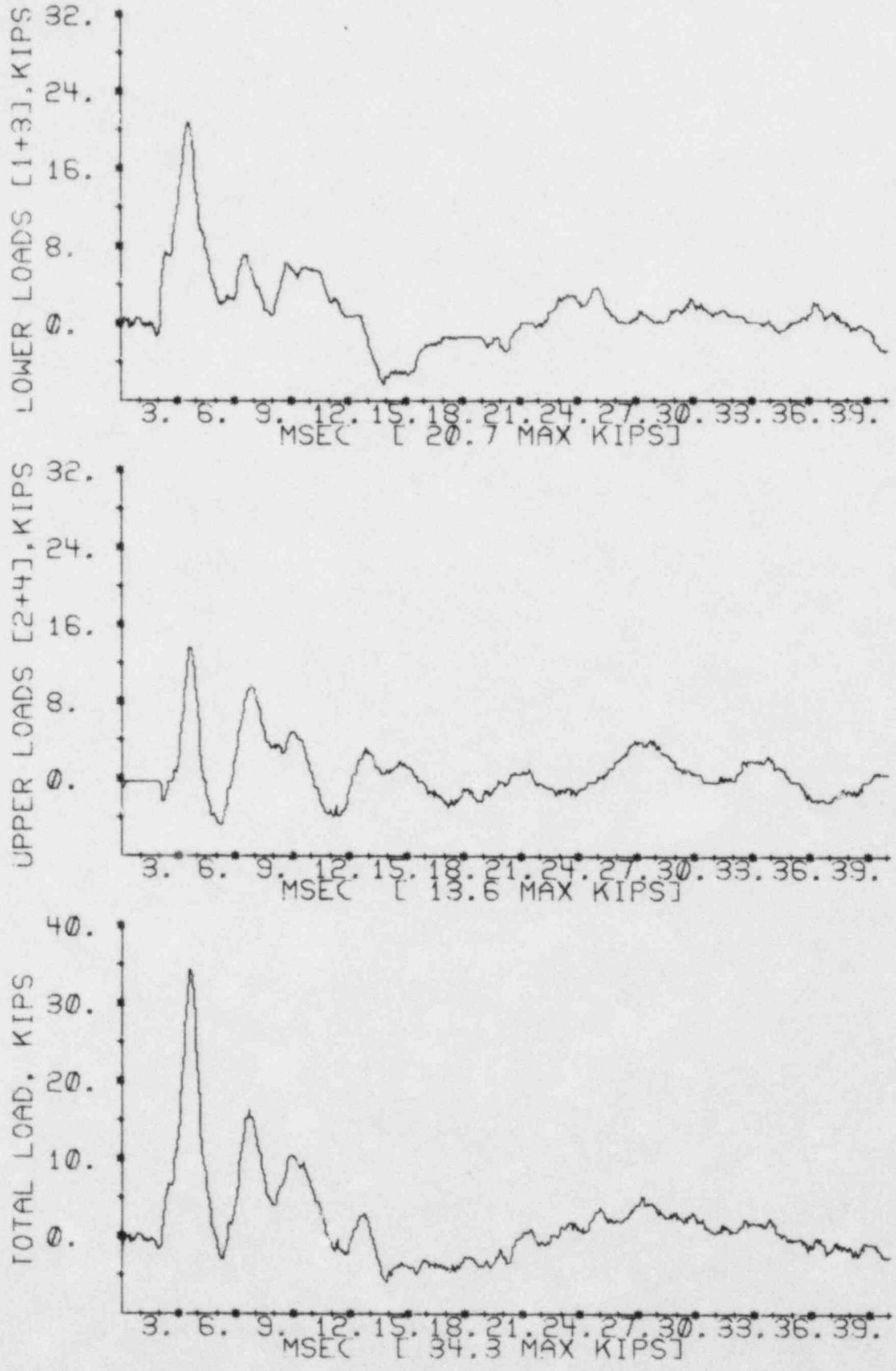

Figure A.3.6-13 Load Cell Data, Experiment Number 20

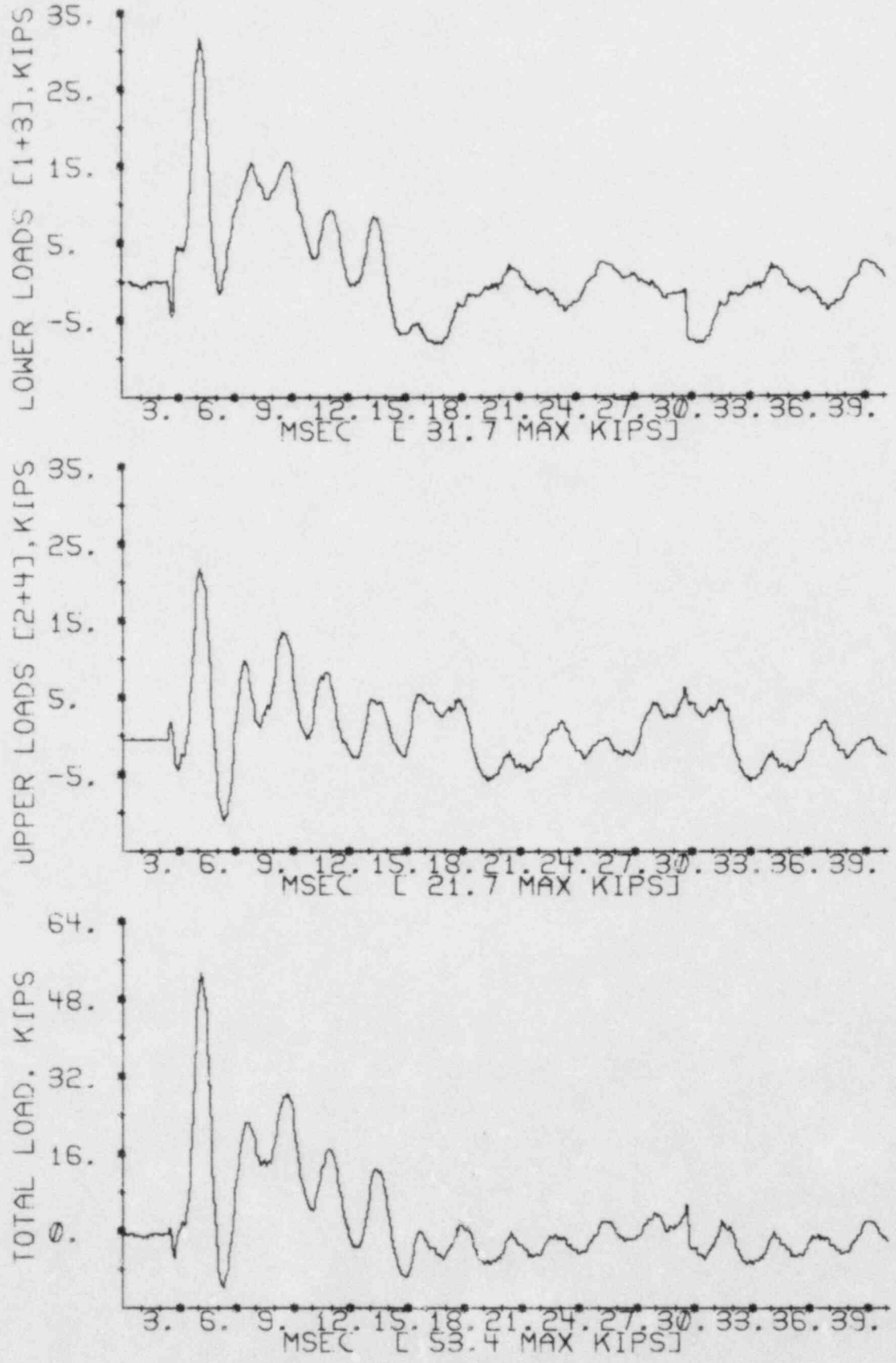

Figure A.3.6-14 Load Cell Data, Experiment Number 25

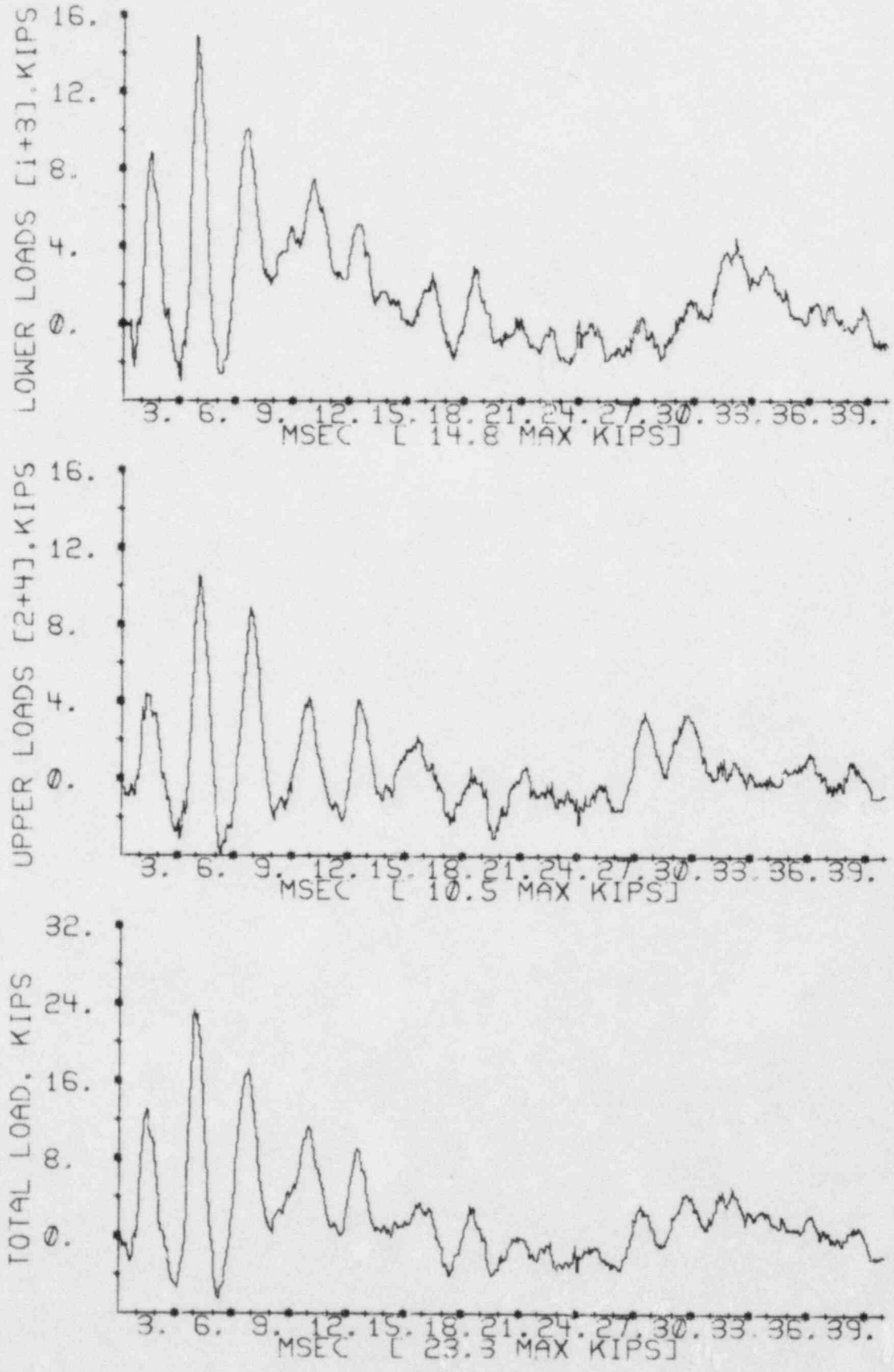

Figure A.3.6-15 Load Cell Data, Experiment Number 48

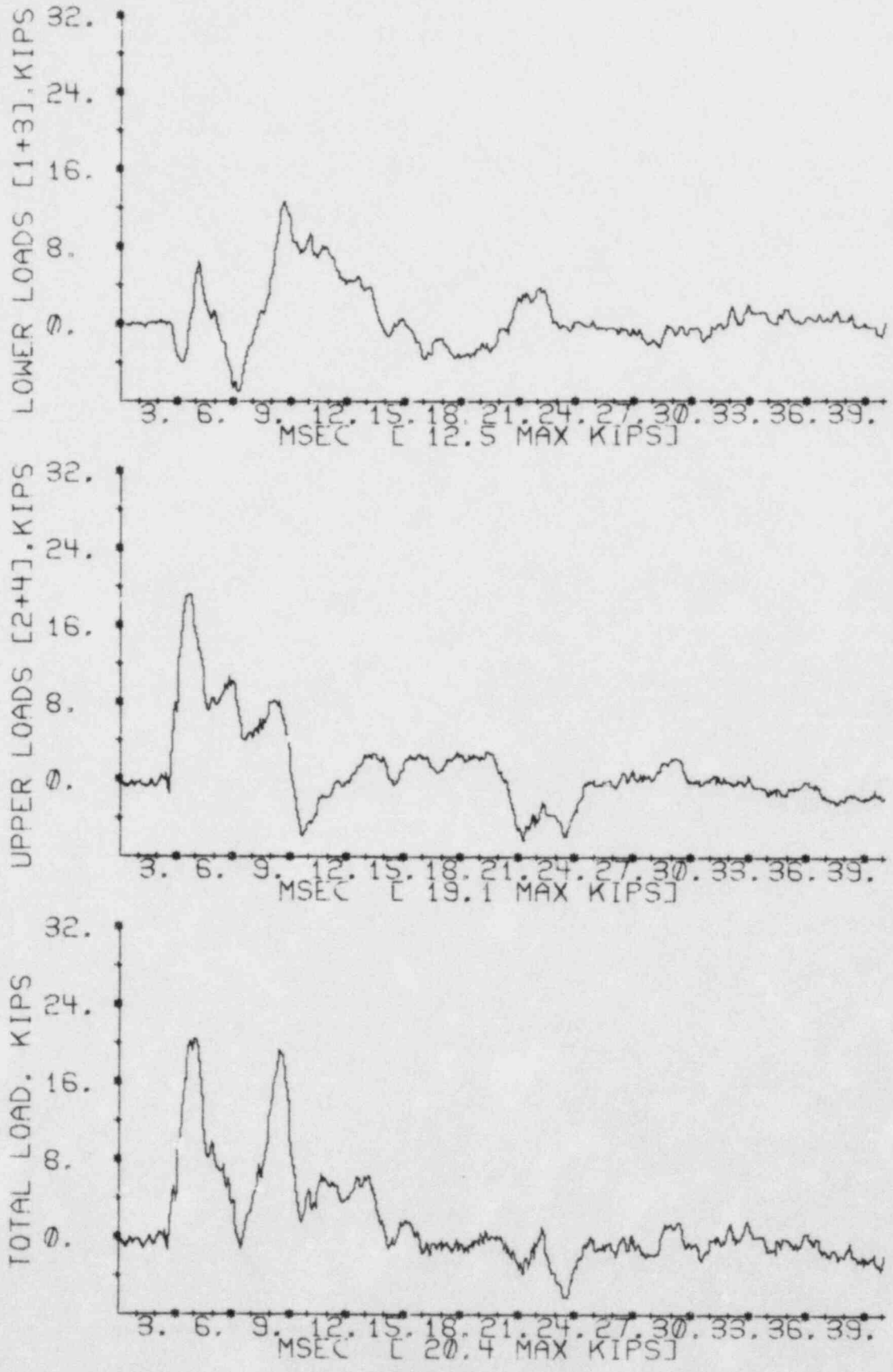

Figure A.3.6-16 Load Cell Data, Experiment Number 31

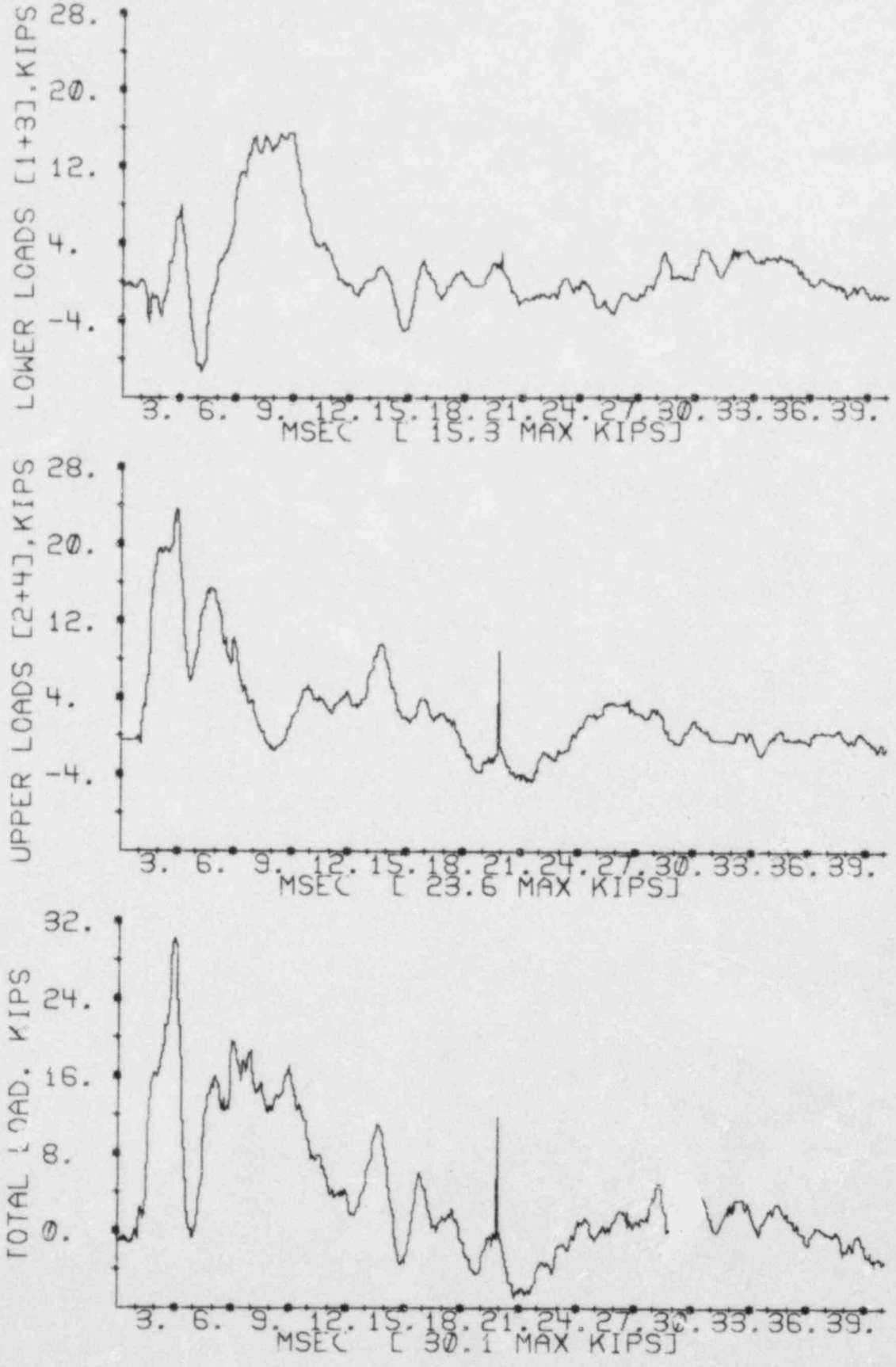

Figure A.3.6-17 Load Cell Data, Experiment Number 27

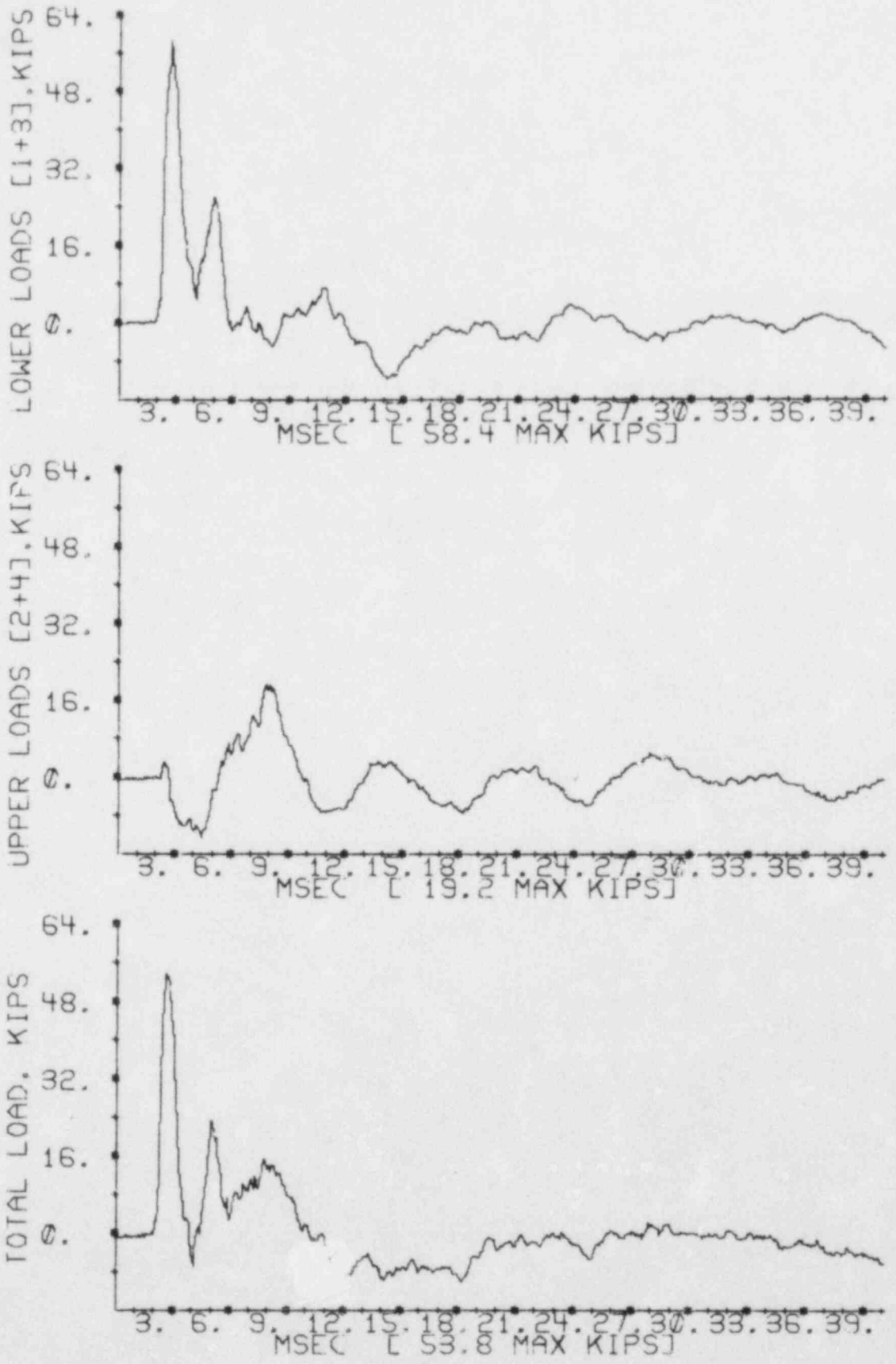

Figure A.3.6-18 Load Cell Data, Experiment Number 16

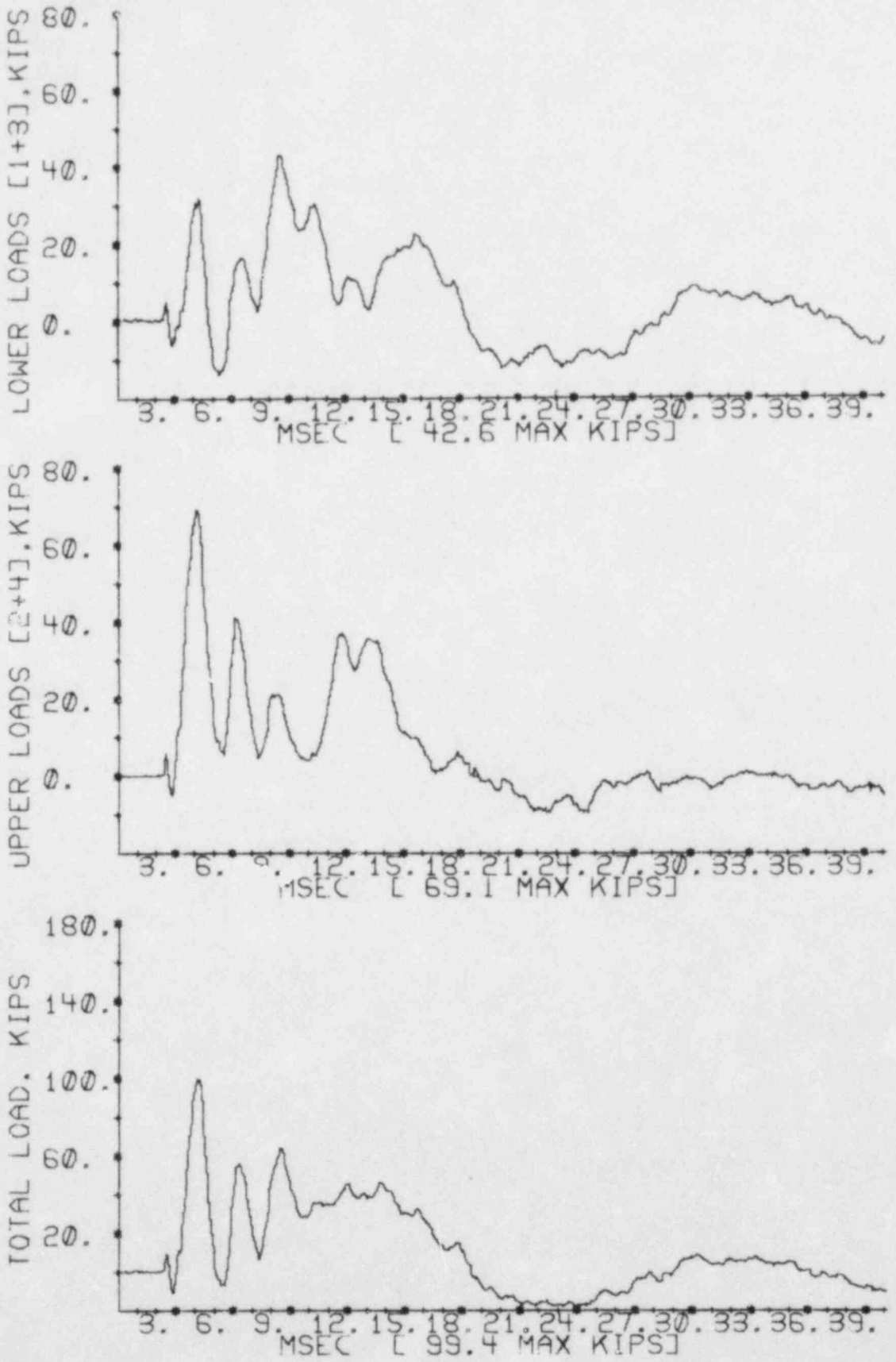

Figure A.3.6-19 Load Cell Data, Experiment Number 46

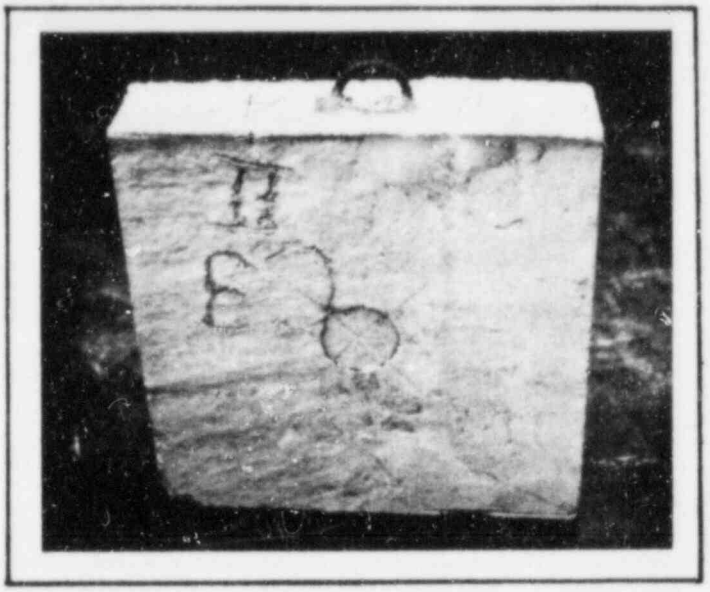

Barrier Front Face

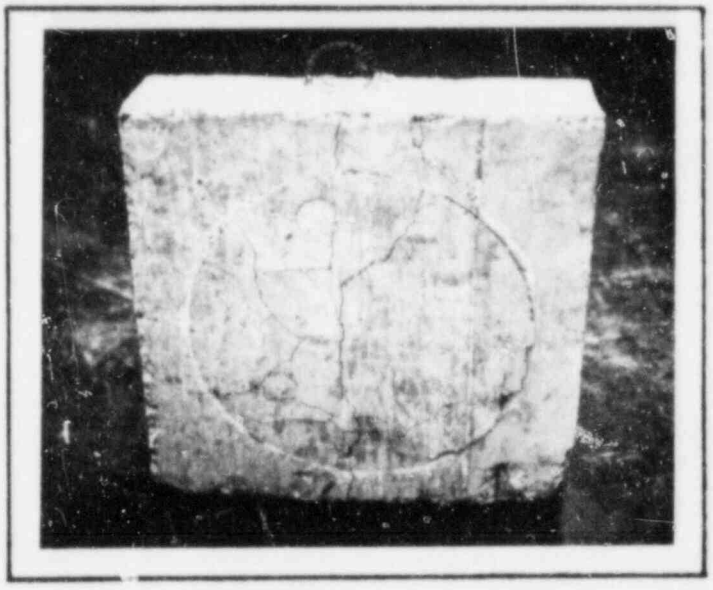

Barrier Rear Face

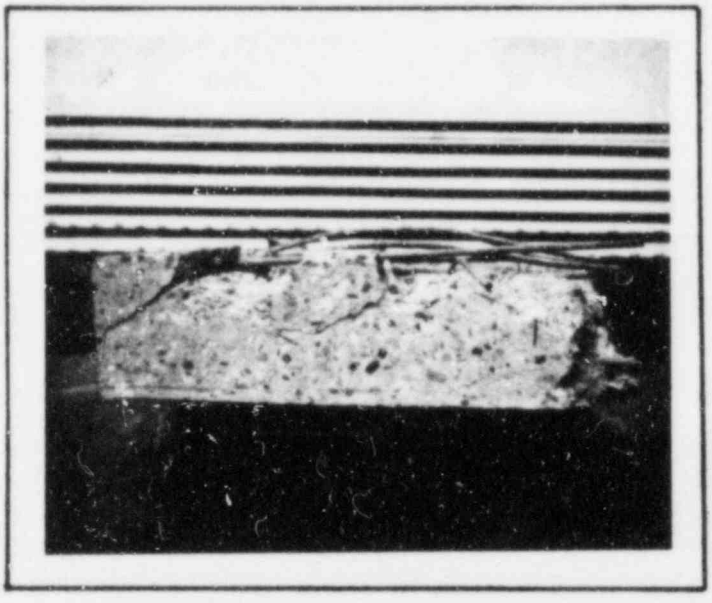

Profile of Rear Rebar or Concrete

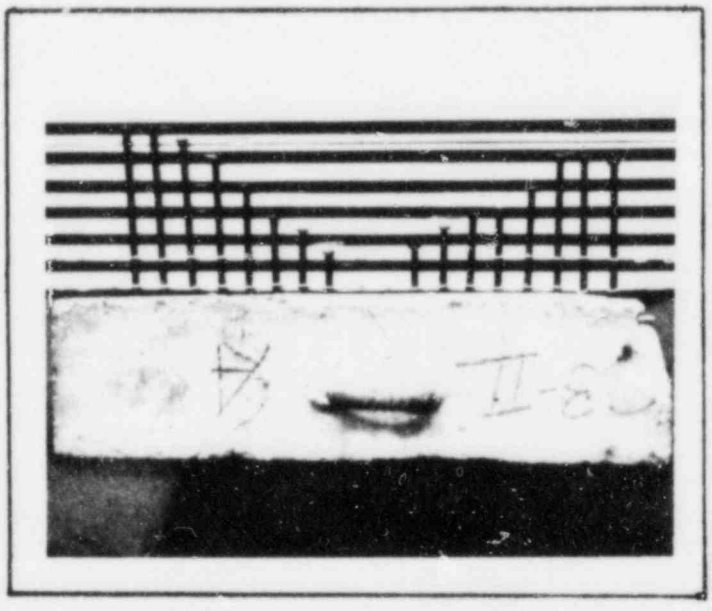

Profile of Back Crater

PUNCHING SHEAR DATA

Maximum Punching Shear Stress: 235 psi
Maximum Static Punching Load: 28.3 kips
Diameter of Applied Load: 3.0 in.
Diameter of Plug in Rear Face: 14.0 in.

BARRIER CHARACTERISTICS

Length: 1.5 ft; Width: 1.5 ft; Thickness: 4.5 in.;
Rebar Size: #2 ; Rebar Spacing, EWEF: 3 in.

Figure A.5-1 Static Punching Shear Test Number 1

Barrier Front Face

Barrier Rear Face

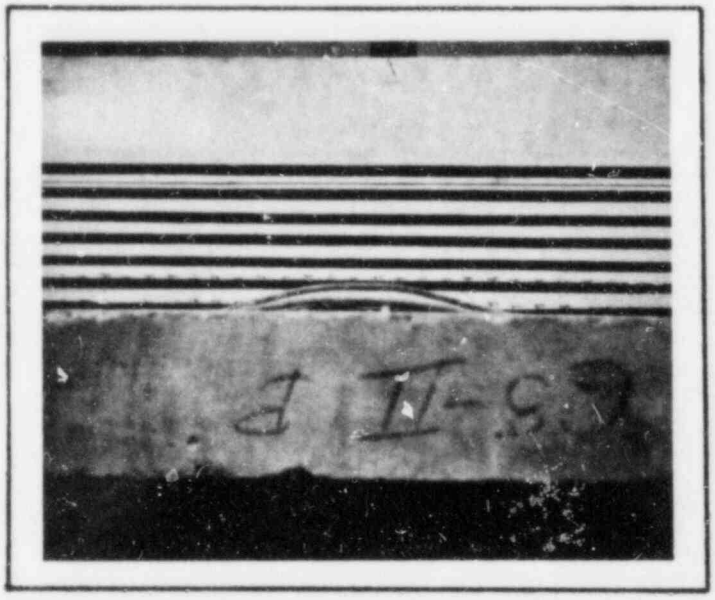

Profile of Rear Rebar or Concrete

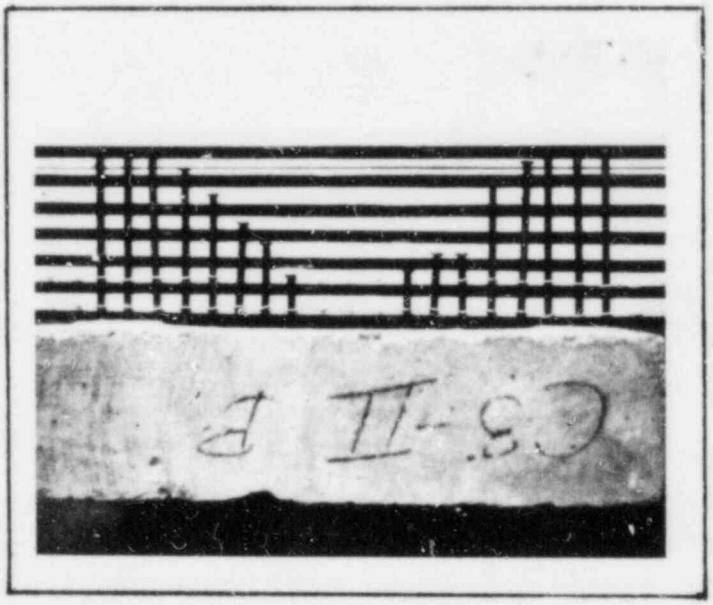

Profile of Back Crater

PUNCHING SHEAR DATA

Maximum Punching Shear Stress: 324 psi
Maximum Static Punching Load: 39.0 kips
Diameter of Applied Load: 3.0 in.
Diameter of Plug in Rear Face: 14.0 in.

BARRIER CHARACTERISTICS

Length: 1.5 ft; Width: 1.5 ft; Thickness: 4.5 in.;
Rebar Size: #2 ; Rebar Spacing, EWEF: 3 in.

Figure A.5-2 Static Punching Shear Test Number 2

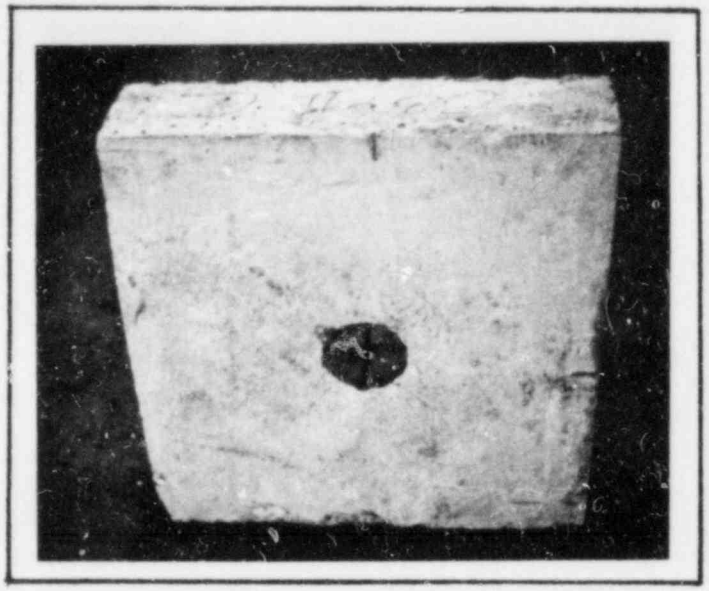

Barrier Front Face

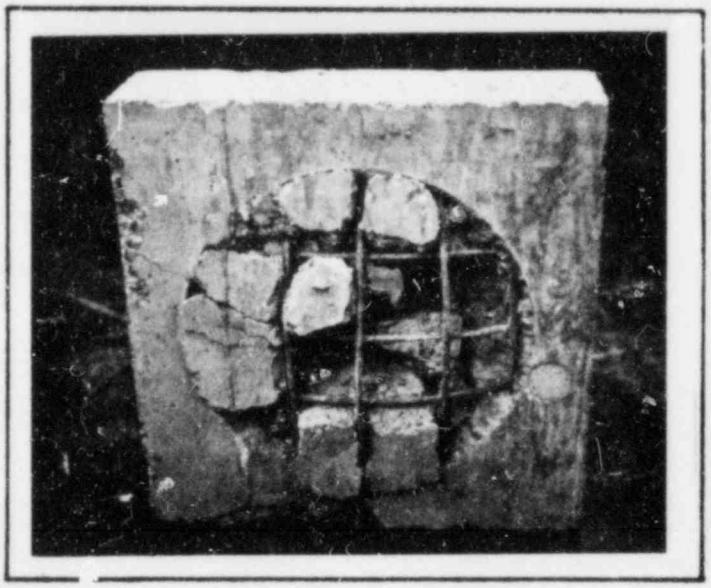

Barrier Rear Face

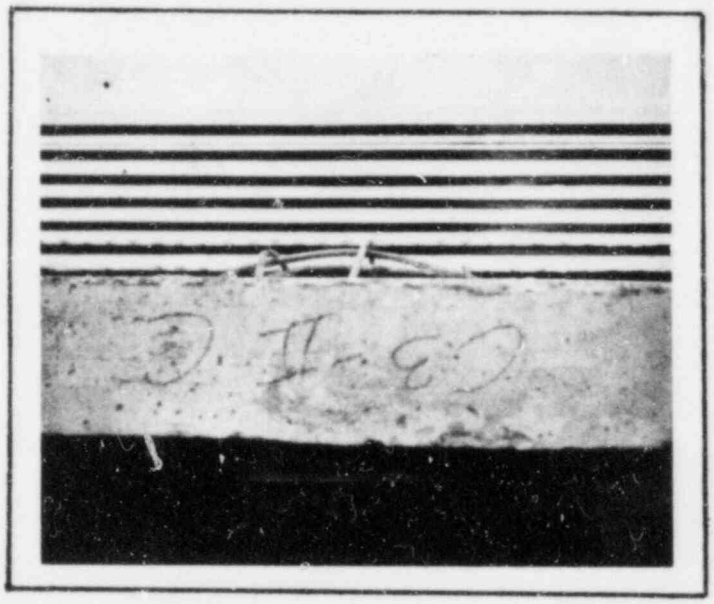

Profile of Rear Rebar or Concrete

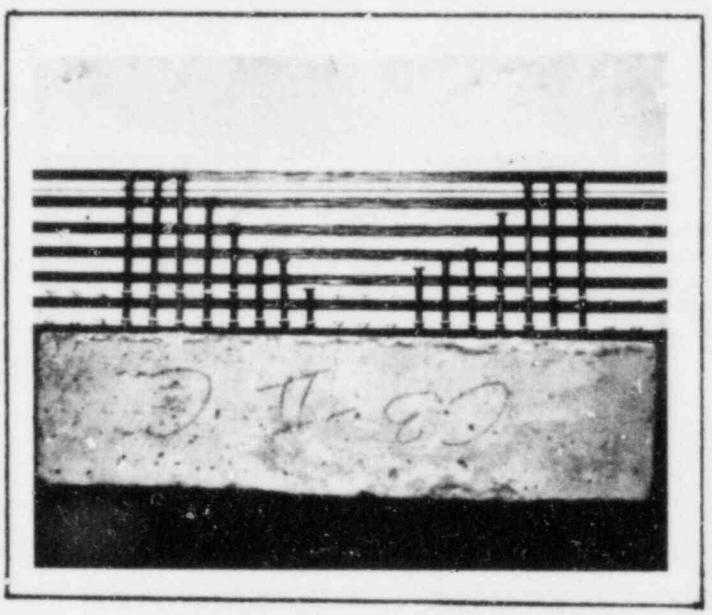

Profile of Back Crater

PUNCHING SHEAR DATA

Maximum Punching Shear Stress: 311 psi
Maximum Static Punching Load: 37.4 kips
Diameter of Applied Load: 3.0 in.
Diameter of Plug in Rear Face: 14.0 in.

BARRIER CHARACTERISTICS

Length: 1.5 ft; Width: 1.5 ft; Thickness: 4.5 in.;
Rebar Size: #2 ; Rebar Spacing, EWEF: 3 in.

Figure A.5-3 Static Punching Shear Test Number 3

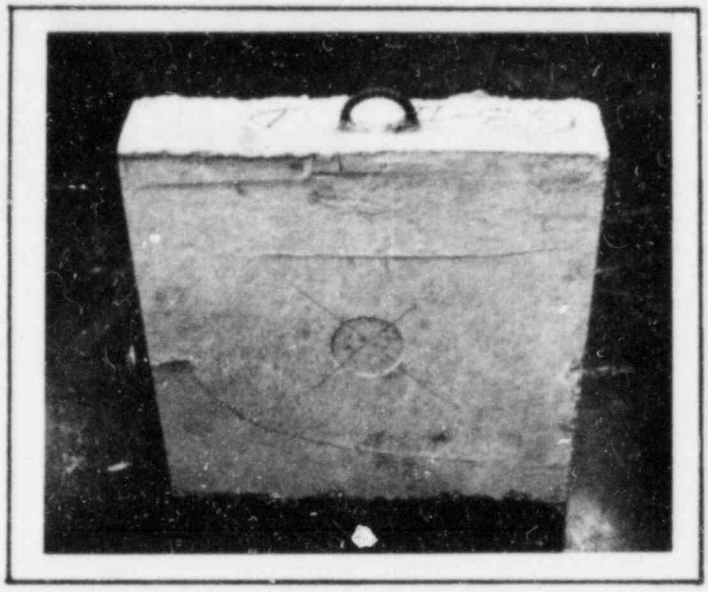

Barrier Front Face

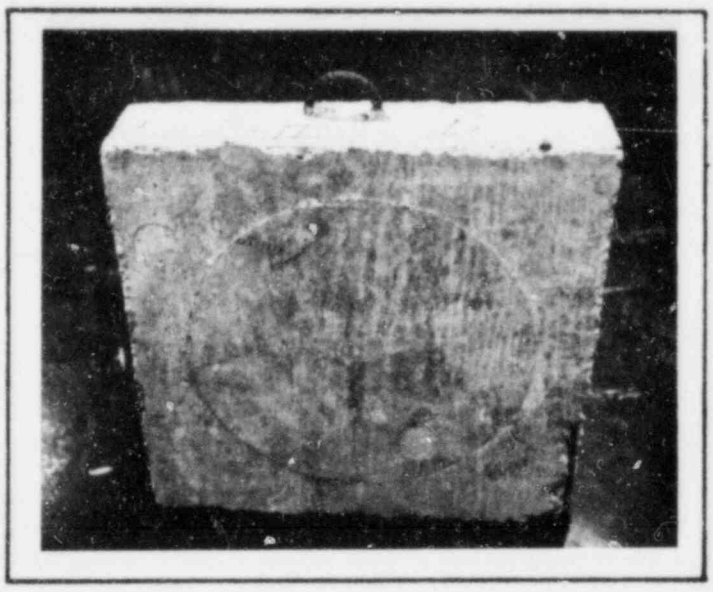

Barrier Rear Face

Profile of Rear Rebar or Concrete

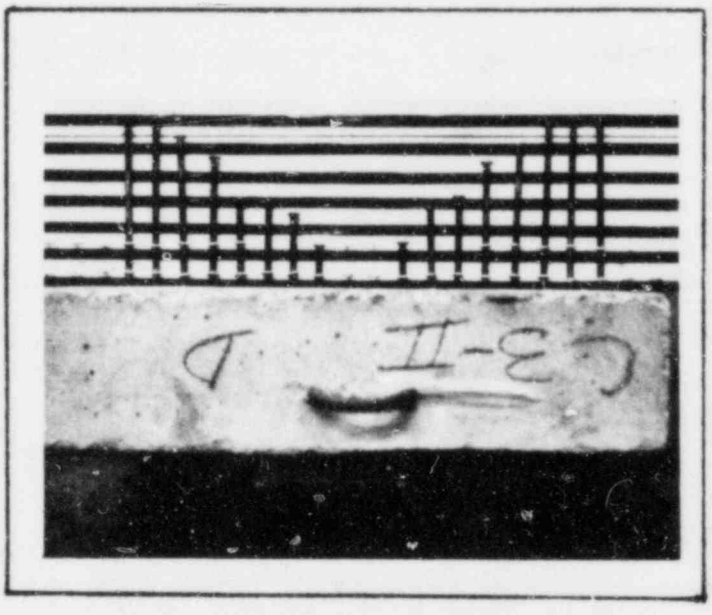

Profile of Back Crater

PUNCHING SHEAR DATA

Maximum Punching Shear Stress: 256 psi
Maximum Static Punching Load: 30.8 kips
Diameter of Applied Load: 3.0 in.
Diameter of Plug in Rear Face: 14.0 in.

BARRIER CHARACTERISTICS

Length: 1.5 ft; Width: 1.5 ft; Thickness: 4.5 in.;
Rebar Size: #2 ; Rebar Spacing, EWEF: 3 in.

Figure A.5-4 Static Punching Shear Test Number 4

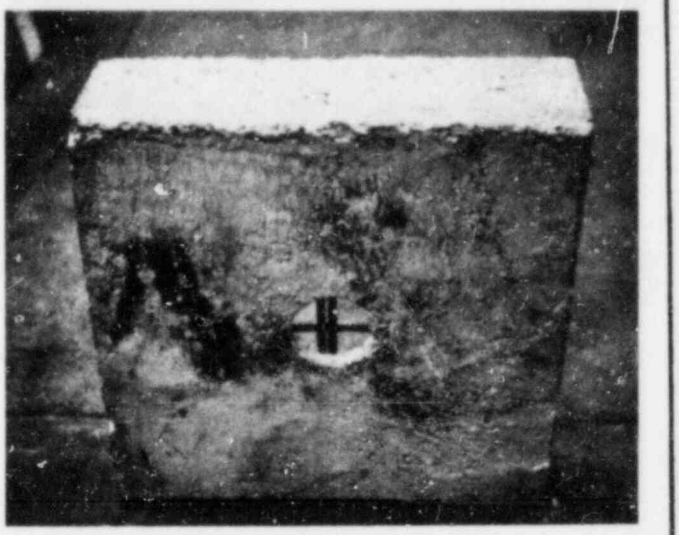

Barrier Front Face

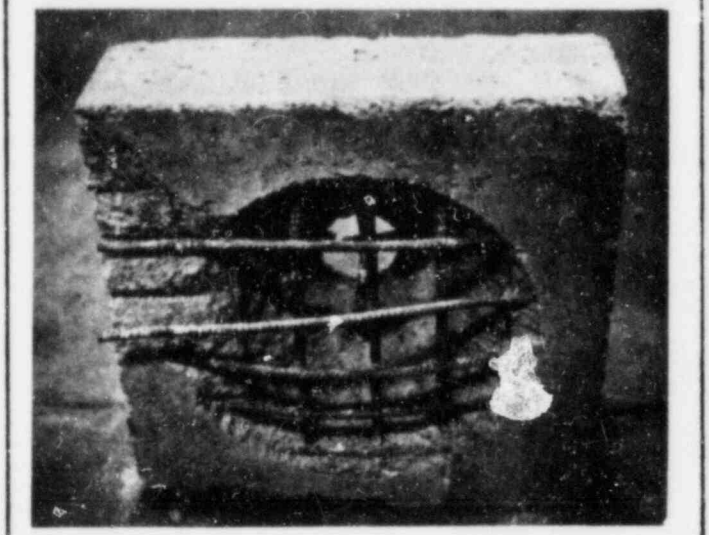

Barrier Rear Face

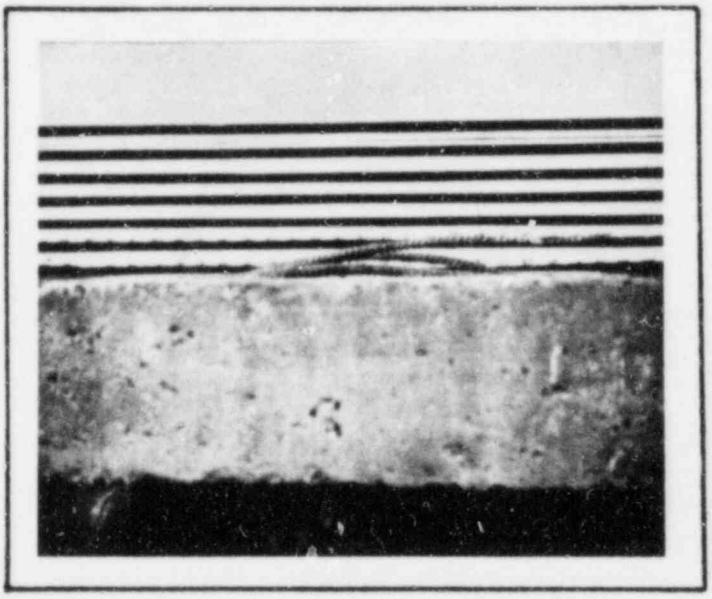

Profile of Rear Rebar or Concrete

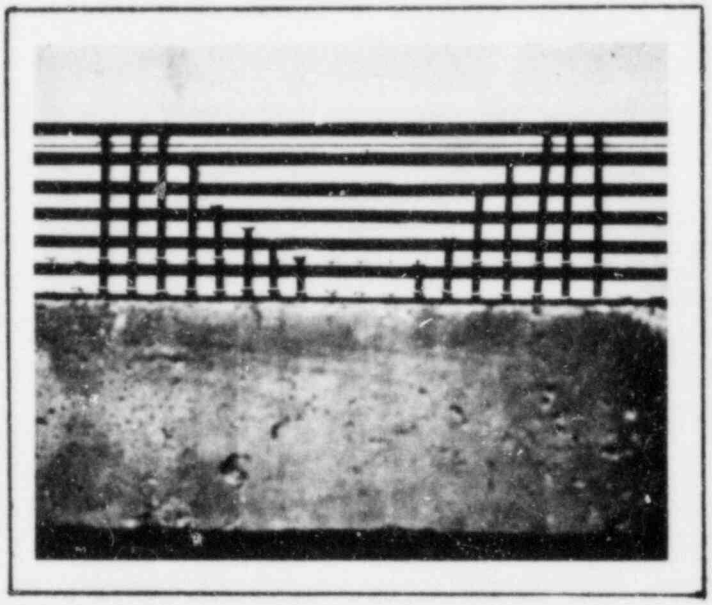

Profile of Back Crater

PUNCHING SHEAR DATA

Maximum Punching Shear Stress: 430 psi
Maximum Static Punching Load: 69.0 kips
Diameter of Applied Load: 3.0 in.
Diameter of Plug in Rear Face: 14.0 in.

BARRIER CHARACTERISTICS

Length: 1.5 ft; Width: 1.5 ft; Thickness: 6.0 in.;
Rebar Size: #3 ; Rebar Spacing, EWEF: 2.5 in.

Figure A.5-5 Static Punching Shear Test Number 5

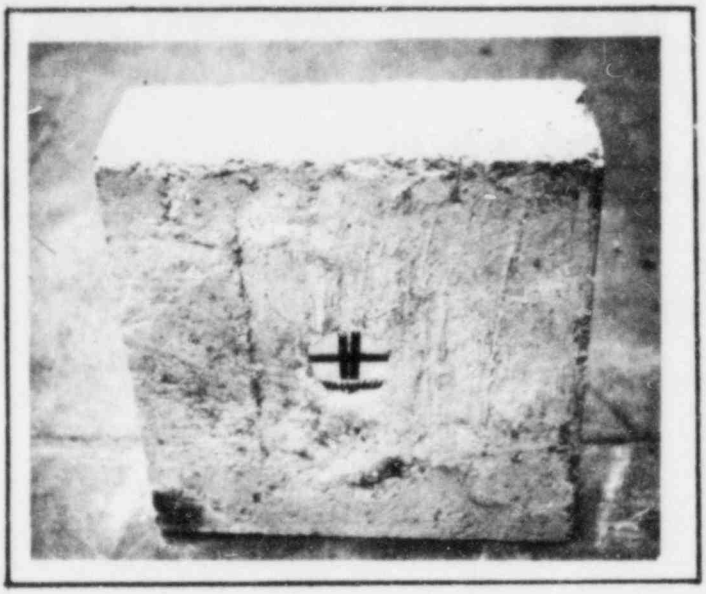

Barrier Front Face

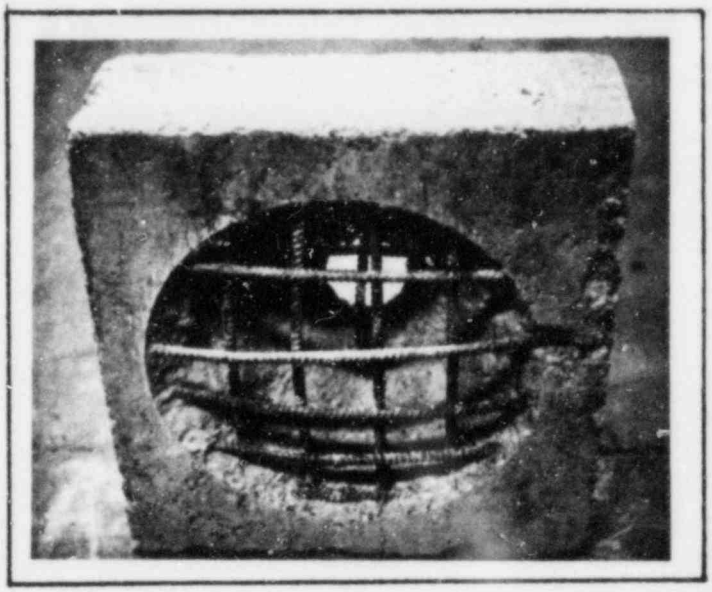

Barrier Rear Face

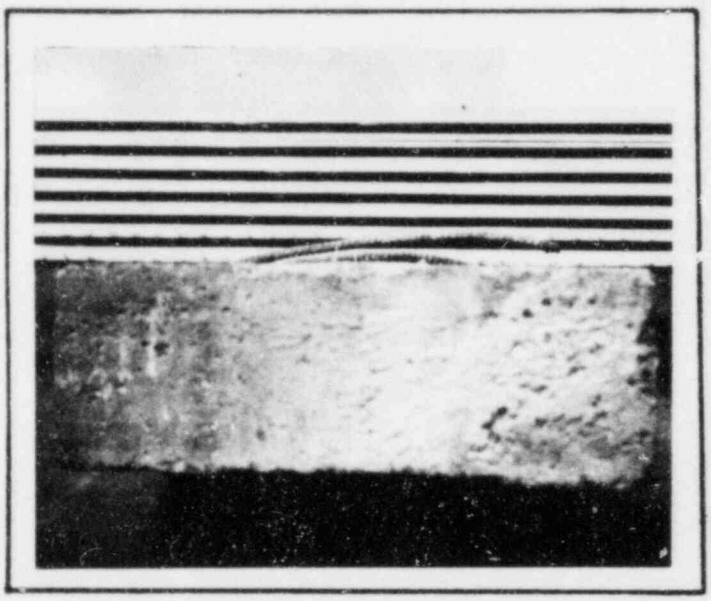

Profile of Rear Rebar or Concrete

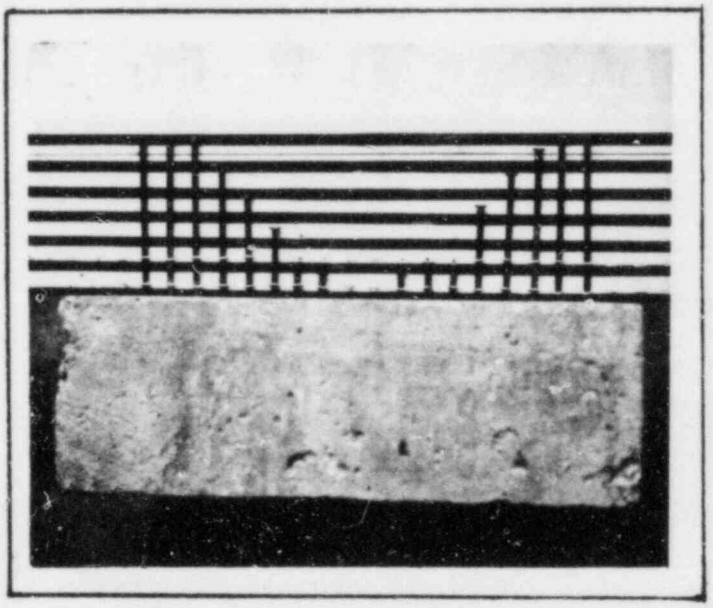

Profile of Back Crater

PUNCHING SHEAR DATA

Maximum Punching Shear Stress: 427 psi
Maximum Static Punching Load: 68.5 kips
Diameter of Applied Load: 3.0 in.
Diameter of Plug in Rear Face: 14.0 in.

BARRIER CHARACTERISTICS

Length: 1.5 ft; Width: 1.5 ft; Thickness: 6.0 in.;
Rebar Size: #3 ; Rebar Spacing, EWEF: 2.5 in.

Figure A.5-6 Static Punching Shear Test Number 6

Barrier Front Face

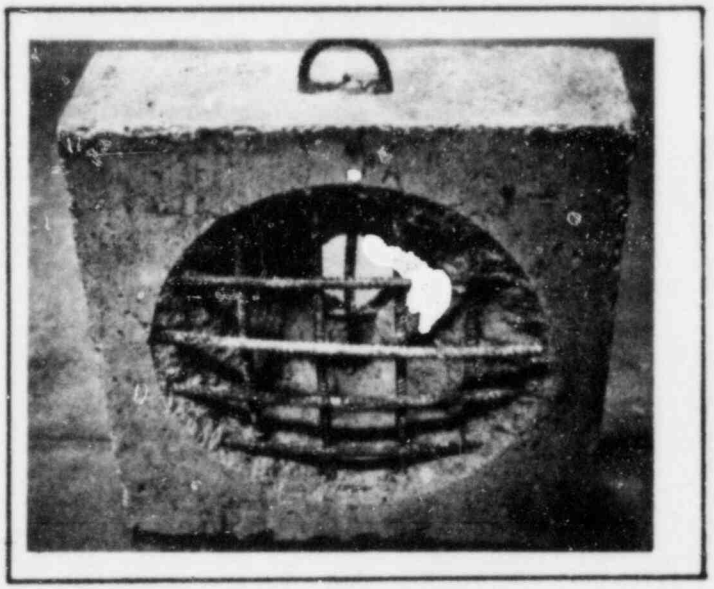

Barrier Rear Face

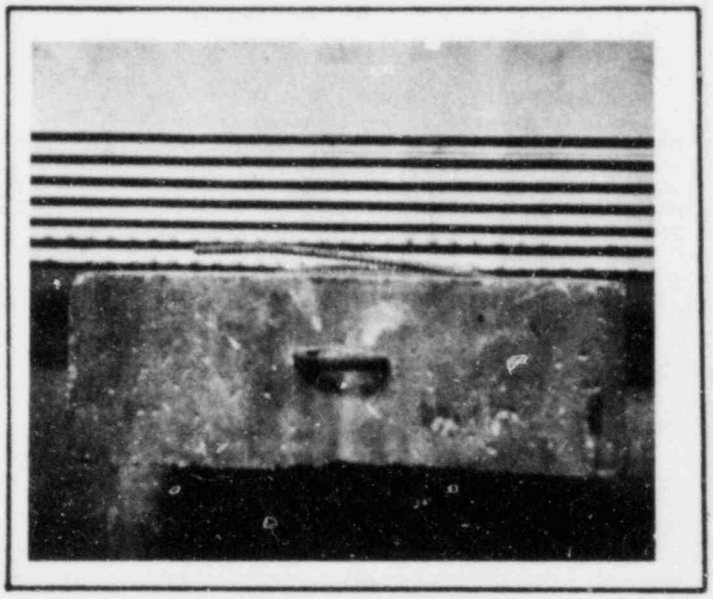

Profile of Rear Rebar or Concrete

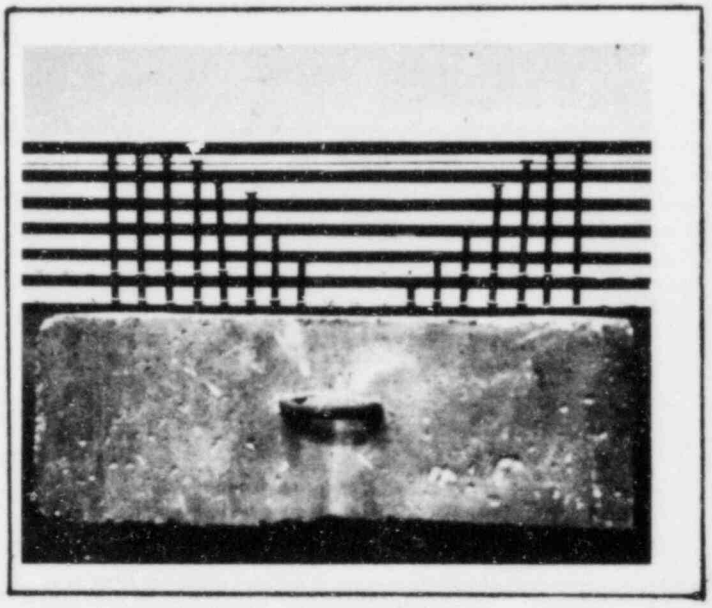

Profile of Back Crater

PUNCHING SHEAR DATA

Maximum Punching Shear Stress: 474 psi
Maximum Static Punching Load: 76.0 kips
Diameter of Applied Load: 3.0 in.
Diameter of Plug in Rear Face: 14.0 in.

BARRIER CHARACTERISTICS

Length: 1.5 ft; Width: 1.5 ft; Thickness: 6.0 in.;
Rebar Size: #3 ; Rebar Spacing, EWEF: 2.5 in.

Figure A.5-7 Static Punching Shear Test Number 7

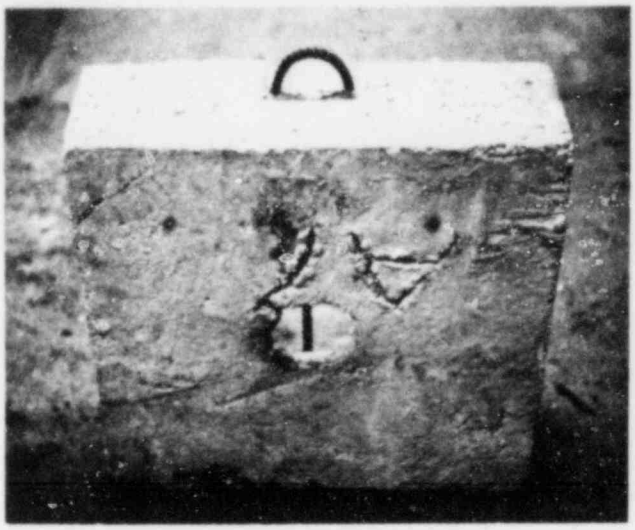

Barrier Front Face

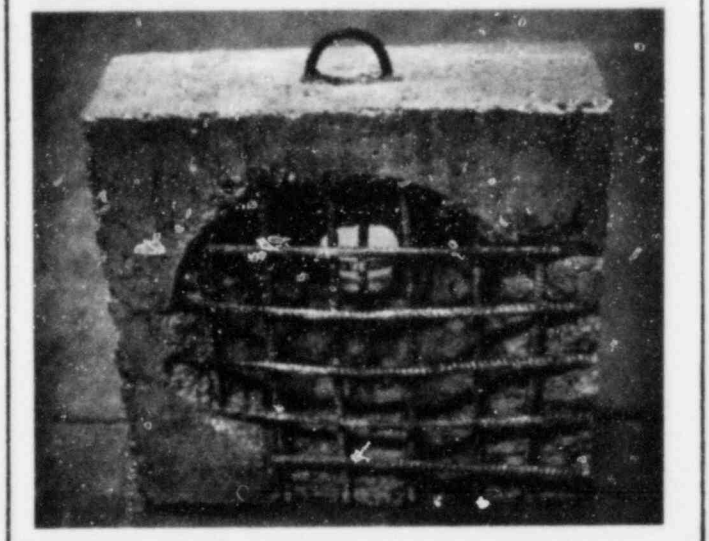

Barrier Rear Face

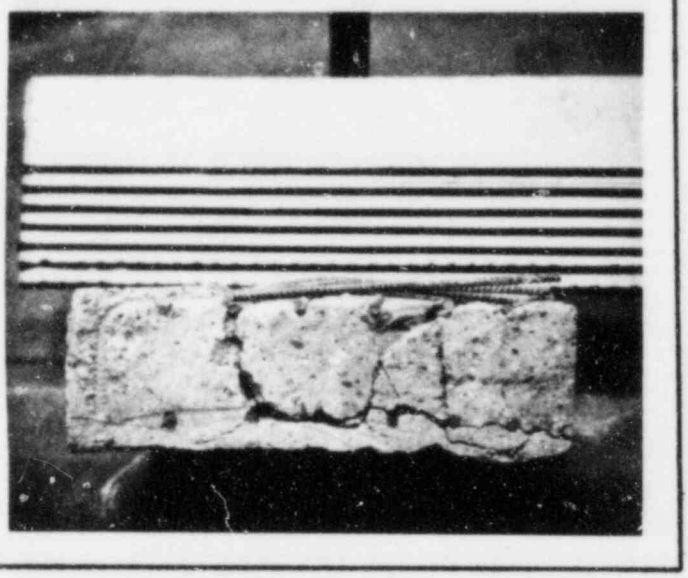

Profile of Rear Rebar or Concrete

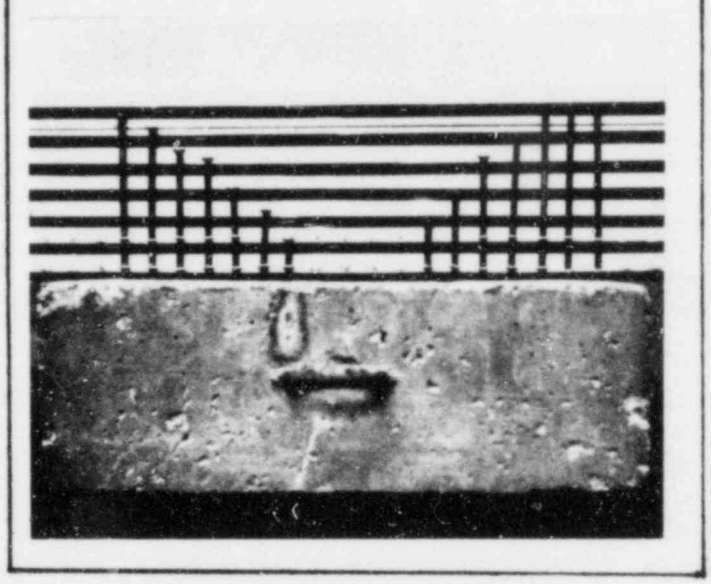

Profile of Back Crater

PUNCHING SHEAR DATA

Maximum Punching Shear Stress: 477 psi
Maximum Static Punching Load: 76.5 kips
Diameter of Applied Load: 3.0 in.
Diameter of Plug in Rear Face: 14.0 in.

BARRIER CHARACTERISTICS

Length: 1.5 ft; Width: 1.5 ft; Thickness: 6.0 in.;
Rebar Size: #3 ; Rebar Spacing, EWEF: 2.5 in.

Figure A.5-8 Static Punching Shear Test Number 8

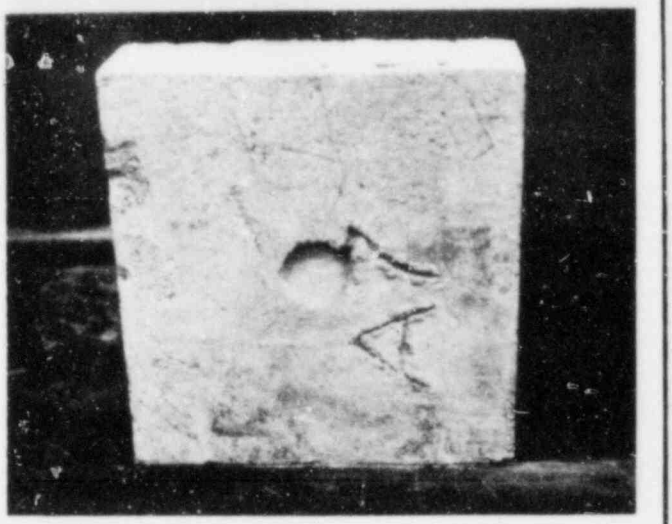

Barrier Front Face

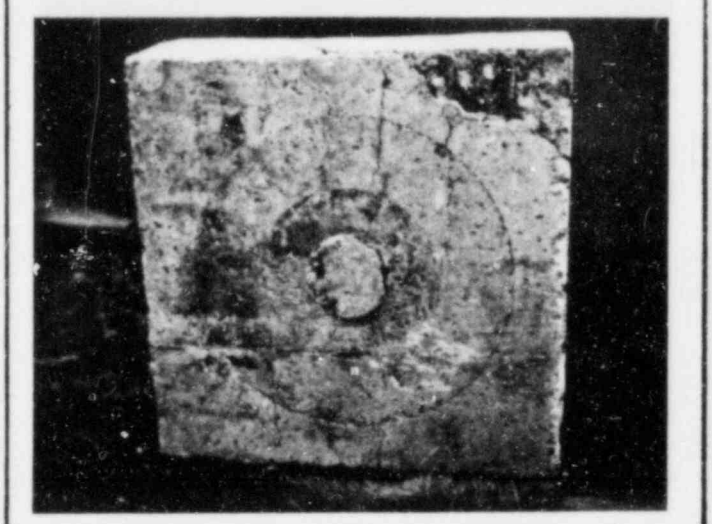

Barrier Rear Face

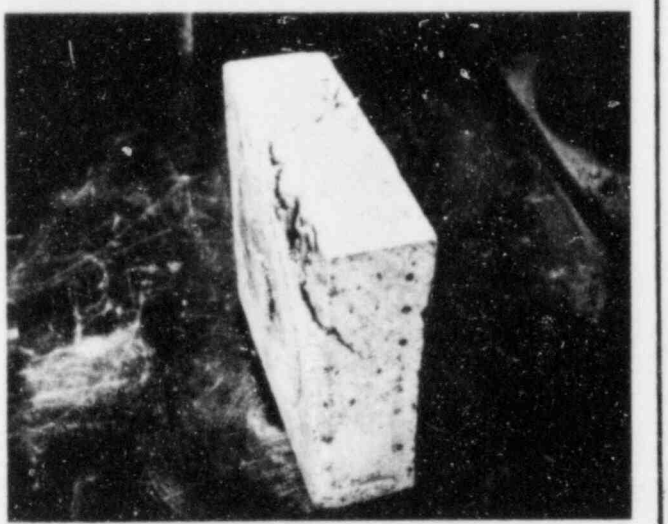

Profile of Rear Rebar or Concrete

Profile of Back Crater

PUNCHING SHEAR DATA

Maximum Punching Shear Stress: 2600 psi
Maximum Static Punching Load: 147.0 kips
Diameter of Applied Load: 3.0 in.
Diameter of Plug in Rear Face: 3.5 in.

BARRIER CHARACTERISTICS

Length: 1.5 ft; Width: 1.5 ft; Thickness: 6.0 in.;
Rebar Size: #3 ; Rebar Spacing, EWEF: 2.5 in.

Figure A.5-9 Static Punching Shear Test Number 9

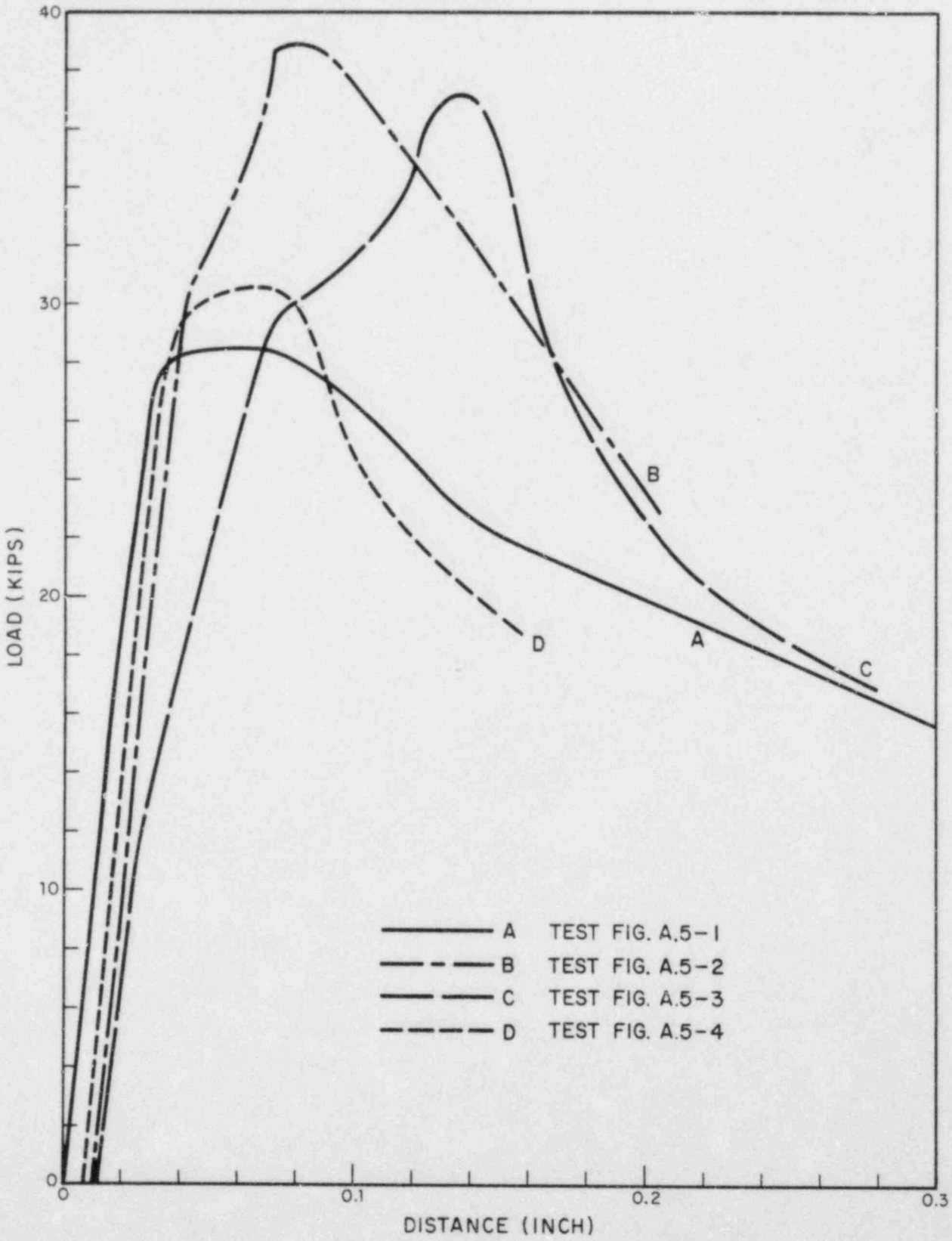

FIGURE A.5-10 FORCE-DEFLECTION CURVES
MOVEMENT OF SHEAR PLUG IN 4.5 IN. THICK
REINFORCED CONCRETE BARRIERS

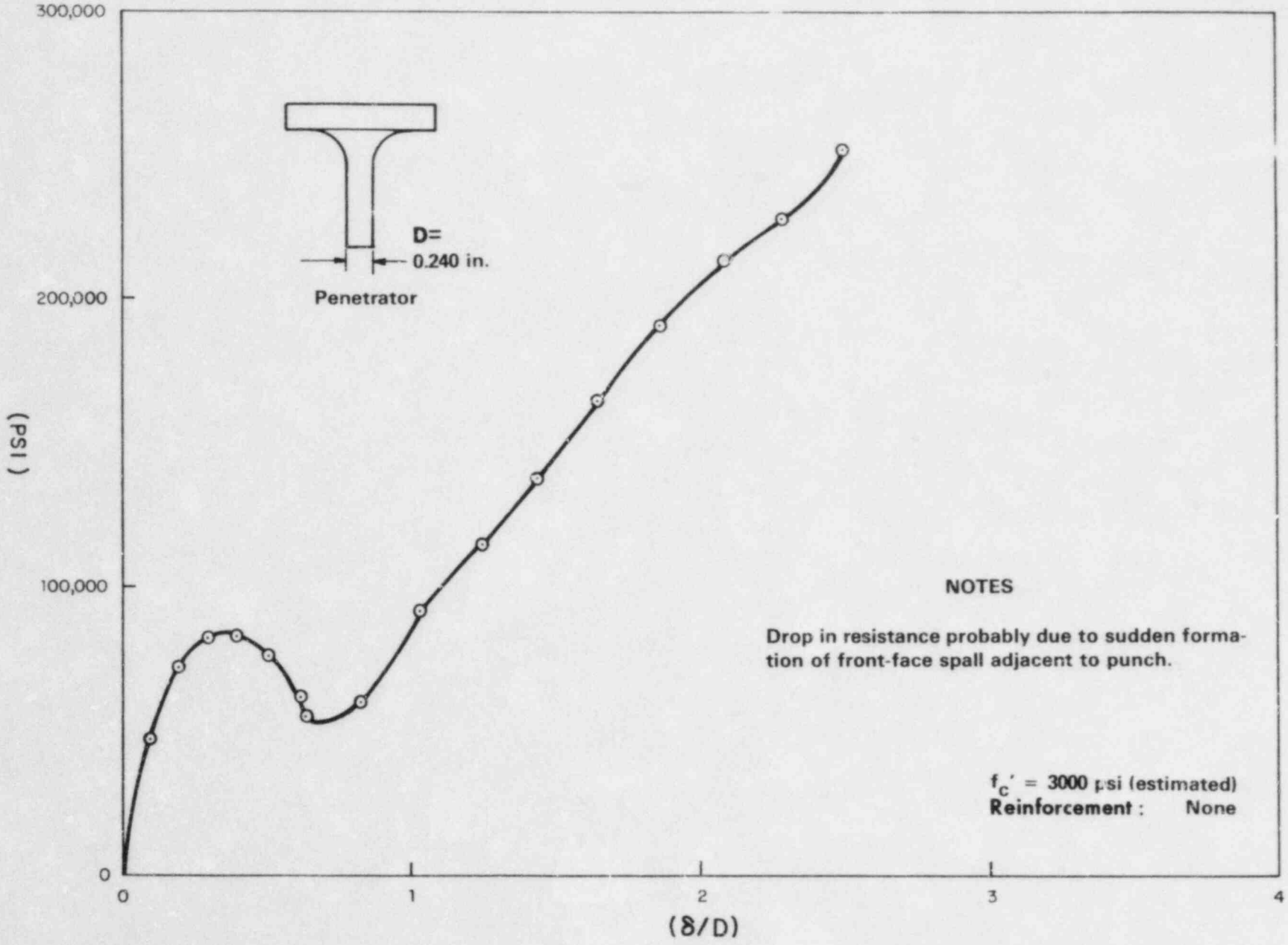

FIGURE A.6-1 STATIC PENETRATION RESISTANCE - TEST I

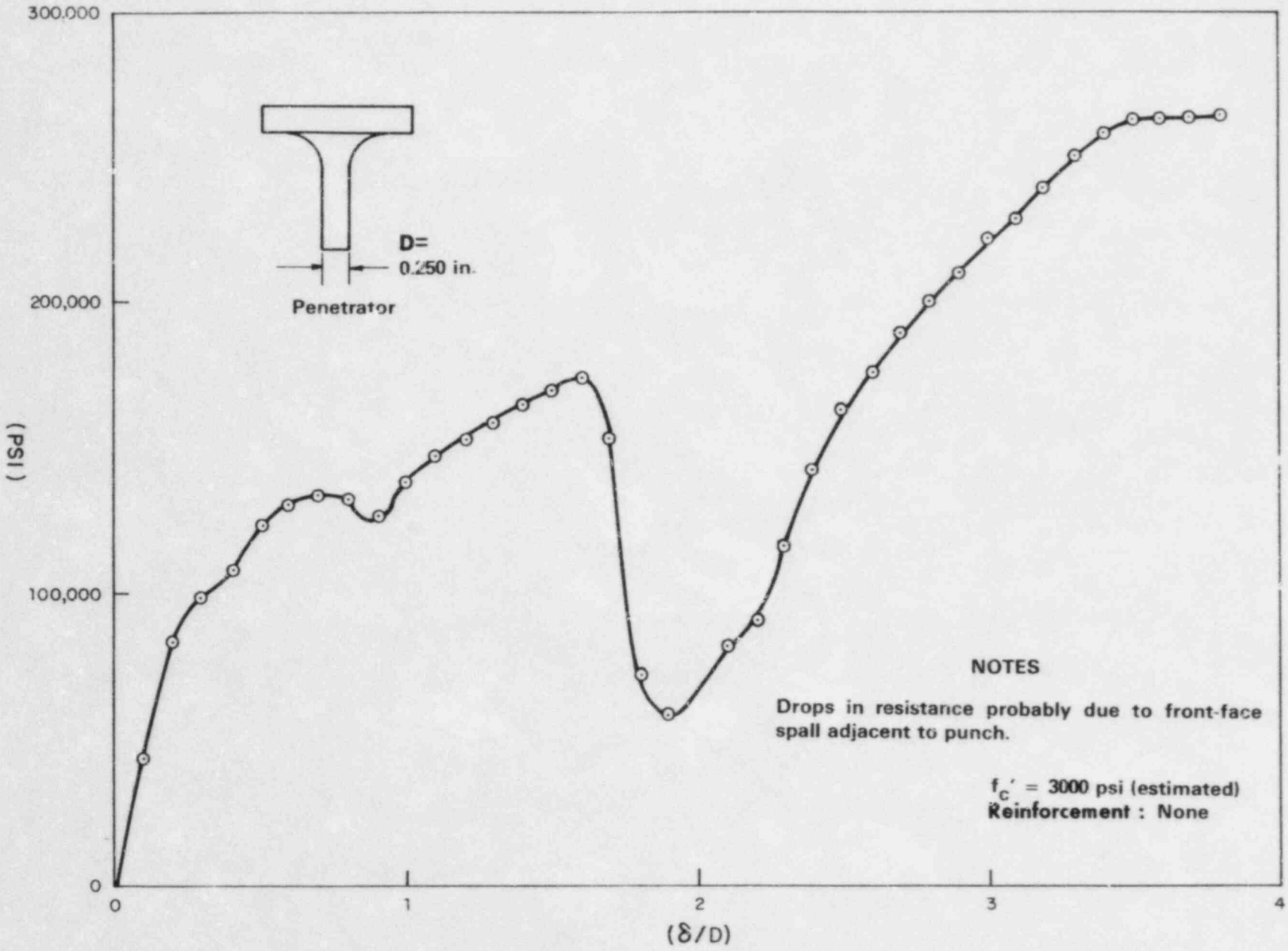

FIGURE A.6-2 STATIC PENETRATION RESISTANCE - TEST II

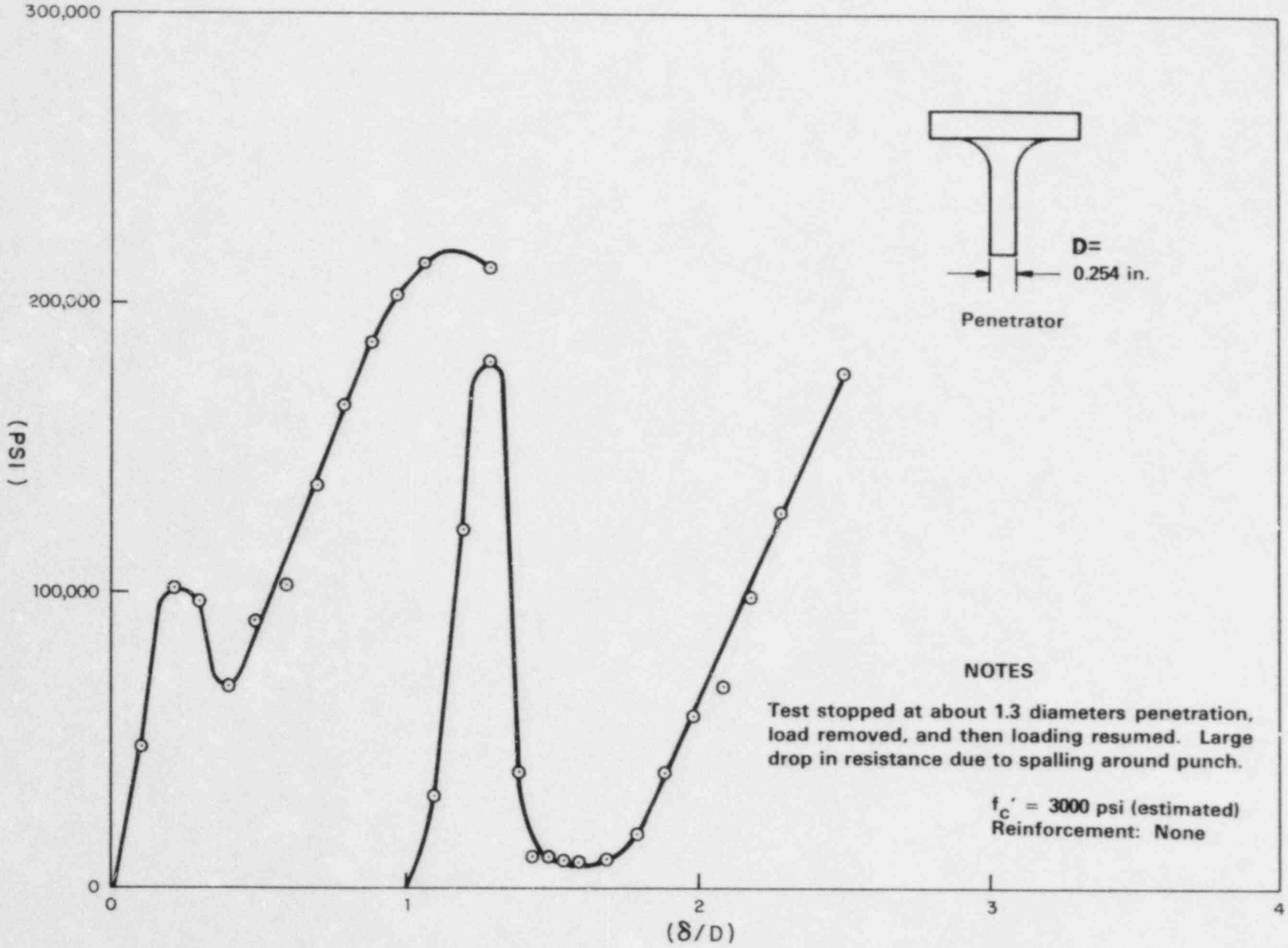

FIGURE A.6-3 STATIC PENETRATION RESISTANCE - TEST III

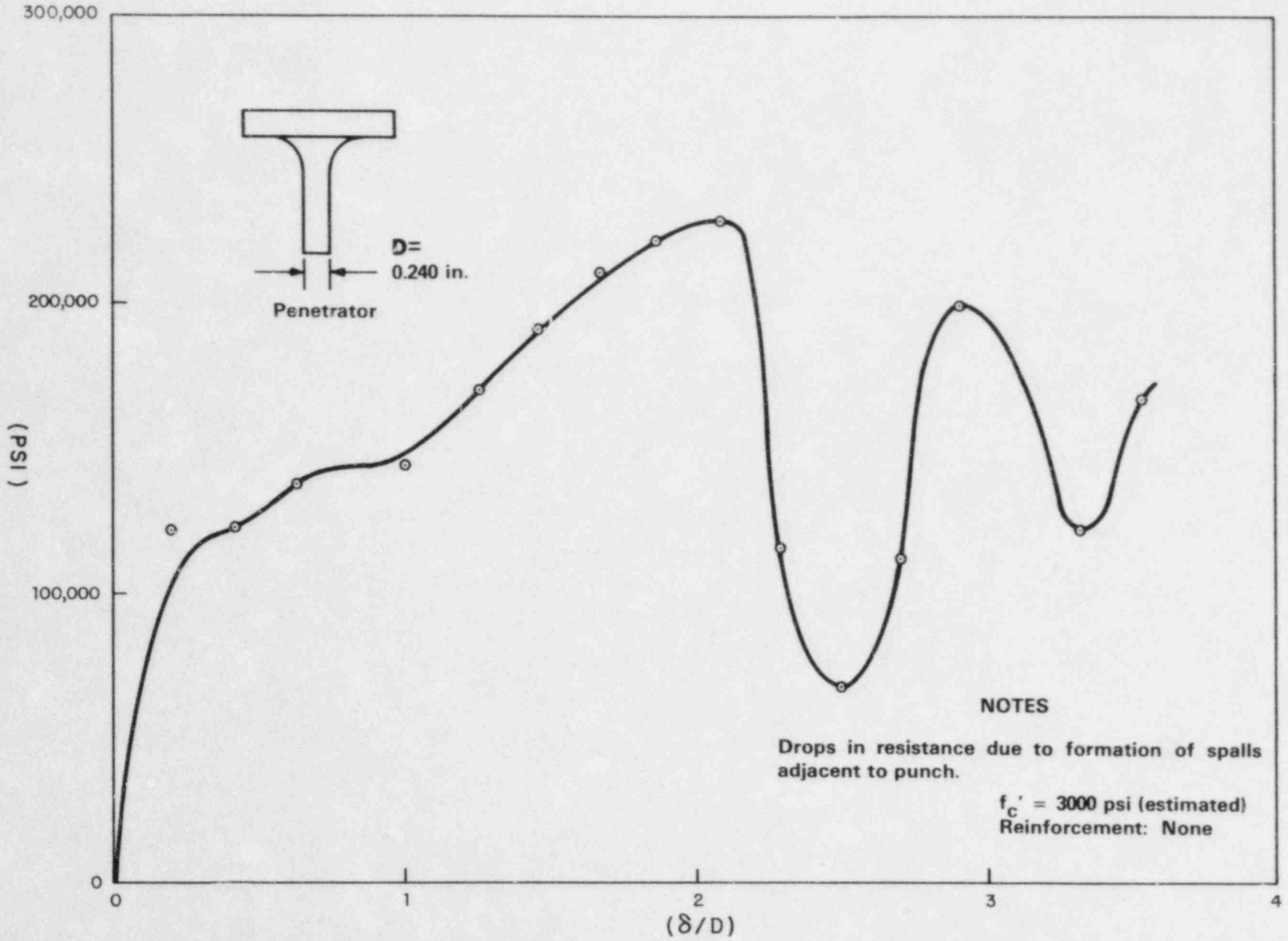

FIGURE A.6-4 STATIC PENETRATION RESISTANCE - TEST IV

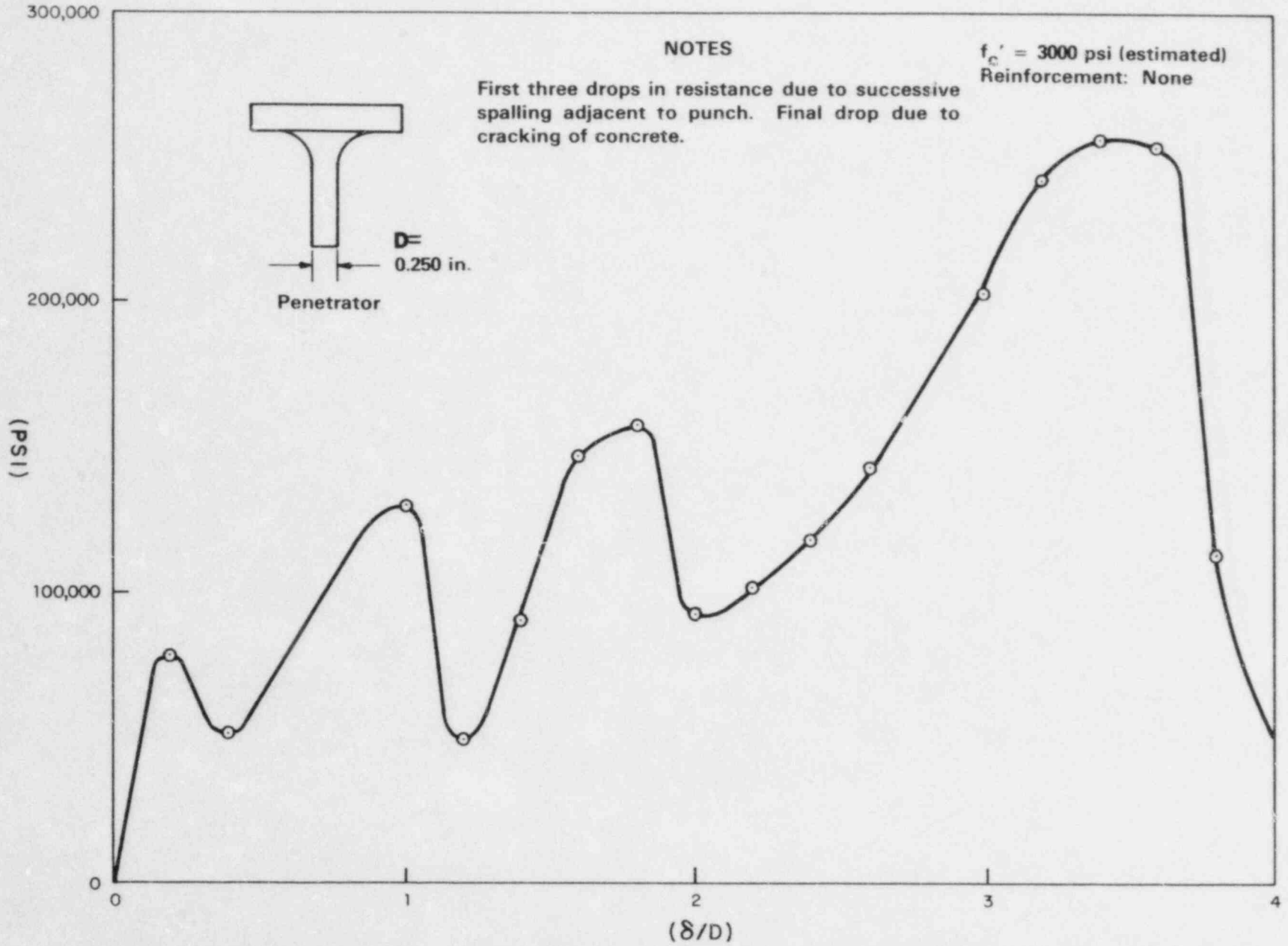

FIGURE A.6-5 STATIC PENETRATION RESISTANCE - TEST V

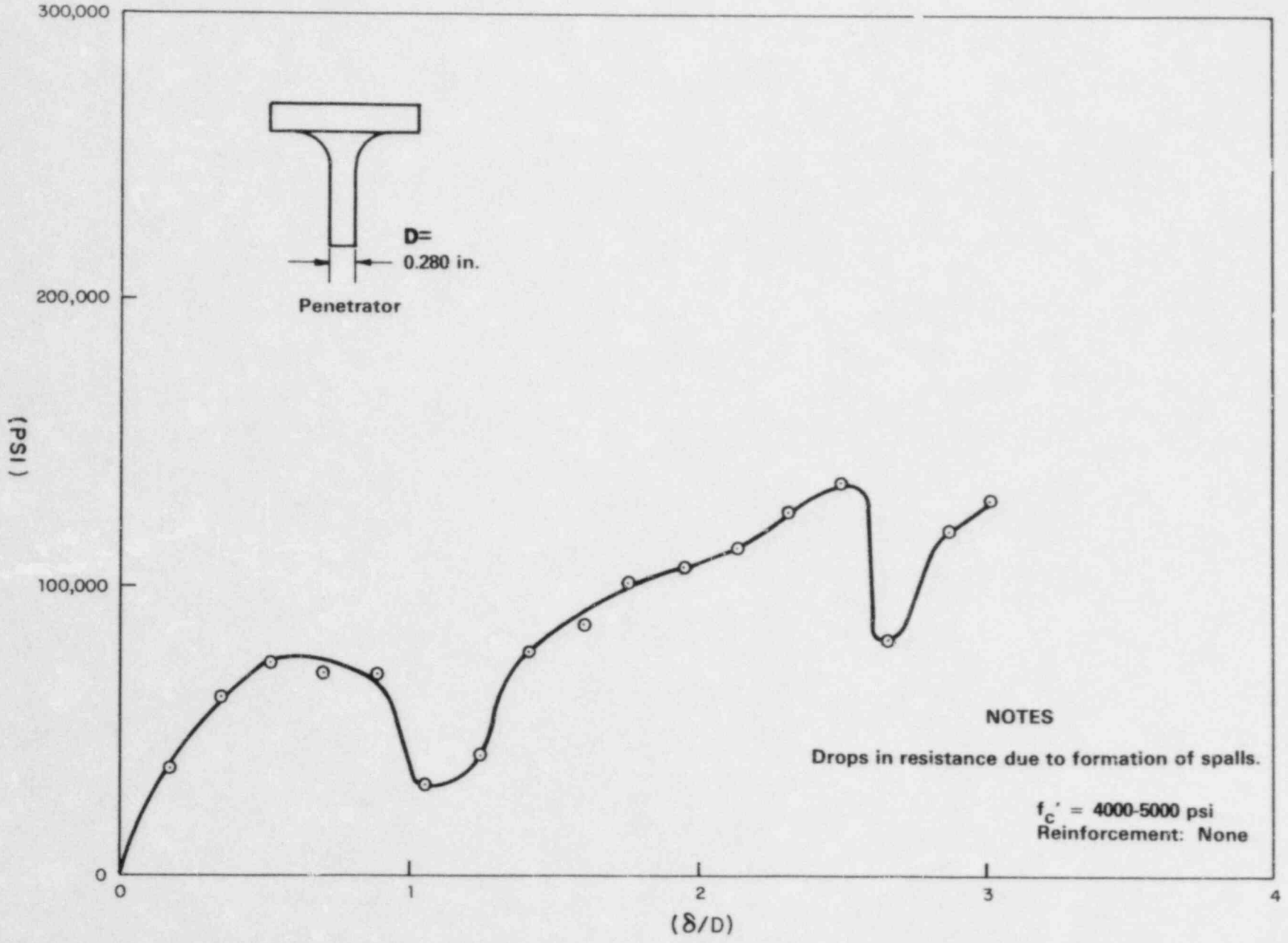

FIGURE A.6-6 STATIC PENETRATION RESISTANCE - TEST VI

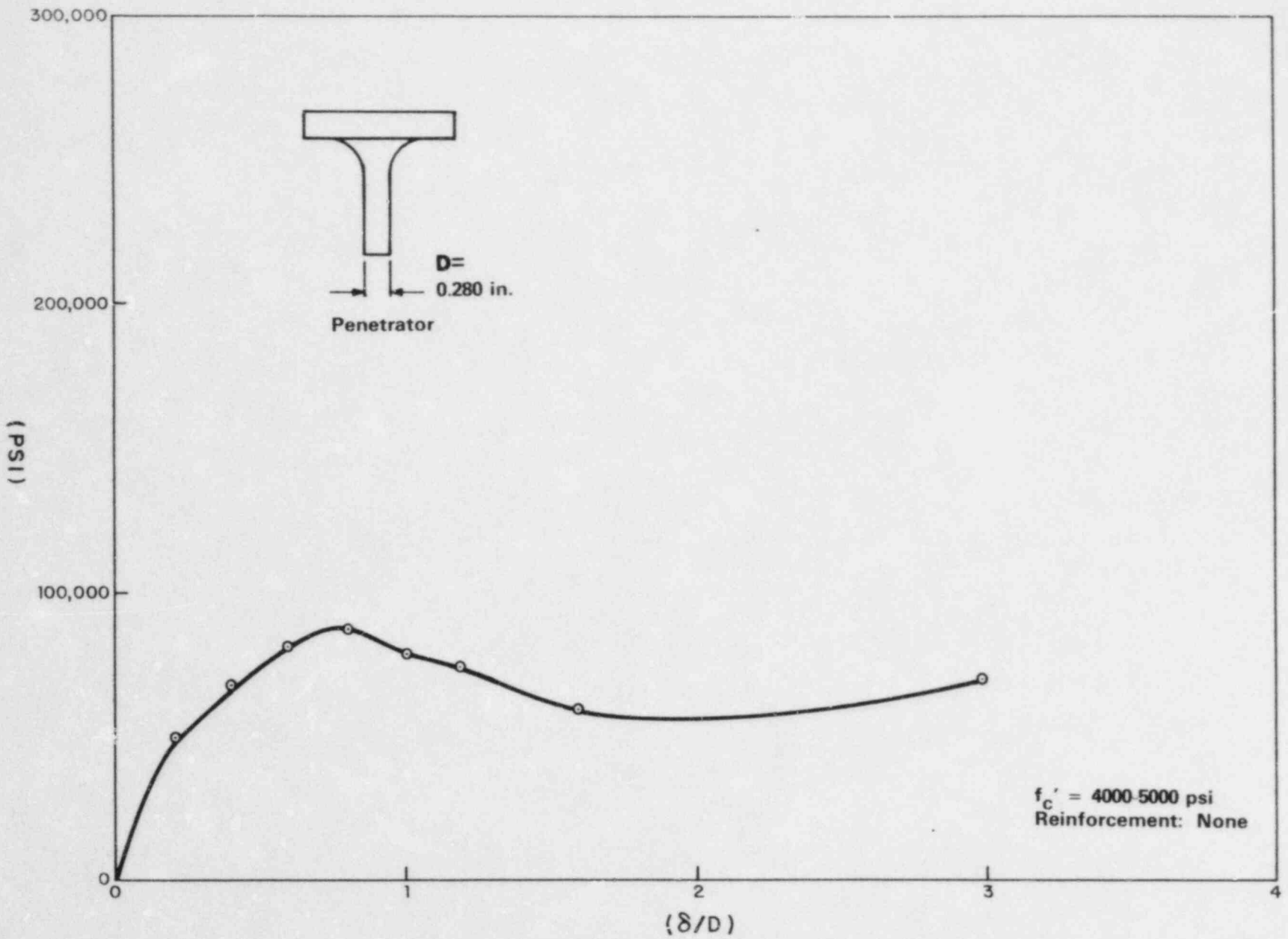

FIGURE A.6-7 STATIC PENETRATION RESISTANCE - TEST VII

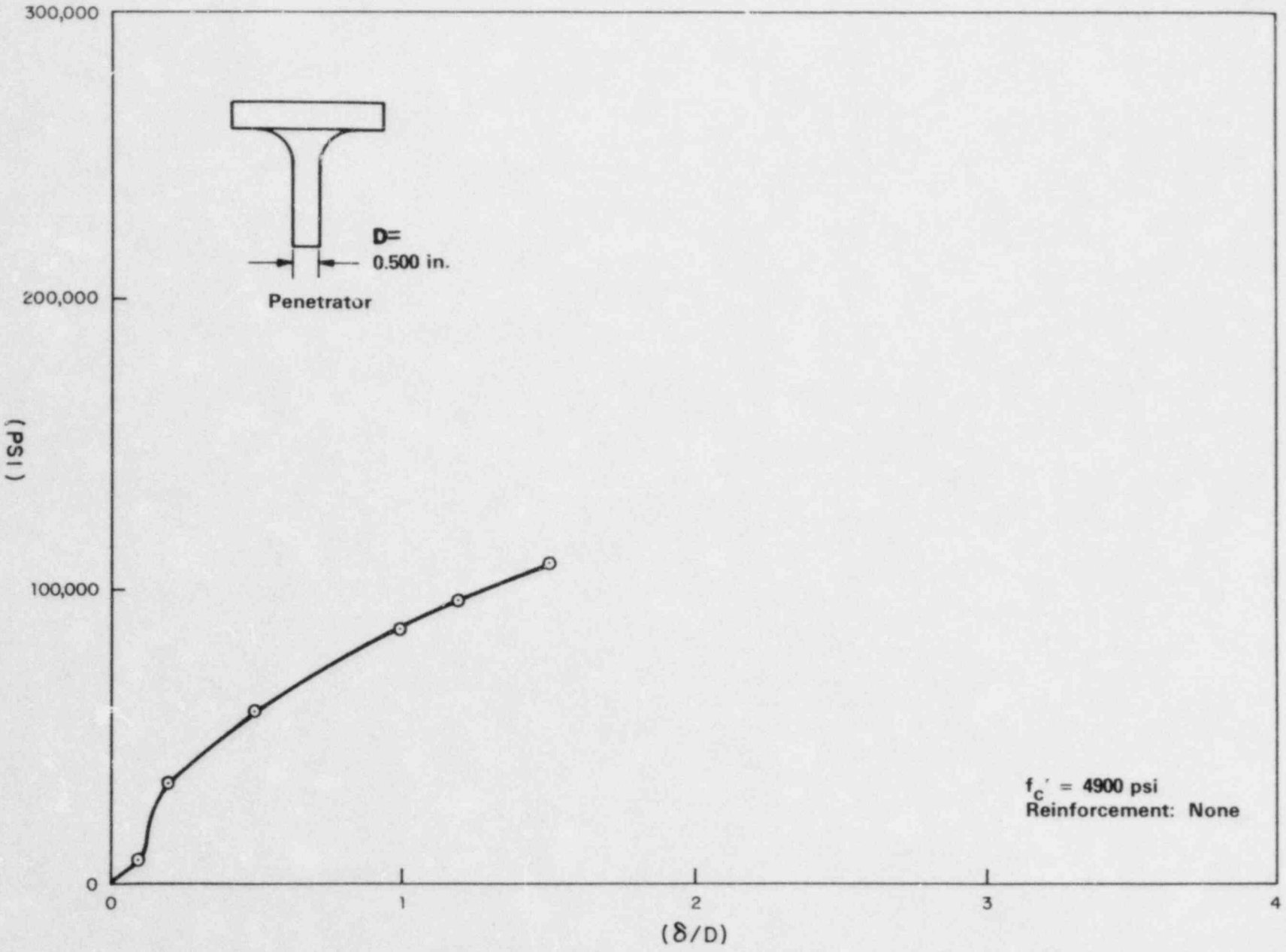

FIGURE A.6-8 STATIC PENETRATION RESISTANCE - TEST VIII

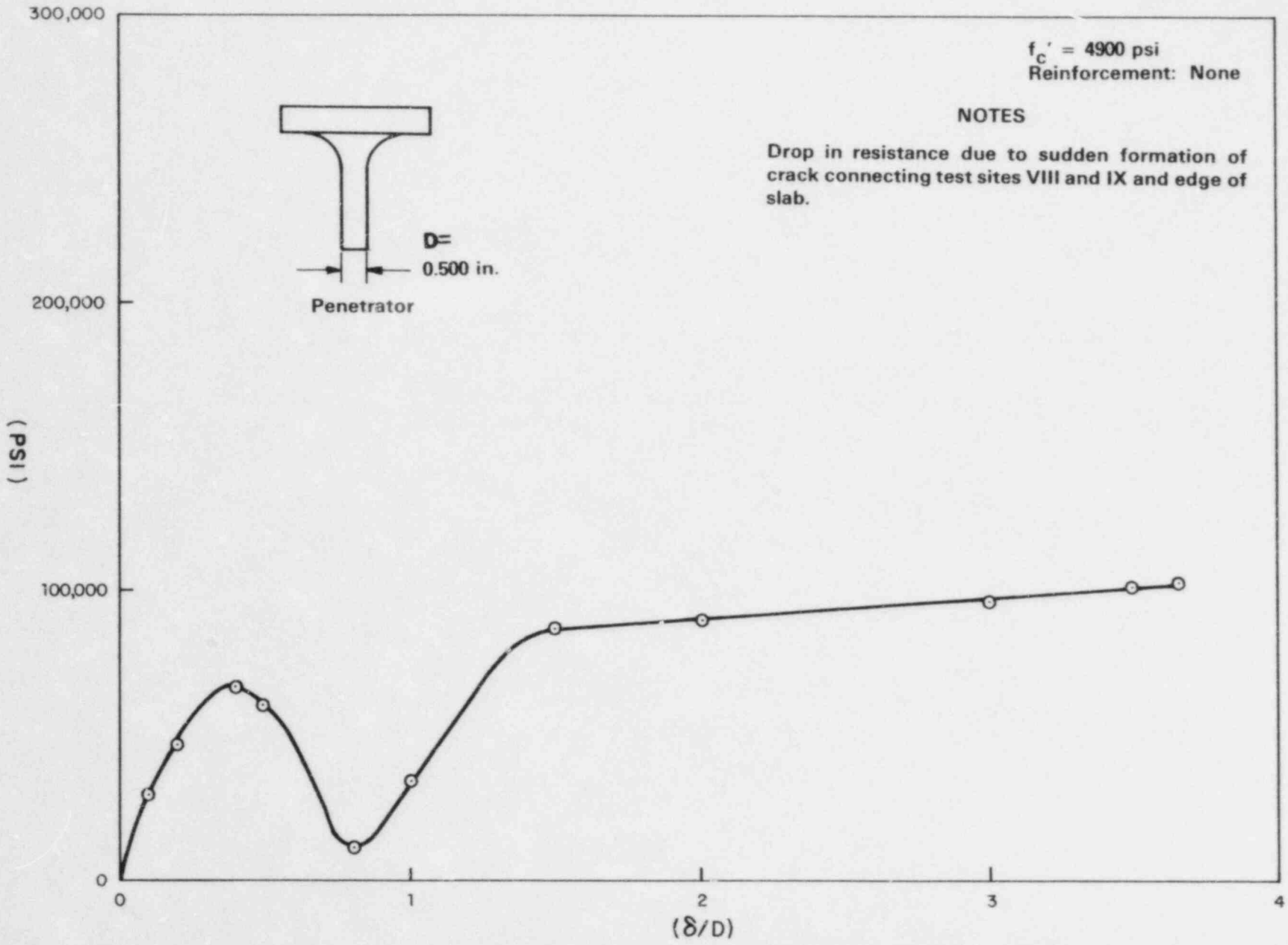

FIGURE A.6-9 STATIC PENETRATION RESISTANCE - TEST IX

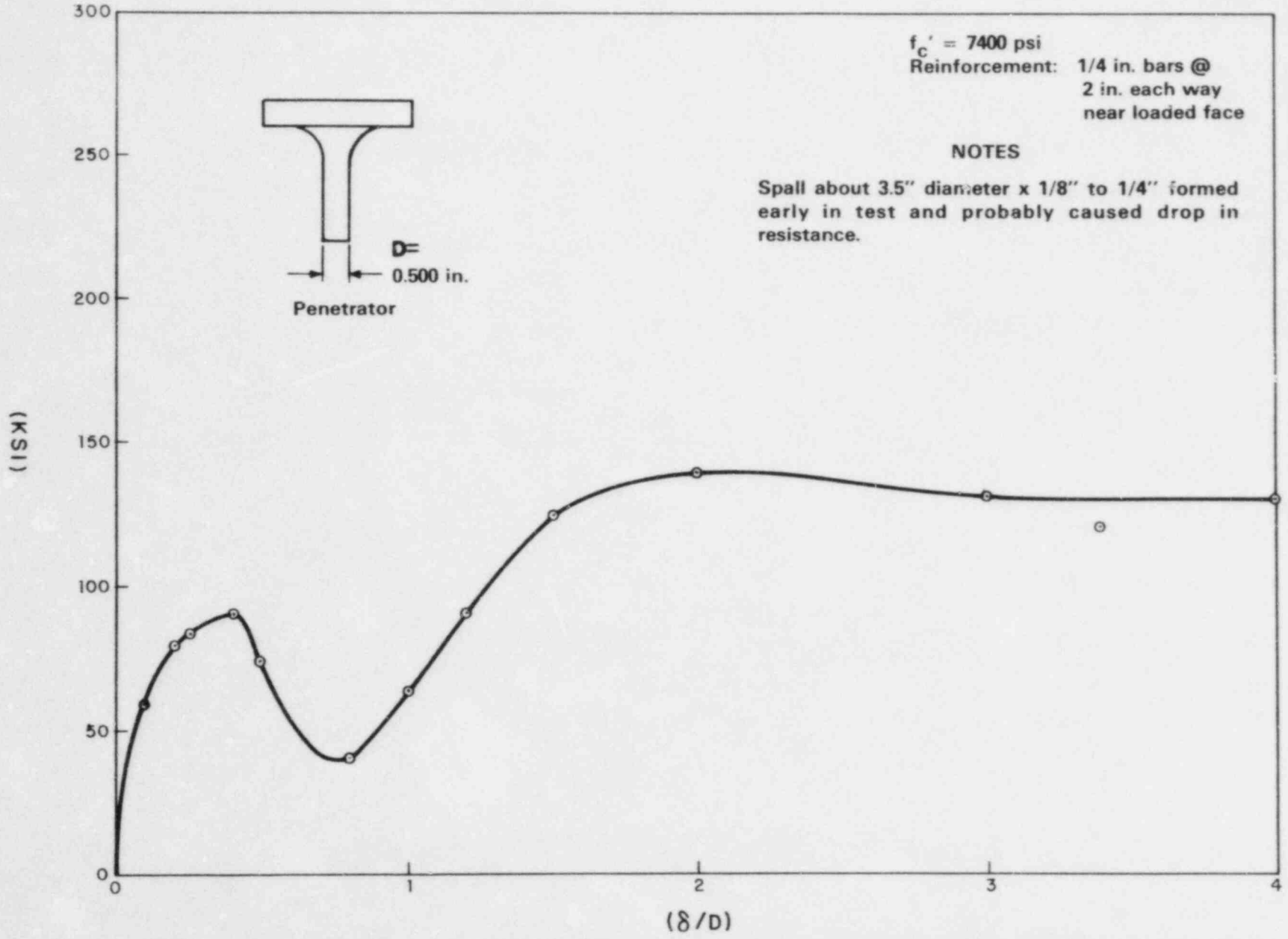

FIGURE A.6-10 STATIC PENETRATION RESISTANCE - TEST X

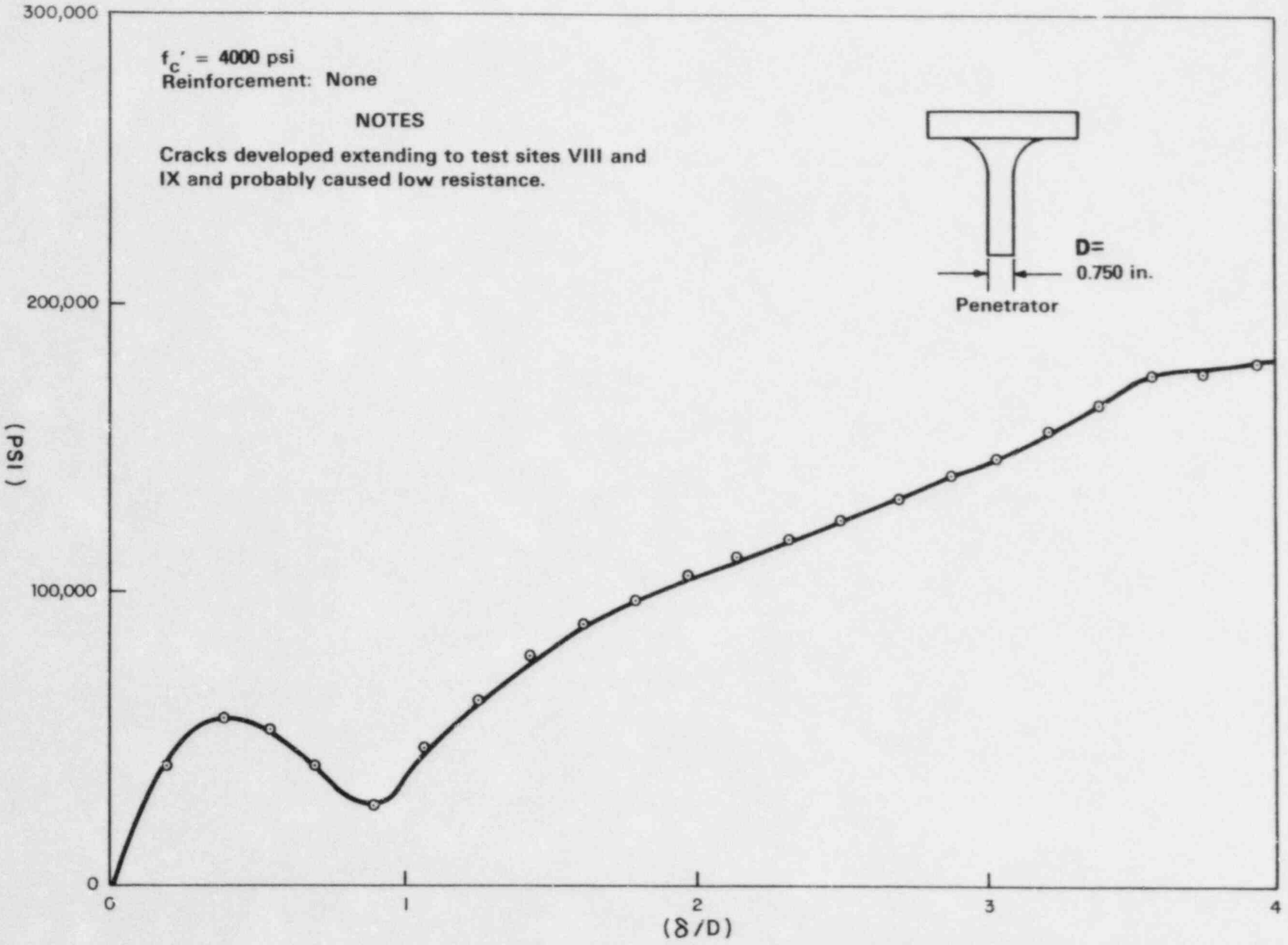

FIGURE A.6-11 STATIC PENETRATION RESISTANCE - TEST XI

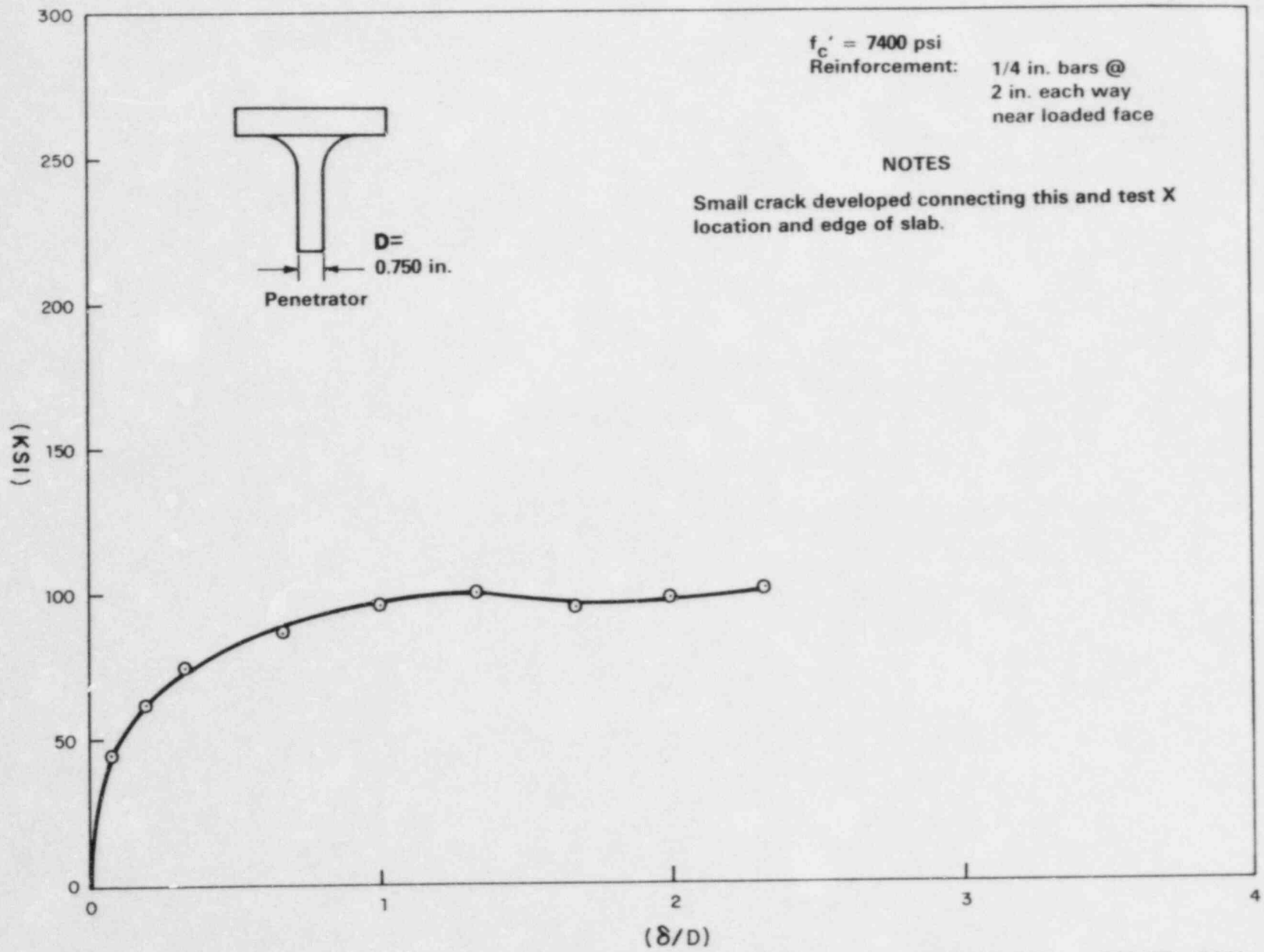

FIGURE A.6-12 STATIC PENETRATION RESISTANCE - TEST XII

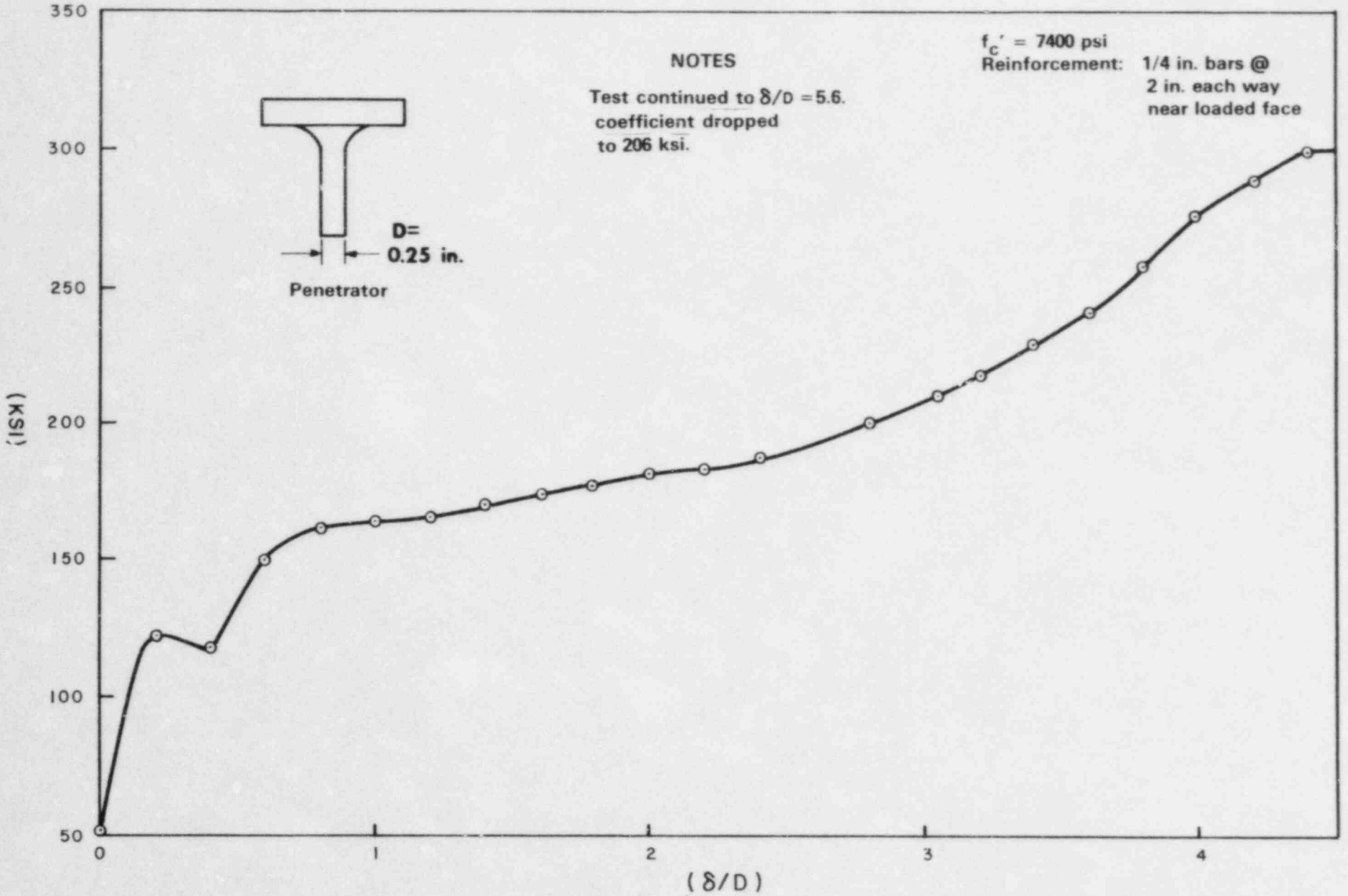

FIGURE A.6-13 STATIC PENETRATION RESISTANCE - TEST XIII

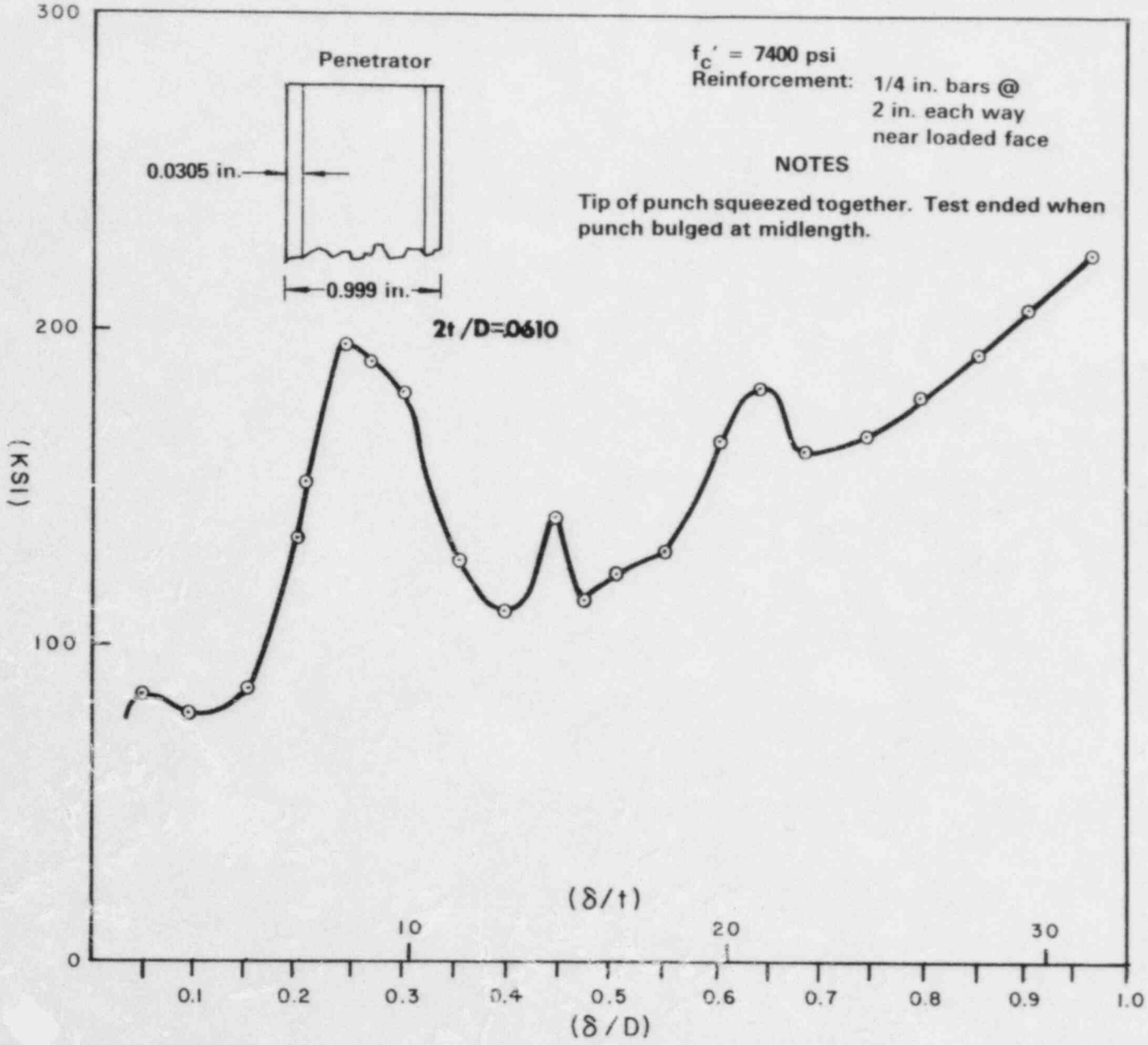

FIGURE A.6-14 STATIC PENETRATION RESISTANCE - TEST XIV

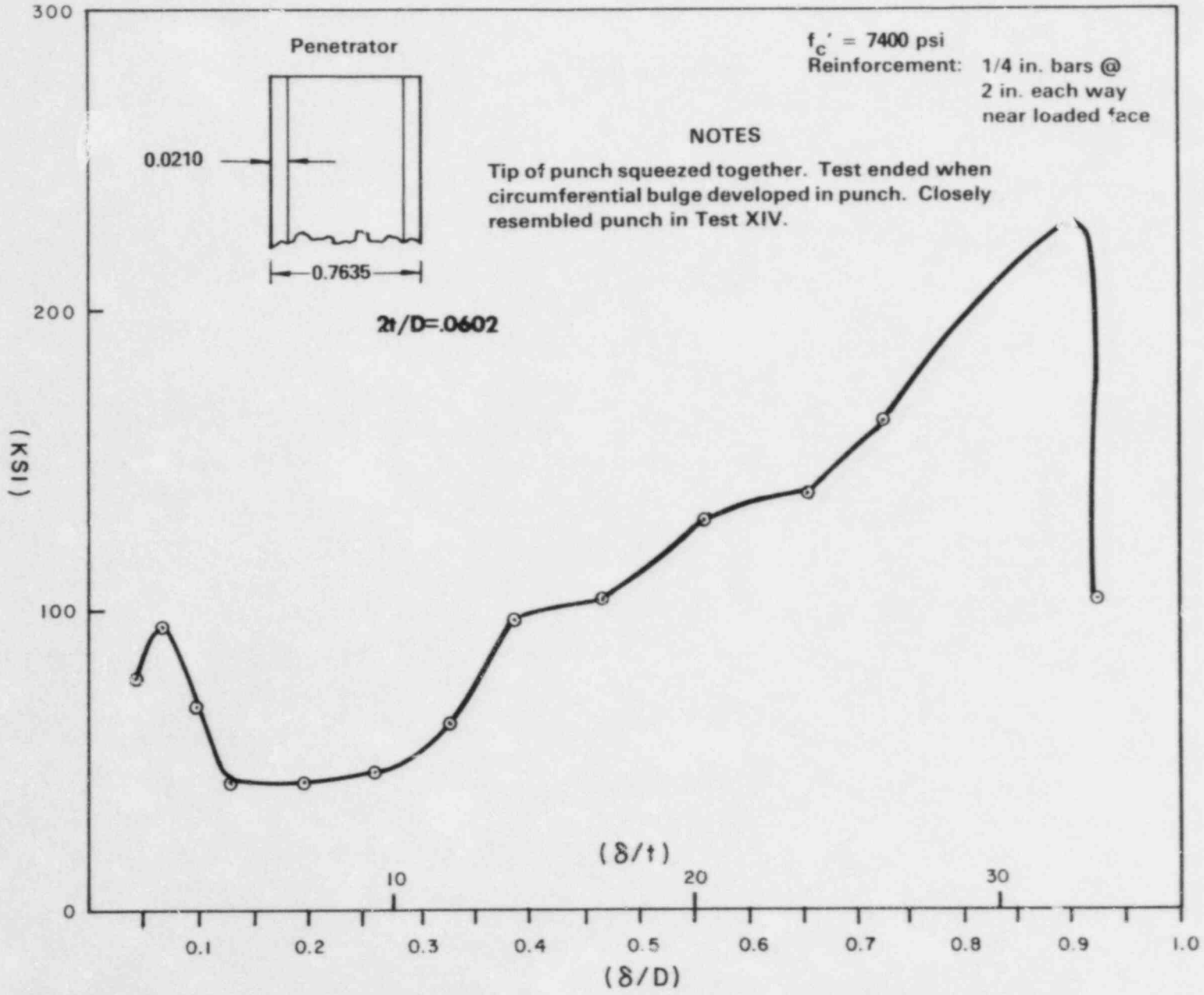

FIGURE A.6-15 STATIC PENETRATION RESISTANCE - TEST XV

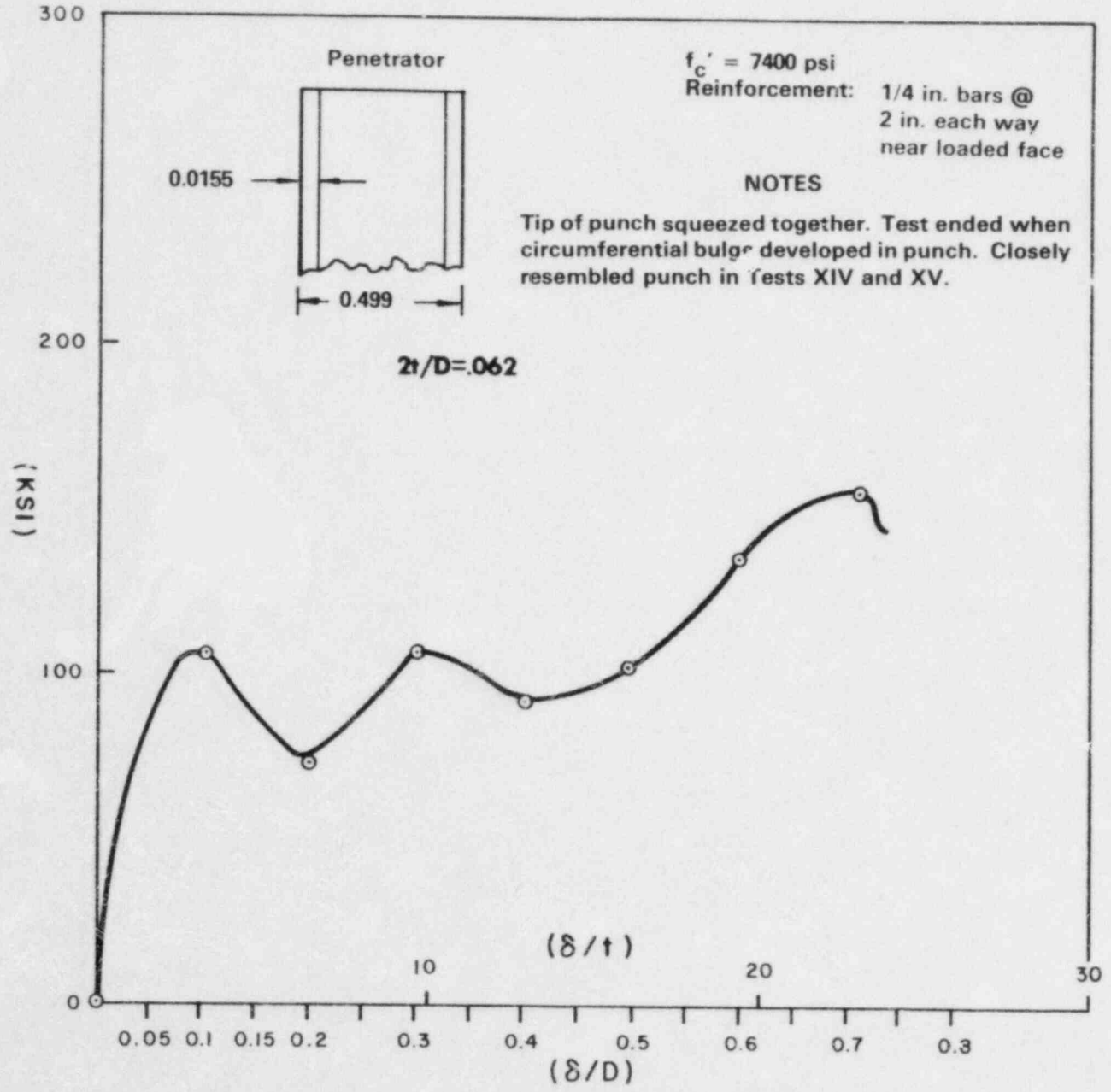

FIGURE A.6-16 STATIC PENETRATION RESISTANCE - TEST XVI

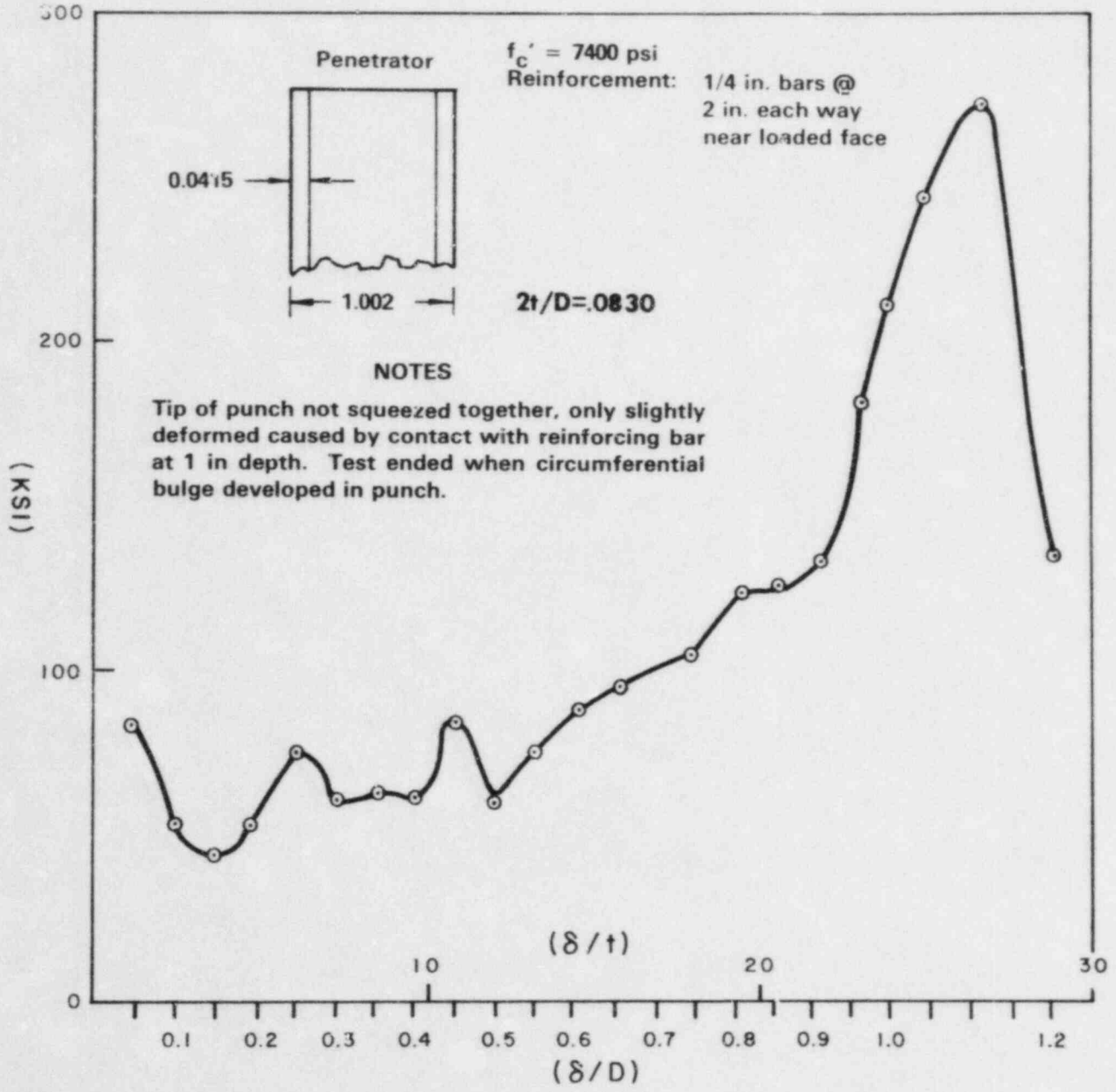

FIGURE A.6-17 STATIC PENETRATION RESISTANCE - TEST XVII

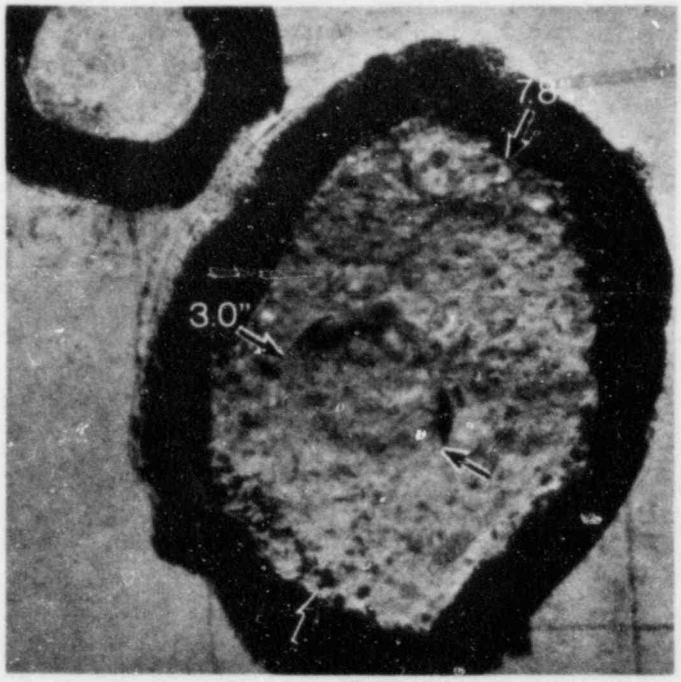

A. IITRI - One-Quarter Size
Test 2 V = 207 fps

B. IITRI -
Test 30

BARRIER

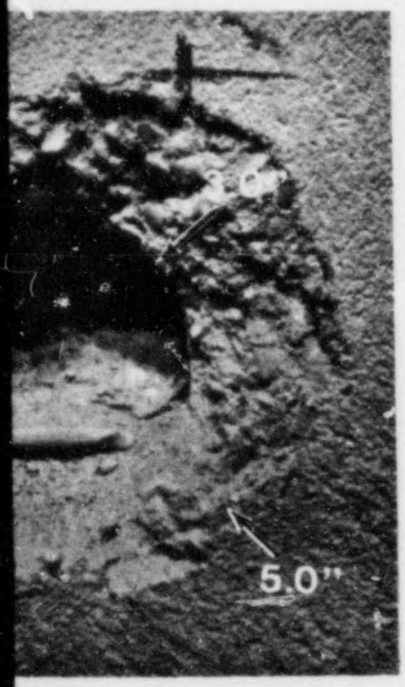

One-Quarter Size
V = 245 fps

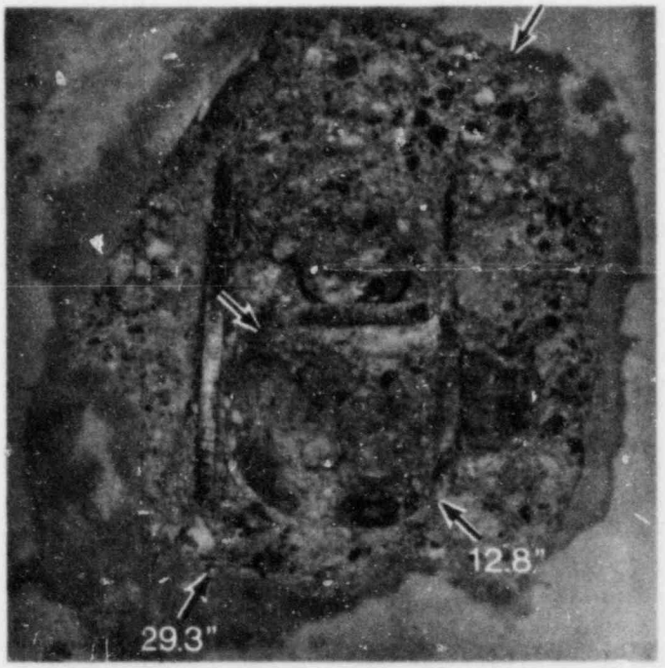

C. Sandia - Full Size
Test 8 V = 202 fps

FRONT FACE

FIGURE A.8.2-1
COMPARISON OF IITRI ONE-QUARTER SIZE WITH SANDIA FULL SIZE MISSILE BARRIER TESTS - 6 IN. AND 24 IN. BARRIERS

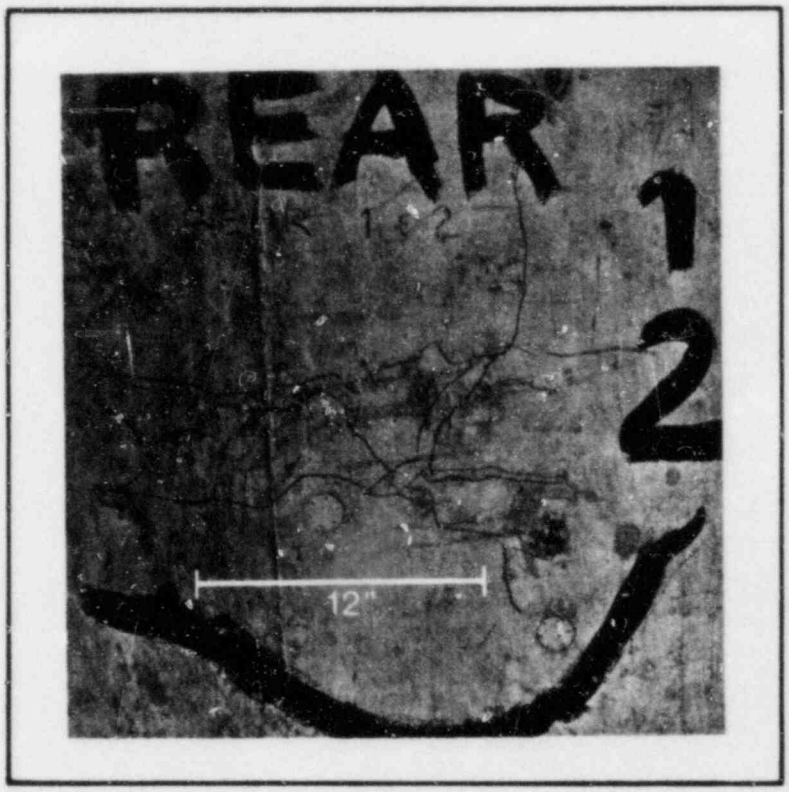

D. IITRI - One-Quarter Size
Test 2 V = 207 fps

E

BARRIER

IITRI - One-Quarter Size
Test 30 V = 245 fps

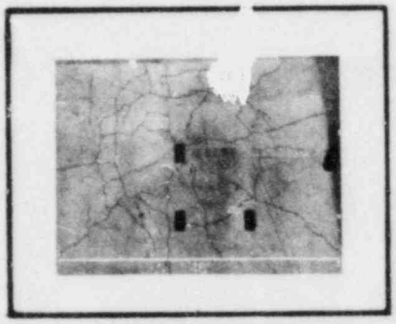

F. Sandia - Full Size
Test 8 V = 202 fps

R REAR FACE

FIGURE A.8.2-2
COMPARISON OF IITRI ONE-QUARTER SIZE WITH SANDIA FULL SIZE MISSILE BARRIER TESTS - 6 IN. AND 24 IN. BARRIERS

G. IITRI - One-Quarter Size
Test 2 V = 207 fps

H. IITRI
Test 3

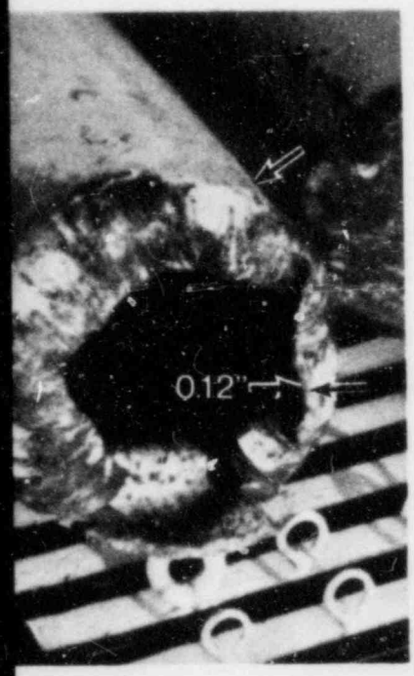

- One-Quarter Size
0 V = 245 fps

I. Sandia - Full Size
Test 8 V = 202 fps

MISSILES

FIGURE A.8.2-3
COMPARISON OF IITRI ONE-QUARTER SIZE WITH SANDIA FULL SIZE MISSILE BARRIER TESTS – 6IN. AND 24 IN. BARRIERS

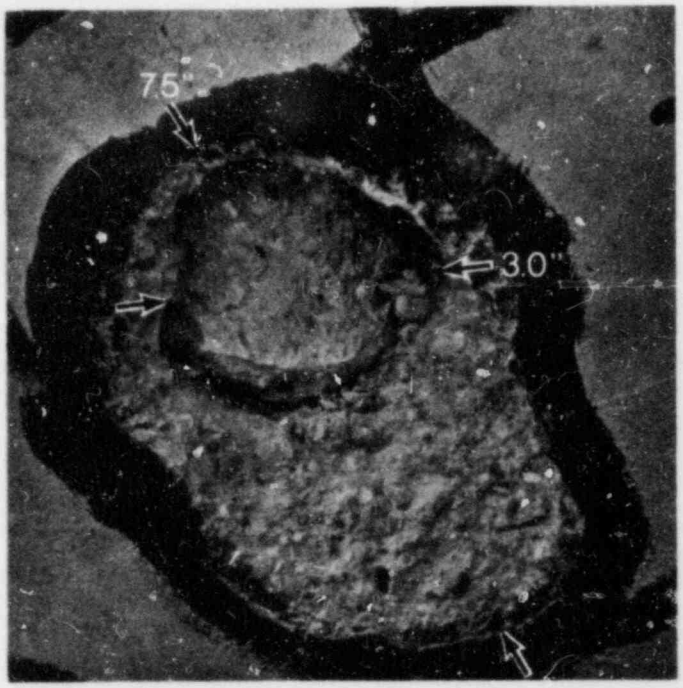

J. IITRI - One-Quarter Size
Test 7 V = 211 fps

K. IITRI -
Test 28

BARRIE

- One-Quarter Size
V = 195 fps

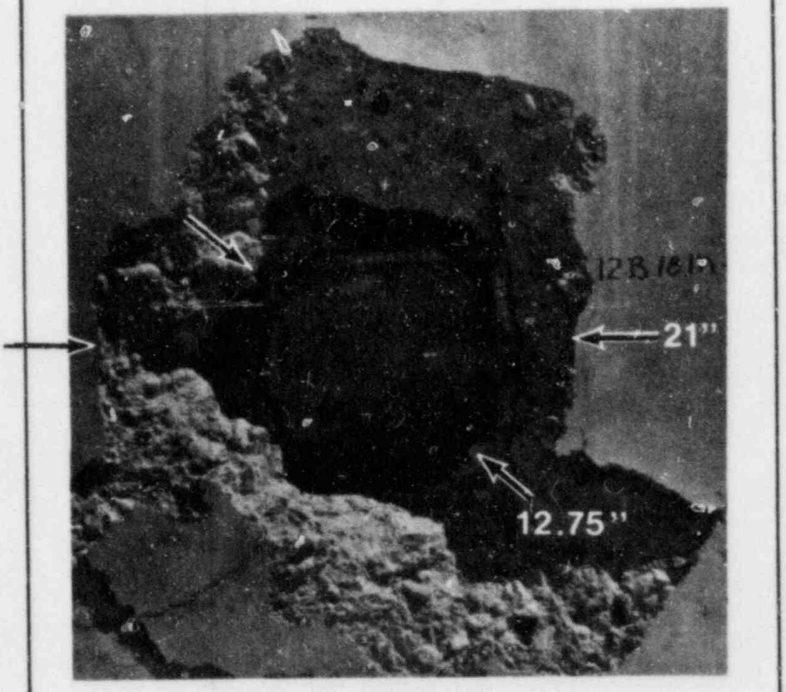

L. Sandia - Full Size
Test 4 V = 202 fps

R FRONT FACE

FIGURE A.8.2-4
COMPARISON OF IITRI ONE-QUARTER SIZE WITH SANDIA FULL SIZE MISSILE BARRIER TESTS — 4.5 IN. AND 18 IN. BARRIERS

M. IITRI - One-Quarter Size
Test 7 V = 211 fps

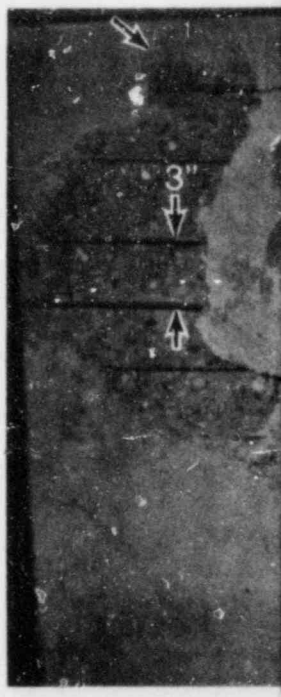

N. IITRI -
Test 28

BARRIE

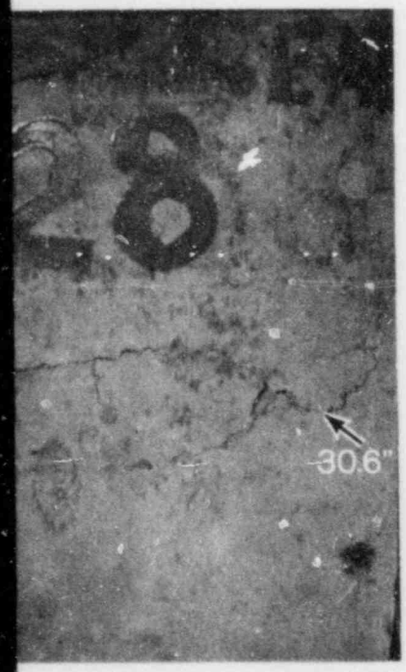

One-Quarter Size
V = 195 fps

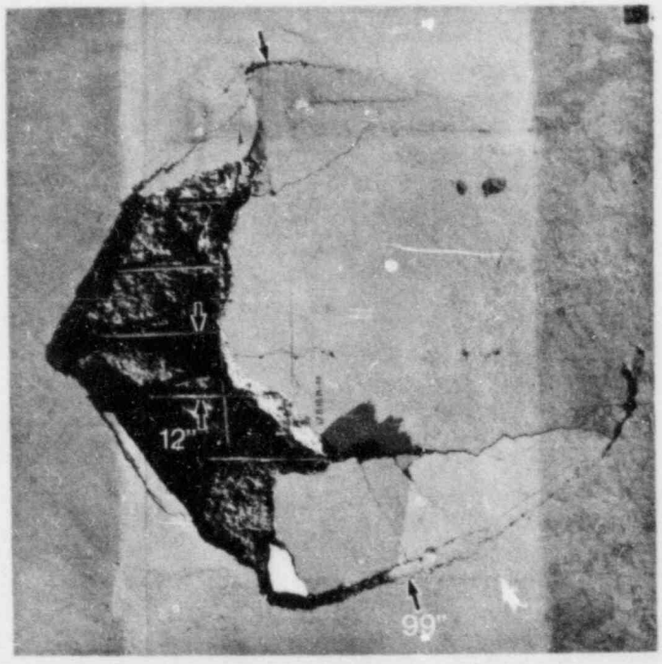

O. Sandia - Full Size
Test 4 V = 202 fps

R REAR FACE

FIGURE A.8.2-5
COMPARISON OF IITRI
ONE-QUARTER SIZE WITH
SANDIA FULL SIZE MISSILE
BARRIER TESTS —
4.5 IN. AND 18 IN. BARRIERS

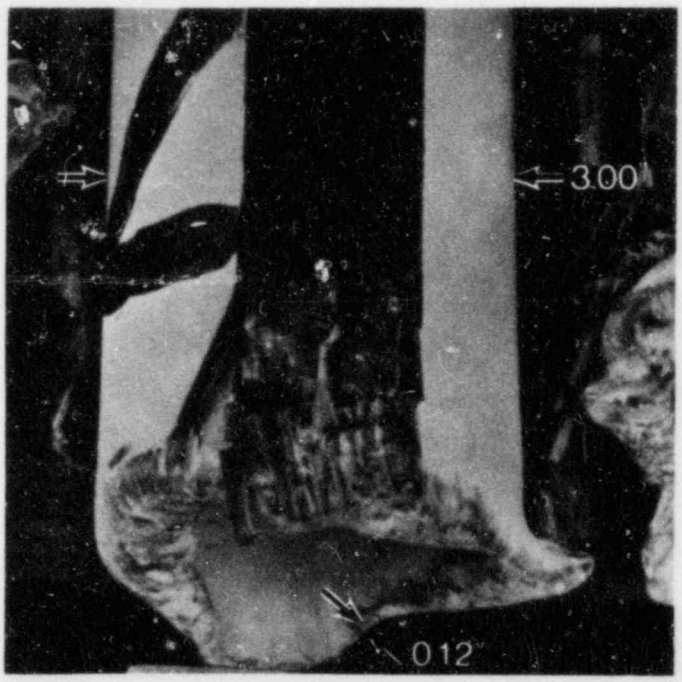

P. IITRI - One-Quarter Size
Test 7 V = 211 fps

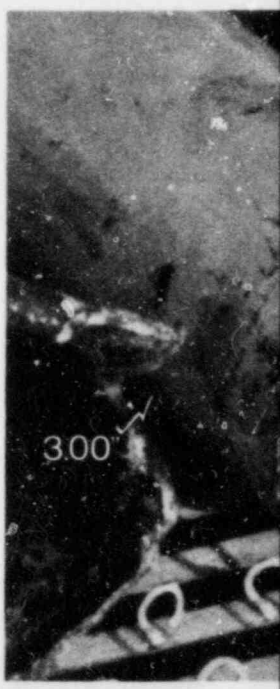

Q. IITRI -
Test 28

M

One-Quarter Size
V = 195 fps

R. Sandia - Full Size
Test 4 V = 202 fps

SSILES

Also Available On
Aperture Card

8403160096-16

FIGURE A.8.2-6
COMPARISON OF IITRI ONE-QUARTER SIZE WITH SANDIA FULL SIZE MISSILE BARRIER TESTS — 4.5 IN. AND 18 IN. BARRIERS

APPENDIX B

EMPIRICAL DESIGN FOR LOCAL RESPONSE

TABLE OF CONTENTS

LIST OF TABLES

LIST OF FIGURES

APPENDIX B

EMPIRICAL DESIGN FOR LOCAL RESPONSE

B.1 PURPOSE

The purpose of this Appendix is to present a design diagram, Figure B.3-1, and procedures for determining reinforced concrete barrier thickness that will preclude scabbing caused by missiles of concern to the nuclear power industry. An additional purpose is to provide a method for designing scab plates to contain secondary concrete missiles.

B.2 SUMMARY

Section B.3 describes the process of scabbing for barriers with thicknesses 1.5 to 3 times the missile diameter. Also described is the design diagram, Fig. B.3-1, and its use in establishing thickness of reinforced concrete barriers to prevent scabbing.

The figure is based primarily on the quarter-scale S&W-IITRI missile barrier test program. However, the accuracy and reliability of the design diagram curves for full-scale predictions are established by comparison with full-scale test data, especially the data obtained in the Bechtel-Calspan program[2]. The level of protection furnished corresponds to the barrier scabbing threshold. The curves shown are also represented approximately by the empirical formulas given in Fig. B.3-1. Another method described allows for the influence of concrete strength when it is less than the strength used in the testing programs.

The design diagram is then, in Section B.4, applied to tornado-borne pipe and automobiles. (Wood missiles fall outside the range of this diagram. The wood utility pole is eliminated as a missile which may cause scabbing as a result of the tests in Appendix A.)

The procedure in Section B.5 for the design of pipe whip barriers uses the kinetic energy of the pipe at impact to determine the effect on the barrier. Kinetic energy is absorbed by crushing of the pipe (possibly up to complete flattening). The degree of flattening determines both the area of contact between pipe and barrier and the final impact force on the barrier. This information and the available kinetic energy are used with Fig. B.3-1 to give a conservative procedure for designing reinforced concrete barriers against scabbing under pipe whip loading.

An illustration of how to apply Fig. B.3-1 to impact from aircraft engines is given in Section B.6. The method is similar to that for the engine of a tornado-borne automobile.

In design for turbine missile impact, the approach used in Section B.7 is to replace a turbine missile (with its complicated geometry) by an equivalent solid cylinder (slug). This cylinder has a contact area that is the mean between the actual contact area of the missile and that of a circle circumscribing the contact area. The equivalent cylinder has the same mass, striking velocity, and kinetic energy as the actual missile. The barrier design process then becomes identical with that for slug impact and is based on Fig. B.3-1.

Figure B.3-1 allows the design of concrete barriers for the above categories of steel industrial missiles. The parameters of primary importance on the figure are the missile kinetic energy, barrier thickness, missile wall thickness, and missile outside diameter. The applicability of this figure is limited to certain ranges of these parameters as shown on the figure.

Section B.8 provides a method for characterizing secondary concrete missiles when the primary missile is traveling at a velocity in excess of the scabbing threshold velocity. It also presents a method for designing scab plates to contain secondary concrete missiles if they should occur.

This Appendix concludes that Fig. B.3-1, a) enables conservative design of barriers for no scabbing, b) takes into account the average or characteristic pressure between missile and barrier, and c) is more reliable and economical when used for missiles similar to those tested than when used for other industrial missiles such as whipping pipes where this method produces less economical designs. This method of designing reinforced concrete barriers to prevent scabbing is a significant improvement over the various methods previously used by the nuclear power industry for the following reasons:

1. Unlike procedures using military formulas (Petry, NDRC, etc), it is based on tests of industrial missiles - pipes and slugs, rather than solid shaped projectiles - at the velocities characteristic of such missiles.

2. Unlike the procedure described in Rotz,[2] this method is size independent (i.e., it is not limited to missiles and barriers of dimensions close to those of the test program) and makes proper allowance for pipe wall thickness and average impact force, which play a very significant role in producing scabbing.

B.3 EVALUATION FOR LOCAL DAMAGE TO REINFORCED CONCRETE BARRIERS

The interaction mechanics of end-on pipe impact against a reinforced concrete barrier from 1.5 to 3 missile diameters in thickness are as follows:

At low velocities, either the pipe wall buckles and deforms (if thin and weak) or it penetrates the concrete a certain distance. In the latter case, the penetration distance can be predicted fairly accurately by assuming the concrete to have a penetration resistance of 50 ksi over the net pipe cross-sectional area. The penetration distance is found by dividing the striking kinetic energy of the missile by the resisting force (50 ksi multiplied by its net cross-sectional area). At low velocities, there is no damage to either the interior or the back face of the barrier.

At some velocity, the barrier begins to experience internal damage. A shear plug in the form of a frustum of a cone of total internal angle about 120 deg is formed. The smaller end of the shear plug coincides with the bottom of the penetration hole of the pipe missile, or with the circle of contact if the missile deforms instead of penetrating. The larger end of the shear plug is outlined by a rough circle of cracks on the rear face of the barrier.

As the striking velocity is increased, the shear plug is displaced more and more and eventually its motion causes scabbing (at first only the reinforcement cover). The scabbing threshold velocity is the primary subject of this Appendix.

The testing that has been performed and on which the present procedure is based covers a certain range of striking velocities, a limited range of ratios of barrier thickness to missile diameter, etc. The ranges of the experimental programs generally correspond to conditions encountered in design. However, care should be taken not to extrapolate much beyond the testing limits.

Figure B.3-1 defines the impact conditions for the scabbing threshold for end-on strikes of pipe and solid cylindrical missiles on reinforced concrete barriers. The limiting conditions of applicability are indicated in the figure. The curves are conservative in that they correspond to the lower limit of the observed data and not to mean values.

The series of converging straight (dashed) lines for $0.25 \leq T/D \leq 1.0$ in Fig. B.3-1 represents a very conservative assumption for the effects of large missiles for which no test data now exists. It is highly important to get experimental data for this T/D band since it is significant in pipe whip and may possibly be in other situations.

Figure B.3-1 applies to steel pipe or slug missiles or the equivalent. It presents the relationships of four parameters: missile kinetic energy/(barrier thickness)^3 = KE/T^3, barrier thickness/missile diameter = T/D, missile wall thickness/missile radius = 2t/D, and the impact force/gross area of impact = σ_{av}. The lowest curve is for solid slugs and the others for pipes of different wall thickness/radius ratios. Note that all lengths are in inches. The scabbing threshold velocity of a given missile-barrier combination can be obtained directly as follows: from the ratios T/D and 2t/D, a point is located on the figure (generally involving interpolation) and the ordinate of that point gives the corresponding value of KE/T^3. With T known, the required missile kinetic energy can be found; and from it and the mass of the missile and the scabbing threshold velocity of the missile can be obtained. On the other hand, finding the required barrier thickness for given impact conditions involves trial and error. First, assume a barrier thickness and find the corresponding kinetic energy. Compare it with the missile energy, and then correct the thickness and repeat the process until a satisfactory design results.

In Fig. B.3-1, no dependence on either barrier reinforcement or concrete strength is shown, provided both lie within conventional design limits (as indicated on that figure). This is because both these parameters appear to have only secondary influence on the scabbing threshold velocity of a particular barrier. For example, in the one-quarter scale S&W-IITRI tests there were two types of 6 in. barriers with reinforcement ratios of 0.32 percent and 0.86 percent each way in each face, respectively. In analyzing the test data, it was found impossible to differentiate between the scabbing thresholds for the two reinforcement levels. (However, there is a difference in behavior at higher velocities and more severe levels of damage.)

The influence of concrete strength (or the absence of such influence) is not clearly established since there were no systematic variations of concrete strength with a given barrier thickness in the S&W-IITRI program. However, there are the following indications: a) in static penetration tests of concrete by solid and hollow cylindrical punches, there was no apparent correlation between penetration resistance and concrete strength when the latter varied over the range of 3.0 ksi - 7.4 ksi; b) in the dynamic tests on model barriers, the 4.5 in. barriers (3.2 ksi concrete) and the 6 in. barriers (3.8 ksi - 4.2 ksi concrete) showed no consistent difference in the initial penetration resistance; c) as shown in Section B.3.1, the predictions of the full-scale tests using Fig. B.3-1 (3.2 ksi - 4.0 ksi concrete) agreed well with the measured data of the Bechtel-Calspan tests (4.4 ksi - 5.8 ksi concrete).

For these reasons, it is considered undesirable to make any allowance for concrete strengths greater than those of the S&W-IITRI tests when using Fig. B.3-1 (3.2 ksi for T/D = 1.5 and 4.0 ksi for T/D = 2.0). On the other hand, pending experimental determination of the effect of lower concrete strength, a conservative allowance for a lower strength can be made in the analysis as is discussed in Section B.3-2 of this Appendix.

B.3.1 Comparison of Fig. B.3-1 Predictions with Full-scale Test Data

The Bechtel-Calspan program contained 17 full-scale tests in which 8 in. slugs and pipes were fired at 12 in., 18 in., and 24 in. reinforced concrete barriers[3]. For nearly every missile-barrier combination, there were two or three tests in which damage levels ranged from no or light scabbing to moderate or severe scabbing. Since this data was not used in preparing Fig. B.3-1, a good indication of the full-scale reliability of that figure is obtained by comparing its predictions with the Bechtel data. Table B.3-1, which is partially taken from Rotz[2], permits this comparison. In Table B.3-1 the next to the last column gives the scabbing velocities deduced from the Bechtel test data by the authors of that report. The last column of Table B.3-1 gives the scabbing threshold velocities predicted by Fig. B.3-1. It can be seen that the Fig. B.3-1 predictions a) agree well with the measured data, and b) except in one case of close agreement, are more conservative by 6 to 17 percent than the velocities deduced from the test data.

The following calculations are typical of those used to obtain the numbers appearing in the final column of Table B.3-1.

Calculation I: Scabbing velocity for Bechtel-Calspan Tests 4F, 3F, and 1F (214 lb, 8 in. diameter slugs against 12 in. barriers).

> T/D = 1.5. From the slug curve of Fig. B.3-1, KE/T^3 = 0.16 ksi. Then KE = 0.16 x 1728 = 276 k-in. The predicted scabbing velocity is given by V^2 = 276(64.4)/(0.214 x 12) = 6934, and V =83 fps.

Calculation II: Scabbing velocity for Bechtel-Calspan Tests 15F and 16F of Table B.3-1 (202 lb, 8 in. Schedule 40 pipe against 12 in. barriers).

> T/D = 12/8.625 = 1.4; 2t/D = 2 x 0.322/8.625 = 0.075. From Fig. B.3-1, KE/T^3 = 0.58 ksi. Then KE = 0.58 x 1728 = 1002. The scabbing velocity is given by V^2 = 1002(64.4)/(0.202 x 12) = 26,621 and V = 163 fps.

A second full-scale test program has been conducted by Sandia Corporation under contract with Electric Power Research Institute (EPRI)[3]. This program utilized the NRC 743 lb 12 in. Schedule 40 pipe missile against 12 in., 18 in., and 24 in. reinforced concrete barriers (3.35 ksi-4.69 ksi concrete). While no special attempt was made to establish threshold scabbing velocities for these barriers, the test results are compatible with the predictions of Fig. B.3-1. For example, against the 24 in. barrier a 202 fps velocity caused only cracks. The predicted scabbing velocity is 269 fps. For the 18 in. barrier, velocities close to 200 fps in four shots all caused scabbing, while two shots at about 155 fps only resulted in back face flaking (see comment in Table B.3-2). The predicted scabbing threshold velocity is 170 fps. For the 12 in. barrier, an impact at 98 fps caused scabbing while another at 92 fps resulted in flaking. The predicted scabbing threshold velocity is 87 fps. Table B.3-2 presents the EPRI-Sandia data together with Fig. B.3-1 predictions.

These consistently conservative discrepancies between the predicted scabbing threshold velocities and those observed in full-scale tests are to be expected since Fig. B.3-1 is based on the lower limits of observed data and not on mean values. This is because Fig. B.3-1 is intended as a set of design curves and is, therefore, expected, on the average, to overpredict damage and underpredict scabbing threshold velocity. The remainder of Section B.3 gives examples of the use of Fig. B.3-1.

B.3.2 Allowance for Barrier Concrete Strength Variation

Figure B.3-1 is believed to give conservative missile barrier scabbing protection for concrete strengths between 3.0 ksi and 4.5 ksi. However, there has not been any systematic experimental determination of the influence of barrier

concrete strength on scabbing phenomena. Pending such a study, it is recommended that, for additional conservatism, corrections be introduced for concrete strengths lower than those on which Fig. B.3-1 is based. However, it is recommended that no allowance for higher strengths be made without experimental justification. The conservatism inherent in both pipe whip and turbine missile design is so great that any correction for barrier strength variation is probably unwarranted.

In Fig. B.3-1, the ordinates are missile kinetic energy divided by barrier thickness cubed (KE/T^3). This has the dimension of stress (ksi). The ordinate can be made dimensionless by dividing it by a stress that is characteristic of the scabbing phenomenon. Probably, the most logical stress to use for this purpose is the punching shear strength of the barrier concrete which is customarily assumed to vary as the square root of its cylinder strength. However, a more conservative assumption is to divide KE/T^3 by the cylinder strength f_c' itself, making the new ordinate dimensionless of the form $(KE/f_c'T^3)$. It is not proposed to redraw Fig. B.3-1 on this basis since the change is simply a device for making a conservative allowance for concrete strength and, at this time, has no other justification. Instead, the suggested allowance for smaller strengths can be made simply by assuming barrier thickness cubed to vary inversely with concrete strength relative to test program strength.

In Fig. B.3-1, data points at T/D = 1.5 are for barriers of about 3.2 ksi concrete, and those at T/D = 2 are for 4.0 ksi barriers. For example, if Fig. B.3-1 indicates that a certain thickness, T, is needed for T/D = 2, a corrected thickness, T', for a 3.0 ksi barrier would be

$$T' = T(4.0/3.0)^{1/3} = 1.1T$$

On this basis, noting that f_c' = 3.2 ksi for T/D = 1.5 on Fig. B.3-1, the following table of corrections has been developed.

Concrete Strength Correction Factors for Thicknesses from Fig. B.3-1*

	T/D = 1	1.5	2	2.5
Barrier f_c' = 3.0	1	1.05	1.10	1.15
3.2	1	1	1.10	1.15
3.5	1	1	1.05	1.10
≥4.0	1	1	1	1.05

*An alternative method of allowing for differences in concrete strengths is to maintain the punching shear capacity of a barrier. The resulting multiplying factors are found to be very slightly smaller than those presented.

B.4 TORNADO MISSILE-BARRIER DESIGN

B.4.1 Tornado-borne Pipe Missiles

The calculation procedure using the curves of Fig. B.3-1 to determine the barrier thickness for a given missile and velocity is as follows: assume a value of barrier thickness T, calculate the corresponding ratios, T/D and 2t/D. From Fig. B.3-1, read off the value of KE/T^3, calculate the kinetic energy (KE), then determine the missile velocity and compare it with the specified velocity. A sample calculaton is summarized below.

For a 12 in. Schedule 40 pipe weighing 743 lbs, determine the barrier thicknesses to prevent scabbing over a range of impact velocities assuming $f_c' \geq 4.0$ ksi. (Note that this pipe is the most damaging of the NRC-specified wood and steel cylindrical tornado missiles.) The 2t/D ratio is 0.06 and the highest of the curves of Fig. B.3-1 applies.

Calculation of Scabbing Threshold Velocity of 743 lbs 12 in. Schedule 40 Pipe for 4.0 ksi Barriers of Given Thicknesses

T (in.)	T/D	KE/T^3 (ksi) (Fig. B.3-1)	KE (in.-kips)	V (fps)	V (mph)
12	0.9	.61	1,050	87	59
13	1.0	.65	1,420	101	69
14	1.1	.66	1,800	114	78
15	1.2	.67	2,250	127	87
16	1.3	.67	2,760	141	96
17	1.3	.68	3,350	155	106
18	1.4	.69	4,020	170	116
19	1.5	.70	4,770	186	127
20	1.6	.70	5,620	201	137
21	1.6	.71	6,560	218	148
22	1.7	.71	7,610	234	160
24	1.9	.73	10,040	269	184
27	2.1	.74	14,620	325	222

According to these calculations, the NRC-specified tornado missile velocities require the following barrier thicknesses for scabbing protection against the 12 in. Schedule 40 pipe:

NRC Zones	V (mph)	V (fps)	KE (in.-kips)	T (in.)
Zone 1	105	154	3,300	17
Zone 2	63	92	1,200	13

B.4.2 Tornado-borne Automobile

The engine of an automobile that strikes a reinforced concrete barrier exerts a

concentrated loading of short duration which is capable of causing scabbing. The body, chassis, etc. contribute to structural response but not to scabbing. The engine applies its loading through whatever is in front of it (bumper, radiator, air conditioner, timing gear mechanism, etc.) so that the loading is not instantaneous such as that of a slug. Moreover, an engine is not a solid block of metal or a slug. Any transverse section through an engine will contain a large proportion of voids.

The ability of a missile to cause scabbing depends on the magnitude of the force it is capable of exerting during impact, as is illustrated by the difference between slugs and pipes, and by the difference between thick-walled and thin-walled pipes. In the case of an engine, this force is determined by the dynamic crushing strength of the weakest cross section toward the front of the engine. The weakest section is most likely to be one which has the smallest solidity ratio, γ, and the dynamic crushing strength would equal the net area of that section multiplied by the compression yield stress, or something slightly higher. Since solidity ratios vary from section to section, a very conservative assumption is to use the average solidity ratio, γ_{av}, in calculating the crushing strength. The average solidity ratio for all cross sections can be found by dividing the weight of the engine by the weight of an equal volume of solid metal. Only those portions of the engine which contribute to its strength in longitudinal compression should be included in this calculation. On this basis, the average impact stress, σ_{av}, is determined for use in Fig. B.3-1 by multiplying γ_{av} times the compression yield stress of the material of the engine. For use of the equation given in Fig. B.3-1, $\gamma = \gamma_{av}$ x compression yield stress/50 ksi. This is because the figure is constructed for missiles producing impact forces equal to 50 ksi times the cross-sectional area.

The calculation of barrier thickness to resist automobile engine-induced scabbing proceeds as follows. The missile weight is that of the engine plus whatever is firmly attached to it. The diameter of the equivalent cylindrical missile is calculated as for the turbine missile (see Section B.7). A barrier thickness is assumed and verified by use of Fig. B.3-1, in which the appropriate curve is the one corresponding to the σ_{av} found above.

Example

Assume that the engine (and those parts which are firmly attached to it) of a 4,000 lb automobile weighs 650 lbs and has a rectangular impact area 1.5 ft by 2.0 ft with a length of 2.0 ft. The circumscribed circle has a diameter of 2.50 ft and an area of 4.91 ft^2. Therefore, the equivalent impact area is 3.84 ft^2 and has a diameter of 2.21 ft. Calculate the scabbing threshold velocity for barrier thicknesses from 12 in. to 24 in. assuming $f_c \geq 4.0$ ksi.

The short block and the head are assumed to be the only portions of the engine which contribute to its longitudinal compressive strength and are assumed to weigh 335 lbs.

γ_{av} = 335/(1.5 x 2. x 2. x 490) = 0.11

Assuming that the compressive yield stress of the engine is 100 ksi,

γ = 0.11 x 100 ksi/50 ksi = 0.22
(Note that this corresponds to σ_{av} = 11 ksi)

For the calculation of the kinetic energy, the entire weight of the engine (650 lbs) is used and the results are given below.

Calculation of Scabbing Threshold Velocity of 650 lb Engine of 4000 lb Automobile for Barriers of Given Thicknesses*

T (in.)	T/D	KE/T^3 (ksi) (Fig. B.3-1)	KE (in.-kips)	V (fps)	V (mph)
12	0.5	.17	300	49	34
13	0.5	.19	410	58	40
14	0.5	.20	550	67	46
15	0.6	.21	720	77	53
16	0.6	.23	940	88	60
17	0.6	.24	1,190	99	68
18	0.7	.26	1,500	111	76
19	0.7	.27	1,860	124	85
20	0.8	.29	2,290	137	94
21	0.8	.30	2,780	152	103
22	0.8	.31	3,350	166	113
23	0.9	.33	4,000	182	124
24	0.9	.34	4,740	198	135

* Note that these numbers include no allowance for the cushioning effect of components ahead of the engine.

According to these calculations, the NRC-specified tornado missile velocities require the following barrier thicknesses for scabbing protection against the 4,000 lb automobile.*

NRC Zones	V (mph)	V (fps)	KE (in.-kips)	T (in.)
Zone 1 (wall)	132	194	4,540	24
Zone 2 (wall)	116	171	3,500	23

Zone 1(roof)	93	136	2,250	20
Zone 2(roof)	82	120	1,750	19

* See note under previous table.

In tests at Sandia Laboratories(*), a 1968 Ford Falcon (3,330 lbs) was impacted into a 16 in. thick concrete wall at a velocity of 52 mph. It was observed that although the car crushed 26 in., the barrier experienced no cracking on either front or rear face, which would indicate that a shear plug was not formed.

In connection with this test, the following calculation can be made. Assume that the engine weighs 400 lbs and has dimensions of 1 ft x 2 ft x 2 ft, and that the short block and the head weigh 275 lbs.

γ_{av} = 275/(1 x 2 x 2 x 490) = 0.14
γ = γ_{av} x 100 ksi/50 ksi = 0.28
D = 1.89 ft (see Section B.4-2)

Calculate the scabbing threshold velocity for the 16 in. barrier. From Fig. B.3-1 T/D = 0.71, KE/T^3 = 0.217, KE = 888 in.-kips and V = 109 fps = 74 mph.

The above calculation is believed to give a conservative estimate of the scabbing threshold velocity. However, due to the paucity of the data, it is recommended that conservative estimates of scabbing threshold velocity be used until further tests have been made.

B.5 PIPE WHIP

No dynamic tests involving pipe whip have been made. In the absence of such information, one must make judicious use of available related data. Such data includes:

1. Missile barrier test data from the S&W-IITRI and other programs;
2. Static test data on the pipe components involved in pipe whip(1).

The mechanics of pipe whip are assumed to be as follows: In a high pressure line a break occurs, either transverse or in the form of a longitudinal split. The jet force of the escaping fluid accelerates the pipe against a barrier intended to protect against such an event. The impacting pipe may be a simple run of piping which will flatten either partially or completely if it has sufficient energy. In complete flattening it ends up as essentially a long solid slug of thickness twice that of the pipe wall and width approximately half the circumference. The work done by the fluid jet up to impact on the barrier becomes the kinetic energy of the pipe which may be uniformly distributed along its length, or in case of rotation about a support, the energy will be distributed as the square of the pipe velocity. In the latter case the maximum energy per length is three times the average. The energy per unit length is a necessary input to the design process.

On the other hand, the impacting pipe may contain a "hard mass" such as an elbow, tee, or valve. It is then necessary to treat this "hard mass" as a separate missile to be designed for, since the attached piping, being lighter and structurally weaker, may possibly be less damaging. As before, the total kinetic energy of the system is obtained from the work of the jet force up to impact. From the distribution of mass and velocity throughout the system, the energy of the "hard mass" is found.

The two different situations that have been described, namely, "hard mass" and uniform pipe impact, require somewhat different treatments. The "hard mass" is handled as a missile in the pipe-slug category, the analysis being directly based on Fig. B.3-1, as follows:

For certain "hard masses," such as pipe elbows, the crushing behavior has been determined in the form of relations among the following parameters: crushing force, crushing distance, flattened contact area, and energy absorbed as function of distance crushed.(1) In general, the force-deflection curve is concave upward and approaches a vertical asymptote at the point of complete flattening, so that only a certain amount of energy can be absorbed up to that condition.

In case the kinetic energy of the "hard mass" is less than that for complete flattening, the crushing distance corresponds to the point where the available energy is absorbed in crushing the "hard mass." This condition determines the final crushing force and the area of the contact surface between missile and barrier. The force divided by the area yields an average contact pressure, σ_{av}, and the essentially elliptical contact surface can be transformed into an equivalent circle of the same area, giving an equivalent diameter D. Fig. B.3-1 can then be used for barrier design since the kinetic energy (KE), the average contact pressure (σ_{av}), and the equivalent diameter of the missile (D) are known. A barrier thickness (T) is assumed, giving T/D. At this T/D and for the curve for the calculated σ_{av} (or an interpolated curve), the ordinate KE/T^3 is read from the figure. Using the assumed T, the allowable kinetic energy is calculated and compared with that which is available. The cycle would be repeated as necessary.

If the available energy exceeds that for complete flattening, the following procedure is used. Let KE_1 be the energy absorbed by the "hard mass" at complete flattening, and KE_2 the balance of the

available energy. The crushing force F and the contact area (A) for complete flattening are known. Then $F/A = \sigma_{av}$ and the area A determines an equivalent contact diameter (D). The energy KE_1 is assumed to act on the barrier as though applied by a missile of contact pressure σ_{av}, while the energy KE_2 is assumed to act as though applied by a solid slug ($\sigma_{av} = 50$ ksi). The design process is as follows:

1. Assume a barrier thickness (T)

2. At the corresponding T/D in Fig. B.3-1, read two ordinates, y_1 and y_2, the first for the calculated σ_{av} and the second for the slug curve ($\sigma_{av} = 50$).

3. Calculate the quantities KE_1/T^3 and KE_2/T^3, using the assumed value of T.

4. If $$\frac{KE_1/T^3}{y_1} + \frac{KE_2/T^3}{y_2} \leq 1$$

   the assumed T is adequate. The cycle may be repeated with improved assumptions for T for adequacy or for economy, as the case may be.

Impacting Length of Pipe

The striking kinetic energy per unit length of pipe is known. If not uniformly distributed, the maximum is used. Since the impact area is a long, narrow band instead of a circle, Fig. B.3-1 cannot be used directly, as was done for the "hard mass" impact.

Scabbing depends on two distinct internal mechanisms within a barrier. First, a shear plug must be formed, and then the shear plug must acquire a certain amount of motion. Shear plug formation occurs when the contact force during impact exceeds for some required time the resistance to shearing failure on the sides of the plug. This mechanism is therefore related to the side area of the plug. On the other hand, the initial movement of the plug is resisted by its mass, proportional to its volume. Thus, the resistance to scabbing under missile impact depends on both the side area and the volume of the formed shear plug. The relative importance of the two resisting mechanisms probably depends on the intensity of the loading, the inertia (volume related) effect being the controlling one for severe loads of short duration, since the shearing mechanism (area related) is probably the more important for smaller loads of longer duration.

These same mechanisms are present, of course, in the scabbing due to impact applied over a narrow contact strip. However, in the case of a strip which would give rise to a long, narrow shear wedge instead of cone, both the side area and the volume of the plug in relation to the impact contact area, are materially smaller than is the case for the circular shear plug. Consequently, for a given contact pressure between missile and barrier, less kinetic energy is required to reach the scabbing threshold for strip loading than for loading on a circle. This reduction in required kinetic energy can be allowed for by introducing an adjusting factor for reducing the ordinates of Fig. B.3-1 for use with strip loading.

The assumption is made that the correcting factor for kinetic energy is of the same order as both the ratio of shear plug surface areas and that of shear plug volumes of linear and of circular plugs having the same impact areas. For 45 deg shear plug side slopes the two ratios, comparing the truncated cone to the truncated wedge, are, respectively, 6 (side area) and 3.4 (volume) for T/D = 2. Since for the severe impacts of pipe whip loading the volume effect is probably the more significant (see above), an energy adjustment ratio of 5 is considered conservative. This factor <u>divides</u> the ordinates of Fig. B.3-1 when strip loading by a length of pipe is considered. Additional geometric correction factors are required in going from circle to strip and from total kinetic energy to energy per unit length of strip. The final result, including the adjustment factor of 5, is

$$KE_L = (4/5\pi)(T^3/D)y$$

In this expression, KE_L = allowable energy per inch of pipe, T = barrier thickness (in.), D = width of strip (in.), and y = the ordinate read from Fig. B.3-1 (ksi).

With the adjustments just described, the design process is basically similar to that outlined for the "hard mass." Force-flattening relations for pipe exist[1] which allow determination of absorbed energy and contact width for deflections up to complete flattening. If the available energy is less than the maximum that can be absorbed in pipe flattening then the maximum force per unit length and the final contact width(D) are known. The final average contact pressure is the ratio of those quantities.

Fig. B.3-1 is used as follows: A barrier thickness T is assumed and T/D calculated. This T/D and the contact pressure (σ_{av}) define an ordinate on the figure. Using the correcting multiplier ($4T^3/5\pi D$) developed earlier, one finds the allowable kinetic energy per unit length of pipe and compares it with that available.

On the other hand, if the available kinetic energy per unit length exceeds the maximum that can be absorbed in flattening, this maximum absorbable energy is designated KE_1 and the balance is KE_2.

The force F and the contact width at complete flattening are known, and from them σ_{av} = F /D is found. A barrier thickness T is assumed and T/D calculated.

Then, in Fig. B.3-1, two ordinates are determined, y_1 for the calculated T/D and for σ_{av}, and Y_2 for the same T/D and for slugs. The assumed thickness is adequate if

$$\frac{KE_1}{(\frac{4T^3}{5\pi D})y_1} + \frac{KE_2}{(\frac{4T^3}{5\pi D})y_2} \leq 1$$

B.6 AIRCRAFT ENGINE IMPACT

The engine is assumed to weigh 1.5 kips and to strike at 150 fps. Assume for illustration that it can be represented as a) a solid steel slug 2 ft in diameter, b) a solid steel slug 3 ft in diameter, or c) a 3 ft circular cylinder of average crushing strength 10 ksi over the entire cross section. (This implies an engine cross section that is roughly 20 percent solid assuming a compressive yield stress of 50 ksi.) It is important to note that the above models of the aircraft engine are chosen for the purpose of demonstrating the design method and do not necessarily represent a real engine.

1. D = 2 ft. Kinetic energy = 1.5 x 150^2 x 12/64.4 = 6,289 in.-kips. Assume a barrier thickness of 3 ft. Then T/D = 1.5. From the slug curve of Fig. B.3-1, the allowable value of KE/T^3 = 0.16 ksi. Then, KE_{all} = 0.16 x 36^3 = 7,408 in.-kips. Since this exceeds the kinetic energy available, the thickness is adequate.

2. D = 3 ft. Kinetic energy = 6,289 in.-kips. Assume a barrier thickness of T = 3 ft. Then T/D = 1. From the slug curve of Fig. B.3-1, KE/T^3 = 0.12. Then, KE_{all} = 0.12 x 36^3 = 5,692 in.-kips. This is inadequate. Assume T = 37 in. From the slug curve of Fig. B.3-1, KE/T^3 = 0.13 ksi. Then, KE_{all} = 0.13 x 37^3 = 6,291 in.-kips. This is acceptable.

3. D = 3 ft. The average crushing stress σ_{av} = 10 ksi. Kinetic energy = 6,289 in.-kips. Figure B.3-1 contains eight curves corresponding to different average missile contact stresses. For 10 ksi, interpolate between 9.5 and 12 ksi. Assume a barrier thickness of 2.5 ft (T/D = 0.83). From Fig. B.3-1, a value of KE/T^3 = 0.34 is calculated. Then KE_{all} = 0.34 x 30^3 = 9,257 in.-kips. This is adequate for the assumed loading condition.

B.7 TURBINE MISSILES

Turbine missiles are characterized by irregular shape, uncertain orientation at impact, high impact velocity, large mass, and high kinetic energy.

The shapes are typically sectors of turbine rotors with linear dimensions from one to five feet, and projected areas of 1.5 ft^2 to 5 ft^2 (depending on orientation). Weights range from 4 kips to 8 kips, and impact velocities from 300 fps to 600 fps. Kinetic energies are in the range of 5,000 ft-kips to 45,000 ft-kips. (For comparison, the kinetic energy of the NRC 12 in. Schedule 40 pipe at 210 fps is only 1,000 ft-kips.)

Examination of Fig. B.3-1 shows that within the range of parameters given, the greater the area of missile contact with the barrier the less kinetic energy is needed to initiate scabbing. For this reason, the assumed impact orientation of a complex missile should be the one offering the greatest contact area. (This orientation produces the largest possible contact force with the shortest possible duration, a condition for maximum scabbing potential.) If scabbing, under the worst orientation, is prevented, no other orientation of the missile is expected to result in perforation.

The missile is modeled as an equivalent solid cylinder having the same weight, velocity, and kinetic energy as the missile. This equivalent cylinder has a circular contact area which is the geometric mean of the actual contact area and the area of the circle circumscribed about the actual contact area. (The geometric mean is the square root of the product of the two areas.)

The above information (the kinetic energy and the effective diameter of the equivalent cylindrical slug) is used with Fig. B.3-1 to find the barrier thickness required to prevent scabbing. In this case, especially, a check should be made to determine if and to what extent the limitations of applicability of that figure are exceeded. (It is recognized that the possible 600 fps velocity of a turbine missile is itself a violation of the limits.)

Example - Turbine Missile Barrier Design

Missile: Westinghouse 44 in. 90 degree segment, weighing 4.25 kips, having a velocity of 600 fps. The maximum projected area is approximately a rectangle 2 ft x 2.4 ft and has an area of 4.7 ft^2. The circumscribed circle has a diameter of 3.1 ft and an area 7.7 ft^2. Therefore, the equivalent solid slug has a contact area which is the geometric mean between 7.7 ft^2 and 4.7 ft^2, or a contact area 6.0 ft^2 with a diameter 2.8 ft.

The kinetic energy of the missile is 4.25 $(600)^2$ 12/64.4 = 285,100 in.-kips. In Fig. B.3-1, assume $KE/T^3 = 0.2$ (an average ordinate of the slug curve). Then

$T^3 = 285,000/0.2 = 1,425,000$ in.^{3} and
$T = 113$ in.
$T = 9.4$ ft

Check: T/D = 9.4/2.8 = 3.4. In the figure, the lowest curve extrapolated to this point will have an ordinate somewhat above 0.2. However, for conservatism, this small correction is not considered and the value already calculated will be kept.

B.8 SECONDARY CONCRETE MISSILES

B.8.1 Secondary Missiles at Impacts above the Scabbing Threshold

Eighteen to twenty of the SWEC-IITRI tests in which the scabbing threshold was definitely exceeded have been examined in order to draw some conclusions about barrier perforation by the missile and about the characteristics of the secondary missiles (e.g., scabbing fragments produced). In spite of considerable apparent scatter among the data, the following conclusions are suggested.

1. There is a correlation between the weight of the impacting missile and the weights of the heaviest scabbing fragments produced by it. In more than half the cases examined, the ratio of the weight of the heaviest fragment to the weight of the missile was between 0.007 and 0.009. In three-quarters of the cases, the ratio was between 0.004 and 0.009, and the maximum observed ratio was 0.011. Reference to Table B.8-1 shows some correlation between missile weight and the total weight of scabbed material.

2. There is a correlation between the maximum fragment velocity and the "velocity excess" of the striking missile. (The velocity excess is the difference between the striking velocity and the scabbing threshold velocity.) In 70 percent of the cases, the ratio of the fragment velocity to the velocity excess was between 0.4 and 0.7. Examination of 8 of the Bechtel-Calspan tests with 8 in. pipes and slugs shows that in half of them the ratio was also between 0.4 and 0.7.

3. There is a correlation between the momentum of the heaviest scabbing fragment and the "momentum excess" of the striking missile. (The momentum excess is the product of the mass of the striking missile and the velocity excess.) In two-thirds of the SWEC-IITRI cases, the ratio of the momentum of the heaviest scabbing fragment to the momentum excess was between 0.004 and 0.007. The largest ratio observed was 0.011.

4. There is very little data about missile perforation. However, all the perforations that occurred in the SWEC-IITRI tests were at velocities approximately twice the scabbing threshold velocity. Moreover, there was one case of no perforation at a velocity of 1.5 times the scabbing threshold velocity. Therefore, it is recommended that until more information is obtained, the perforation velocity should be conservatively taken as 1.5 times the scabbing threshold velocity for $1.0 \leq T/D \leq 3.0$.

This information will be useful in situations where a level of damage more severe than that of scabbing thereshold may be allowed in the design of a barrier. (For example, when a second barrier is located behind the main barrier or any equipment behind the main barrier either has a significant level of resistance to scabbing particles or is located far enough away.)

Example - Secondary Missile Characteristics

An aircraft engine weighing 1.5 kips, three feet in diameter, having a velocity of 150 fps, strikes a 30 in. reinforced concrete barrier. Behind the barrier is a 1.5 in. steel radiation containment shell. In this illustration, the engine is assumed, very conservatively, as discussed in Section B.4-2, to be equivalent to a solid slug.

The missile has a kinetic energy of 6,289 in.-kips. The ratio, T/D, equals 0.83, and from the slug curve of Fig. B.3-1 the scabbing threshold value of $KE/T^3 = 0.10$. Then, at the scabbing threshold,

$KE_{all} = 0.10\ (30)^3 = 2,745$ in.-kips

This is considerably under the available kinetic energy. The scabbing threshold velocity is calculated:

$2745 = 1.5\ (12)\ V^2/64.4$
with the result, $V = 99.1$ fps

The velocity excess is 50.9 fps.

From the previous discussion of scabbing fragments and perforation, the following estimates can be made:

1. The heaviest fragment of barrier concrete probably weighs between

6 lbs and 14 lbs, and possibly as much as 15 lbs–20 lbs.

2. Fragment velocities probably lie within the range of 20 fps - 36 fps.

3. The maximum momentum of individual fragments is probably in the range of 0.01 k-sec to 0.02 k-sec, with a possible maximum of 0.03 k-sec.

4. Perforation of the 30 in. reinforced concrete barrier by the aircraft engine is a possibility. The solution to this problem requires a moderate thickening of the outer barrier or determination that possible secondary missiles, including the engine, are acceptable.

B.8.2 Scab Plates

Scab plates have long been used in military structures to protect personnel and equipment against flying pieces of concrete set in motion by projectile impact on the outside surface. Their design has been by rule of thumb, based on experience. In nuclear protective structures, scab plates may also play a role, for example when it becomes necessary to upgrade existing construction. A rational approach to the design of scab plates has been developed and is presented in the following paragraphs. First, consider the physical basis of the proposed design method.

A missile striking a reinforced concrete barrier at a velocity above the scabbing threshold velocity causes separation of pieces of rear-face concrete. With increasing severity of impact the weight, velocity, momentum, and kinetic energy of the scabbed material all increase. At the perforation threshold, the missile itself can pass through the barrier, either going between the reinforcing mesh or rupturing enough rebars to make way for itself. The role of the scab plate is to stop these secondary missiles and, if necessary, the attacking missile as well. The scab plate is attached to the barrier by means of a pattern of anchors to which it is normally welded. In the following development it is assumed that the strength of the anchors, or the connection to them, is less than the strength of the plate, so that the plate can lift away from the barrier over a certain region surrounding the impact location. This has the advantage of causing the energy that has to be absorbed to be distributed over a significant area of plate beyond the actual loaded area. The anchor resistance is a critical parameter of the system. If too large, the effect is to concentrate the energy absorption within a small plate area, with more likelihood of failure of the plate.

The design process consists of the following steps:

1. Prediction of the amount and areal distribution of the kinetic energy leaving the rear face of the barrier; this is a function of barrier and missile parameters and of the difference between the impact velocity and the scabbing threshold velocity.

2. Prediction of the amount and pattern of the resulting deformation produced in the plate, including the maximum plastic strain. This determination is very dependent on the following parameter.

3. Determination of the ratio of the anchor resistance (size and spacing of anchors) to the yield strength of the plate.

4. Comparison of the maximum strain produced in the plate with the maximum allowable strain.

B.8.3 Back-Face Phenomena - Analysis of Test Data

The following information is sought:

1. The energy or momentum leaving the rear face of a barrier (or the weight and velocity of scabbed material) as a function of impact conditions beyond the scabbing threshold.

2. The areal distribution of this energy, momentum, or scabbed material.

Ten of the S&W-IITRI quarter-scale tests can be used for this analysis. They are reported in Table B.8-1, which also summarizes the analysis. The data are arranged in order of the ratio of the impact velocity to the scabbing threshold velocity (V/V_c). Columns 21, 22, 23 and 24 present the information required for scab plate design, namely, the fraction of the impact kinetic energy present in the scabbed concrete, the fraction in the missile (if it perforates), and the size of the region where all this energy is concentrated. Getting that information requires knowledge of scabbing weights and velocities and missile exit velocity. These data can only be roughly estimated from observations taken during the S&W-IITRI test program. However, in order to verify and improve the accuracy of that data, advantage was taken of the fact that the momentum leaving the face can be determined in two ways: (1) by consideration of scabbing weights and velocities and missile exit velocity, as mentioned above, and (2) from the difference between the missile impact momentum and the impulse recorded at the barrier support. Columns 9 and 17 of

Table B.8-1 show the two sets of results. It must be mentioned that the close agreement in most of the cases involving barrier perforation is not proof of exactness, but rather is the result of adjustments made in the scabbing weights and velocities. The justification for making these adjustments is to improve the calculation of back-face kinetic energies as much as possible. When perforation did not occur, the scabbing particle momentum was so small that it could not be measured by means of the support impulse.

Any conclusions drawn from Table B.8-1 are subject to several restrictions that are due to the limited range of parameters of the test program:

1. Barrier thickness/missile diameter ratio (T/D) $1.0 < T/D < 3.0$
2. Missile velocity not more than 2.5 times the scabbing threshold
3. Barrier reinforcement between 0.3 and 1.0 percent each way in each face
4. Concrete strength between 3.0 and 4.5 ksi.

With these restrictions, the following conclusions can be drawn:

1. The perforation threshold velocity is approximately twice the scabbing threshold velocity for pipe missiles (Line M6 in Table B.8-1).
2. Below the perforation threshold, the back-face kinetic energy is only one to two percent of the striking energy.
3. Above the perforation threshold, the weight of scabbed material increases by a factor of two or more and there is a much greater increase in the kinetic energy.

   When perforation occurs, exiting missile kinetic energy and the scab material energy can be of the same order of magnitude, each on the order of ten percent of the missile impact energy.
4. Without perforation, the scab material comes from a circle of diameter B, between two and three times the barrier thickness, (basically the rebar cover) and with a fairly uniform velocity. With perforation, the damaging kinetic energy comes from the core of the shear plug within a circle of diameter 1.2 to 1.5 the barrier thickness.
5. The reinforcement ratio has a very significant influence on back-face phenomena for missile velocities above the scabbing threshold. For missile velocities near the scabbing threshold, as mentioned in Section A.9.7, Appendix A, the reinforcement ratio is not significant. Comparison of lines M16 and M17 in Table B.8-1 shows that heavy reinforcement (0.86 percent) reduces all scabbing measurements, especially weight of material, momentum, and kinetic energy, in comparison to light reinforcement (0.32 percent). The overall reduction in kinetic energy is about 25 percent. It should be emphasized that the majority of the tests analyzed were on barriers with 0.44 percent reinforcement so that these conclusions are expected to be conservative when applied to the standard S&W tornado barrier with approximately twice as much steel.

B.8.4 Recommendations - Back-Face Kinetic Energy

The following is recommended for reinforced concrete barriers with reinforcement ratios greater than 0.5 percent each way in each face:

V/V_c =	1.0-1.5	1.5-2.0	2.0-2.5
KE_R/KE_I =	0.025	$(0.45V/V_c - 0.65)$	0.25
B =	D+1.5T	D+0.7T	D

Here V and V_c are actual and scabbing velocities, KE_R back-face kinetic energy, and KE_I impact energy.

Note: For reinforcement ratios between 0.3 and 0.5 percent, increase KE_R by 10 percent.

B.8.5 Scab Plate Deflection

The scab plate is assumed to be pushed away from the barrier to which it is anchored by a force consisting of a more or less uniform pressure applied over a circular area of diameter B. The effect is to separate the plate from the barrier over a somewhat larger circular area, within which the plate anchors have failed. Restraint is provided by the innermost line of unbroken anchors. The deformed plate is stretched plastically. The energy absorbed in plastic deformation of the plate is equal to the work done by the uplifting force. If it is assumed that this static configuration is approximately the same as that produced by the back-face kinetic energy, then that energy can be equated to the absorbed static plastic work.

Fig. B.8-1 shows a cross section of deformed plate. The total lifting force is P. The stress in the radial direction

is the plate yield stress, σ_y. Taking any horizontal cross section of the deformed plate and summing vertical forces gives the relation

$$P = 2\pi r \sigma_y t \sin \psi.$$

But $\tan \psi = -\frac{dv}{dr} = -v'$. Then

$$P = -2\pi \sigma_y t r v'/(1 + v'^2)^{\frac{1}{2}} \qquad (B.8\text{-}1)$$

Letting $c = P/2\pi \sigma_y t$ (B.8-2)

the previous equation becomes

$$v' = -c/(r^2 - c^2)^{\frac{1}{2}}$$

and $v/c = \cosh^{-1} b/c - \cosh^{-1} r/c$ (B.8-3)

The parameter c has the dimension of length and it corresponds physically to that radius at which the slope of the equilibrium surface of the deformed plate, if continued inward, would become vertical. Therefore c must always be less than a.

The distance b, where liftoff ceases, is determined by the ratio of anchor strength to the yield strength of the plate. Let the strength of each anchor connection be Q and the average spacing of anchors around the b-circle be s. (Note: if s is small compared to b then it is approximately equal to 1.18 times the rectangular spacing of anchors.) From Fig. B.8-1, $Q = \sigma_y t\, s \sin\psi_b$

where $\tan \psi_b = -v'_b = 1/\beta$.

From equilibrium

$$\left(\frac{\sigma_y st}{Q}\right)^2 = 1 + \beta^2 \qquad (B.8\text{-}4)$$

Then the liftoff boundary radius, b, is found by substituting $\beta = -\frac{1}{v'_b}$ from Eq. B.8-4 into B.8-2 with

$$\frac{b}{c} = \sqrt{1+\beta^2} = \frac{\sigma_y ts}{Q} \qquad (B.8\text{-}5)$$

Then Eq. B.8-3 becomes

$$\frac{v}{c} = \cosh^{-1} \sqrt{1+\beta^2} - \cosh^{-1} r/c \qquad (B.8\text{-}3')$$

The approximate energy absorbed in plastic deformation can be found by assuming that all points on the scab plate displace vertically, with zero radial displacement. The only strain in the plane of the plate is in the radial direction and equals $\varepsilon = \sqrt{1+v'^2} - 1$ which is approximately

$$\varepsilon = v'^2/2 = \frac{c^2}{2(r^2-c^2)} \qquad (B.8\text{-}6)$$

Then the energy absorbed in plastic deformation is

$$E = 2\pi\sigma_y t \int \varepsilon r\, dr = \pi\sigma_y t\, c^2 \int_a^b \frac{r}{r^2-c^2}\, dr$$

or

$$E = \frac{\pi\sigma_y t\, c^2}{2} \ell n \frac{\beta^2}{\frac{a^2}{c^2} - 1} = \frac{\pi\sigma_y t\, c^2}{2} \ell n\, 2\, \varepsilon_m \beta^2 \qquad (B.8\text{-}7)$$

Some additional energy is absorbed by plastic deformation within the region inside the radius, a. If that circular area of radius, a, is bulged into a spherical segment of a dome having the same base radius, it can be shown that the absorbed energy is of the order $\pi\, \sigma_y t\, c^2$. For the conditions envisaged here, this energy is small compared to that given in Eq. B.8-7 and is ignored.

The maximum strain is found at radius a with the help of Eq. B.8-6. It is

$$\varepsilon_m = \frac{1}{2(\frac{a^2}{c^2}) - 1} \qquad (B.8\text{-}8)$$

This maximum resulting strain must not exceed the specified allowable strain, a function of the plate material and also of the strains in the two other principal directions - circumferential and thickness directions. Note that in plastic deformation there is essentially conservation of volume so that the sum of the three principal strains equals zero.

The design strain limit for scab plates is 0.5 of the ultimate uniform strain of the scab plate material. This limit is analagous to the limit of pipe whip restraints acting in tension as specified in NUREG-75/087 Section 3.6.2[5]. For symmetric biaxial tensile loading with two principal stresses equal, as occurs in a spherical shell under uniform pressure, the perpendicular strains in the plane of the surface are equal but their value at the onset of instability is approximately one-half the ultimate load strain in simple tension. For this reason, the permissive value of ε_m from Eq. B.8-8 should not exceed one half the strain at ultimate stress in simple tension.

B.8.6 Recommended Design Procedure

1. Determine the back-face kinetic energy and its areal distribution. For barriers with reinforcement ratios greater than 0.5 percent each way in each face, use:

V/V_c =	1.0-1.5	1.5-2.0	2.0-2.5
KE_R/KE_I =	0.025	$(0.45V/V_c - 0.65)$	0.25
	$B = D+1.5F$	$D+0.7T$	D

(For barrier reinforcement ratios between 0.3 and 0.5 increase E by 10 percent.)

2. For the interior region of the barrier, design the scab plate and its anchors by the following process. The quantities σ_y, E_m, and $a = B/2$ are known. Assume reasonable values of plate thickness, t, and anchor spacing s. Find b, the limiting radius of plate liftoff by combining Eqs. B.8-5 and B.8-7, e.g.

$$\left(\frac{b}{a}\right)^2 = \frac{1}{1+2\varepsilon_m}\left(2\varepsilon_m + e^{\frac{E(1+2\varepsilon_m)}{\pi\sigma_y t a^2 \varepsilon_m}}\right) \qquad \text{(B.8-9)}$$

The required anchor strength, Q, is found from a combination of Eqs. B.8-4 and B.8-8, e.g.

$$Q = \frac{\sigma_y t s a}{b}\,\frac{\sqrt{2\varepsilon_m}}{\sqrt{1+2\varepsilon_m}} \qquad \text{(B.8-10)}$$

The process can be repeated with different assumed values of t and s until a satisfactory and economical result is reached. For a preliminary design, the above equations can be approximated by

$$\frac{b}{a} \approx e^{\frac{E}{2\pi\sigma_y t a^2 \varepsilon_m}} \qquad \text{(B.8-11)}$$

$$Q = \frac{\sigma_y t s a}{b}\sqrt{2\varepsilon_m} \qquad \text{(B.8-12)}$$

3. Near a barrier boundary, to allow for the reduced area of plate available for absorbing energy, the back-face kinetic energy is doubled (i.e., two E) in calculating thickness, anchor design, and uplift radius, b'. For interior (>b' from boundary), use E to design anchors and calculate b.

Example: Given a 743-lb 12-in. Schedule 40 pipe at 211 fps. with 6,200 in-kips energy. Design scab plates for interiors of (a) 18-in. and (b) 12-in. barriers, assuming impact to occur away from a barrier boundary.

(a) 18-in. Barrier. V_c = 170 fps and V/V_c = 1.24. Therefore, the back-face kinetic energy E = 0.025 (6200) = 155 in-kips and B = 12 + 1.5(18) = 39 in., so that a = 19.5 in. Let the plate characteristics be σ_y = 40 ksi and ε_m^2 = 0.035.

Assume t = 0.25 in. and s = 12 in. Then from the approximate expressions (11) and (12)

b = 23.5 in. and Q = 26.4 kips.

Next try an alternative arrangement. Let t = 0.125 in. and s = 12 in. Then, approximately,

b = 28.25 in. and Q = 11 kips

The exact formulas give for the last assumptions

b = 28.5 in. and Q = 10.2 kips

It is important to observe that this calculated value of Q is an upper limit. Increasing it will result in plate strains above the allowable 0.035, and vice versa. For example, if Q is reduced to 8 kips while s, t, E, and σ_y are unchanged, there results

b = 32.4 in. and ε_m = 0.026

(Note that Q is bond strength, tensile strength, or plate connection strength, whichever is least.)

(b) 12-in. Barrier. V_c = 87 fps and V/V_c = 2.43. Perforation is expected. Then the back-face kinetic energy E = 1550 in-kips and B = 12.75 in., so that a = 6.375 in. Plate material characteristics are the same as before.

Assume t = 2 in. and s = 18 in. From the approximate expressions

b = 55.7 in. and Q = 43.6 kips

Next try t = 1.5 in. and s = 18 in. Then, approximately,

b = 115 in. and Q = 15.9 kips

By the exact equations, the last assumptions give

b = 135.8 in. and Q = 13.4 kips

B.9 CONCLUSIONS

Procedures are presented for missile barrier design for scabbing protection. Fig. B.3-1 is based on the results of the S&W-IITRI test program. Consequently, the accuracy and economy is greater for missiles similar to those tested than for missiles with significantly different characteristics. Design for tornado-borne pipe missiles is dependable and economical. Both pipe whip design and turbine missile design involve certain assumptions which increase the conservatism and consequently reduce the economy of the resulting designs.

This method, using Fig. B.3-1 to design barriers to prevent scabbing, is an improvement over the existing methods[2] because it takes into consideration pipe wall thickness and the average pressure between missile and barrier which have been shown to have a significant role in the ability of the missile to produce scabbing.

B.10 REFERENCES

(1) Peech, J.M., Roemer, R.E., Pirotin, S.D., East, G.H., Goldstein, N.A., "Local Crush Rigidity of Pipes and Elbows", Transactions of the 4th International Conference on Structural Mechanics in Reactor Technology, San Francisco, California, 15-19 August 1977.

(2) Rotz, J.V. "Results of Missile Impact Tests on Reinforced Concrete Panels", Second ASCE Speciality Conference on Structural Design of Nuclear Plant Facilities, Vol. 1A, New Orleans, 1975.

(3) Stephenson, A.E., "Full-Scale Tornado-Missile Impact Tests", November 19, 1976.

(4) Stephenson, A.E., "Tornado Vulnerability Nuclear Production Facilities", April, 1975.

(5) NUREG-75/087, Section 3.6.2 "Determination of Break Locations and Dynamic Effects Associated with the Postulated Rupture of Piping." U.S. Nuclear Regulatory Commission.

TABLE B.3-1

COMPARISON OF BECHTEL-CALSPAN DATA WITH FIG. B.3-1 PREDICTIONS

1. Test No.	2. Missile Type	3. Missile Wt (lbs)	4. Barrier Thickness (in.)	5. Missile Velocity (fps)	6. Spall Damage	7. Scabbing Velocities Derived from Bechtel Test Data (fps)	8. Scabbing Velocities Predicted from Fig. B.3-1 (fps)
4F	Slug	214	12	122	Moderate		
3F	Slug	214	12	214	Severe (hole)	100	83
1F	Slug	213	12	340	Severe (perf.)		
17F	Slug	213	18	161	None		
18F	Slug	213	18	207	Incipient	200	174
2F	Slug	213	18	337	Severe		
11F	Slug	213	24	295	None		
12F	Slug	215	24	377	Light	350	288
15F	Pipe	202	12	135	None	180	159
16F	Pipe	202	12	209	Light		
5F	Pipe	205	18	210	None	320	302
6F	Pipe	209	18	319	Incipient		
7F	Pipe	209	24	370	None	470	477
8F	Pipe	208	24	470	Incipient		
9F	Pipe	210	24	475	Incipient		
19F	Pipe	132	18	370	None	400	379
20F	Pipe	132	18	455	Moderate		

Columns 1 through 6 from Table 2 of Ref. 2. Column 7 from Ref. 2.

TABLE B.3-2

COMPARISON OF EPRI-SANDIA DATA WITH FIGURE B.3-1 PREDICTIONS
DAMAGE TO REINFORCED CONCRETE BARRIERS DUE TO
743 LB 12 IN. SCHEDULE 40 PIPE

Barrier Thickness T (in.)	Concrete Strength f_c' (ksi)	Velocity V (fps)	Damage	Predicted Scabbing Threshold Velocity (Fig. B.3-1) V (fps)
24	3.8	202	Cracks	269
18	3.4	202	Scabbing	170
18	3.6	198	Scabbing	170
18	4.5	203	Scabbing	170
18	4.7	213	Scabbing	170
18	4.3	157	Flaking*	170
18	4.2	152	Flaking*	170
18	4.3	143	Cracks	170
12	3.7	143	Perforation	87
12	3.6	98	Scabbing	87
12	3.4	92	Flaking*	87

*Note that the term 'flaking' is used to indicate extensive back-face cracking with small particles of cement falling off with no velocity. This level of damage occurs after shear plug formation but before the scabbing threshold has been reached.

TABLE B.8-1

BACK FACE PHENOMENA

		1	2	3	4	5	6	7	8	9	10	11	12	13	14	15	16	17	18	19	20	21	22	23	24
		Missile																							
Line	Test	T		W	V	V_c	V/V_c	$\frac{WV}{g}$	$\int F dt$	T-8	A_{cov}	W_{cov}	W_e	W_p	12_{+13}	V_{sc}	V_m	Mom	KE_{sc}	KE_m	KE_I	$\frac{KE_{sc}}{KE_I}$	$\frac{KE_m}{KE_I}$	$\frac{B}{T}$	$\frac{B-D}{T}$
P7	28	4.5	P	13.5	195	150	1.3	81.8	79.0	-	120	5.2	5.2	0	5.2	50	0	8.1	202	0	7,971	.025	0	2.7	2.0
P29	18	6L	S	23.5	128	95	1.35	93.4	101.0	-	130	6.0	6.0	0	6.0	15	0	2.8	21	0	5,979	.004	0	2.2	1.7
M5	4	4.5	P	12.35	216	150	1.44	82.8	82.6	-	120	5.2	5.2	0	5.2	30	0	4.8	73	0	8,947	.008	0	2.7	2.0
P26	14	6L	S	12.7	205	135	1.5	80.8	110.0	-	135	6.0	6.0	0	6.0	25	0	4.7	58	0	8,288	.007	0	2.2	1.7
M6	29	4.5	P	12.0	296	150	2.0	110.3	61.0	49.0	340	15.0	5.0	9.5	14.5	100	10	48.8	2,251	19	16,325	.14	.001	1.5	.83
M16	31	6L	P	28.2	329	160	2.6	288.0	98.0	190.0	500	21.7	7.2	20.0	27.2	110	110	189.0	5,110	5,298	47,397	.11	.11	1.5	1.0
P9	12	4.5	P	12.5	317	150	2.1	123.1	67.5	55.6	300	13.0	4.3	9.0	13.3	110	40	61.0	2,499	311	19,505	.13	.02	1.4	.73
M17	27	6H	P	28.25	340	160	2.1	298.3	143.0	155.0	410	17.8	5.9	14.0	19.9	105	105	157.0	3,407	4,836	50,710	.07	.10	1.5	.7
M7	13	4.5	P	11.6	329	150	2.2	118.5	37.5	81.0	270	12.0	4.0	9.4	13.4	100	100	78.0	2,081	1,801	19,497	.11	.09	1.45	.8
P10	10	4.5	P	12.35	403	150	2.7	154.6	105.0	50.0	300	13.0	4.3	9.0	13.3	105	0	43.4	2,277	0	31,145	.07	0	1.4	.73

Notes: In First Column, P = primary shot at barrier, M = second or third shot at barrier. Line and test No. 5 refer to Tables A.3.3-1, A.3.3-2, 3.5-1 3.5-2 in Appendix A

Col.
1: Barrier thickness T, and for 6 in. whether light (L = 0.32 percent) or heavy (H = 0.86 percent) reinforcement. 4.5 in. have 0.44 percent.
2: P = standard 3 in. pipe with 0.122 in. wall; S = 3 in. slug
3: Missile weight, lb
4: Missile velocity, fps
5: Scabbing threshold velocity, fps - Col. 6: Velocity ratio
7: Missile momentun, lb-sec
8: Impulse of force-time record at barrier support, lb-sec. Note that P26 record is questionable.
9: Missile impact momentum, lb-sec - support impulse = momentum leaving back of barrier
10, 11: Area of back-face rebar exposed, $in.^2$ and weight of 0.5 in. rebar cover lost, lb
12: Effective weight of lost rebar cover, assumed same for momentum and for kinetic energy, lb
13: Weight of shear plug material actually lost during impact, lb
14: Total effective weight of scabbed material, lb
15: Maximum velocity of scabbed materials as deduced from maximum distance thrown, fps
16: Missile exit velocity as deduced from distance of travel and from velocity of scabbed material, fps
17: Calculated exit momentum, lb-sec: Cols. 14 x 15 + 3 x 16 ÷ by g. Compare with Col. 9
18, 19: Kinetic energy of scabbed concrete and of perforating missile from data of Cols. 3, 14, 15, and 16, ft-lb
20: Original missile kinetic energy from Cols. 3 and 4 ft-lb: Col. 21:22: Ratios of scabbing and missile exit energy to original missile energy
23: B = diameter of scabbing material carrying most of the kinetic energy, in.
24: This shows the dependence of B on both missile diameter (D) and barrier thickness (T). Note the influence of reinforcing ratio in comparing lines M16 and M16.

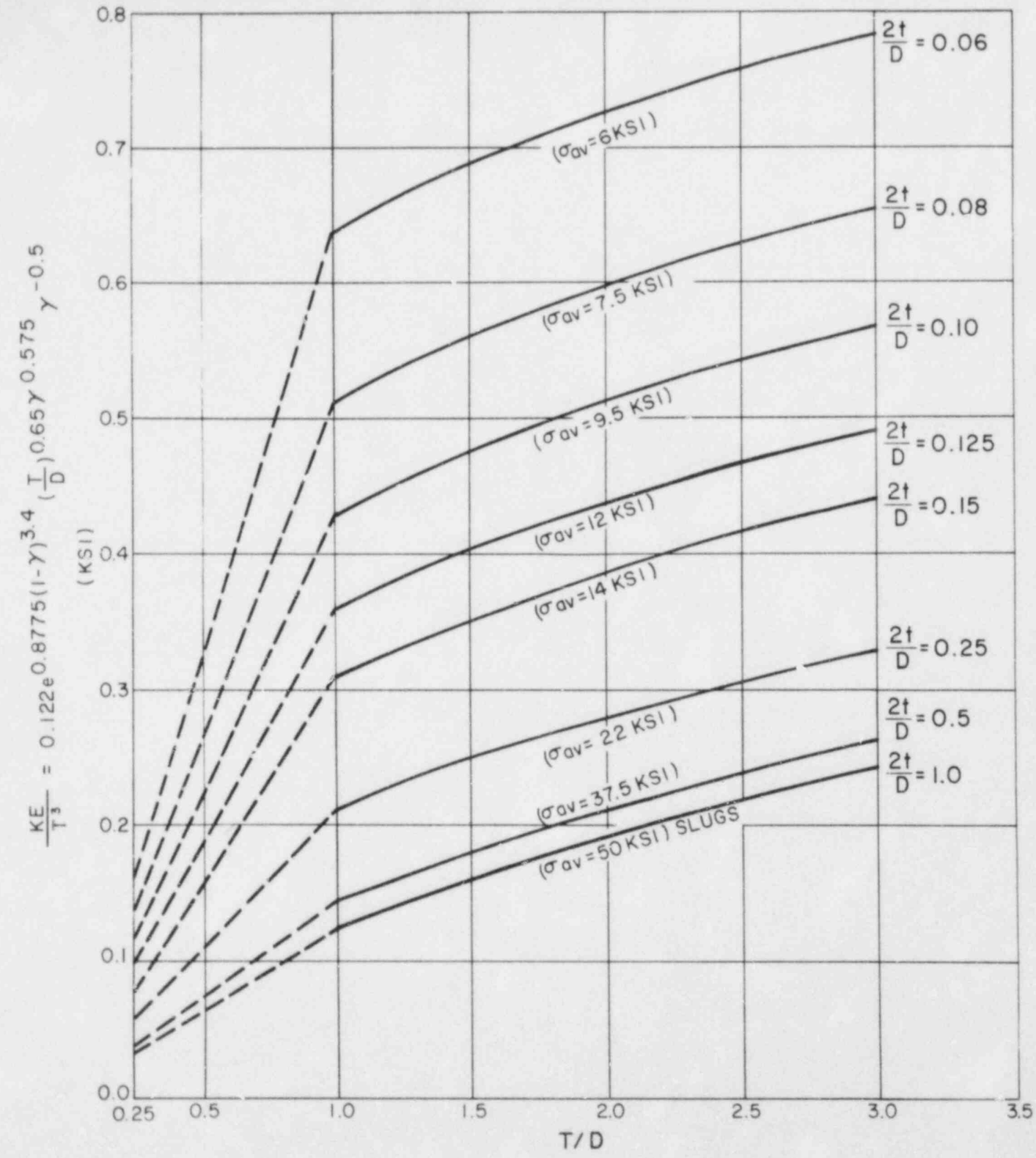

——— BASED ON TEST DATA

– – – A CONSERVATIVE EXTRAPOLATION

$\gamma = \frac{2t}{D}(2 - \frac{2t}{D}) = $ (SOLIDITY RATIO)

KE = KINETIC ENERGY (IN-KIPS)

T = BARRIER THICKNESS (IN.)

t = PIPE WALL (IN.)

D = PIPE O.D. (IN.)

f_c = (3-4.5 KSI) CONCRETE COMPRESSIVE STRENGTH AT TIME OF MISSILE IMPACT

MISSILE VELOCITY (75-250 FPS)

BARRIER REBAR PERCENTAGE ≥ 0.3

$\sigma_{av} = \frac{\text{IMPACT FORCE}}{\text{GROSS AREA}} = (50\text{ KSI})\frac{A\text{ NET}}{A\text{ GROSS}} = 50\gamma$

FIGURE B.3-1 SCABBING THRESHOLD LIMIT-STEEL PIPES OR SLUGS ON REINFORCED CONCRETE BARRIERS

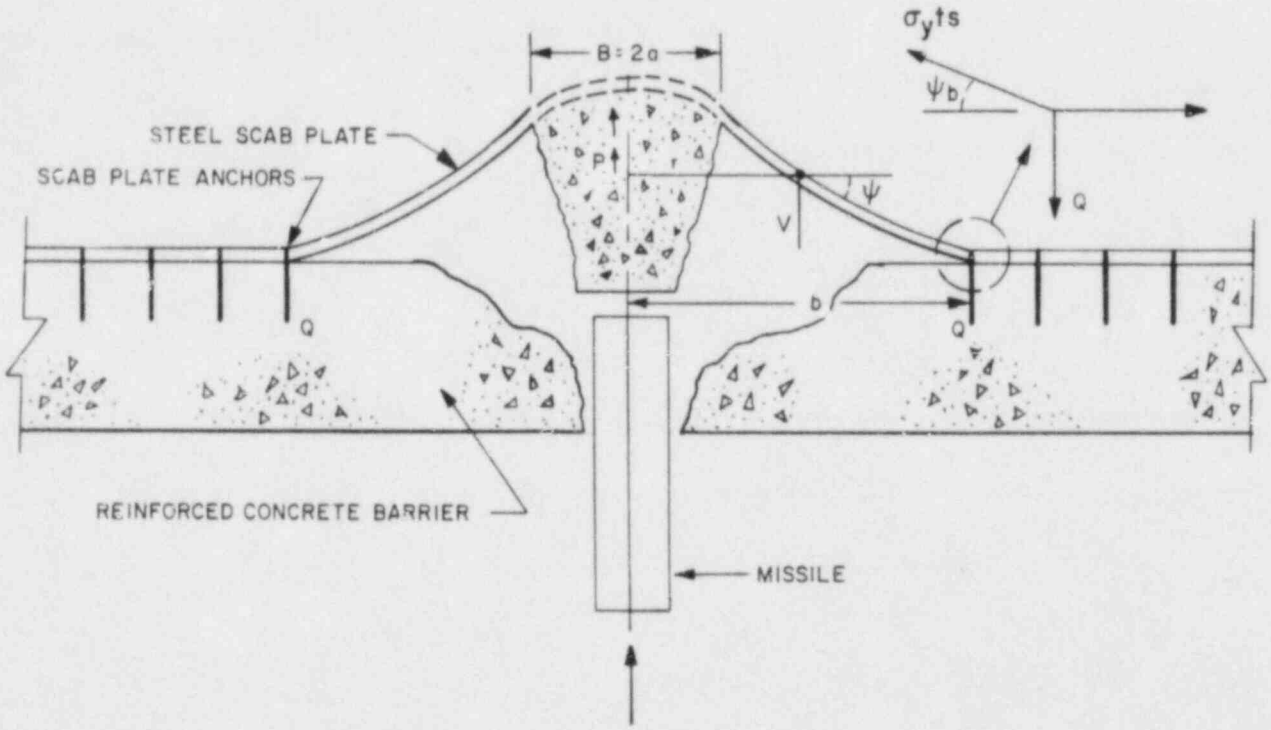

FIGURE B.8-1 DEFORMED SHAPE & FORCES ACTING ON SCAB PLATE

SWECO 7703
EMTR-801
September 1977

APPENDIX C

TIME HISTORY ANALYSIS FOR OVERALL STRUCTURAL RESPONSE

Stone & Webster Engineering Corporation

TABLE OF CONTENTS

LIST OF TABLES

LIST OF FIGURES

APPENDIX C

TIME HISTORY ANALYSIS

FOR OVERALL STRUCTURAL RESPONSE

C.1 PURPOSE

The purpose of this Appendix is to develop methods for determining overall barrier deflection due to missile impact, static loads, and other dynamic loads acting together in a load combination equation.

C.2 SUMMARY

The deflection of a barrier due to missile impact, static loads and other dynamic loads acting together in a load combination equation is determined by solving the equation of motion for the barrier by two independent methods which give the same results and employ the same assumptions.

The equation of motion for a barrier is solved; a) by numerical integration and, b) in closed analytical form. In both solutions the barrier is represented by an equivalent mass and a nonlinear spring which can describe the barrier force deformation relationship.

The missile is characterized by its mass and striking velocity. In addition, the average impact force between missile and barrier is required.

The missile-barrier contact force acts to decelerate the missile and to accelerate the barrier, and continues to act until a common velocity at the impact point is attained. Thereafter, missile and barrier move together until they come to rest at the maximum barrier deflection.

If the duration of the impact interval (to achieve a common velocity) is very short compared to the time in which the barrier comes to maximum displacement, the impact can be treated on the basis of an instantaneous impulse between missile and barrier, considerably simplifying the analysis. The representation of the missile as an instantaneous impulse is realistic only when the duration of impact is short compared to the time it takes the barrier to come to maximum displacement. Otherwise, the instantaneous impulse method is too conservative and a square wave of force versus time is used to transfer the missile momentum to the barrier.

The permissible ductility ratio, μ, limiting barrier deflection for bending, compression, and shear, is defined as the ratio of the maximum acceptable displacement x_m to the displacement at the effective yield point x_y in bending.

Where barriers are required to carry other loads or where there is only one barrier provided to stop a missile and protect against secondary missiles, the maximum allowable ductility is 10 or less depending on how shear and compression influence the flexural response of the barrier.

Where reinforced concrete barriers are not required to carry other loads and where a second barrier such as a wall or floor is located between the primary barrier and the missile protected area, the primary barrier may be designed to act in tension, similar to a mechanical pipe whip restraint. In this case, the maximum barrier deflection is based on half of the ultimate uniform strain in the rebar. This limit for reinforced concrete barriers acting in tension is the same as the limit for pipe whip restraints.

C.3 SINGLE MASS TIME HISTORY ANALYSIS OF BARRIER STRUCTURAL RESPONSE

C.3.1 General Description

Structural response to missile impact is calculated here using a single equivalent mass and a nonlinear (elasto-plastic) spring to model the dynamic response characteristics of the barrier. The single equivalent mass in the equation of motion for the barrier is the sum of the barrier equivalent mass plus any missile mass in contact with the barrier, traveling at the same velocity as the barrier. When the impulse is short compared with the duration of the barrier response, the barrier mass, not the barrier structural resistance to deformation, stops the missile. In this case, structural response is based upon an initial impulse of zero duration described below. This produces the same structural response as obtained by Williamson and Alvy[3], Eq. (14).

On the other hand, when the impulse of the missile acting on the barrier is not short enough to be treated as instantaneous, the interaction between missile and barrier is

represented by means of a constant force acting for a finite time. The magnitude of that force is determined by the crushing resistance of the missile or the penetration resistance of the barrier, whichever governs. The force remains constant until either the missile and barrier have reached the same velocity or the barrier has come to rest. In the former case, the combined system - missile with barrier - continues to deflect until brought to rest by the barrier's resistance to deformation. Depending on the parameters of the system, the final deflection obtained for an interaction of finite duration may be considerably smaller than when the entire momentum transfer is assumed to take place instantaneously, as is illustrated later.

The analytical and numerical methods presented here can take into account four types of static and dynamic loadings, as required by the load combination equation in the SAR.

Load Type 1: static loads (static pressure differential or weight of a horizontal barrier)

Load Type 2: dynamic suddenly applied constant load (fluid jet, or dynamic pressure differential)

Load Type 3: square wave impulse of finite duration (force of penetrating or crushing missile)

Load Type 4: initial impulse of essentially zero duration (i.e., very much shorter than the duration of the barrier structural response)

The mass of the missile which applies its load to the barrier via a square wave, Load Type 3, is M_3. The mass of the missile associated with an instantaneous transfer of momentum, Load Type 4, is M_4.

The physical mechanism of the missile-barrier interaction is as follows: The impact force decelerates the missile and accelerates the barrier. The deflection of the barrier is aided by any static and dynamic forces normal to its surface and by any initial impulse; the barrier deflection is opposed by the barrier's structural resistance, initially elastic and finally plastic, represented by a bilinear resistance-deflection relation. The constant plastic resistance is determined by yield-line theory, taking no credit for any catenary or curvature influence. The missile and barrier continue to move under the action of the various forces, usually until both have achieved a common velocity. After that, the missile and barrier are assumed to form a single degree of freedom system having kinetic energy which is dissipated in producing further deflection. A somewhat different physical process can sometimes occur when the plastic structural resistance is larger than the constant missile contact force. In that case, the barrier may come to rest before the missile and the barrier reach a common velocity.

C.3.2 Allowable Barrier Deflection

Where only one barrier is placed between a missile source and a missile protected zone or where a barrier is required to carry other loads, the maximum barrier deflection is expressed in terms of a ductility ratio, $\mu = X_m/X_y$. The maximum allowable ductility ratios for different loading conditions are specified by the NRC[8].

The maximum allowable ductility ratio of 10 or less, specified by the NRC, can be a small fraction of the deflection capacity of a barrier. The limit of 10 is based on tests of simply supported beams such as those reported by Gaston, Siess, and Newmark[9].

Simply supported two-way slabs, end restrained two-way slabs, and end restrained beams all have considerably more deflection capacity to failure than do simply supported beams. This is because the reinforcing bars act in catenary tension after the flexural hinge capacity is exhausted. For two-way slabs, there is an additional resisting force due to the formation of compression rings in the barrier about the point of applied load. Anderson, Hansen, Murphy, Newmark and White[10] described the additional capacity of these barriers in design of blast resistant structures. Section 8-7 of Anderson et al.[10] states:

"The Catenary Effect. The yield line theory gives only a partial explanation of the behavior of a plate or slab supported on more than two opposite sides and loaded laterally. In addition to the bending action that has been discussed, there is a complex membrane action as well.

In the case of a square plate with four-side support, the bulging at the center tends to pull opposite sides of the plate toward each other. This effect is strongest for a central strip and does not exist for a strip adjacent to a supported edge. As a consequence, the middle area of the plate is in tension and the outer parts in compression. This has two effects: a) the membrane action supplies some load carrying capacity, and b) the tension and compression fields alter the plastic hinge moments to be used in the yield line theory. It should be noted that the membrane action, just mentioned, is not confined to two-way slabs. A similar effect will be encountered in one-way slabs and beams the ends of which are so anchored as to prevent movement toward

each other during flexure. In this case, the lengthening of the member as it deflects gives rise to tension which carries a part of the applied load, thus increasing the load capacity of the member, especially at large deflections."

Wood[1] describes membrane tension in two-way slabs. Figure C.3-1 taken from Wood[1] shows that two-way slabs have considerably increased force capacity and deflection capacity above that determined using bending yield line analysis and a ductility of 10 based on simply supported beams.

The tension mechanism described above for two-way slabs and beams anchored at their ends is used in barrier design when:

1. There is a second barrier between the primary barrier acting in tension and the missile protected area. The second barrier is designed to stop scabbing particles from the primary barrier,
2. the primary barrier is not required to carry other loads,
3. the missile geometry is such that it cannot slip between the rebar pattern, and
4. the rebar is continuous in the barrier and fully developed in the barrier support.

The maximum deflection of reinforced concrete barriers acting in tension is determined by the maximum allowable strain in the rebar. For barriers acting in tension, meeting the conditions (1.) through (4.) above, the maximum allowable rebar strain is half of the ultimate uniform strain of the rebar. This is analagous to the maximum strain permitted by the NRC[11] for mechanical pipe whip restraints.

C.3.3 Barrier Equilibrium Equation and Transformation Factors

The basic equation of motion of the barrier is

$$M_e a = F_e - R_e \qquad \text{(C.3-1)}$$

where

$M_e = M_{be} + M_4$: Prior to the missile and barrier reaching a common velocity, M_e equals barrier equivalent mass M_{be}, plus the mass, M_4, associated with the initial impact of zero duration, Load Type 4. Thereafter,

$M_e = M_{be} + M_3 + M_4$: After missile and barrier reach a common velocity, M_e equals the sum of the barrier equivalent mass M_{be} plus the missile mass from Load Types 3 and 4.

a = barrier acceleration

F_e = sum of static and dynamic forces or equivalent forces causing changes of motion

R_e = equivalent barrier resistance to deformation

Prior to missile mass M_3 and barrier reaching a common velocity, F_e equals

$$F_e = F_{e_1} + F_{e_2} + F_{e_3}$$

where F_{e1}, F_{e2} and F_{e3} are equivalent forces for load types one, two, and three in Section C.3.1. After missile mass M_3 and barrier reach a common velocity, F_e equals

$$F_e = F_{e_1} + F_{e_2}$$

Load Type 4 from Section C.3.1 is a very high force from a hard missile or component which is on the barrier for a very short interval of time. This force causes the barrier equivalent mass, M_{be} plus the missile mass M_4 to have an initial velocity before loads F_{e2} or F_{e3} cause any motion. This velocity is

$$V_o = I_4/(M_{be} + M_4)$$

Load Type 4 is not applied to the barrier explicitly. Rather, the barrier is given an initial velocity which results from the impulse I_4 of load F_{e4}. The impulse is applied to the combined mass of the barrier and the missile M_4 since they are assumed to travel together after impact.

Load Type 1 is a static load which causes the barrier to have an initial displacement before loads F_{e2} and F_{e3} cause any motion. This displacement is

$$X_o = F_{e_1} X_y/R_{ey}$$

where X_y and R_{ey} are the displacement and resisting force of the barrier at its effective yield point.

In order to know when the missile force F_{e3} terminates, it is necessary to monitor the velocity of the missile mass M_3. This is done as follows

$$V_3 = (I_3 - \sum F_{e_3}\, dt)/M_3$$

When the missile velocity V_3 decreases to the velocity of the barrier, the mass M_3 no longer pushes on the barrier with force F_{e3}. From this time on, the barrier and missile M_3 are assumed to travel together until the barrier stops. I_3 is the original momentum of missile mass M_3.

Although the barrier deflection pattern takes on different configurations in the elastic and plastic stages, the values used for the mass and load transformation factors, K_m and K_L, are determined for the plastic configuration since the barrier deflection is predominantly in the plastic range. The barrier equivalent mass M_{be} is determined from

$$M_{be} = K_m M_b \qquad \text{(C.3-2)}$$

where

M_b = total mass in barrier yield mechanism

K_m = mass transformation factor so that the model and prototpype barriers have the same kinetic energy and same displacement

$$K_m = \sum m_b \phi^2 \, dA/M_b \qquad \text{(C.3-3)}$$

where

m_b = mass per unit area of barrier
ϕ = normalized displacement of barrier

dA = increment of barrier area

The equivalent forces acting on the barrier from the missile, other dynamic loads and static loads are determined as follows

$$F_e = K_L \, F \qquad \text{(C.3-4)}$$

where

K_L = load transformation factor determined so that the model and prototype forces do the same work on the barrier assuming same displacements for model and prototype barriers.

$$K_L = \sum f \, dA/F \qquad \text{(C.3-5)}$$

where

f = force per unit area of barrier mechanism

F = total force on barrier

A different equivalent force is determined for each load acting on the barrier.

The barrier equivalent resisting force R_e is determined from

$$R_e = R \qquad \text{(C.3-6)}$$

where

R = barrier resisting force for a concentrated load producing a specified displacement

C.3.4 Missile Force for Load Type 3

The missile force for Load Type 3 in Section C.3.1 is determined by one of the following methods:

1. The force for Load Type 3 is equal to the kinetic energy of the missile divided by the distance the missile permanently deforms. This method is used when there is no significant penetration or shear plug movement compared with missile deformation in actual tests.

2. If actual test data for (1.) above are not available, then the Load Type 3 for constant cross-section missiles is the lesser of missile material yield stress or 50 ksi confined concrete bearing stress times the net cross-sectional area of the missile.

3. If the missile does not maintain a constant cross-section at the point of impact, Load Type 3 is set equal to the peak of a force-crush curve for the missile, where the area under the curve equals the kinetic energy of the missile. If the area under the force-crush curve is less than the kinetic energy of the missile, the momentum corresponding to the balance of the energy is applied as instantaneous impulse, Load Type 4.

C.3.5 Numerical Solution for Equation of Motion

The numerical solution for the barrier equation of motion is performed starting from an instant of time when the displacement and velocity of the barrier and the missile and the forces acting on them are known. The numerical solution of the barrier equation of motion given here is accomplished in a manner similar to Biggs[4], Chapter 1. The differences are: a) the barrier has an initial velocity from an instanteous impulse of high force capacity missile components, b) the applied force of the missile remains on the barrier until missile and barrier come to a common velocity; then it is taken off, and c) the mass of the high force capacity missile components M_4 and the mass M_3 of the lower force capacity missile components which penetrate or crush significantly are added to the equivalent mass of the barrier after they attain a common velocity with the barrier.

Equation C.3-1 establishes the acceleration. The velocity and position of the barrier at the end of a time interval dt are

$$V_n = V_{n-1} + a \, dt \qquad \text{(C.3-7)}$$

$$X_n = X_{n-1} + V_{n-1} \, dt + .5 \, a \, dt^2 \qquad \text{(C.3-8)}$$

where

V_n = velocity at end of time interval dt

V_{n-1} = velocity at beginning of time interval dt

X_n = barrier displacement at end of time interval dt

X_{n-1} = barrier displacement at beginning of time interval dt

a = barrier acceleration assumed constant during time interval

dt = time increment for numerical integration of the equations of motion. It is set between 2 and 20 microseconds depending on the time duration of missile force.

The example used for illustration is an automobile weighing 4,000 lb (1,810 kg) which strikes a 2 ft reinforced concrete barrier at 194 fps (59 meters per second), NRC[7]. The engine and transmission are assumed to weigh 650 lb and assumed to be a rigid component which applies a concentrated impulse to the barrier of 3.85 kip-sec. The remaining 3,350 lb of body and chassis carry a momentum of 20.15 kip-sec. The crushing resistance of this component is assumed to be 300 kips and to be essentially constant as long as crushing continues.

The assumption of body-chassis crushing strength is based on the results of a test performed by Sandia Laboratories[4]. The test consisted in projecting an automobile head-on against a reinforced concrete barrier. The following data describe the test:

Weight of auto:	originally 2,715 lb, modified for test to 3,330 lb
Impact velocity:	76.3 fps
Damage to barrier:	none
Damage to automobile:	26 in. crushing

The average crushing resistance of the body and chassis can be determined by calculating their kinetic energy and dividing that energy by the crushing distance. Assuming 16 percent of the original weight to be engine and transmission this calculation gives:

$$26\ R/12 = (3.3 - 2.715x.16)\ 76.3^2/64.4$$
$$R = 119.6 \text{ kips}$$

Since the automobile used in the example is heavier than the one tested, the crushing resistance R is greater. Assuming resistance proportional to weight, there results

$$R = 119.6 \times 4000/2714 = 176 \text{ kips}$$

For conservatism, this is increased to 300 kips for the example.

Table C.3-1 through C.3-6 give the results of the numerical solution for 24 in. barriers with spans of 10 ft, 15 ft, and 30 ft. Two different load conditions are considered for each span. They are:

1. 4,000 lb auto body and auto engine considered as applying a zero duration impulse (Load Type 4). This gives identical results to Williamson and Alvy Equation 14.

   Impulse: 24 kip-sec.

2. auto body with 20.15 kip-sec momentum considered as applying a square wave impulse with crush force of 300 kips (Load Type 3), and auto engine with 3.85 kip-sec momentum considered as a pure impulse (Load Type 4).

The top half of each table gives the data on missile, barrier, and other loads acting on the barrier. The bottom half presents a summary of the numerical integration of the barrier equation of motion.

Table C.3.7 gives the deflection and ductility of tornado-borne missiles listed in NUREG-75/087, Section 3.5.1.4[7]. This table shows that the ductility is less than 10 for all missiles when the barrier is loaded simultaneously with tornado wind.

C.3.6 Analytical Solution for Equation of Motion

This analytical solution is presented to verify the numerical solution in Section C.3.5 and to offer an alternative to a computer program for the single mass time history analysis of barrier deflection.

The analysis predicts the structural response of an elasto-plastic missile barrier to any combination of the four kinds of loads given in Section C.3.1.

Load Types 2 - 4 are specifically treated in the analytical development that follows, and in which the static loading is assumed to be zero. The result is a system of formulas which permit the determination of both the maximum structural deflection x_m and the ductility ratio $\mu = x_m/e$, where e = the elastic limit deflection of the barrier. The duration of the impact phase of the process can also be found if required.

The effect of a simultaneous static loading is determined by means of a correction of the results of the purely dynamic loading analysis, as is discussed later.

Two different situations occur, according to whether the elastic limit is reached before or after the end of the impact phase.

The impact phase ends when the missile and the barrier (at the point of impact) have the same velocity. Following that time the missile and barrier are assumed to remain in contact and to decelerate together until motion ceases. Under some conditions, the barrier comes to rest before the missile does. This happens for high momentum missiles where the force stopping the missile (Load Type 3) is less than the barrier resistance, R.

The final result of the analysis is expressed in terms of μ, the ratio of the final deflection to the elastic limit deflection of the barrier.

The following symbols are used:

- $e\ (= x_y)$ = elastic limit deflection of barrier (ft)
- F = constant missile impact force (lbs), Load Type 3
- F' = $F + P$
- G = $\beta RmV/F' \sqrt{MRe} = \tan\gamma$
- I = Initial impulse (lb-sec) = $m_i V = \beta mV$, Load Type 4
- M_{be} = equivalent mass of barrier (slugs) (Eq. C.3-1)
- M = $M_{be} + m_i$
- m = missile mass associated with force $F(=M_3)$
- m_i = missile mass associated with initial impulse $I(=M_4)$
- $m + m_i$ = total impacting mass
- P = suddenly applied constant force of indefinite duration Load Type 2 (Eq.C.3-3)
- Q = equivalent static force, Load Type 1 (Eq. C.3-3)
- R = constant plastic equivalent resistance of barrier (Eq. C.3-5)
- t = time (sec)
- $t_1, t_2 \ldots$ = durations of successive stages of response
- V = impact velocity of missile (fps)
- x = deflection of barrier (ft)
- $x_1, x_2 \ldots$ = deflection at ends of successive stages
- $x_y\ (=e)$ = elastic limit deflectionn
- y = displacement of missile mass m after impact
- $\dot{x}, \dot{y} \ldots$ = dx/dt, $dy/dt \ldots$
- β = m_i/m
- λ^2 = R/Me
- γ = $\tan^{-1} G$
- μ = final deflection/e = ductility ratio

Case A. ELASTIC LIMIT IS REACHED DURING PENETRATION/CRUSHING STAGE

Stage 1: $0 \le x \le e$, $\dot{y} > \dot{x}$

Equations of motion are

$$\ddot{y} = -F/m \qquad \ddot{x} + Rx/Me = F'/M$$

$$\dot{y} = V - Ft/m \qquad x = \frac{F'e}{R}(1-\cos\lambda t) + \frac{I}{\lambda M}\sin\lambda t$$

$$\dot{x} = \frac{F'e}{R}\lambda\sin\lambda t + \frac{I}{M}\cos\lambda t$$

Find time t_1 when $x = e$ by setting $x = e$. Then $\cos(\lambda t_1 + \gamma) = (1-R/F')\cos\gamma$

where (C.3-9)

$$\gamma = \tan^{-1}\beta RmV/F' \sqrt{MRe} = \tan^{-1} G$$

If $(1-R/F')\cos\gamma \le -1$, the barrier remains elastic.

The condition for Case A to occur is:

$$\sin\lambda t_1 + G\cos\lambda t_1 + \frac{F}{F'}\frac{M}{m}(\lambda t_1) \le \frac{MG}{m\beta} \qquad \text{(C.3-10)}$$

Stage 2: This stage ends when $\dot{y} = \dot{x}$.

Equations of motion (new time origin) are

$$\dot{y} = V - \frac{F}{m}(t_1 + t) \qquad \ddot{x} = \frac{F'-R}{M}$$

$$\dot{x} = \frac{F'e\lambda}{R}\sin\lambda t_1 + \frac{I}{M}\cos\lambda t_1 + \frac{F'-R}{M}t$$

$$x = e + \frac{F'e\lambda t}{R}\sin\lambda t_1 + \frac{It}{M}\cos\lambda t_1 + \frac{F'-R}{2M}t^2$$

Then, equating $\dot{x} = \dot{y}$ find t_2 from

$$\lambda t_2 = \frac{MG/m\beta - M\lambda t_1/m - \sin\lambda t_1 - G\cos\lambda t_1}{1 + MF/mF' - R/F'} - \lambda t_1 \qquad \text{(C.3-11)}$$

However, if $R > F'$ the barrier mass M may come to rest at time t_2 before $\dot{y} = \dot{x}$. To determine if this happens (only possible if $R > F'$) calculate t_2', from

$$\lambda t_2' = \frac{\sin\lambda t_1 + G\cos\lambda t_1}{R/F' - 1} - \lambda t_1 \qquad \text{(C.3-11A)}$$

If $t_2' \le \lambda t_2$ or if λt_2 from Eq. C.3-11 is negative, then motion ceases at t_2'

$$\mu = 1 + \frac{F'}{R}(\lambda t_2')\left[\sin\lambda t_1 + G\cos\lambda t_1 + (1-R/F')\frac{\lambda t_2'}{2}\right] \qquad \text{(C.3-12A)}$$

However, if $F' > R$ or if $\lambda t_2' > \lambda t_2$, then Stage 3 follows, in which masses M and m move together until they come to rest at a final barrier deflection x_3.

During Stage 3 the deceleration is

$$-\ddot{x} = \frac{R-P}{M+m}$$

At the beginning of Stage 3, velocity and deflection are Stage 2 final values

$$\dot{x}_2 = \frac{F'e\lambda}{R}\sin\lambda t_1 + \frac{I}{M}\cos\lambda t_1 + \frac{F'-R}{M}t_2$$

$$x = e + \frac{F'e}{R}\lambda t_2 \sin\lambda t_1 + \frac{It_2}{M}\cos\lambda t_1 + \frac{F'-R}{2M}t_2^2$$

The final deflection $x_3 = x_2 + (\dot{x}_2)^2/2\ddot{x}$, and

$$\mu = \frac{x_3}{e} = 1 + \frac{F'}{R}(\lambda t_2)\left[\sin\lambda t_1 + G\cos\lambda t_1 + \frac{1}{2}\left(1 - \frac{R}{F'}\right)\lambda t_2\right] + \frac{1+\frac{m}{M}}{2\left(1-\frac{P}{R}\right)}\left(\frac{F'}{R}\right)^2\left[\sin\lambda t_1 + G\cos\lambda t_1 + \left(1-\frac{R}{F'}\right)\lambda t_2\right]^2 \qquad \text{(C.3-12)}$$

$$\text{and } \lambda t_3 = \frac{1+\frac{m}{M}}{1+\frac{P}{R}}\left(\frac{F'}{R}\right)\left[\sin\lambda t_1 + G\cos\lambda t_1 + (1-R/F')\lambda t_2\right]$$

Case B: PENETRATION/CRUSLING STAGE ENDS BEFORE ELASTIC LIMIT IS REACHED

Stage 1: Ends when $\dot{y} = \dot{x}$, $x < e$

Equations of motion are the same as for Stage 1 of Case A.

Stage 1 end at time t_1 when $\dot{y} = \dot{x}$. This time is given by the equation

$$\sin\lambda t_1 + G\cos\lambda t_1 + \frac{F}{F'}\frac{M}{m}(\lambda t_1) = \frac{MG}{m\beta} \qquad \text{(C.3-13)}$$

The condition for Case B to occur is

$$\cos\lambda t_1 - G\sin\lambda t_1 \geq 1 - \frac{R}{F'} \qquad \text{(C.3-14)}$$

Velocity and deflection at the end of Stage 1 are

$$\dot{x}_1 = \frac{F'e\lambda}{R}\sin\lambda t_1 + \frac{I}{M}\cos\lambda t_1$$

$$x_1 = \frac{F'e}{R}(1-\cos\lambda t_1) + \frac{I}{M\lambda}\sin\lambda t_1$$

Stage 2: Ends when barrier comes to rest. Use work and energy principle. At the end of Stage 1, the strain and kinetic energies are

$Rx_1^2/2e$ and $\frac{M+m}{2}(\dot{x}_1)^2$, respectively. At the end of Stage 2 the strain energy $= R(x_2 - e/2)$, and the kinetic energy $= 0$. Then

$$Rx_1^2/2e + \frac{M+m}{2}(\dot{x}_1)^2 = R(x_2 - e/2)$$

and then

$$\mu = \frac{x_3}{e} = \frac{1}{2}\left\{1 + \left(\frac{F'}{R}\right)^2\left[(1-\cos\lambda t_1 + G\sin\lambda t_1)^2 + \left(1+\frac{m}{M}\right)(\sin\lambda t_1 + G\cos\lambda t_1)^2\right]\right\} \qquad \text{(C.3-15)}$$

or, alternatively

$$\mu = \frac{1}{2} + \left(\frac{F'}{R}\right)^2\left[1-\cos\lambda t_1 + \sin\lambda t_1 + G + \frac{1}{2}G^2 + \frac{m}{2M}(\sin\lambda t_1 + G\cos\lambda t_1)^2\right] \qquad \text{(C.3-16)}$$

The limiting condition for Case B occurs with only an initial impulse $I = m_i V$ and no force F. Then, since $M = M_{be} + m_i$,

$$\mu = \frac{1}{2}\left(1 + \frac{I^2}{Re M}\right)/\left(1-\frac{P}{R}\right) \qquad \text{(C.3-17)}$$

The results that have been presented for dynamic response with no accompanying static loading can be corrected as follows when a static load Q also acts.

A uniformly distributed constant static loading can be represented for the dynamic analysis by means of an equivalent concentrated constant force Q, according to Eq. C.3-3. Since this force is capable of doing work during a structural displacement it contributes to the final deflection of the system. Its importance depends on its magnitude compared to the structural resistance (R) of the barrier.

Allowance for the effect of Q on maximum deflection is made as follows: The force Q alone produces in the barrier an elastic deflection Qe/R which uses up a fraction Q/R of its elastic limit deflection e, leaving what can be called a psuedo-elastic limit deflection e' (=e - Qe/R). Likewise, the presence of Q reduces the remaining available plastic resistance from the value R to R - Q = R', where R' can be termed the psuedo-plastic resistance.

The dynamic loads can next be applied to the new substitute system characterized by e' and R' instead of the actual e and R. The calculations lead to a value of x_m' (Eq. C.3-12, C.3-12A, C.3-15, or C.3-16 as the case may be) which is the final deflection of the system beyond or in addition to the starting deflection e' caused by Q. Finally, the actual maximum deflection of the barrier relative to its unstrained configuration is

$$x_m = x_m' + e'$$

and the ductility ratio is

$$\mu = x_m/e = \frac{x_m'}{e} + \frac{Q}{R}$$

C.3.7 Williamson and Alvy Solution

The Williamson and Alvy[3] method of calculating structural response is broken down into, (a) the case with missile penetration and (b) the case with no penetration. This method is used as a basis of comparison by the NRC[8]. The tornado missile which produces the most structural response is the 4,000 lb auto which does not penetrate the barrier.

Therefore, the case of no penetration in Williamson and Alvy is discussed here in detail. Because the penetration of missiles of concern to nuclear power plant design varies so widely for the spectrum of missiles and because the penetration of any given design basis missile is not documented, structural response is not based on penetration. Rather, it is based on the force of the missile on the barrier.

Equation 14 in Williamson and Alvy establishes how much reinforcing steel is needed in a barrier of given thickness for a missile with momentum equal to M_m times V_m. This method of calculating structural response does not necessarily predict structural response for moving objects striking barriers at a nuclear facility.

Equation 14 is derived here in a more direct way than given in Williamson and Alvy [3].

The kinetic energy and momentum of the missile are

$$KE_m = .5\, M_m\, V_m^2$$

$$\text{Momentum} = M_m\, V_m$$

The velocity of the barrier after impact is determined by assuming that the missile and barrier remain together after impact. By conservation of momentum, the velocity of the barrier and missile moving together after impact is

$$V_{b+m} = V_m\, M_m / (M_m + M_{be}) \qquad \text{(C.3-18)}$$

The kinetic energy after impact is

$$KE_{m+b} = .5\, M_m^2\, V_m^2 / (M_m + M_{be}) \qquad \text{(C.3-19)}$$

where

M_m = mass of missile
V_m = velocity of missile
M_{be} = equivalent mass of barrier
V_{b+m} = velocity of missile and barrier traveling together after impact

The kinetic energy of the system after impact is absorbed by structural response. The structural properties are

R = equivalent barrier plastic resisting force

X_y = barrier yield displacement
X_m = maximum barrier displacement
μ = ductility defined by X_m/X_y

Equating the energy of structural response to the kinetic energy of the system after impact gives

$$RX_m - .5\, RX_y = .5\, M_m^2\, V_m^2 / (M_{be} + M_m) \qquad \text{(C.3-20)}$$

$$R^2\, (\mu - .5)/k = .5\, M_m^2\, V_m^2 / (M_{be} + M_m) \qquad \text{(C.3-21)}$$

where the barrier stiffness k is defined by

$$X_y = R/k \text{ and } X_m = \mu X_y \qquad \text{(C.3-22)}$$

The period T of the system is

$$T = 2\pi \left((M_{be} + M_m)/k \right)^{\frac{1}{2}} \qquad \text{(C.3-23)}$$

The resisting force of the barrier R then becomes

$$R = \frac{2\pi\, M_m\, V_m}{T} \left(\frac{1}{2\mu - 1} \right)^{\frac{1}{2}} \qquad \text{(C.3-24)}$$

Equation C.3-24 is the same as Equation 14 in Williamson and Alvy[3].

Equation C.3-24 produces the same deflection as Load Type 4 for the missile where the momentum of the missile is transferred to the barrier as an initial velocity before the barrier offers any structural response.

C.3.8 Comparison of Numerical and Analytical Methods with Williamson and Alvy Results

The method proposed by Williamson and Alvy for predicting the structural response of a missile barrier to impact by a nonpenetrating missile is based on the assumption that the duration of the impact is very short compared to the time required for the barrier to reach its maximum deflection. The loading is treated as a concentrated impulse. This assumption is too conservative, as is evident from consideration of the data presented in the Table C.3-8.

A missile having a certain finite crushing strength will exert a total force of approximately that amount during the impact interval. The duration of the crushing process is then determined from consideration of the initial momentum. When that crushing or loading interval is not extremely short compared to the total reaction interval, consideration of that fact is necessary. The methods of analysis presented here take account of the fact that the crushing and/or penetrating interval is of finite duration. (Note that all the results presented in Table C.3-8 use the same data given in Tables C.3-1 through C.3-6.)

The reason for conservatism in the Williamson and Alvy method is that it only allows the equivalent of Load Type 4 in Section C.3.4. In this load case, the momentum of the missile is transferred to the barrier before the barrier offers structural resistance.

In Table C.3-8, Load Type A is a zero duration impulse, Load Type 4, which gives results identical to those of Williamson and Alvy. Load B is the combination of an initial rigid mass impulse of 5.85 kip-sec with a square wave impulse of 20.15 kip-sec and force 300 kips, Load Types 3 and

4. It is apparent in Table C.3-8 that for the short span the difference is considerable but that it remains very significant for the longer spans as well.

C.3.9 Application to Other Missiles

The method of determining barrier structural deflection to missile impact loads, static loads, and other dynamic loads required by a load combination equation, given in Sections C.3.1 through C.3.4, has many possible applications for predicting the effects of missiles striking reinforced concrete barriers at nuclear power plants.

An example is a whipping ruptured pipe striking a reinforced concrete barrier.

The whipping pipe motion during impact is considerably more complicated than the head-on impact of an auto or tornado driven pipe striking end-on. A whipping pipe may strike a barrier near the pipe elbow. It may also strike sequentially along a line when a long section of pipe impacts the barrier. In the first case, structural deflection is calculated using a circular yield mechanism around the point where the elbow strikes. In the second case, structural deflection is calculated using a rectangular yield mechanism surrounding the line of impact.

As a whipping pipe strikes a barrier, the metal on the impact side of the pipe exerts a large force to bring it to a sudden stop. Then a lower force is exerted on the barrier as the pipe crushes. If the pipe has sufficient energy, it will not be stopped by the time the back surface of the pipe arrives at the barrier. In this case a second force of large magnitude is exerted on the barrier to stop the rear surface of the pipe.

The momentum of the front surface of the pipe in the impact area is assumed to act like Load Type 4 in Section C.3.1, an instantaneous impulse. The crushing of a pipe is represented by Load Type 3 where the magnitude of the square wave is the maximum force from force deflection crush curves for pipes, from Peech et al.[5], needed to absorb the energy of the whipping pipe. The energy of a whipping pipe used to determine the maximum force from crush curves is the total kinetic energy of a whipping pipe less the kinetic energy of the initial impact surface of the pipe, given above as an instantaneous impulse.

If the total crush energy of the elbow, defined by Peech et al.[5] is not sufficient to absorb the kinetic energy of the whipping pipe, remaining after the front surface of the pipe has impacted the barrier as an instantaneous impulse, the excess kinetic energy is absorbed as an instantaneous impact, Load Type 4, of the rear side of the pipe impacting the barrier. The two Type 4 loads representing the front and rear surfaces of the pipe impacting the barrier are applied for simplification and conservatism at the beginning of the impact process.

C.4 CONCLUSIONS

The conclusions to be drawn from this Appendix are:

1. A 2 ft thick reinforced concrete barrier with No. 11 rebar at 10 in., on centers each way and each face, having concrete strength of 3 ksi and rebar yield strength 40 ksi can withstand the impact of the tornado-generated missiles given in NUREG-75/087, Section 3.5.1.4[7] combined with tornado wind. The ductility is less than 10.

2. The methods of analysis formulated in this Appendix can be used to conservatively design barriers for structural response. These methods apply to tornado-generated missiles, whipping pipes, aircraft, dropped equipment, and ruptured components from pressurized and rotating systems and equipment.

3. Structural response is limited to a ductility of 10 or less if the barrier is carrying other loads or if it is the only barrier separating the missile from a missile protected zone.

4. Reinforced concrete barriers are designed to go into the tension resisting mechanism for anchored beam barriers and membrane tension of two-way slab barriers when there is a second barrier downstream of the primary barrier which can stop secondary concrete missiles and when the primary barrier is not required to carry other loads. The maximum barrier tension strain in this case is the same as is permitted for pipe whip restraints, NUREG-75/087, Section 3.6.2.[11]

5. Estimating structural response for barriers at nuclear power facilities using the method for non-penetrating missiles in Williamson and Alvy[3] is too conservative. The method presented in this Appendix is used by Stone & Webster.

6. The method of calculating structural response given in this Appendix is the same whether the missile penetrates or not, and does not depend on a

determination of the depth of penetration. Since penetration of missiles of concern to nuclear power plants is not well documented, the method of determining structural response given in this Appendix is used by Stone & Webster instead of the method given in Williamson and Alvy for penetrating missiles.

C.5 REFERENCES

(1) Wood, R.H., "Plastic and Elastic Design of Slabs and Plates", The Ronald Press Co., New York, N.Y., 1961.

(2) ASTM-A615-75, "Standard Specification for Deformed and Plain Billet Steel Bars for Concrete Reinforcement."

(3) Williamson, R.A., and Alvy, R.R., "Impact Effects of Fragments Striking Structural Elements," Holmes & Narver, Inc., Anaheim, California, Revised November 1973.

(4) Stephenson, A.E., "Tornado Vulnerability Nuclear Production Facilities," Sandia Laboratories, Environmental test Department, April 1975.

(5) Peech, J.M., Roemer, R.E., Pirotin, S.D., East, G.H. and Goldstein, N.A., "Local Crush Rigidity of Pipes and Elbows", Transactions of the 4th International Conference on Structural Mechanics in Reactor Technology, San Francisco, California, 15–19 August 1977.

(6) Biggs, J.M., "Introduction to Structural Dynamics", McGraw-Hill Book Company, 1964.

(7) NUREG-75/087, Section 3.5.1.4, "Missiles Generated by Natural Phenomena", U.S. Nuclear Regulatory Commission.

(8) NUREG-75/087, Section 3.5.3, "Barrier Design Procedures", U.S. Nuclear Regulatory Commission.

(9) Gaston, J.R., Siess, C.P., and Newmark, N.M., "An Investigation of the Load-Deformation Characteristics of Reinforced Concrete Beams Up to the Point of Failure", Civil Engineering Studies, Structural Research Series No. 40, University of Illinois, December 1952.

(10) Anderson, P.E., Hansen, R.J., Murphy, H.L., Newmark, N.M., and White, M.P., "Design of Structures to Resist Nuclear Weapons Effects", ASCE-Manuals of Engineering Practice-No. 42, American Society of Civil Engineers, 1961.

(11) NUREG-75/087, Section 3.6.2, "Determination of Break Location and Dynamic Effects Associated with the Postulated Rupture of Piping," U.S. Nuclear Regulatory Commission.

TABLE C.3-1

4,000 LB AUTO V=59 METERS/SEC**INSTANTANEOUS MOMENTUM TRANSFER SPAN = 10.0 FT

****

DATA ON MISSILE, BARRIER, AND LOAD COMBINATION EQUATION

****

BARRIER YIELD MECHANISM SPAN = 10.0 FT ** BARRIER THICKNESS = 24.0 "
P = 0.007632 = AS/(B*D) = STEEL RATIO ** DEPTH TO CENTROID OF TENSION STEEL = 20.44 "
FC = 3.0 KSI ** FY = 40. KSI ** YIELD LINE FORCE = 12.6*MP

0.0 KIPS EQUIVALENT STATIC FORCE ** LOAD 1
0.0 KIPS EQUIVALENT CONSTANT DYNAMIC FORCE ** LOAD 2
0.0 KIP-SEC MISSILE IMPULSE RESISTED BY FORCE AT BARRIER SUPPORT PLUS BARRIER INERTIA DURING MOMENTUM TRANSFER ** LOAD 3
24.000 KIP-SEC MISSILE IMPULSE RESISTED ONLY BY BARRIER INERTIA DURING MOMENTUM TRANSFER ** LOAD 4
97.5 FPS BARRIER INITIAL VELOCITY DUE TO LOAD 4

BARRIER EQUIVALENT WEIGHT	MISSILE WEIGHT LOAD 3	MISSILE WEIGHT LOAD 4	BARRIER PLASTIC FORCE	BARRIER EFFEC. YIELD DEFLECTION	BARRIER PERIOD
KIPS	KIPS	KIPS	KIPS	FT	SEC
3.927	0.000	4.000	1482.2	0.0116	0.0061

****

RESULTS OF TIME HISTORY ANALYSIS FOR MISSILE IMPACT WITH OTHER LOADS

****

1 TIME HISTORY NUMBER	2 DURATION OF LOAD 3	3 MISSILE FORCE LOAD 3	4 FORCE AT BARRIER SUPPORT	5 TIME OF MAX BARRIER DEFLECTION	6 MAXIMUM BARRIER DEFLECTION	7 MAXIMUM BARRIER DUCTILITY	8 MAXIMUM BARRIER VELOCITY	9 FINAL BARRIER RESISTING MECHANISM
	SEC	KIPS	KIPS	SEC	FT		FT/SEC	
1	0.0	0.0	1482.2	0.016258	0.7960	68.42	97.49	MEMBRANE TENSION

TABLE C.3-2

4,000 LB AUTO V=59 METERS/SEC**INSTANTANEOUS MOMENTUM TRANSFER SPAN = 15.0 FT

****

DATA ON MISSILE, BARRIER, AND LOAD COMBINATION EQUATION

****

BARRIER YIELD MECHANISM SPAN = 15.0 FT ** BARRIER THICKNESS = 24.0 "
P = 0.007632 = AS/(B*D) = STEEL RATIO ** DEPTH TO CENTROID OF TENSION STEEL = 20.44 "
FC = 3.0 KSI ** FY = 40. KSI ** YIELD LINE FORCE = 12.6*MP

0.0 KIPS EQUIVALENT STATIC FORCE ** LOAD 1
0.0 KIPS EQUIVALENT CONSTANT DYNAMIC FORCE ** LOAD 2
0.0 KIP-SEC MISSILE IMPULSE RESISTED BY FORCE AT BARRIER SUPPORT PLUS BARRIER INERTIA DURING MOMENTUM TRANSFER ** LOAD 3
24.000 KIP-SEC MISSILE IMPULSE RESISTED ONLY BY BARRIER INERTIA DURING MOMENTUM TRANSFER ** LOAD 4
60.2 FPS BARRIER INITIAL VELOCITY DUE TO LOAD 4

BARRIER EQUIVALENT WEIGHT	MISSILE WEIGHT LOAD 3	MISSILE WEIGHT LOAD 4	BARRIER PLASTIC FORCE	BARRIER EFFEC. YIELD DEFLECTION	BARRIER PERIOD
KIPS	KIPS	KIPS	KIPS	FT	SEC
8.835	0.000	4.000	1482.2	0.0262	0.0138

****

RESULTS OF TIME HISTORY ANALYSIS FOR MISSILE IMPACT WITH OTHER LOADS

****

1 TIME HISTORY NUMBER	2 DURATION OF LOAD 3	3 MISSILE FORCE LOAD 3	4 FORCE AT BARRIER SUPPORT	5 TIME OF MAX BARRIER DEFLECTION	6 MAXIMUM BARRIER DEFLECTION	7 MAXIMUM BARRIER DUCTILITY	8 MAXIMUM BARRIER VELOCITY	9 FINAL BARRIER RESISTING MECHANISM
	SEC	KIPS	KIPS	SEC	FT		FT/SEC	
1	0.0	0.0	1482.2	0.016398	0.5011	19.14	60.21	MEMBRANE TENSION

TABLE C.3-3

4,000 LB AUTO V=59 METERS/SEC**INSTANTANEOUS MOMENTUM TRANSFER SPAN 30.0 FT

****

DATA ON MISSILE, BARRIER, AND LOAD COMBINATION EQUATION

****

BARRIER YIELD MECHANISM SPAN = 30.0 FT ** BARRIER THICKNESS = 24.0 "
P = 0.007632 = AS/(B*D) = STEEL RATIO ** DEPTH TO CENTROID OF TENSION STEEL = 20.44 "
FC = 3.0 KSI ** FY = 40. KSI ** YIELD LINE FORCE = 12.6*MP

0.0 KIPS EQUIVALENT STATIC FORCE ** LOAD 1
0.0 KIPS EQUIVALENT CONSTANT DYNAMIC FORCE ** LOAD 2
0.0 KIP-SEC MISSILE IMPULSE RESISTED BY FORCE AT BARRIER SUPPORT PLUS BARRIER INERTIA DURING MOMENTUM TRANSFER ** LOAD 3
24.000 KIP-SEC MISSILE IMPULSE RESISTED ONLY BY BARRIER INERTIA DURING MOMENTUM TRANSFER ** LOAD 4
19.6 FPS BARRIER INITIAL VELOCITY DUE TO LOAD 4

BARRIER EQUIVALENT WEIGHT	MISSILE WEIGHT LOAD 3	MISSILE WEIGHT LOAD 4	BARRIER PLASTIC FORCE	BARRIER EFFEC. YIELD DEFLECTION	BARRIER PERIOD
KIPS	KIPS	KIPS	KIPS	FT	SEC
35.342	0.000	4.000	1482.2	0.1047	0.0553

****

RESULTS OF TIME HISTORY ANALYSIS FOR MISSILE IMPACT WITH OTHER LOADS

****

1 TIME HISTORY NUMBER	2 DURATION OF LOAD 3	3 MISSILE FORCE LOAD 3	4 FORCE AT BARRIER SUPPORT	5 TIME OF MAX BARRIER DEFLECTION	6 MAXIMUM BARRIER DEFLECTION	7 MAXIMUM BARRIER DUCTILITY	8 MAXIMUM BARRIER VELOCITY	9 FINAL BARRIER RESISTING MECHANISM
	SEC	KIPS	KIPS	SEC	FT		FT/SEC	
1	0.0	0.0	1482.2	0.018938	0.2115	2.02	19.64	BENDING YIELD LINE

TABLE C.3-4

4,000 LB AUTO V=59 METERS/SEC** 650 LB ENGINE - 3,350 LB BODY AND FRAME SPAN = 10.0 FT

****

DATA ON MISSILE, BARRIER, AND LOAD COMBINATION EQUATION

****

BARRIER YIELD MECHANISM SPAN = 10.0 FT ** BARRIER THICKNESS = 24.0 "
P = 0.007632 = AS/(B*D) = STEEL RATIO ** DEPTH TO CENTROID OF TENSION STEEL = 20.44 "
FC = 3.0 KSI ** FY = 40. KSI ** YIELD LINE FORCE = 12.6*MP

0.0 KIPS EQUIVALENT STATIC FORCE ** LOAD 1
0.0 KIPS EQUIVALENT CONSTANT DYNAMIC FORCE ** LOAD 2
20.150 KIP-SEC MISSILE IMPULSE RESISTED BY FORCE AT BARRIER SUPPORT PLUS BARRIER INERTIA DURING MOMENTUM TRANSFER ** LOAD 3
3.850 KIP-SEC MISSILE IMPULSE RESISTED ONLY BY BARRIER INERTIA DURING MOMENTUM TRANSFER ** LOAD 4
27.1 FPS BARRIER INITIAL VELOCITY DUE TO LOAD 4

BARRIER EQUIVALENT WEIGHT	MISSILE WEIGHT LOAD 3	MISSILE WEIGHT LOAD 4	BARRIER PLASTIC FORCE	BARRIER EFFEC. YIELD DEFLECTION	BARRIER PERIOD
KIPS	KIPS	KIPS	KIPS	FT	SEC
3.927	3.350	0.650	1482.2	0.0116	0.0061

****

RESULTS OF TIME HISTORY ANALYSIS FOR MISSILE IMPACT WITH OTHER LOADS

****

1 TIME HISTORY NUMBER	2 DURATION OF LOAD 3	3 MISSILE FORCE LOAD 3	4 FORCE AT BARRIER SUPPORT	5 TIME OF MAX BARRIER DEFLECTION	6 MAXIMUM BARRIER DEFLECTION	7 MAXIMUM BARRIER DUCTILITY	8 MAXIMUM BARRIER VELOCITY	9 FINAL BARRIER RESISTING MECHANISM
	SEC	KIPS	KIPS	SEC	FT		FT/SEC	
1	0.003520	300.0	1482.2	0.003520	0.0517	4.45	27.20	BENDING YIELD LINE

TABLE C.3-5

4,000 LB AUTO V=59 METERS/SEC** 650 LB ENGINE - 3,350 LB BODY AND FRAME SPAN = 15.0 FT

****

DATA ON MISSILE, BARRIER, AND LOAD COMBINATION EQUATION

****

BARRIER YIELD MECHANISM SPAN = 15.0 FT ** BARRIER THICKNESS = 24.0 "
P = 0.007632 = AS/(B*D) = STEEL RATIO ** DEPTH TO CENTROID OF TENSION STEEL = 20.44 "
FC = 3.0 KSI ** FY = 40. KSI ** YIELD LINE FORCE = 12.6*MP

0.0 KIPS EQUIVALENT STATIC FORCE ** LOAD 1
0.0 KIPS EQUIVALENT CONSTANT DYNAMIC FORCE ** LOAD 2
20.150 KIP-SEC MISSILE IMPULSE RESISTED BY FORCE AT BARRIER SUPPORT PLUS BARRIER INERTIA DURING MOMENTUM TRANSFER ** LOAD 3
3.850 KIP-SEC MISSILE IMPULSE RESISTED ONLY BY BARRIER INERTIA DURING MOMENTUM TRANSFER ** LOAD 4
13.1 FPS BARRIER INITIAL VELOCITY DUE TO LOAD 4

BARRIER EQUIVALENT WEIGHT	MISSILE WEIGHT LOAD 3	MISSILE WEIGHT LOAD 4	BARRIER PLASTIC FORCE	BARRIER EFFEC. YIELD DEFLECTION	BARRIER PERIOD
KIPS	KIPS	KIPS	KIPS	FT	SEC
8.835	3.350	0.650	1482.2	0.0262	0.0138

****

RESULTS OF TIME HISTORY ANALYSIS FOR MISSILE IMPACT WITH OTHER LOADS

****

1 TIME HISTORY NUMBER	2 DURATION OF LOAD 3	3 MISSILE FORCE LOAD 3	4 FORCE AT BARRIER SUPPORT	5 TIME OF MAX BARRIER DEFLECTION	6 MAXIMUM BARRIER DEFLECTION	7 MAXIMUM BARRIER DUCTILITY	8 MAXIMUM BARRIER VELOCITY	9 FINAL BARRIER RESISTING MECHANISM
	SEC	KIPS	KIPS	SEC	FT		FT/SEC	
1	0.004540	300.0	1482.2	0.004540	0.0378	1.45	13.28	BENDING YIELD LINE

TABLE C.3-6

4,000 LB AUTO V=59 METERS/SEC** 650 LB ENGINE - 3,350 LB BODY AND FRAME SPAN = 30.0 FT

****

DATA ON MISSILE, BARRIER, AND LOAD COMBINATION EQUATION

****

BARRIER YIELD MECHANISM SPAN = 30.0 FT ** BARRIER THICKNESS = 24.0 "
P = 0.007632 = AS/(B*D) = STEEL RATIO ** DEPTH TO CENTROID OF TENSION STEEL = 20.44 "
FC = 3.0 KSI ** FY = 40. KSI ** YIELD LINE FORCE = 12.6*MP

0.0 KIPS EQUIVALENT STATIC FORCE ** LOAD 1
0.0 KIPS EQUIVALENT CONSTANT DYNAMIC FORCE ** LOAD 2
20.150 KIP-SEC MISSILE IMPULSE RESISTED BY FORCE AT BARRIER SUPPORT PLUS BARRIER INERTIA DURING MOMENTUM TRANSFER ** LOAD 3
3.850 KIP-SEC MISSILE IMPULSE RESISTED ONLY BY BARRIER INERTIA DURING MOMENTUM TRANSFER ** LOAD 4
3.4 FPS BARRIER INITIAL VELOCITY DUE TO LOAD 4

BARRIER EQUIVALENT WEIGHT	MISSILE WEIGHT LOAD 3	MISSILE WEIGHT LOAD 4	BARRIER PLASTIC FORCE	BARRIER EFFEC. YIELD DEFLECTION	BARRIER PERIOD
KIPS	KIPS	KIPS	KIPS	FT	SEC
35.342	3.350	0.650	1482.2	0.1047	0.0553

****

RESULTS OF TIME HISTORY ANALYSIS FOR MISSILE IMPACT WITH OTHER LOADS

****

1 TIME HISTORY NUMBER	2 DURATION OF LOAD 3	3 MISSILE FORCE LOAD 3	4 FORCE AT BARRIER SUPPORT	5 TIME OF MAX BARRIER DEFLECTION	6 MAXIMUM BARRIER DEFLECTION	7 MAXIMUM BARRIER DUCTILITY	8 MAXIMUM BARRIER VELOCITY	9 FINAL BARRIER RESISTING MECHANISM
	SEC	KIPS	KIPS	SEC	FT		FT/SEC	
1	0.019338	300.0	827.7	0.019338	0.0585	0.56	4.19	ELASTIC

TABLE C.3-7

BARRIER DEFLECTION AND DUCTILITY FOR
TORNADO-BORNE MISSILES PLUS 360 MPH TORNADO WIND*

Missile	Velocity (meters per second)	Momentum kip-sec	Barrier Span (ft)	Barrier Deflection (ft)	Barrier Ductility
114.6 lb wood plank	83	0.97	10	0.0038	0.33
114.6 lb wood plank	83	0.97	30	0.0121	0.12
286.6 lb 6 in. Sch 40 pipe	52	1.52	10	0.0034	0.30
286.6 lb 6 in. Sch 40 pipe	52	1.52	30	0.0162	0.16
8.8 lb 1 in. steel rod	51	0.05	10	0.0004	0.04
8.8 lb 1 in. steel rod	51	0.05	30	0.0048	0.05
1124.4 lb utility pole	55	6.30	10	0.0114	0.98
1124.4 lb utility pole	55	6.30	30	0.0523	0.50
749.6 lb 12 in. Sch 40 pipe	47	3.59	10	0.0125	1.08
749.6 lb 12 in. Sch 40 pipe	47	3.59	30	0.0327	0.31
4000.0 lb auto	59	24.00	10	0.0520	4.47
4000.0 lb auto	59	24.00	30	0.0629	0.60

* Barrier data: 2 ft concrete f_c' = 3 ksi No. 11 rebar Grade 40 10 in. on center each way and each face

TABLE C.3-8

COMPARISON OF BARRIER DUCTILITY RATIOS PREDICTED BY ANALYTICAL AND NUMERICAL METHODS WITH WILLIAMSON AND ALVY METHOD

Missile: Auto: weight = 1810 kg, velocity = 59 mps

Barrier: 24 in. concrete No. 11 rebar at 10 in. on center each way and each face

Line No.	Span (ft)	Missile Load Type	Analytical Method	Numerical Method	Williamson & Alvy Method
1	10	A*	68.42	68.42	68.42
2	10	B**	4.56	4.45	N.A.
3	15	A	19.14	19.14	19.14
4	15	B	1.47	1.45	N.A.
5	30	A	2.02	2.02	2.02
6	30	B	0.56	0.56	N.A.

*A 24 kip-sec initial impulse for auto body and engine

**B 3.85 kip-sec initial impulse for engine and 20.15 kip-sec square wave for auto body with 300 kip crush strength

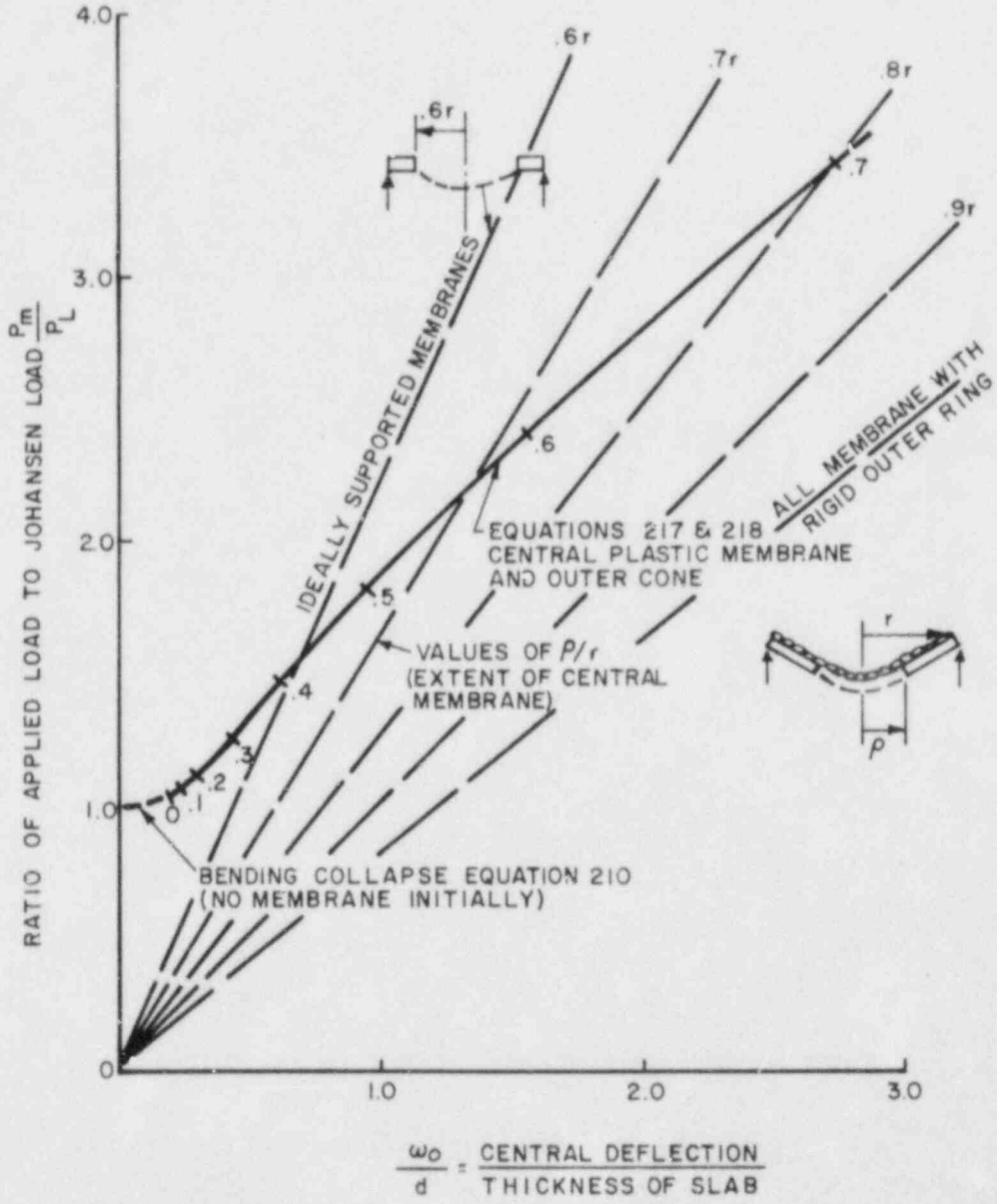

FIGURE C.3-1

EFFECT OF TENSILE MEMBRANE ACTION ON SUPPORTED CIRCULAR SLAB

(From Fig. 86a in Wood[1])